AUTOMATED MULTIFREQUENCY MEASUREMENTS OF IONOSPHERIC MOVEMENTS

BY

DAVID NOEL WARREN-SMITH B.Sc.

A Thesis

presented for the degree of

Master of Science

at the

UNIVERSITY OF ADELAIDE

(Physics Department)

NOVEMBER 1979

Awarded May 1980

TABLE OF CONTENTS

LIST OF ILLUSTRATIONS

SUMMARY

The experimental data described in this thesis have been obtained with a fully automated ground based equipment which measures the angle of arrival of electromagnetic waves reflected from the ionosphere at a number of selected frequencies. The measurements are made sequentially at the successive frequencies at a maximum rate of one measurement every two or three seconds. Near-vertical incidence c.w. signals from a transmitting station 32 km distant from the receiver site are used to investigate the travelling waves in the ionosphere. Electron density profile analysis together with spectral analysis of the angle of arrival data yields estimates of the vertical trace velocities of the ionospheric waves. This data is then interpreted in terms of the dispersive properties of atmospheric gravity waves in order to estimate horizontal parameters associated with the waves. The interpretation of the data is extended with the use of a geometrical simulation of ionospheric reflection in the presence of an assumed travelling sinusoidal reflecting surface.

STATEMENT

To the best of the author's knowledge this thesis contains no material previously published or written by another person, except where due reference is made in the text. It contains no material which has been submitted or accepted for the award of any other degree or diploma in any university.

(D.N. WARREN-SMITH)

ACKNOWLEDGEMENTS

The author would like to acknowledge the help and encouragement given to him by the two supervisors for this thesis: Dr. R.A. Vincent of the Radio Physics Group of the Physics Department at the Adelaide University and to Mr. P.L. George of the Ionospheric Studies Group, Defence Research Centre Salisbury (D.R.C.S.).

The data described in this thesis were obtained using equipment at the Weapons Research Establishment (now D.R.C.S.) with the permission of the director. The equipment used to obtain the data was developed jointly by members of Cybernetics Electronics Group (D.R.C.S.) and Ionospheric Studies Group (D.R.C.S.) for the use of Ionospheric Studies Group, and was based on concepts developed by Ionospheric Studies Group over preceding years. The contribution of the author to this development was the design of the microcontroller and computer interface circuitry and to write the computer software for the system.

The experimental program was made possible by the kind provision of transmitting equipment and a transmitter site operator at the Kersbrook site as well as the use of the receiving site equipment at St. Kilda and the Ionosonde station at Salisbury, by Ionospheric Studies Group under the leadership of Mr. P.L. George. Special thanks are due to Mr. A. Eason for ensuring that all required equipment was made available.

The electron density profile data used in chapter 5 and described in the section on real height analysis in chapter 2 was supplied and scaled by Ionospheric Studies Group. Assistance has also been received with the production of drawings and photographic work.

FRONTISPIECE

Direction of arrival data for two signals reflected from the ionosphere at near vertical incidence displayed as components of zenith angle.

KERSBROOK TEST W004B 4/1/76 ZENITH ANGLE PLOT PAGE 1

1: 5.3800 MHZ FINE FILTER 2 K=0.25 4756 POINTS MEANS: NS -0.73 EW 5.96 :W004AA

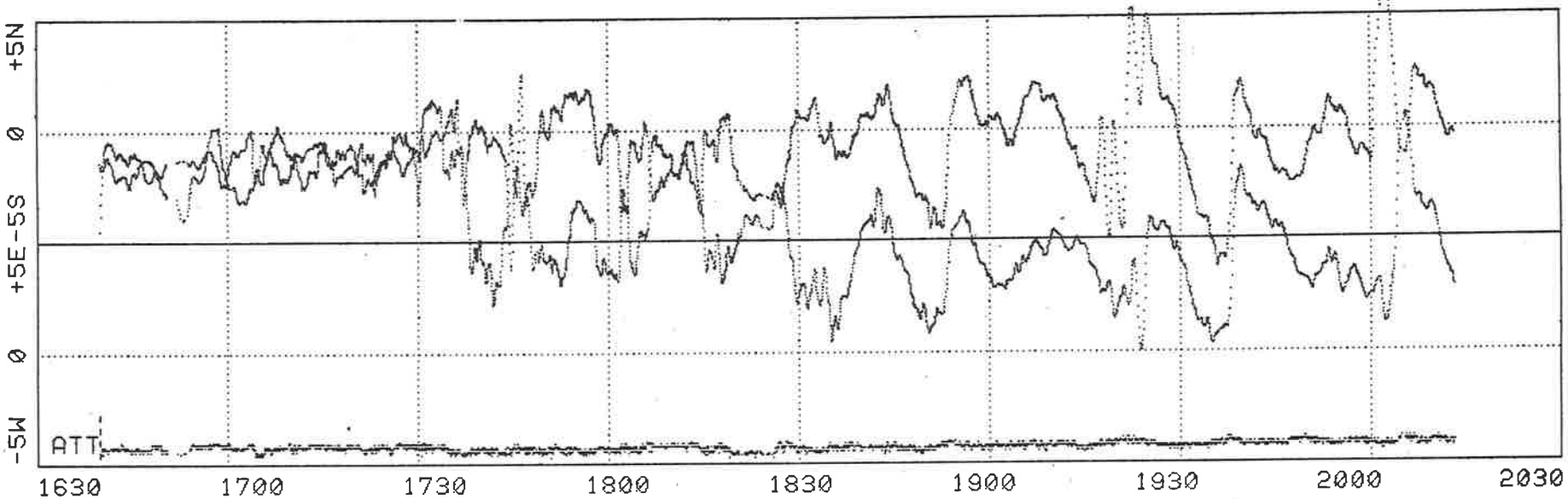

2: 5.7450 MHZ FINE FILTER 2 K=0.25 2415 POINTS MEANS: NS -1.14 EW 3.91 :W004AB

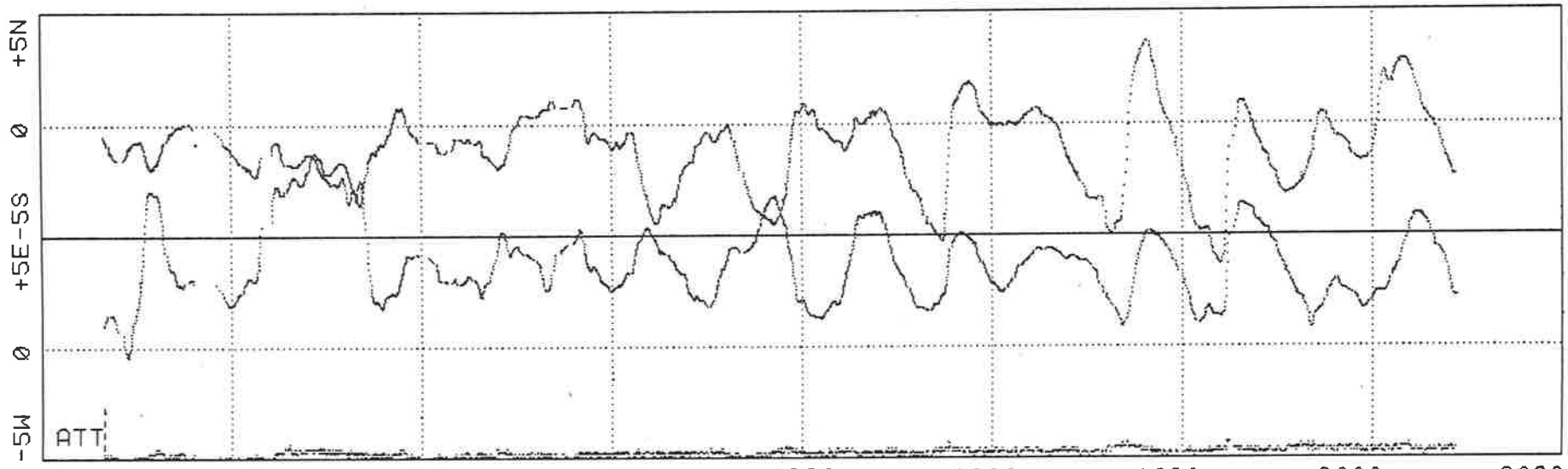

CHAPTER 1

INTRODUCTION

1.1 GENERAL INTRODUCTION

This thesis describes experiments carried out with equipment that has been designed to automate the measurement of the direction of arrival of electromagnetic waves propagated via reflection from the ionosphere. Whilst the ionosphere does act as a remarkably good mirror for e.m. waves propagated in this way, it is observed that the direction of arrival of these waves is subject to a continual wandering over a small angular range of a few degrees, depending on the obliquity of the signals. This wandering effect is attributed to a large extent to the presence of internal gravity waves that propagate through the earth's atmosphere at ionospheric heights. The effects of these waves are commonly known as travelling ionospheric disturbances (TID's), particularly when they are of large amplitude. The local effect of these disturbances is to create tilts in the ionospheric medium that is responsible for the reflection of the e.m. waves that impinge on it.

This thesis is mainly concerned with observations on ionospheric movements by means of e.m. wave propagation at near vertical incidence. It is found that propagation may occur via the F region or the E region, or both, or may switch from one to the other. In the data base obtained in the measurement runs made with the equipment, multimode reflection in the form of switching between E and F modes was commonly observed with occasional brief periods of pure E or F region reflection. This thesis is not concerned with small scale irregularities or scintillations.

For many communication purposes the effects of travelling ionospheric disturbances may not be significant, however, where accuracy is required

such as for direction finding purposes or for communications with highly directional antennas it is desirable to be able to characterise the effects which they produce. The collection of data with manual or semi automatic equipment presents a formidable manual effort. Furthermore the results are subject to the effects of fatigue, subjective bias, and inattentiveness introduced by the operator. Automatic equipment, besides being essentially free of these effects if properly designed, can also be given a degree of agility that a human operator does not possess.

The main features of the experimental equipment are described in chapter 2. Paragraphs 2.1 to 2.4 are an abreviated version of a report on the technical aspects of the experimental equipment (Warren-Smith and Steer, 1977). Although the technicalities of automation of the equipment are not without interest, the main emphasis in this thesis is on the analysis and interpretation of the experimental records obtained. The raw data that will be presented is in the form of orthogonal components of phase data related to the direction of arrival of the received signal as a function of time. Ionograms from the Salisbury ionosonde station are used in some of the data analyses. Processing procedures applied to the data are also given in chapter 2, paragraphs 2.7 to 2.12. This introductory chapter discusses previous studies of ionospheric movements and alternative methods of observation with special reference to direction of arrival methods of measurement.

Significant progress in the understanding of any physical phenomenon can only be made when experimental observations are accompanied by a theoretical approach. The last part of this introductory chapter considers briefly the development and experimental verification of gravity wave theory and the dispersion relations for the atmosphere at ionospheric altitudes. The dispersion relationships through the use of appropriate

mathematical techniques are fundamental to an understanding of the dynamics of atmospheric processes and source mechanisms for travelling ionospheric disturbances. The first order perturbation theory of internal gravity waves is considered in chapter 5 where it is used for estimating horizontal and other parameters of the wave motions exhibited in the data.

1.2 INVESTIGATION OF IONOSPHERIC MOVEMENTS

An observation of the effects of travelling ionospheric disturbances was made by Munro (1950) and co-workers as early as 1939 from continuous virtual height (h't) recordings then being made at Sydney and Canberra. A three station system of spaced observing points was established in 1947 for the purpose of studying these disturbances. Synchronised pulse transmissions on a single frequency and a cathode ray tube display were used in conjunction with a continuous moving photographic strip to make simultaneous recordings of effective height from the three stations. These recordings enabled times of occurence of disturbances to be determined at the mid points between the transmitting stations and the receiving station. The directions and velocities of the disturbances were then determined from the records. Velocities ranging from 80 to 160 m/s were observed with directions that bore a marked seasonal variation. Similar experiments were carried out by Bramley and Ross (1951) and others. A later paper, Munro (1953), described complexities, associated with the disturbances, that appeared on the (h't) records. These were the characteristic X, Y and Z traces, which were explained by means of a geometrical construction as being due to reflection from a concave isoionic moving surface in the ionosphere. The moving disturbance is depicted as a wave in which the electron density in the ionosphere is alternately more and less dense with a progressive change in phase with height thus giving the wave a vertical

as well as horizontal component of velocity. The asymmetry leading to Y and Z traces was accounted for by the differential retardation in the discrete reflections when multiple reflections were present, due to variations in the gradient of electron density in different parts of the wave motion.

In a further paper, Munro (1958), detailed statistics of daily, monthly, and yearly occurences, velocities and directions of disturbances were given. A mean velocity of 130 m/s was found with azimuthal directions varying between 30 degrees east of north in winter to 120 degrees in summer. All the results given were, however, taken with a single frequency of 5.80 Mhz, and on disturbances which produced clearly defined complexes on the records. Further tests were considered necessary to determine what variation could be expected with altitude.

Comparisons were also made between the Munro method of measurement and alternative methods of measurement (Heisler, 1963). The method of Mitra (1949) was noted to produce results not in agreement with the Munro method. A significant difference between the two methods is that the separation of reflection points for the Munro method is approximately 20 km whereas for the Mitra method receiving elements were some 100 m apart and used an amplitude fading method of observation. The paper of Heisler (1963) also gave a summary of the characteristics of disturbances that had been established up to that time. It was particularly noted that the method of measurement used could have a selective effect on the scale or other characteristics of the effects observed. Disturbance effects had been observed ranging from large scale phenomena, Heisler (1958), with a predominant direction from the pole to the equator but with comparatively infrequent occurrence to small scale phenomena that were present more or less continuously.

Further investigations of the directions and velocities of travelling ionospheric disturbances were made in the northern hemisphere by Jones (1969) using the doppler method of phase path measurement developed by Davies and Baker (1966). A three station array was established with reflection points arranged in an equilateral triangle with sides of approximately 40 km. Three frequencies were used in one arm of the array to allow vertical as well as horizontal trace components of velocity to be measured. The experimental results show an annual variation of direction very similar to that given by Munro (1958) except that at the equinoxes velocities were to the west instead of to the east as determined by Munro, in the southern hemisphere. At the solstices the directions of TID movement were essentially from the direction of the winter pole, in both hemispheres. The magnitudes of velocities obtained were similar to those obtained by Munro, except that actual velocity was obtained and not just the horizontal component. The results of Jones were checked by an experiment carried out by Walton (1971), who found essential agreement.

A later suggestion is made by Davies and Jones (1971) that the differences in directions of the travelling waves at the equinoxes were a consequence of the time of observations which were usually made at a particular time of day. This suggestion is in agreement with an earlier review of ionospheric movements of Briggs and Spencer (1954), in which it was shown that ionospheric movements at this time of year were to the east in the morning and to the west in the afternoon. Calculations by Hooke (1970a,b,c) show that the response of the ionised constituents of the ionosphere to motion of the neutral atmosphere induced by TID's can be appreciably anisotropic depending on the azimuth of the TID with respect to the inclination of the Earth's magnetic field and the orientation of the sun. The suggestion is made that this anisotropy in conjunction with the

known sensitivity of ionospheric sounding equipment can account to a large degree for the statistical behaviour of the observed directions of TID movements.

Wave like irregularities in the E region have been studied by Vincent (1972) using the Buckland Park aerial array near Adelaide. The averaged velocities of the irregularities were compared with neutral wind measurements made by the Adelaide meteor system and found to be in reasonable agreement. This agreement was interpreted as evidence of selection of gravity waves due to critical layer winds at the altitude of the E layer. The wave like irregularities were shown to be of small amplitude and to produce specular reflections of the radio signals used for observations. Variability of the wave effects observed was such that multiple off vertical reflections could at times be inferred.

Systematic tilts in the ionosphere have been studied by Morgan (1974). A small systematic tilt was shown to occur and to vary as a function of solar zenith angle.

1.3 THE EFFECT OF IONOSPHERIC DISTURBANCES ON DIRECTION FINDING TECHNIQUES

When direction finding methods were applied to high frequency signals for which the ionosphere provided the means of propagation over the required distances, deviations in the measured bearings of the signals could be seen. The deviations continued to be seen when improvements to direction finding equipment ruled out the possibility of instrumental errors as the cause of the deviations. A review of direction finding techniques, Ross (1947), describes equipment in use, problems and possible directions of future development after the second world war. The Adcock system and the spaced loop direction finder were the favoured techniques at the time, but the advantages, such as potential for wave interference

reduction, and problems of wide aperture systems were considered and it was conceded that wide aperture systems would have a place in future developments. The effect of lateral deviations introduced into bearing readings on signals reflected from the ionosphere was considered. These lateral deviations were noted to be worst at very short range (<90 km), to improve progressively as range increased but to deteriorate once again at ranges where multi-hop propagation occured.

A review paper by Gething (1966) contains an extensive list of references to direction finding techniques, problems and systems in use. The U-Adcock system and circularly disposed arrays of wide aperture such as the Wullenweber systems were described amongst others. The latter systems employed a rapidly rotating commutator and a system of delay lines in conjunction with a cathode ray tube display to form either a broad beam for signal identification or a deep null pattern which gave the bearing of the received signal directly on the cathode ray tube display. Bearing accuracies approaching 0.1 degree have been reported for this type of system (Jones and Reynolds, 1975). In practice, this accuracy was only achievable on ground wave signals. R.M.S errors of 2 to 4 degrees were common for ionospherically propagated signals, depending on obliquity.

The effect on the direction of a radio signal after reflection from the tilted ionosphere has been considered by Croft and Fenwick (1963) with a mirror reflection model for the case of oblique propagation. A selection of charts were computed and presented which relate the tilt of the mirror to the distant point of intersection of the ray path of the signal on the Earth's surface, or the nearest point to which the ray returns if it does not again intersect the Earth's surface. The three dimensional geometry of tilted mirror like reflection, following the method of Bramley (1953), suitable for short oblique paths is developed in chapter 4. A single

sinusoidal reflecting surface is applied to this model.

A description of techniques which preceded the development of the automated equipment described in this thesis are given by Treharne et. al. (1965) and Treharne (1967) where the potential of vertical triangulation using skywaves is considered for the purpose of radio location from a single site. Approximate methods of solving the oblique path geometry are described with a view to improving the estimation of the distance to the remote transmitting source to be located. A technique of amplitude ratio measurements with a system of spaced antennas was used to determine the elevation angle and bearing of the received signal. The measurement technique adopted for the equipment described in this thesis is, however, the interferometer principle described by Ross et. al. (1951). A sum and difference principle in conjunction with a cathode ray tube display was used for measurement and observation of the phases of the received signals in two orthogonal pairs of aerials. The elevation angle and bearing were then calculated from the measured phase angles. For the equipment described in this thesis a digital method of phase measurement has been used which is amenable to computer control and for storage of data on magnetic tape or for obtaining printed results in real time after processing in the computer.

Since there is no known way of predicting the occurence of TID's, efforts have been made to devise practical schemes for allowing for their effects for the purpose of improving the accuracy of direction finding systems. A selection of schemes for doing this are described by Jones and Reynolds (1975). In one scheme a spaced array of doppler sounders was provided at the mid point of the path to the distant transmitting station from which the tilt in the ionosphere at this point could be determined and then used for correcting the bearing indicated by the direction finding

system. Experimental verification of the feasibility of this method has been described by Jones, Kantarizis and Morgan (1975). A second technique is to take bearing measurements on a second transmitter of known location in the vicinity of the one to be observed. Problems were experienced with wave interference effects when multimode propagation was present, although some success was reported for unimodal signals. The second transmitter needs to be in the near vicinity of the known transmitter and to be operating on close to the same frequency for good correlation of observed tilts to be obtained. A third possibility is to make simultaneous measurements of bearing and doppler shift, with a view to determining ionospheric tilts remotely through the use of oblique signals. There are, however, difficulties associated with each of these schemes for use in an operational direction finding system. Further discussion of these and other possible techniques are described by Gething (1978).

The application of a ray tracing model to the demonstration of the effect of TID's on range errors when vertical triangulation schemes are applied to radio location applications at short ranges has been described by George (1972), where the tilt is measured in the vicinity of the direction finding station. Errors in the application of simple tilt correction schemes are described and the improvement in accuracy to be achieved by allowing for these errors is demonstrated.

A significant problem experienced with the use of narrow aperture direction finding equipment such as the U-Adcock system is the fluctuations in indicated bearing due to multipath wave interference. This problem has been graphically demonstrated by Hayden (1961) who showed that bearing errors of as much as 90 degrees to the mean bearing of a pair of incomming rays could result from wave interference effects. This source of error can also occur in wide aperture systems although to a lesser extent.

A commonly used device to overcome this problem is to use pulse transmissions to take advantage of the different times of flight for pulses propagating by different ionospheric modes and by gating the pulses from the required mode into the phase measurement circuitry. An advantage of this technique is that it allows directions of arrival of different modes to be determined individually.

If observations are made over a period of time, the effect of wave interference error can be averaged out and the resulting mean phase tends towards the phase of the strongest mode present or towards the centre of the angular spectrum if different modes are of similar strength (Burtnyk et. al., 1965). Burtnyk et. al. have also considered the reliability of ambiguity resolution for wide aperture arrays through the use of an additional orthogonal set of receiving aerials of narrower aperture and have concluded that ambiguity resolution is feasible for all but a small percentage of the time if the measured phases are averaged for a suitable time before use. Precautions taken to ensure unimodal reception for the equipment described in this thesis are given in chapter 2.

Resolution of individual modes using swept frequency, continuous wave signals has been demonstrated by Rice (1973) using a 32 element wide aperture array with a separate receiver connected to each antenna element. Examples given by Rice show both the separation of individual modes and also the bearings of signals received in each mode. The extraction of this greater degree of information about the received signals is only achieved at the expense of providing spatial sampling in a wide aperture array with dimensions exceeding a kilometer in the broadside direction to the remote signal source together with the requisite matched receiving equipment and on-line computing facilities.

1.4 THE DEVELOPMENT OF ACOUSTIC-GRAVITY WAVE THEORY

Initial efforts to develop a satisfactory theory to account for the behaviour of travelling ionospheric disturbances were hindered by the non linear character of the differential equations governing the upper atmosphere considered as a tenuous fluid. Progress in developing a first order theory to provide a starting point for an understanding of the main features of atmospheric motions at ionospheric altitudes depended on a choice of assumptions to simplify the equations. The first adequate solution to this problem was that of Hines (1960). The gravity wave theory of ionospheric irregularities was further considered and reinforced in a Napier Shaw prize essay (Hines, 1963). The latter paper besides reviewing the gravity wave theory also considered systematic wind structures in the upper atmosphere such as winds due to tidal effects. A review of atmospheric waves in the ionosphere along similar lines was given by Beer (1972).

The theory was applied to the behaviour displayed by long lasting meteor trails that were revealed by radar observations. Radar installations for tracking meteor trails had been set up to make observations of wind structures at heights of 80 to 115 km where the ionisation produced by meteors was greatest. It was noted that during the course of a few minutes the meteor trails became distorted, displaying the effects of horizontal winds that varied in direction within a vertical scale of a few kilometers. The winds deduced from these observations displayed predominantly horizontal flow with a horizontal scale that was much greater than their vertical scale and with the scales of both increasing greatly with height. The randomness exhibited in these wave motions was given as an indication of the presence of a spectrum of waves. An approximate treatment of the effects of viscosity, which increases with

height in inverse proportion to the gas density was shown to account for the vertical scale size of the observed wind motions. It was shown that the effect of viscosity would be to progressively exclude the smaller scale motions with increase in altitude. The expected exponential increase in amplitude with altitude was demonstrated to be approximately realised in the observations.

Reflection of waves at a thermal barrier was given as a second mechanism for the restriction of the observed spectrum of wave motions. The dominant modes displayed at an altitude of 90 km were shown to be in good agreement with the theoretically expected spectrum of waves, from a source inferred to be in the lower or middle atmosphere. Arguments were advanced for a gravity wave explanation of ionospheric drift observations as opposed to a wind driven explanation. It was pointed out that a wave interpretation did not require an additional explanation for the presence of the irregularities and could account for the sudden change in direction of the irregularities sometimes observed. It was noted that the movements observed would represent phase progressions of the waves and not component velocities of air parcel movements, although the air parcel movements themselves could represent quite appreciable wind systems.

F region TID's such as those described by Munro (1958) were also accounted for by means of gravity wave theory. A 'leaky' ducting mechanism provided an explanation of the downward phase progression accompanied by an obliquely upward flow of energy. The thermal decline at heights of 50 - 80 km provided a reflection mechanism which partially reflected waves back into the lower atmosphere and provided a partial ducting mechanism in the horizontal direction allowing energy to progressively leak into the upper atmosphere with horizontal distance.

A number of papers have appeared subsequently describing further work suggested by Hines (1960). Pitteway and Hines (1963) consider the effect of including viscous damping in the equations and confirmed the conclusion that an increase in amplitude with height would be balanced by the increasing effect of viscous damping giving rise to a dominant wavelength at a given height. Thermal conductivity was shown to be similar in its effect to viscous damping. The effect of allowing for arbitrary variations of temperature and background wind with height was considered by Pitteway and Hines (1965). Reflection and ducting of atmospheric waves which result from these effects were studied. Further effects and filtering of gravity waves due to background winds was considered by Hines and Reddy (1967). The relationship between gravity waves in the atmosphere and their effect on ionisation density as observed by ionospheric sounding equipments was considered by Hooke (1968). Verification of gravity wave theory at F region heights is considered in chapter 5.

A review of large scale TID's with particular emphasis on source mechanisms was given by Francis (1975). In this review the term TID was reserved for large well defined events. Wave events of the scale described were not identified in the data base for this thesis, but the review is of interest as a source of references to work that has been done on realistic atmospheric models and to excitation mechanisms of gravity waves. Descriptions were given of a number of large scale TID observations. In this thesis the term TID is not restricted to large scale events.

CHAPTER 2

DESCRIPTION OF THE EXPERIMENT

2.1 EQUIPMENT AND FACILITIES

The experimental equipment is comprised of a computer controlled interferometer facility. The facility was developed to the point where near simultaneous measurements of the direction of arrival of up to ten h.f. radio signals reflected by the ionosphere could be made. Typically, each signal would be sampled in turn with all the required steps of tuning the receiver to the selected frequency, level adjustments, calibration and measurement sequence being carried out under computer control for each signal. Some two or three seconds is required to carry out the complete procedure for each signal, under average conditions.

Software was written to provide a machine language interactive keyboard operating system. This operating system provided flexible arrangements for setting up the required parameters, sequence of operations and real time processing and display requirements by entering simple commands at the keyboard. Real time computation and print out of azimuth and elevation angles for each signal was provided to facilitate monitoring of the course of an experiment. Data storage was provided on small magnetic tape reels.

A photograph of the equipment is shown in figure 1. A PDP-8L computer occupies the rack on the left, together with associated peripheral equipment including a memory expansion unit and a dual dectape unit. Control equipment with computer interface and subsystem interface circuitry, power supply and HP3330A frequency synthesizer occupy the centre rack. The RACAL twin channel communications receiver type RA153 together with measurement equipment and receiver subsystems occupy the right hand rack. A small

table is normally placed adjacent to the ASR-33 teletype machine but was removed for the photograph. A small amount of equipment associated with the interferometer aerial interface is housed in a separate rack which does not appear in the picture.

2.2 AERIAL ARRAY

Figure 2 is a view of the interferometer aerial array which occupies a field near the equipment building. The interferometer consists basically of two pairs of horizontal dipole aerials that are accurately surveyed into position. One pair is sited in a north-south direction and the other pair in an east-west direction. The separation of the dipoles in each pair is 73.15 m (240 feet). A measurement of the phase difference of the signals appearing in each of the two pairs of dipoles is sufficient to determine the direction of arrival of the incoming radio wave at the selected frequency without ambiguity, provided that the frequency is sufficiently low and that the direction of arrival of the radio wave is from near the zenith. For higher frequencies and for oblique signals an ambiguity arises from grating lobes due to the spacing of the dipole pairs. The ambiguity is resolved by making phase measurements at an additional two pairs of orthogonal aerials at one quarter of the spacing of the main array.

In the practical realisation of the interferometer each horizontal dipole as described so far actually consists of two crossed dipoles arranged at 45 degrees to the north-south direction. These crossed dipoles are connected with a phasing circuit to form a circularly polarized antenna (Phillips, 1951). The direction of polarization can be selected remotely. The horizontal dipoles have a polar diagram which is directed vertically, ensuring that ionospherically propagated signals are given preference over ground wave signals. Only six crossed dipole aerials are actually used

FIGURE 2.1 View of the equipment racks

FIGURE 2.2 View of the interferometer aerial array

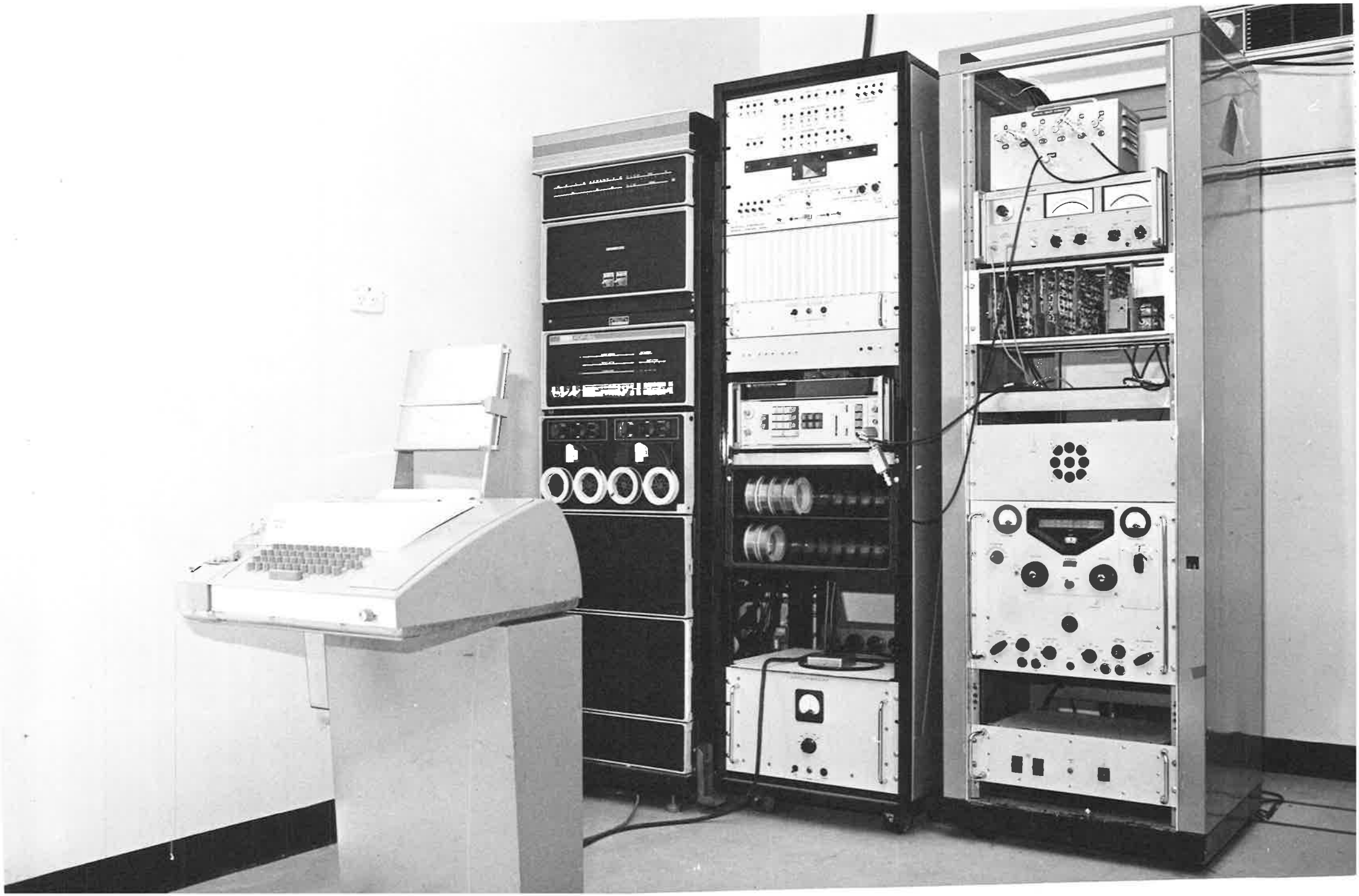

since the short base line pairs can share one dipole each with the long base line pairs.

2.3 RECEIVER AND PHASE MEASUREMENT CIRCUITRY

A block schematic of the receiver, phase measurement and associated circuitry is shown in figure 3. The Racal RA153 twin channel communications receiver amplifies the selected high frequency signals received by the selected pair of aerials and converts these signals to 100 kHz intermediate frequency signals. The differential phase angle of the intermediate frequency signals is measured by the phase measurement circuitry provided that certain test conditions are satisfied.

The aerial multicoupler units comprise pairs of identical wideband isolating amplifiers. These units allow additional experimental systems to share the same antenna array. They also provide a gain of 10 db together with some increase in sensitivity. The aerial switching unit allows for connection of either the required pair of aerials or the calibration signal. The calibration signal is provided by a programmable HP3330A frequency synthesizer. The output frequency of the synthesizer is set under programme control to the selected operating frequency. The calibration signal is applied to each receiver through a resistive divider network at the aerial switching unit input. The required receiver input signal level is set by a dual matched programmable attenuator unit.

The receiver is capable of being tuned in the frequency range 1 MHz to 30 MHz. However, the maximum usable frequency is limited to 13 MHz by the frequency synthesizer. The receiver provides two separate signal paths, balanced to 1 db in amplitude and 15 degrees in phase, to produce two i.f. signals at 100 kHz, at which the phase is measured. Due to the phase and gain imbalances which vary with both receiver control settings and signal

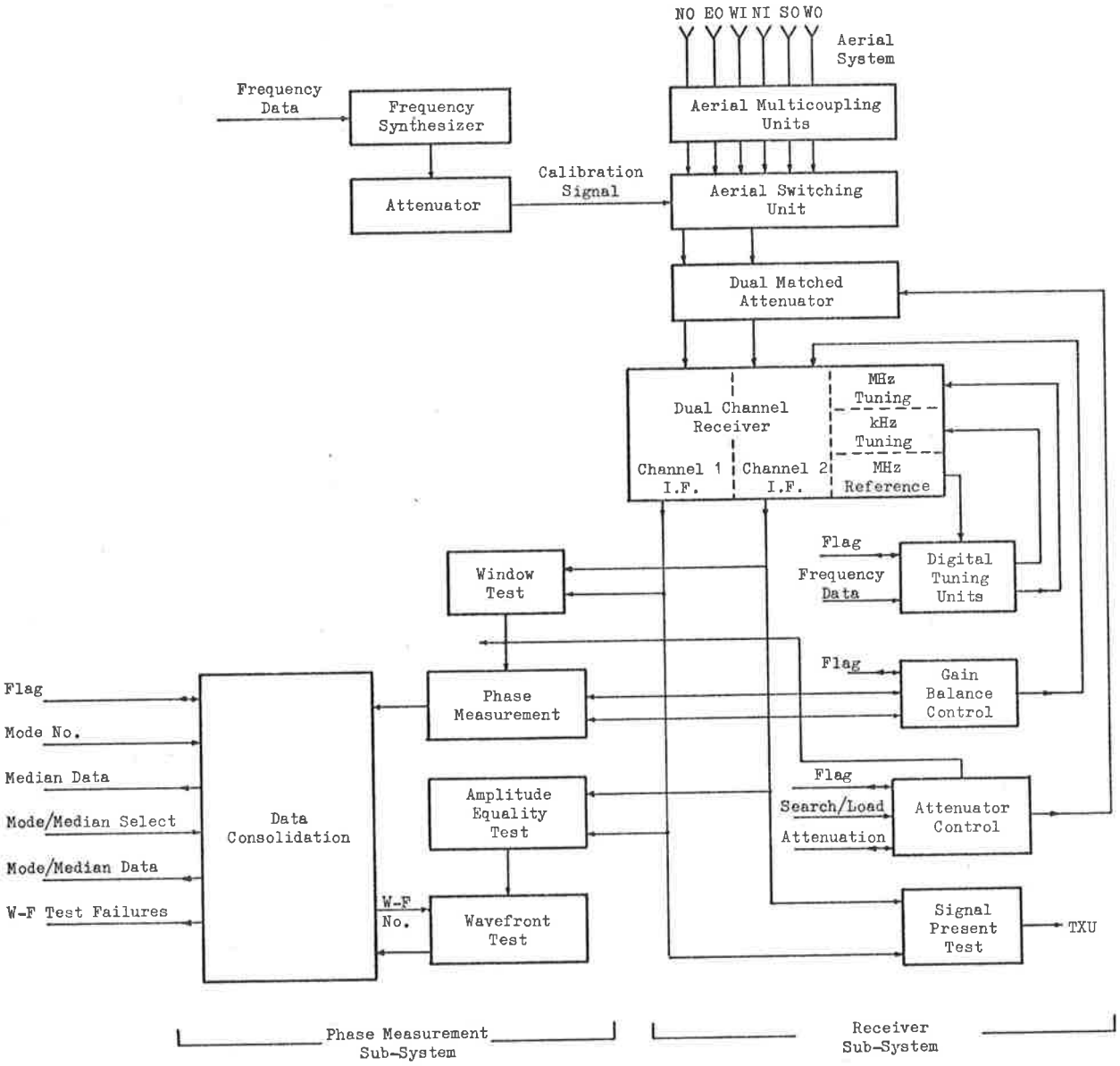

Figure 2.3 Block schematic of the dual channel receiver and phase measurement circuitry

level, a number of calibration and control functions are necessary to ensure that phase measurements are accurate to within 2 degrees. A calibration sequence is carried out prior to every set of phase measurement readings. During this sequence gain imbalance is corrected by the action of the gain balance control circuit. The phase imbalance is then measured and stored as a correction for subsequent phase measurements. In order to reduce the differential phase shift due to signal level variations, the i.f. signal levels are controlled to fall within a 10 db dynamic range prior to the measurements being taken. This action is carried out by the dual matched attenuator in conjunction with the attenuator control unit. The attenuator can be locked at a given setting or allowed to step until the required signal level is achieved. The R.F. gain control of the receiver is preset manually so that the 60 db dynamic range of the attenuator covers the expected range of input signal levels.

The two channels of the receiver are tuned by the same local oscillators. Two local oscillator signals are required to control the megahertz and kilohertz contents of the frequency to be received. The Wadley system of band selection (see; RACAL Communications Incorporated, operating manual) is used in the receiver. Approximately 200 ms is requird to tune the receiver to a new frequency.

The phase difference between the two i.f. signals is measured on a cycle to cycle basis by counting the number of pulses of a clock between zero cross over points on the two i.f. signals. In order that this should provide a direct measurement of the phase angle and to avoid errors resulting from variations in the i.f. signal frequency, the clock is controlled to be a fixed multiple of the i.f. signal frequency for variations of up to 8 percent in the nominal frequency of 100 kHz. The clock frequency is 256 times that of the i.f. so that 360 degrees is represented by 256 in the

phase measurement system. The resolution of the phase measurement system is therefore approximately 1.4 degrees.

The phase measurement circuitry is prevented from operating if any of three test conditions are not satisfied. Measurements are taken only when both i.f. signal levels fall within a given range. This test is indicated on figure 3 as a window test. In an attempt to ensure that only quasi-unimodal propagation is considered, measurements are only taken when amplitudes across the array are equal to within a preset tolerence which is small by comparison to that permitted in the window test. A further test for unimodality in the received signals is to use i.f. cycles only when a given number of preceding cycles meet the amplitude equality test. The number of preceding cycles to test can be selected under computer control to values in the range 0 to 7. This test is shown on figure 3 as a wave-front test. A fourth test is provided, with an output that can be tested directly by the microcontroller to be described in the next section. This comparative test circuit was set with a threshold just above the receiver noise floor and determined if a signal was present or not.

Raw phase measurements are collected in the data consolidation circuitry. This circuitry consists of a hardware histogram circuit, implemented with random access memory. One memory word is reserved for each of the 256 possible measurement values. A consolidated phase measurement is considered to be complete when the most frequently occurring value exceeds a pre-determined number of occurrences given by 32n+31 where n is a single digit in the range 0 to 7. The most frequently occurring value is the mode of the set of readings. Hardware circuitry was provided which could then determine the median value of the set of readings. Either the mode or median value could be made available as the final phase reading taken by the phase measurement system.

2.4 CONTROLLER AND INTERFACE CIRCUITRY

A control and interface circuit was constructed to allow complete system interconnection. A programmable microcontroller within this unit provides a sequencing capability for one complete calibration and phase measurement cycle, including the transfer of one set of data to the computer. The measurement sequence is initiated by the computer after the required frequency and other parameters have been transferred to the controller from the computer. Interface circuitry provides interconnection to the computer on the one hand and to the receiver, calibration and phase measurement circuitry on the other hand.

A very much simplified block diagram of the controller subsystem is shown in figure 4. The manual control and display panel which can be seen at the top of the centre rack in figure 1 is not included in figure 4. The control and display panel was used for monitoring whilst the equipment was under computer control and for test purposes during development. At the top of figure 4 it can be seen that there is a flow of parameters from the computer through appropriate interface gate circuitry to a set of registers. These registers hold such information as the selected frequency, initial attenuator setting and other initialisation parameters. This information is then available to the subsystems until changed by the computer. In the centre of figure 4 it can be seen that there is a similar flow of data and parameters from the subsystems to the computer. The phase measurement data and sample time are collected in an additional set of registers. Transfer of this data to the computer is initiated by the microcontroller when a complete set of data has been collected, through the direct memory access facility of the computer into a preselected buffer area in the computer's memory.

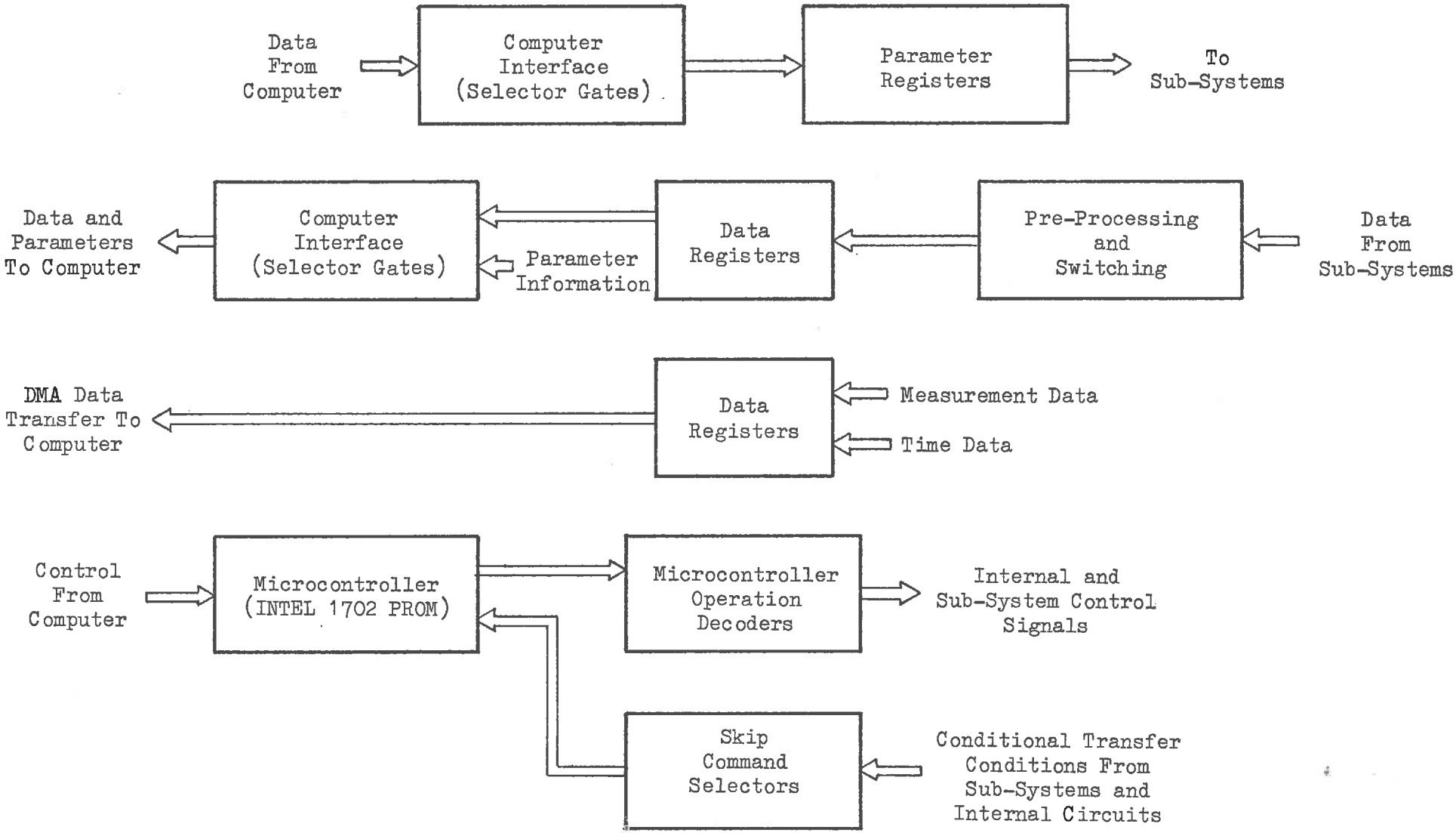

Figure 2.4 Controller block diagram

The microcontroller is shown at the bottom of the block diagram. The microcontroller is a programmable sequencing device. It can generate a number of control pulses on individually selected lines. These pulses initiate such actions as the gain balance control function or initiate tuning of the receiver. The microcontroller can execute conditional as well as unconditional branch operations to any step in the sequence by means of a second set of individually selected lines which sense the conditions to be tested. The microcontroller thus has the capability of responding to circumstances as they arise and to step to a new sequence step or loop back to a previous step as required.

In the case of many of the receiver subsystems, the microcontroller initiates a sub-sequence controlled within the subsystem. In these cases, the conditional branching facility is used to execute a waiting loop until a flag signal within the subsystem is set. The previously mentioned examples of gain balance control and receiver tuning are cited. To avoid a possible indefinitely long waiting period, a time limit test is included in the waiting loop in a number of cases. If the time limit expires, the microcontroller programme branches to an exit sequence and signals the computer.

The microcontroller circuitry is based on an INTEL 1702 PROM device which provides a fixed non-volatile memory to hold the programme. This device can be programmed in the laboratory. An assembler programme was written to assist in firmware development. This assembler could be run on the computer or any other similar PDP-8 computer system. The assembler will accept a source file generated with the operating system software of the computer and will produce both a fully coded octal and decimal listing of the microcontroller programme and a specially coded paper tape which can be fed directly into an INTEL PROM programmer.

2.5 EXPERIMENTAL ARRANGEMENT

The experimental data for this thesis was taken in December 1975 with a few additional days in January 1976. The arrangement provided for the experiment can be seen in figure 5. The interferometer and computer system was installed at the St. Kilda receiver site. A collection of four transmitters were operated in c.w. mode at the Kersbrook site, some 32 km to the east. The output power for three of the transmitters was 10 watts whilst the fourth transmitter had an output power of 30 watts. The frequencies used were 3.84 Mhz, 5.38 Mhz, 5.745 Mhz and 6.7155 Mhz. Vertical incidence ionograms were taken from the Salisbury ionosonde station at 5 minute intervals during some of the data runs. Since the equipment is automatic in operation when once set up it was possible to leave the equipment unattended on occasions. Several overnight runs were made. The c.w. transmissions could be monitored on a separate receiver and the presence of interfering signals checked for and noted.

Since the transmitting site was comparatively close to the receiver site, signals reflected from the ionosphere had a direction of arrival close to the zenith. All the data collected from the experimental configuration is in the form of time series phase angle data, related to the near vertical angle of arrival of the signals. The final setting of the dual matched attenuator was also recorded but is not specifically used in the analyses. The analyses of the data are supported by the ionogram data from the Salisbury ionosonde station.

2.6 DATA ANALYSIS PROCEDURES

The raw data from the experimental equipment is in the form of ASCII coded files on small magnetic tape reels. These files contain heading and parameter information followed by lines of data. Each line of data con-

tains the results of one complete measurement sequence carried out under the control of the microcontroller. Each data line starts with a single identification digit which is followed by the sample time, coarse and fine pairs of phase readings and the attenuator setting. Parameter lines also start with an identification digit and contain the frequency and other fixed settings for the corresponding data lines. Data for different frequencies can therefore be unambiguously identified during subsequent processing.

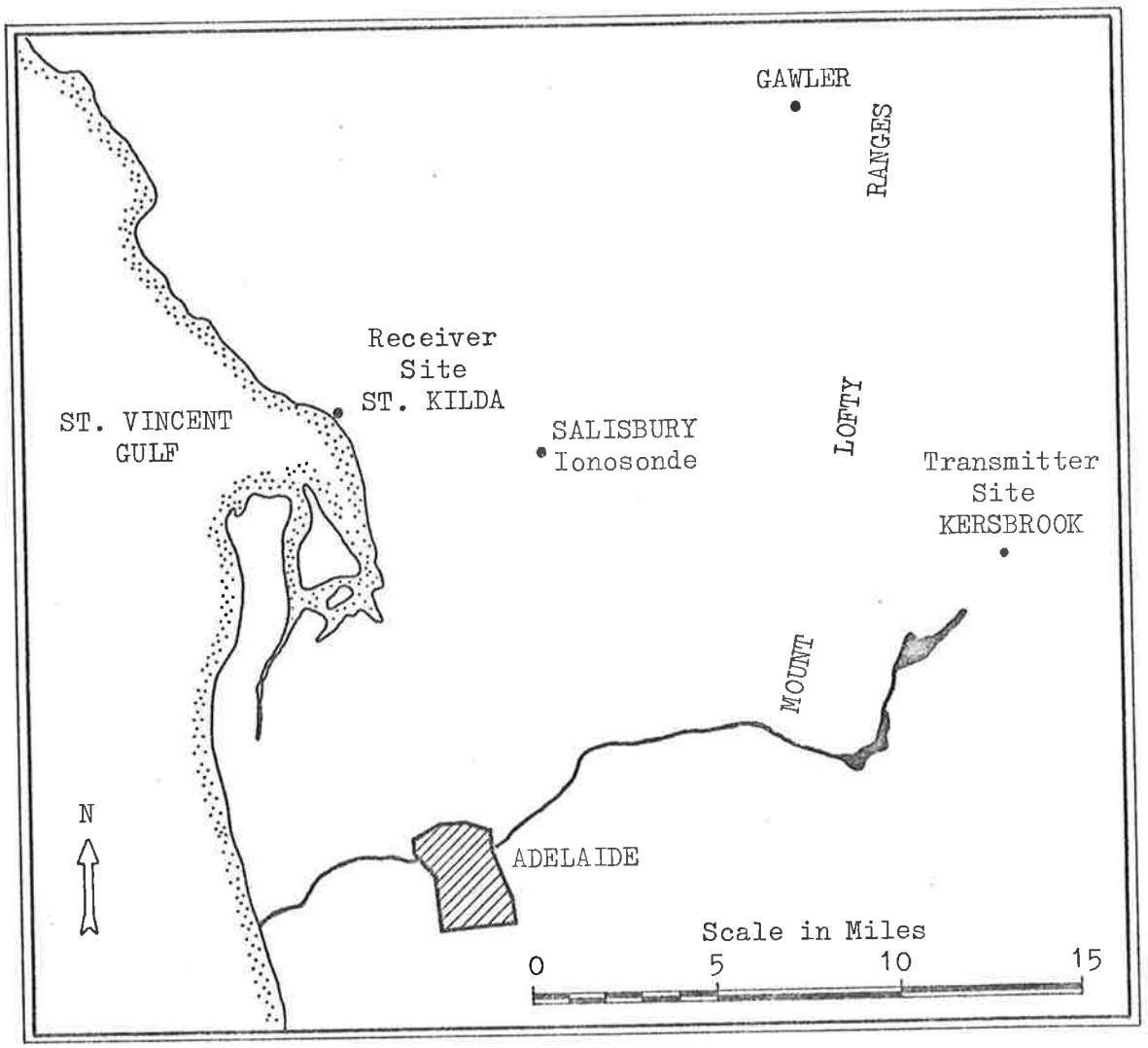

FIGURE 2.5 Map showing the location of the receiver site, transmitter site and Salisbury ionosonde

All data collected were transferred from the small magnetic tape reels onto standard ANSI format 10 1/2 inch magnetic tape reels. Individual data files on these tapes are labelled with a code that includes the day of the year during which the data were taken and the sequence of the data during the day.

Computer programmes were written to provide a range of data analysis procedures for the data. A PDP-11 computer with plotting facilities was used for much of the data processing. The relationship amongst the main procedures can be seen in figure 6. Each box in figure 6 represents a computer programme or choice of programmes. The general purpose programmes will be described in this chapter and the remainder in subsequent chapters.

The first programme accepts a selected raw data file as input and extracts data corresponding to a specified parameter line. A secondary file in direct numerical form is generated from the input data. The secondary data file contains heading and parameter information followed by zenith angle components from the coarse or fine phase data, decimal time and attenuator settings. An exponential smoothing algorithm may be applied to the zenith angle data which enhances the quick look presentation of the data. The programme may also plot the output data. All secondary data files including files produced by further processing procedures are given a standard format to facilitate handling. These files can be accepted by the plotting section of the input data conversion programme. Numerical operations and other details of the various programmes are given in subsequent sections.

A special programme was written to provide a test facility for some of the data analysis procedures. This programme accepts a secondary data file as input and generates another secondary file with time information copied from the input file and zenith angle data replaced with sine wave data,

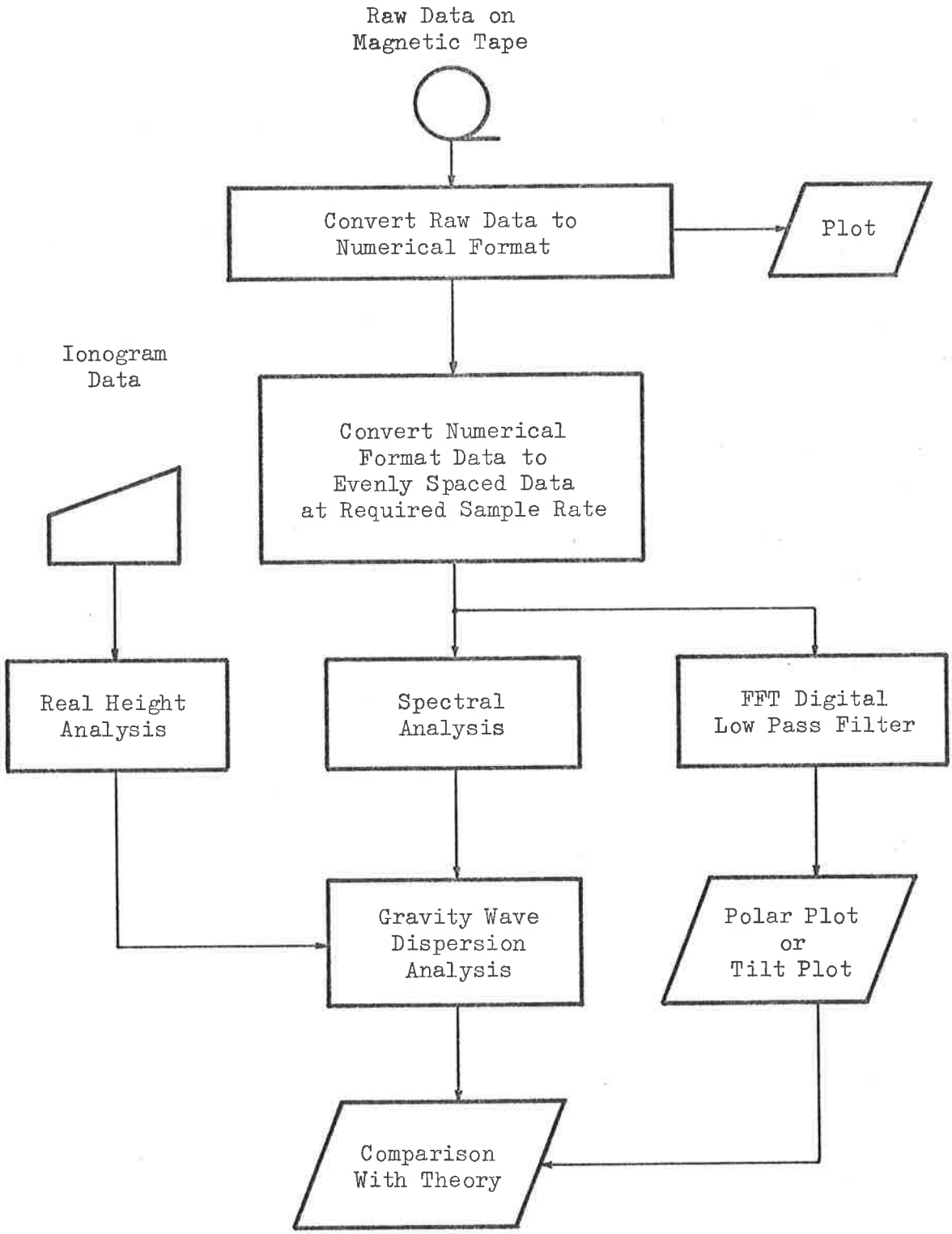

Figure 2.6 Flow diagram of data analysis procedures

square wave data and/or random data. Any number of sine waves can be generated and added together, with period, amplitude and phase specified for each one. A choice of uniformly distributed or Gaussian distributed random data can be added to the sine waves.

2.7 INPUT DATA CONVERSION AND PLOTTING PROGRAM

The primary function of this programme is to transform the ASCII formatted raw data files into direct access numerical files. The phase angle data obtained from the phase consolidation circuitry is converted into north-south and east-west angle components which closely approximate the zenith angle components of the incoming wave normal.

The direction cosines of the incoming ray are obtained from the relation:

$$\text{Cos}\,\alpha = \frac{\phi\lambda}{2\,\pi d} \tag{2.1}$$

where ϕ is the consolidated phase angle; λ is the wavelength of the received signal and d is the spacing of the antennas, which is 240 feet for the fine spacing antennas and 60 feet for the coarse spacing antennas. The compliment of the angle α obtained from this is a good approximation to a zenith angle component for zenith angles of less than 10 degrees. After inserting physical conversion factors the relationship:

$$Z = 90.0-57.2958\ \text{Arccos}\ \frac{\phi D}{87.8432f} \tag{2.2}$$

is obtained, where f is the frequency of the incoming wave in Mhz and D has the value 1 for the fine antenna spacing and 4 for the coarse antenna spacing.

The resulting zenith angle is brought into the range $-90 \leq Z \leq 90$ by subtracting 180 degrees from it if it is greater than 90 degrees. The

quantisation step size for the zenith angle data can be obtained from (2). At a frequency of 3.84 Mhz this gives approximately 0.24 degrees for the fine spacing data and 1.0 degrees for the coarse spacing data. At the 6.7155 Mhz frequency the step sizes are 0.14 degrees and 0.55 degrees respectively.

The plotting section of the programme provides for two annotated zenith angle plots. These plots include the north-south and east-west zenith angle components separately, the time in hours-minutes form and the attenuator settings. Central summer time is used throughout. The plots are composed of data representing the results of individual measurements or individual processed data points. If available, the ordinary and extraordinary ray marker is plotted, and represents the time at which a change was made to the polarization setting. The O-ray setting is represented on the zenith angle plots as a short vertical dashed line above the attenuator setting data at the bottom of each plot. The X-ray setting is similarly represented by a short vertical dotted line.

Quick look presentation of the data is enhanced by means of the exponential low pass filter option. The characteristics of this recursive digital filter are given in appendix A. This filter has been chosen for its simplicity of implementation in the FORTRAN programme. The required degree of smoothing is achieved by specifying two parameters. The first parameter specifies the filter configuration and the second parameter specifies the degree of smoothing required. Filter configuration type 1 provides second order smoothing in the forward direction through the data. Filter configuration type 2 provides a second smoothing pass backwards through the data following a forward pass, thus providing a zero phase shift version. A value between zero and one is specified for the second parameter depending on the degree of smoothing required. The smaller the value chosen for this

parameter the greater the degree of smoothing performed. A value of 0.25 was typically used, with a type 2 configuration.

2.8 DATA COMPOUNDING PROGRAMME

The experimental data was produced at irregular intervals, typically of a few seconds apart. The spectral analysis techniques used required uniformly spaced data. The experimental data was also produced at a faster rate than was required for data processing. The excess data usefully provided some degree of initial smoothing.

A data compounding programme was written which could read an input secondary file and produce another secondary file in which all input data points within successive uniformly spaced intervals of time were averaged to produce uniformly spaced samples with times assigned to the centres of the intervals. The first interval was set to start at the time of the first data point from the input file. In the averaging process north-south and east-west components were averaged separately. The attenuator settings data was also averaged. Typically up to ten input points would be averaged to form one output point depending on sample rate (specified as samples per hour) required. An option was provided which enabled gaps in the data to be filled in by linear interpolation between the nearest two data points. Linear interpolation in this way is less severe than setting data points in gaps to zero since there is an inherent offset in the data due to the fact that the transmitter site is not co-located with the receiver site.

The data compounding programme allows successive data files taken on a given day to be concatenated. The gap between successive files can also be filled in by linear interpolation if required. Thus a single secondary data file can be produced containing all the data from a given day with uniformly spaced sample intervals.

A useful option is provision for changing the heading stored in the output secondary file. Treated files can be identified by incorporating additional information in the new heading.

2.9 SPECTRAL ANALYSIS PROGRAMME

The spectral analysis programme has been adapted from a multivariate spectral analysis programme in use by the Radio Physics Group of the Physics Department at the University of Adelaide. The adaptations provided for the present programme are mainly related to input file handling and to the plotting of results. A modified procedure for smoothing of power spectral estimates is described in Appendix B.

The spectral analysis programme allows two secondary data files to be read as input and a series of procedures may then be applied to the two sets of data from these files. The available procedures will be described in their order of application.

The first procedure is that of mean or mean and trend removal. The procedure consists of determining the least squares straight line fit to the data and subtracting this line point by point from the data. Each component of the data is treated separately. The next procedure is to apply a 10% cosine bell weighting function to the data. A function of the form:

$$\frac{1}{2}\left\{1 - \cos\frac{\pi k}{N}\right\} \qquad (2.3)$$

is applied to the kth data point for the first and last 10% of the data. N is the nearest integer to 10% of the available data points read in from an input data file. The input routine for the programme can read a specified number of input data points up to 512 from an input data file. If fewer than 512 data points are available, the balance required to make up 512 points are filled in with zeros. The application of zeros to the data does

not affect the resulting spectra other than to reduce the available resolution. At the conclusion of this step the two sets of data are ready for the application of Fast Fourier Transforms to obtain the raw spectra for the data. The operation performed by the FFT procedure is given by:

$$F_x(k) = \frac{1}{N} \sum_{n=0}^{N-1} x(n) e^{-j2\pi nk/N} \tag{2.4}$$

where: x(n) is one of the sets of input samples,

N=512 is the number of data points to be transformed,

and $F_x(k)$ is the kth raw spectral estimate on the x input data set.

On completion of the FFT procedure the power, co and quadrature spectra are computed from the relations:

$$\begin{aligned} G_x(k) &= F_x^2 real(k) + F_x^2 imag(k) \\ G_y(k) &= F_y^2 real(k) + F_y^2 imag(k) \\ C_{xy}(k) &= F_x real(k) F_y real(k) + F_x imag(k) F_y imag(k) \\ Q_{xy}(k) &= F_x real(k) F_y imag(k) - F_x imag(k) F_y real(k) \end{aligned} \tag{2.5}$$

Confidence in the spectral estimates is increased by the application of smoothing to each of the above four sets of estimates (Otnes and Enochson, 1972). The simplest procedure to apply is to average every M estimates and assign the centre frequency of each set of averaged values to be the frequency for the set. The value of M to apply to this procedure can be specified. The value to choose is a compromise between the degree of confidence that can be placed in the spectral estimates obtained and the resolution of the resulting spectra. An idea of the order of magnitude of the confidence interval that might be expected can be gained from the following example. A 90% confidence interval in a power spectral estimate for a value of M of 8, on the assumption that the smoothed spectral estimate is a χ^2-variable, is approximately 5.2 db. In other words, there is a 90%

confidence that the power spectral estimate is within -2.2 db and +3.0 db of its real value when 8 successive raw spectral estimates have been averaged. Alternative smoothing schemes, with the same objective, are possible and may have advantages. An alternative scheme, used in chapter 5 is described in appendix B.

A correction factor given by:

$$16T/7NM(N-L-1) \tag{2.6}$$

is applied to all of the spectral estimates. T is the total duration of the sample including added zeros and L is the number of zeros added. This is done in preference to normalisation of the spectral estimates and has the advantages of providing a degree of physical significance to the values obtained for the spectral estimates which are then called power spectral density estimates. A derivation of this factor as well as a more detailed discussion of its usefulness is given in appendix C.

The final processing procedures are to generate the cross spectrum amplitude and phase functions and the coherence function. These functions are defined by the relations:

$$\begin{aligned} G_{xy}(k) &= |F_x(k)F_y^*(k)| \\ &= |C_{xy}(k)-jQ_{xy}(k)| \end{aligned} \tag{2.7}$$

$$\theta_{xy}(k) = \text{Arctan}\frac{Q_{xy}(k)}{C_{xy}(k)} \tag{2.8}$$

$$\begin{aligned} \gamma_{xy}(k) &= \frac{G^2_{xy}(k)}{G_x(k)G_y(k)} \\ &= \frac{C^2_{xy}(k)+Q^2_{xy}(k)}{G_x(k)G_y(k)} \end{aligned} \tag{2.9}$$

The results of the analysis are both printed in tabular form and plotted graphically. The vertical axes on the spectral plots are marked from 0 db to -30 db in 5 db steps. The vertical axis on the phase plot is marked

from +180 degrees to -180 degrees. The horizontal axis on all the plots are marked from zero to 30 cycles per hour in steps of 5 cycles per hour.

2.10 FFT DIGITAL LOW PASS FILTER

The bandwidth available at the receiver i.f. output was appreciably greater than necessary for the purpose of analysis of the data, which resulted in the unnecessary introduction of noise. Some reduction in this bandwidth is achieved by the data compression programme. However, the bandwidth is still greater than required for some purposes. An FFT digital filter programme was written which allows an arbitrary low pass cut off frequency to be specified at the time of use of the programme.

A cut off frequency is specified and applied in the frequency domain to an initially uniform frequency distribution of unit magnitude and zero phase. Allowance is made for the two sided nature of the frequency domain distribution when FFT,s are used. The frequency distribution is then transformed into the time domain to allow truncation of the weighting function to be performed. A suitable cosine weighting function is applied to the truncated weighting function to eliminate any possible discontinuity at the point of truncation. Again allowance is made for the two sided nature of the time domain weighting function. The weighting function is re-normalised to avoid alteration to the total weighting following truncation procedures. Truncation of the time domain weighting function is necessitated by the presence of the Gibb's phenomenon. The Gibb's phenomenon is such that a damped transient appears in the FFT filter output, both preceding and following a discontinuity in the data. It is found that the Gibb's phenomenon can be eliminated if the time domain weighting function is truncated at a time interval equal to half the period of the cut off frequency. This action implies a considerable compromise with the ideal

frequency response characteristic required. The resulting frequency response is, however, still adequate for the purpose intended. The Gibb's phenomenon if present would be intolerable for visual presentation of data plots and for further processing use.

The final frequency response function is obtained by transforming the truncated weighting function back to the frequency domain. North-south and east-west components of the required input data sample are then separately transformed into the frequency domain, complex multiplied point by point with the frequency response function and then finally transformed back to the time domain. A new secondary data file is produced containing the reconstructed filtered data. The input data sample is not required to have exactly the required number of data points. Evenly spaced input data at the required sampling points is obtained by quadratic interpolation from the nearest input data points. No undesirable effects are evident from the use of input data interpolation. The attenuator settings are not altered by the filter programme. The option for changing the heading is provided to allow a simple means of identification for treated data.

The performance of the filter can be seen in figure 7. This figure was generated by replacing the north-south component of the filter output secondary file with the frequency domain response function suitably scaled. Square wave input test data was obtained from the sine-square wave test programme. In the top half of figure 7 the weighting function has been truncated as described and it can be seen that there is no trace of the Gibb's phenomenon on the resulting rounded square wave. In the lower half of figure 7 the weighting function was only lightly truncated resulting in a more rapid cut off to the frequency response. The severe effect of the Gibb's phenomenon can be seen in the rounded square wave form output of this filter.

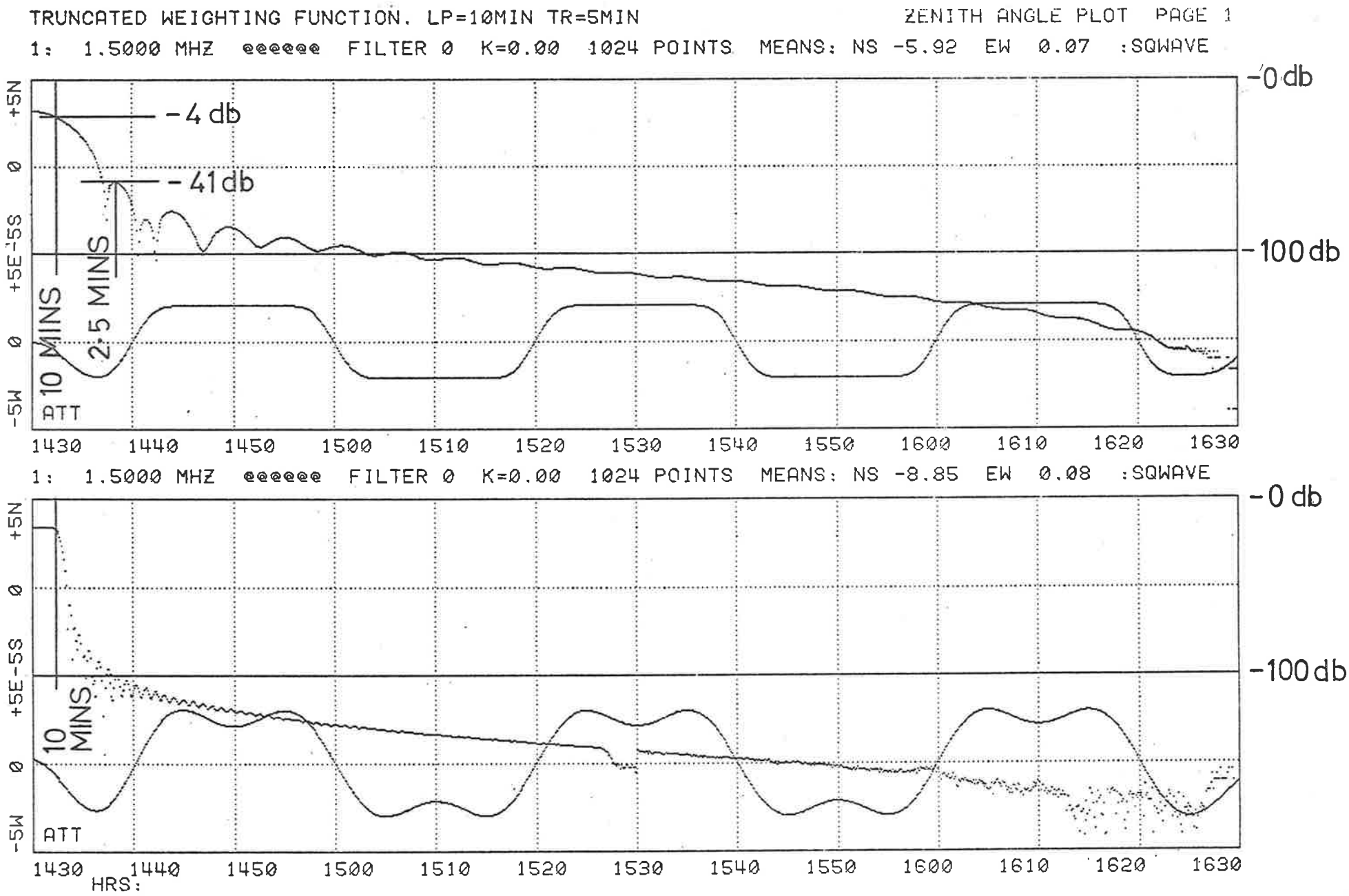

Figure 2.7 Response of the FFT digital filter

2.11 POLAR PLOTTING PROGRAMME

The polar plotting programme will accept up to four secondary data files as input and plot selected portions of these data files in the form of a polar plot. The input data are corrected to true zenith angles prior to plotting.

By reference to figure 8 it can be seen that the zenith angle γ is related to the angles α and β by the direction cosine relationship:

$$\cos^2\alpha + \cos^2\beta + \cos^2\gamma = 1 \tag{2.10}$$

from which:

$$\gamma = \text{Arcsin}\sqrt{\cos^2\alpha + \cos^2\beta} \tag{2.11}$$

If $\alpha' = \frac{\pi}{2} - \alpha$ and $\beta' = \frac{\pi}{2} - \beta$ are the angle components produced by the input data conversion programme, stored in the input data file, then in terms of these angles:

$$\gamma = \text{Arcsin}\sqrt{\sin^2\alpha' + \sin^2\beta'} \tag{2.12}$$

The azimuth angle is calculated from:

$$\phi = \text{Arctan}\ \frac{\cos\beta}{\cos\alpha}$$

$$= \text{Arctan}\ \frac{\sin\beta'}{\sin\alpha'} \tag{2.13}$$

A correction of +180 degrees has to be made to this angle if α' is negative. The corrected zenith angles are then computed from:

$$\alpha'' = \gamma\cos\phi$$

$$\beta'' = \gamma\sin\phi \tag{2.14}$$

The above formulae for ϕ and γ convert the data to azimuth and true zenith angle respectively.

A polar plot is one form of time series plot of these quantities. Time series plots of azimuth and true zenith angle against a linear time axis were not provided, for data processing purposes. These would have

been useful if oblique signals had been included for study.

The polar plotting programme provides markers at five minute intervals for each trace on the plot. These markers are the same decimal digit used to identify data lines in the original data. For all of the data presented these markers represent the signal frequency that produced the trace according to a fixed arrangement of the digits. The start and finish of each trace is also marked with the time in hours-minutes format.

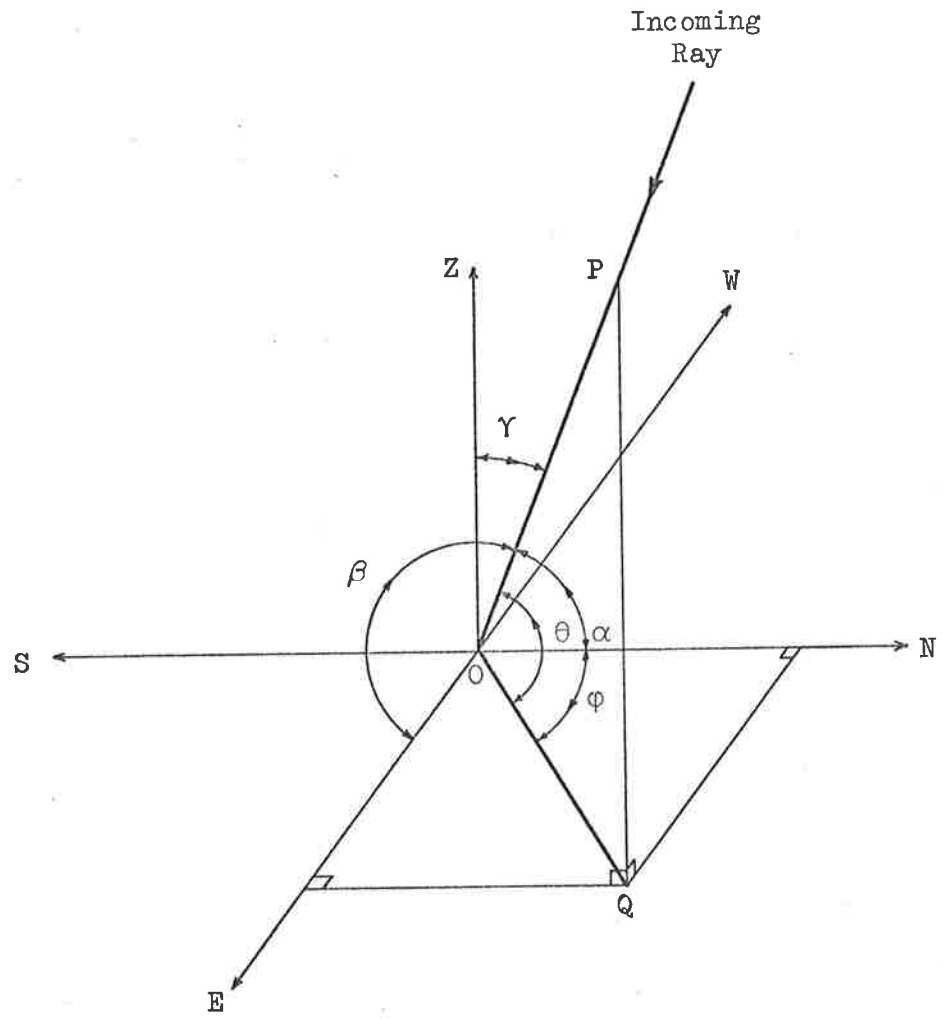

FIGURE 2.8 Diagram defining the component angles for computation of zenith angles

2.12 REAL HEIGHT ANALYSIS

Vertical incidence ionograms were taken at the Salisbury ionosonde station during many of the data runs. Ionograms at fifteen minute intervals were scaled and applied to an electron-density profile analysis programme for selected periods of data. The profile analysis programme provides both electron densities and true reflection heights for scaled frequencies for the ordinary ray component from the vertical incidence ionograms. The electron density profile analysis programme in use, is that of Doupnik (1963). An authoritative comparative study of profile analysis methods is given by McNamara (1978). An earlier review of this subject is that of Thomas (1959). Useful information is also contained in the URSI handbook (Piggott and Rawer, 1972).

The quantities that are required to be derived from the profile analysis data are the scale height H at the peak of the layer and the real heights of reflection at the frequencies of the signals used for the experiment. The calculation of the scale height H is done by use of the parabolic layer approximation from the Chapman layer theory. An expression for a parabolic layer approximation for the F_2 layer peak from which the scale height can be calculated is derived in appendix D:

$$N = N_m \left\{ 1-\tfrac{1}{2}\left| \frac{h-h_m}{H} \right|^2 \right\} \qquad (2.15)$$

where:

N_m is the electron density at the peak of the layer,

h_m is the height of the peak of the layer,

H is the scale height at the peak of the layer,

and N is the electron density (in electrons/cc) at the true height h (in km).

These quantities can be seen in figure 9a. It is found that a parabola is a good fit to the true height electron density data at the layer peak. A parabola of the form:

$$N = a_0 + a_1 h + a_2 h^2 \tag{2.16}$$

is fitted to the data in the vicinity of the layer peak using the numerical method of least squares. By equating coefficients in (15) and (16) the scale height for the layer can be found from:

$$H = \frac{1}{2a_2}\sqrt{\tfrac{1}{2}a_1^2 - 2a_0 a_2} \tag{2.17}$$

Although not required for further analysis, the maximum electron density of the layer, and the height at which it occurs can be found from:

$$N_m = -2H^2 a_2$$
$$h_m = -a_1/2a_2 \tag{2.18}$$

In fitting the parabola (16) to the data, at least three values of N,h are required. In practice four or five values could be used which allowed an estimate of the goodness of fit of the data to be made. A typical case is plotted in figure 9b.

To obtain the reflection height for the ordinary ray component at a specified frequency below the critical frequency, use is made of the relationship between electron density and plasma frequency:

$$N = 1.24 \times 10^4 f^2 \tag{2.19}$$

where f is in Mhz. Expression (19) is substituted into (16) which is then solved for h.

To obtain the reflection height for the extraordinary ray component at the specified frequency use is made of the relation between the ordinary and extraordinary ray:

$$f_x^2 - f_x f_B \simeq f_o^2 \tag{2.20}$$

where $f_B = 2.8B = 1.68$(Mhz) is the gyrofrequency of electrons in a magnetic

field of strength B (gauss) (appropriate to Salisbury) and f_o is as given in (19). After substitution of (20) into (19) an expression is obtained for N:

$$N = 1.24 \times 10^4 (f^2 - ff_B) \qquad (2.21)$$

from which the reflection height for the X-ray can be found by the same procedure as for the O-ray.

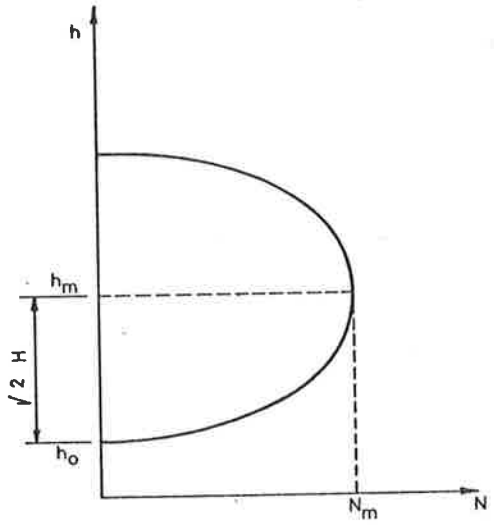

(a)

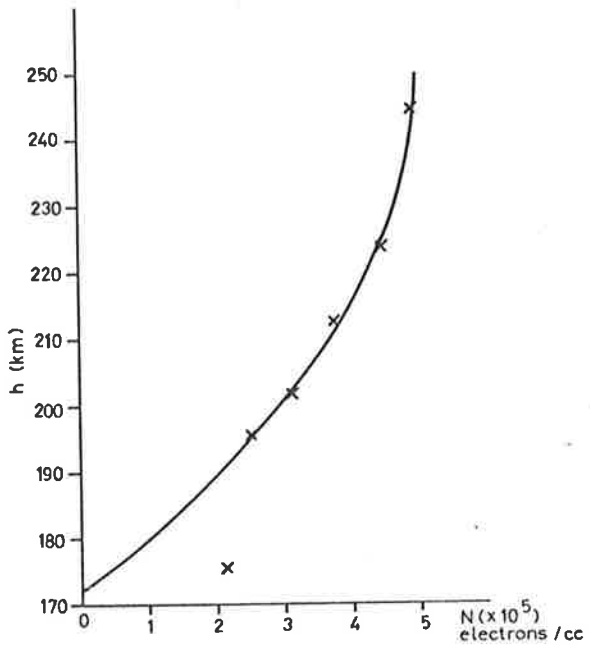

(b)

FIGURE 2.9 (a) Parabolic layer approximation
(b) A typical plot (Ionogram for 1500 20/12/75)

CHAPTER 3

EXPERIMENTAL RESULTS

3.1 INTRODUCTION TO THE EXPERIMENTAL DATA

In spite of the short duration of the experimental programme, more data was collected than it has been possible to analyse completely, with the methods described in this thesis. This chapter presents a selection of zenith angle plots as well as a few other plots of the data obtained from the experimental program. A complete list of the data obtained is given in appendix E. Only some of this data is included in this chapter. To avoid unneccessary repetition, plots of much of the data have been omitted entirely. Some data is displayed in chapter 5, where it is used to illustrate the gravity wave method of analysis. General features of the data are described in the following section and illustrated with the selected plots.

3.2 DESCRIPTIONS OF DATA PLOTS

Data taken on 7/12/75 provided an opportunity to compare direction of arrival data and effective height (h't) data. Zenith angle data for the single frequency of 5.38 Mhz is plotted in figure 1 according to the procedure outlined in section 2.7. A three station plot of effective height measured with a frequency close to 6 Mhz and with reflection points in the same general locality, kindly supplied by Ahmed (1977), is shown in figure 2. It can be seen that the two plots show little obvious correlation. The geometrical analysis of chapter 4 indicates that this is to be expected. The direction of arrival method is sensitive to small amplitude wave motions and less sensitive to large amplitude movements of the ionospheric medium as a whole. The h't record in figure 2 shows

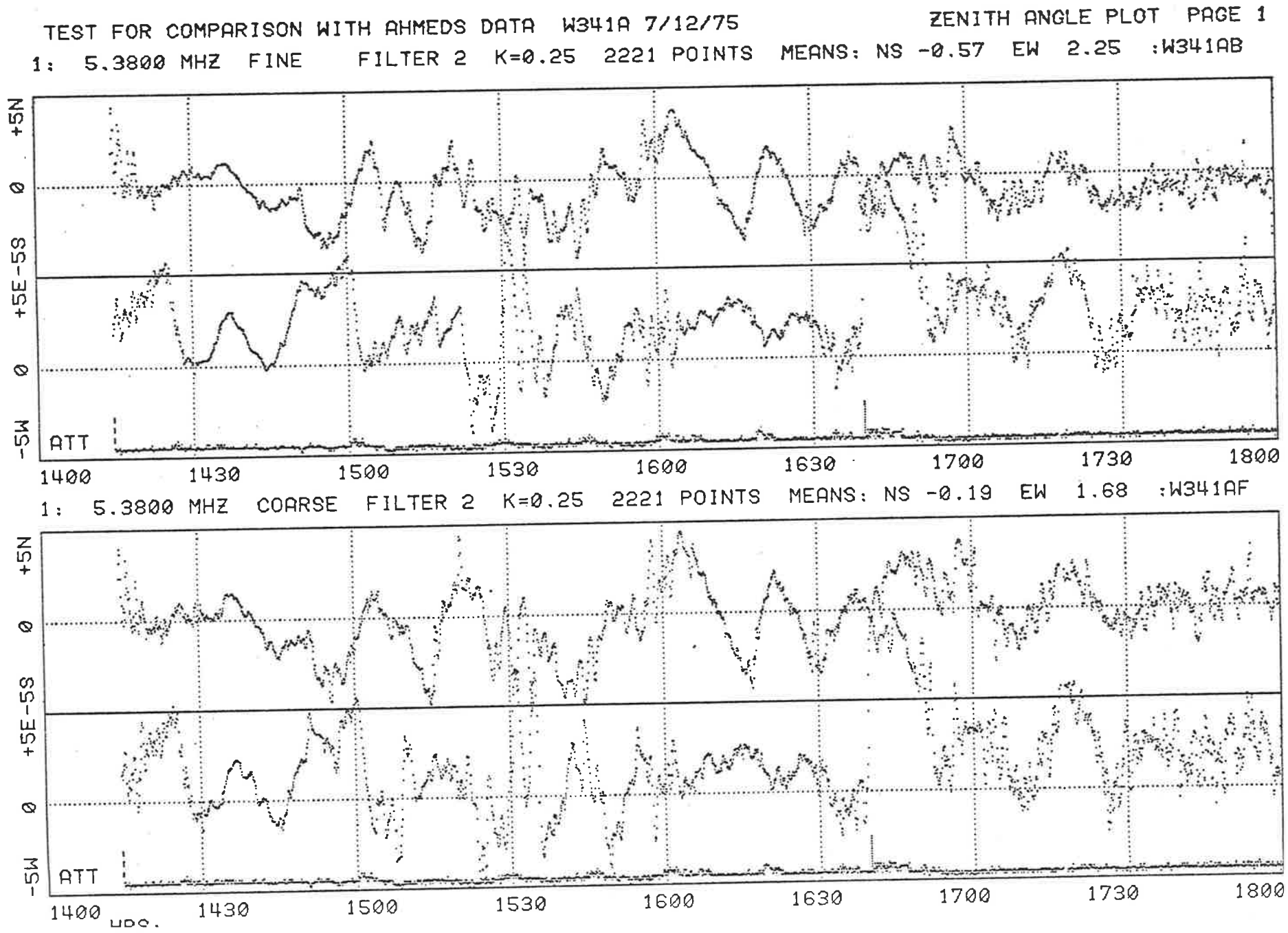

Figure 3.1 Zenith angle plot: For comparison with (h't) data

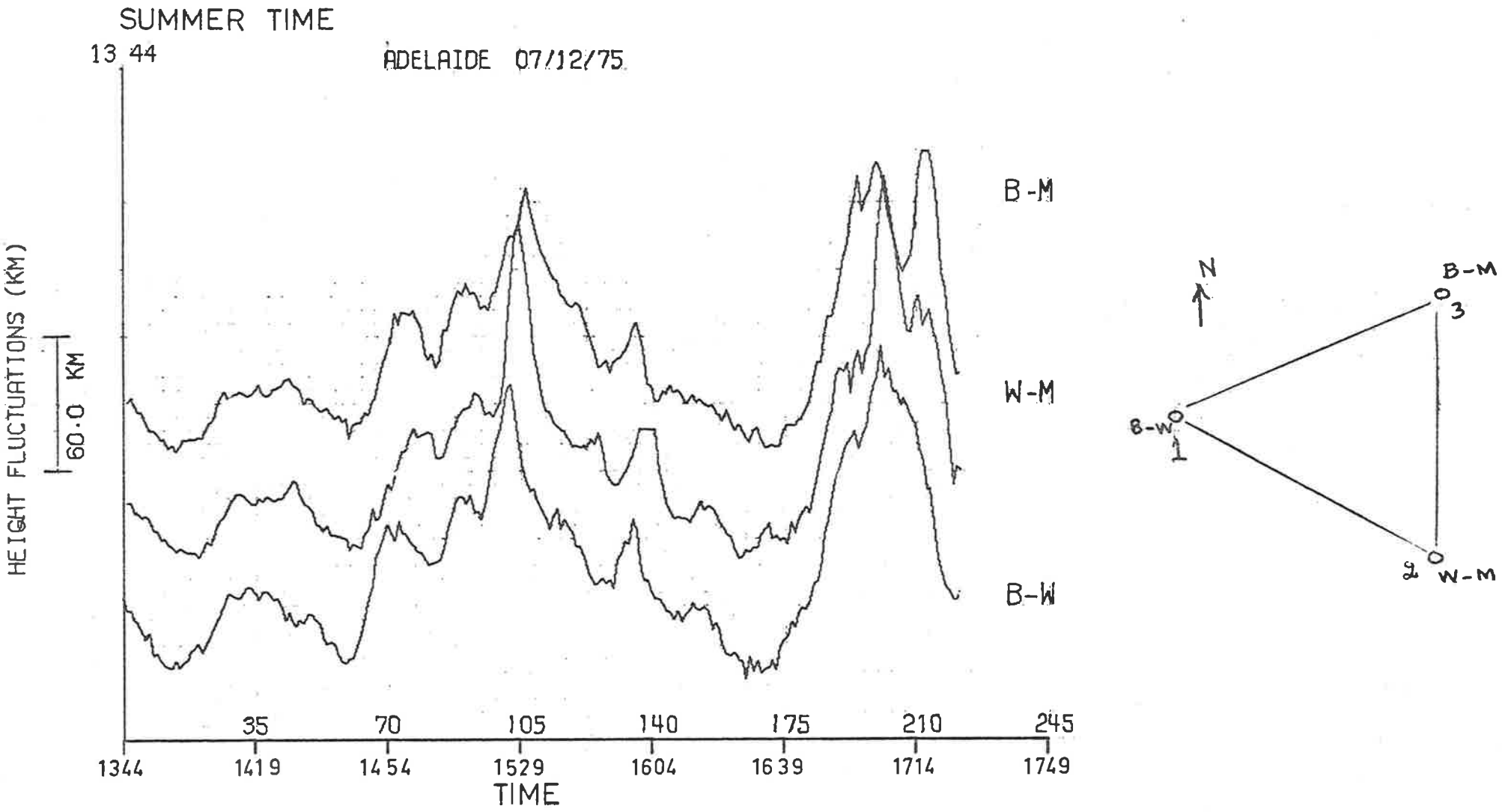

Figure 3.2 Three station (h't) record

movements in the effective height of the reflection point of over 100 km. Atmospheric wave motions can be expected to exist over the whole of the real depth in the ionosphere represented by these effective height variations.

A large shift in the direction of arrival of the signal towards the east can be seen in figure 1 at approximately 1640 hours when the extraordinary ray component was switched into use. This event provides an illustration of the effect of magnetoionic splitting, on the direction of arrival of the ionospheric components of the signal. Figure 1 also provides an illustration of the close correlation that exists in this case between the directions measured by the fine spacing (73.15 m) antennas and the directions measured by the coarse spacing (18.29 m) antennas. This result indicates that no ambiguity correction is required for the frequency in use and for the near vertical direction of arrival of the signals. This result also implies that reasonably plane waves were being received. Ambiguity correction becomes necessary for oblique signals at a frequency with a wavelength equal to twice the fine antenna spacing multiplied by the sine of the angle of incidence of the received signal, i.e. at a frequency of 2.05 Mhz for a signal at grazing incidence. Both the fine and coarse signals should be smoothed, as is done in figure 1, prior to the necessity of ambiguity correction being considered.

Compounded zenith angle data for day 346 is shown in figure 3. The early morning data is characterised by the effects of interference, particularly on the higher frequencies. Of particular interest is the period of sporadic E (E_S) reflection that occured between 1200 and 1400 hours. Since the transmitting station is located to the east of the receiving station reflection from the E layer results in zenith angles with a greater bias to the east than for F layer reflection. Filtered data for

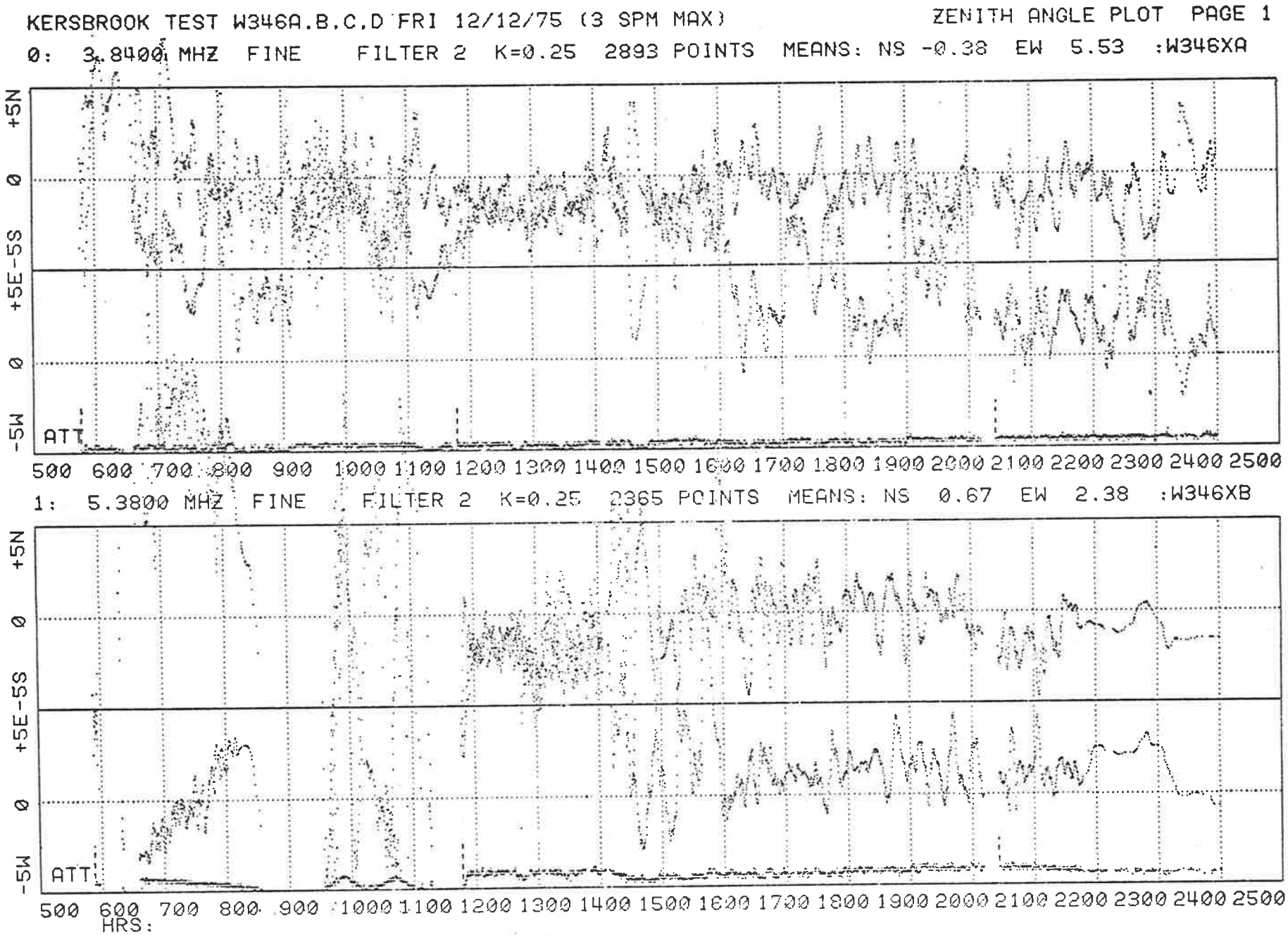

Figure 3.3 Compounded zenith angle data for day 346
(a) 3.84 and 5.38 Mhz plots

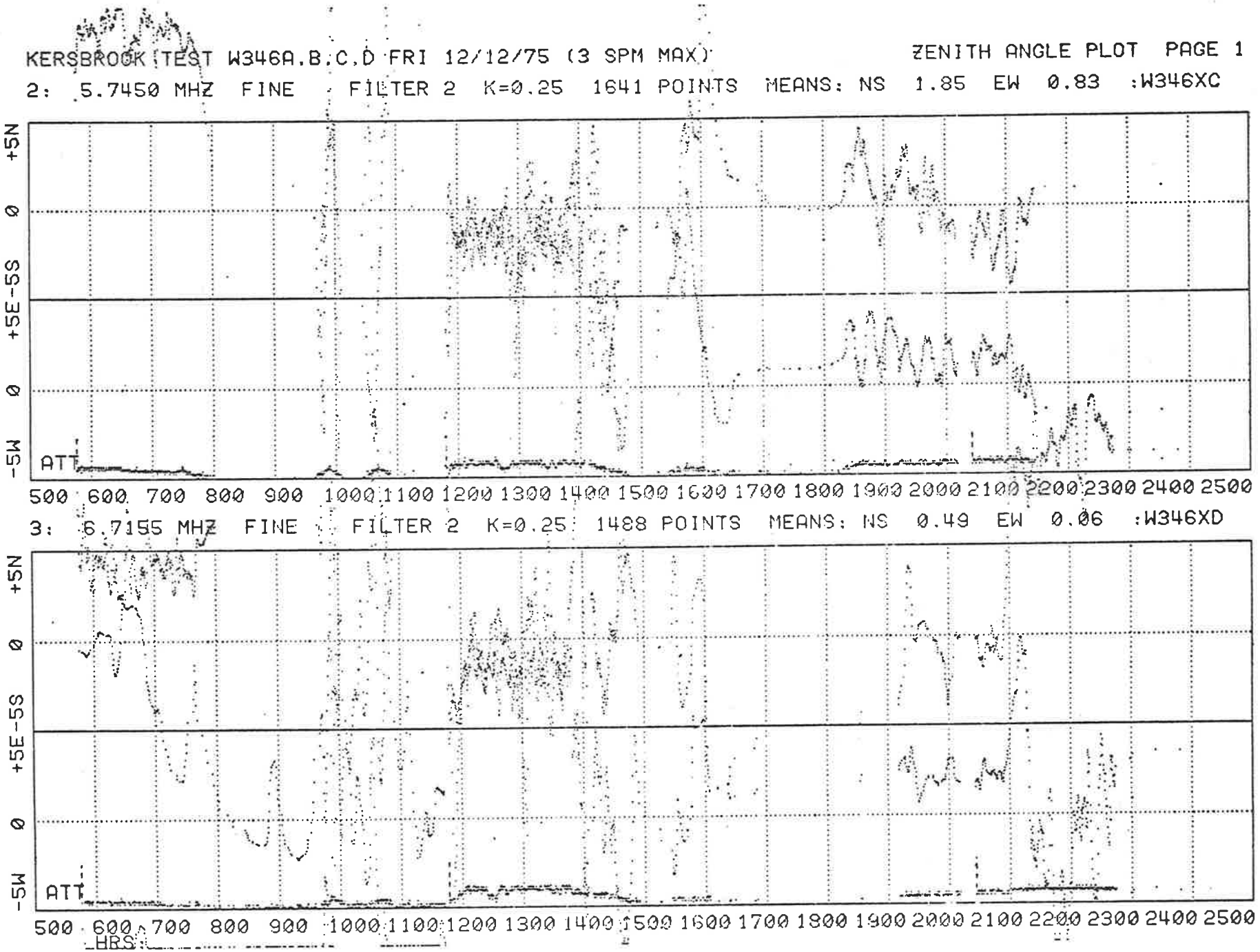

Figure 3.3 Compounded zenith angle data for day 346
(b) 5.745 and 6.7155 Mhz plots

the period 1200 to 1400 hours is shown in figure 4 and a series of ionograms covering this period is shown in figure 5(a). The correlation with E_S is evident from these figures.

The two higher frequency plots in figure 4 display a brief transition to F mode reflection. This occurs at approximately 1255 hours on the 5.745 Mhz signal and at approximately 1300 hours on the 6.7155 Mhz signal. Reflection at the higher frequencies is noticably rougher than for the lower frequency signals. A number of remarkable sinusoidal events can be seen in the 6.7155 Mhz trace, such as the one occurring at 1230 hours. Polar plots for the period 1240 to 1320 hours are shown in figure 6. Spectra made for the period of the E_S occurrence tend to lack dynamic range. Spectra for the 5.745 Mhz and 6.7155 Mhz signals for the period 1210 to 1343 hours are shown in figure 7. Besides the peak in these spectra at low frequencies, two additional slight peaks can be seen at periods of 4.3 minutes and 2.3 minutes for the 6.7155 Mhz signal and at periods of 6.6 minutes and 2.4 minutes for the 5.745 Mhz signal, for the north-south components. For the east-west components, peaks in the spectra can be seen at 6.6 minutes and 3.2 minutes for the 6.7155 Mhz signal and at 6.0 minutes and 3.5 minutes for the 5.745 Mhz signal. Further samples of this type of data would be necessary for firm conclusions to be drawn from these results, but it is possible that the periodicities noted represent phase path effects following passage through the E layer.

Figure 8 has been chosen to display the variation in measured zenith angles that can occur between four received signals. At the lowest frequency of 3.84 Mhz E layer reflection predominates over the whole sample except for a brief period when the O ray was selected. At the next higher frequency of 5.38 Mhz switching between E layer and F layer reflection can be seen. The next higher frequency of 5.745 Mhz displays predominantly F

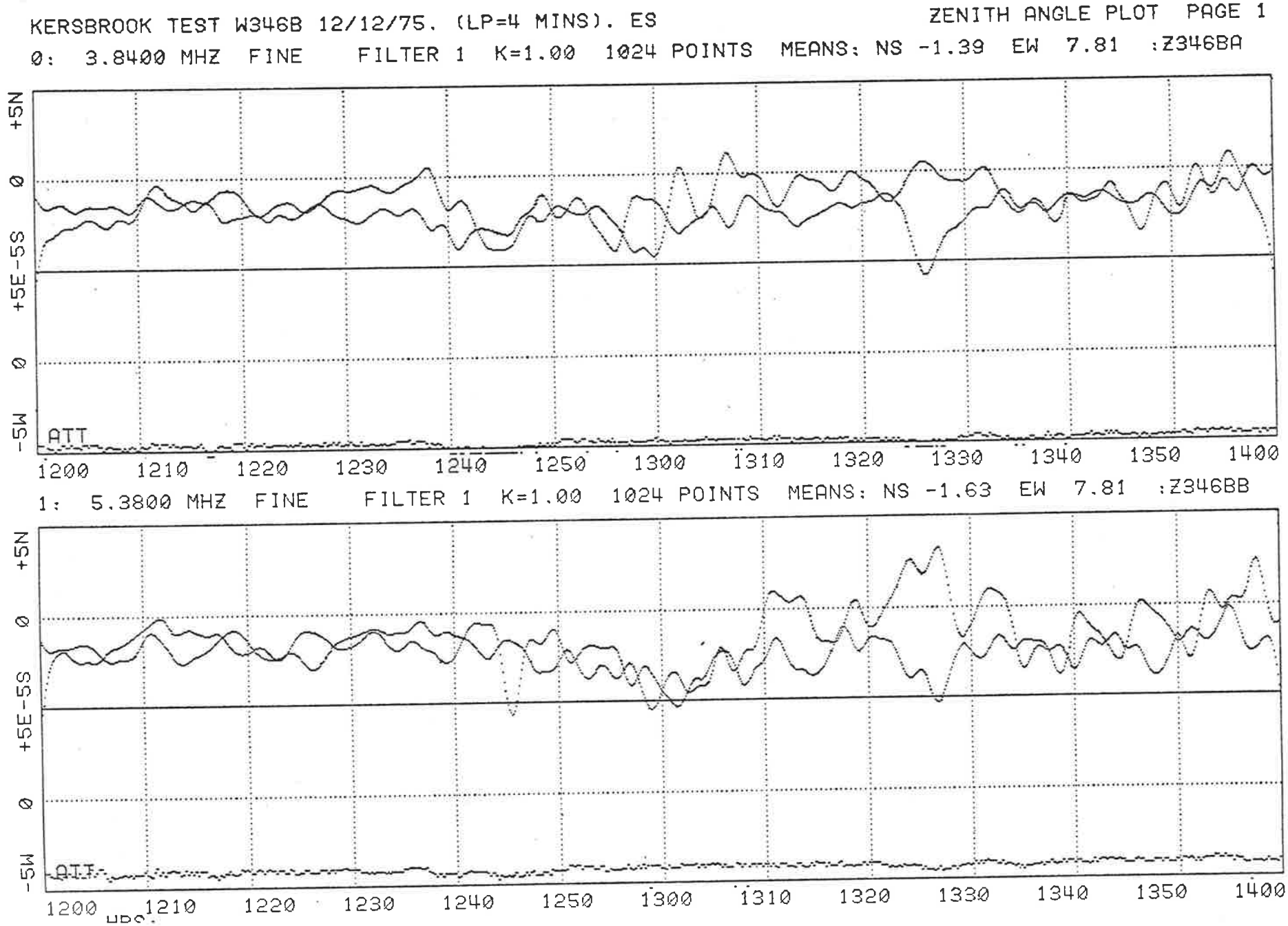

Figure 3.4 Low pass filtered data for period 1200 to 1400 hours on day 346 showing reflection from sporadic E layer (a) 3.48 and 5.38 Mhz plots.

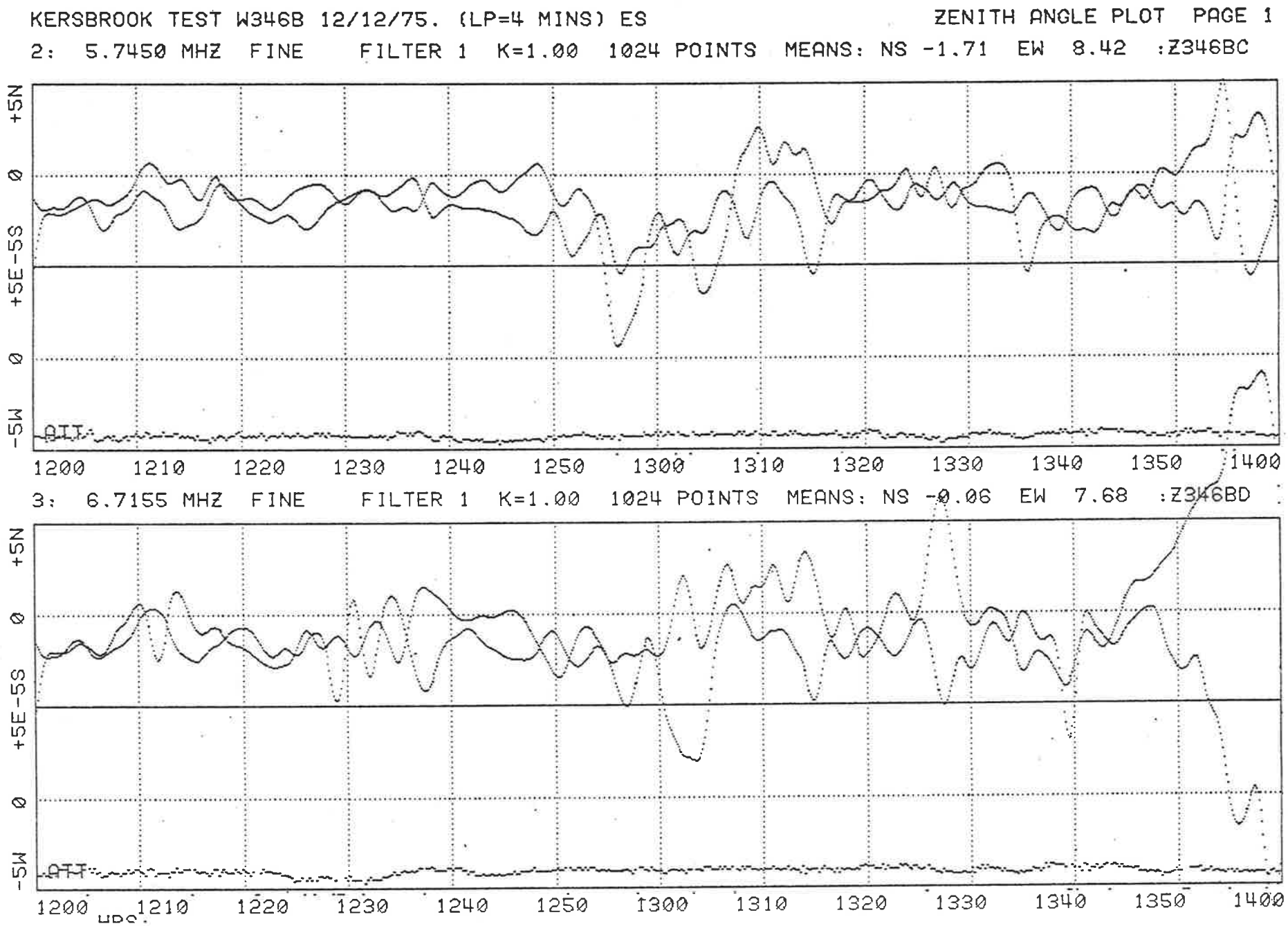

Figure 3.4 Low pass filtered data for period 1200 to 1400 hours on day 346 showing reflection from sporadic E layer (b) 5.745 and 6.7155 Mhz plots

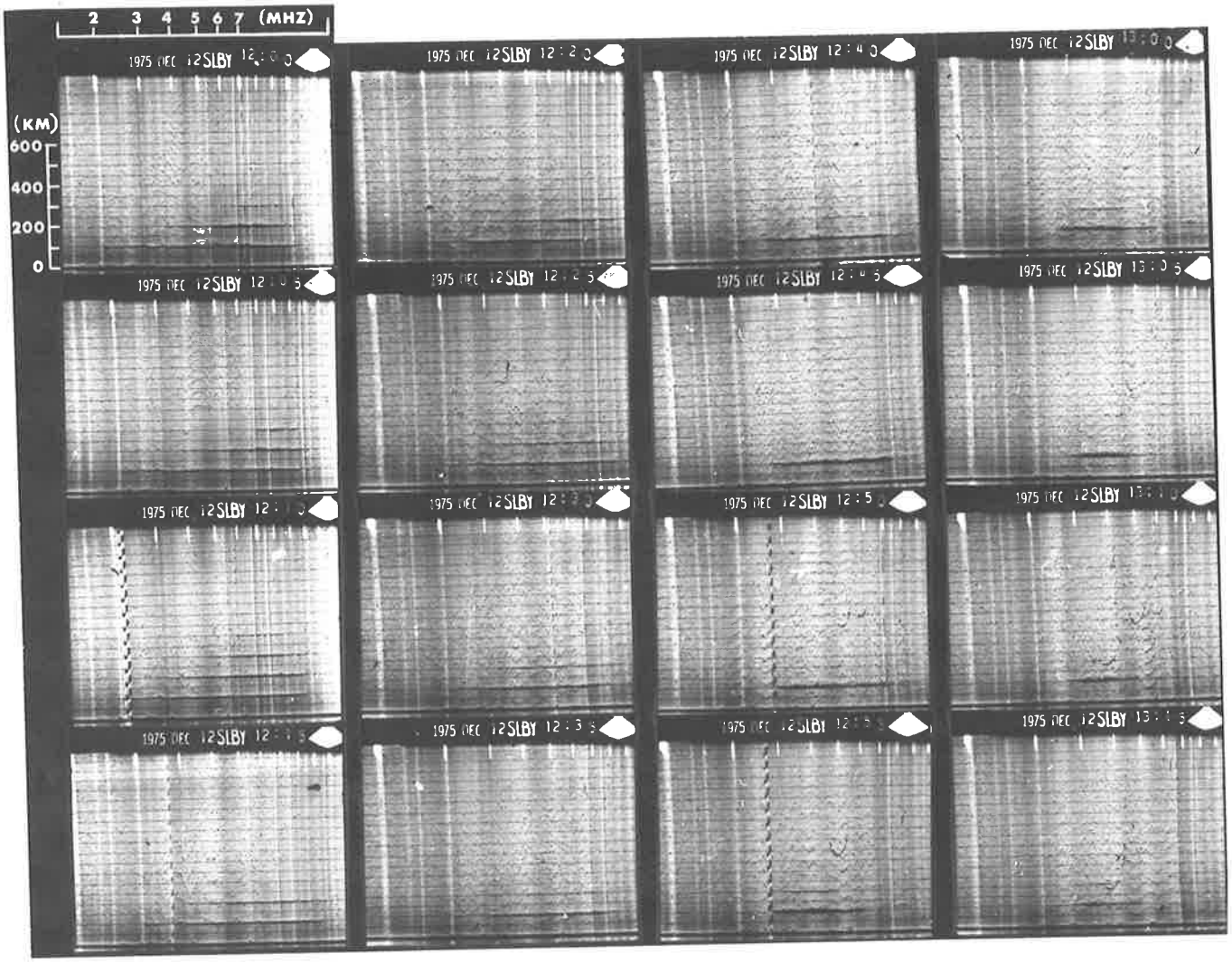

Figure 3.5 (a) Series of ionograms for the period 1200 to 1315 hours on day 346 showing blanketing sporadic E traces

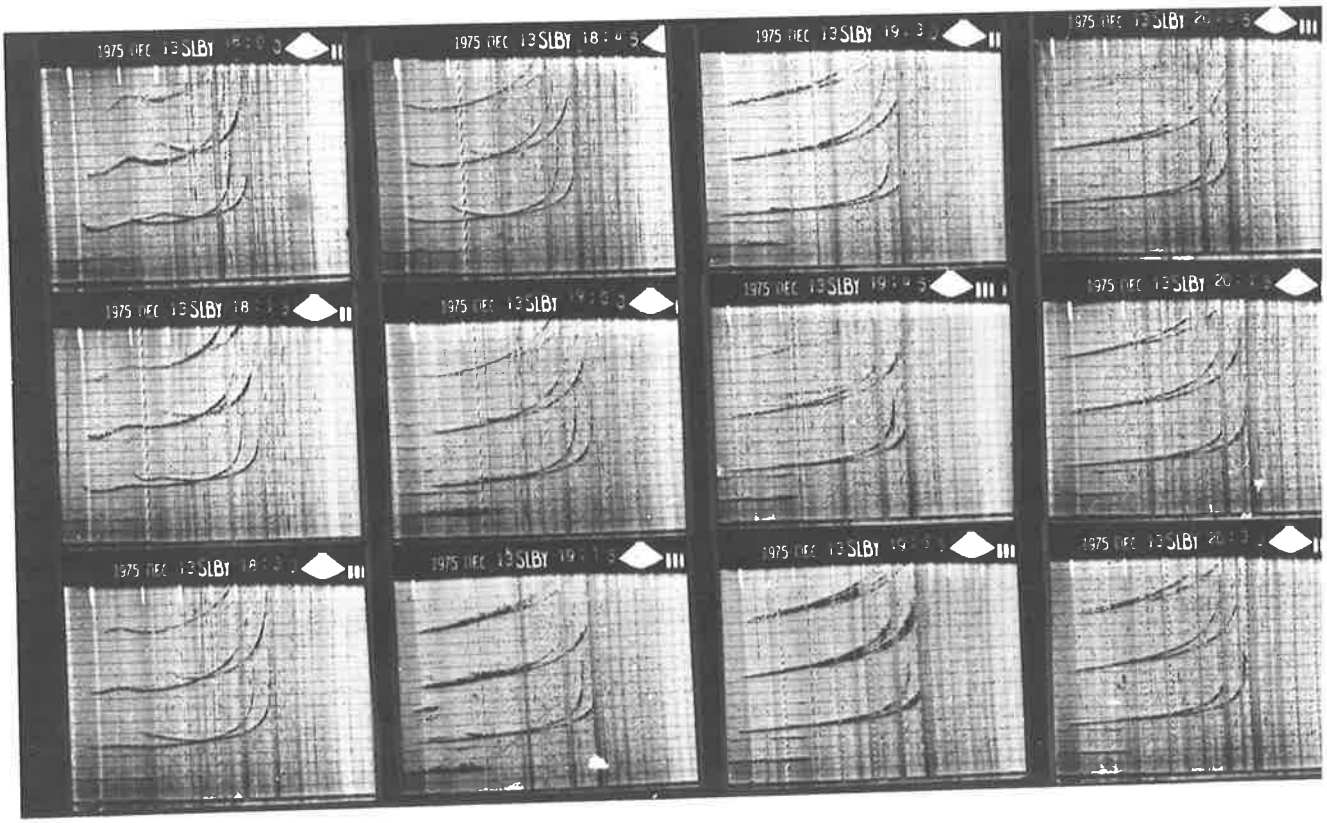

Figure 3.5 (b) Series of ionograms during the period 1800 to 2030 hours on day 347

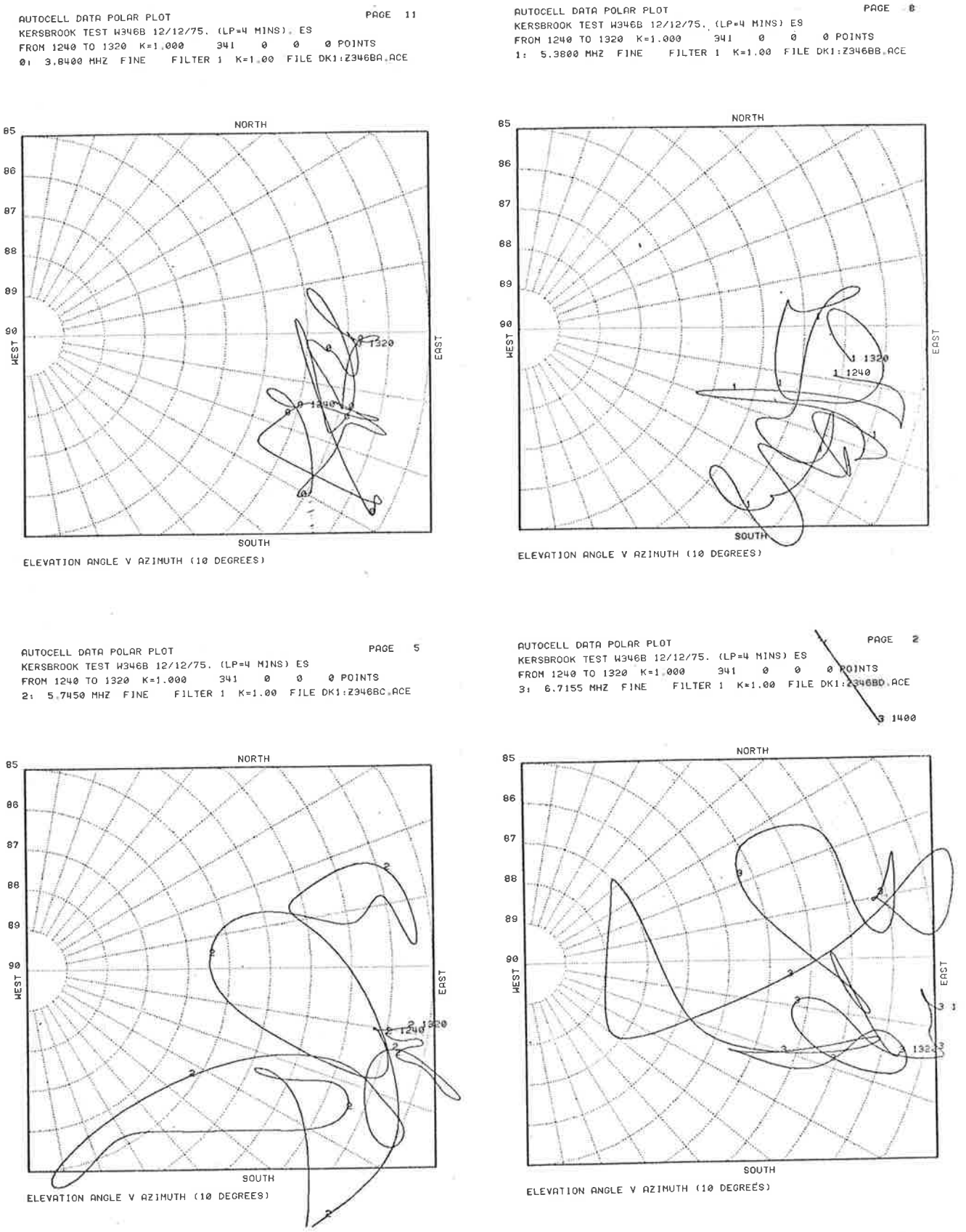

Figure 3.6 Polar plots of filtered zenith angle data for the period 1240 to 1320 hours.
(3.84, 5.38, 5.745, 6.7155 Mhz frequencies)

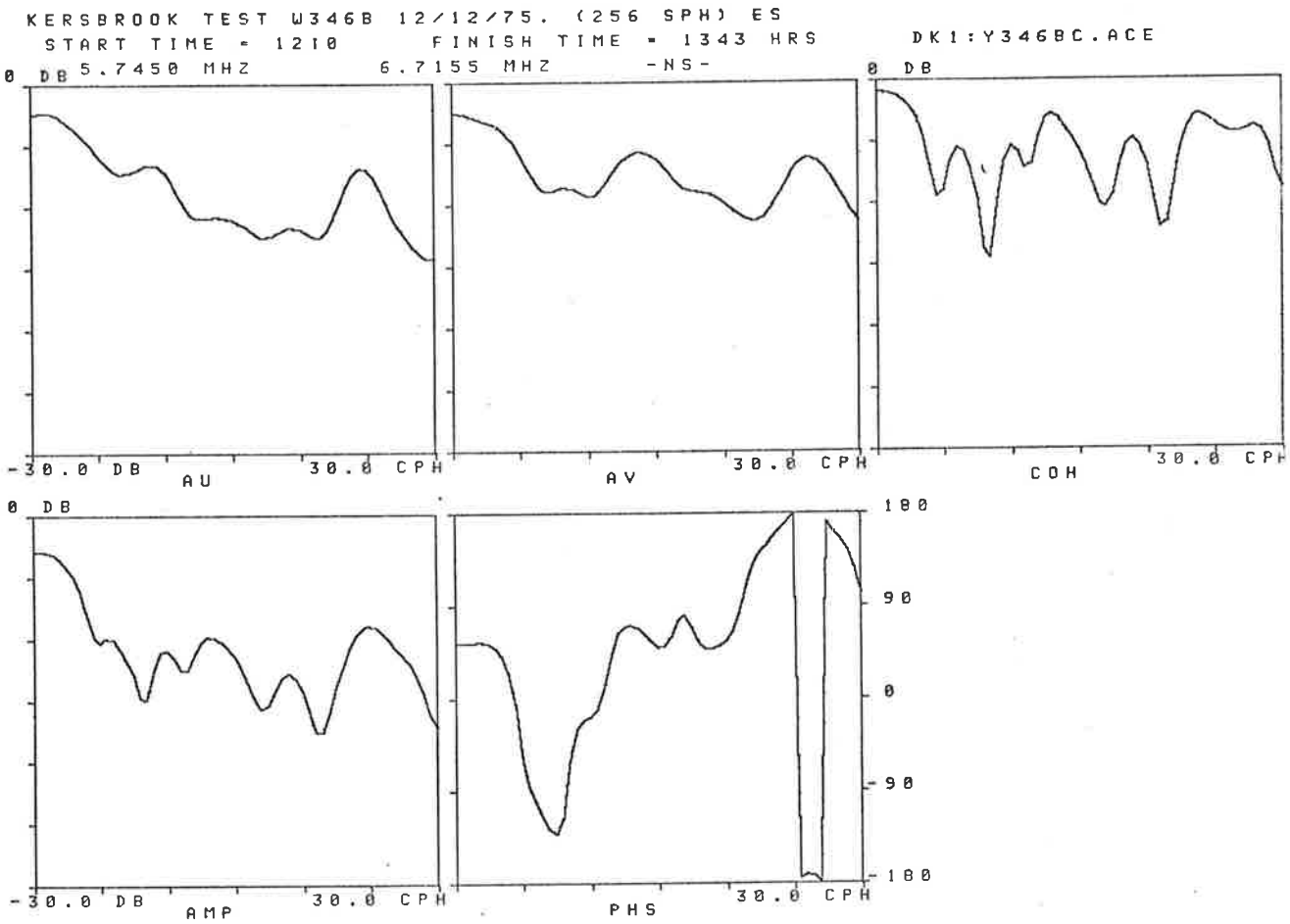

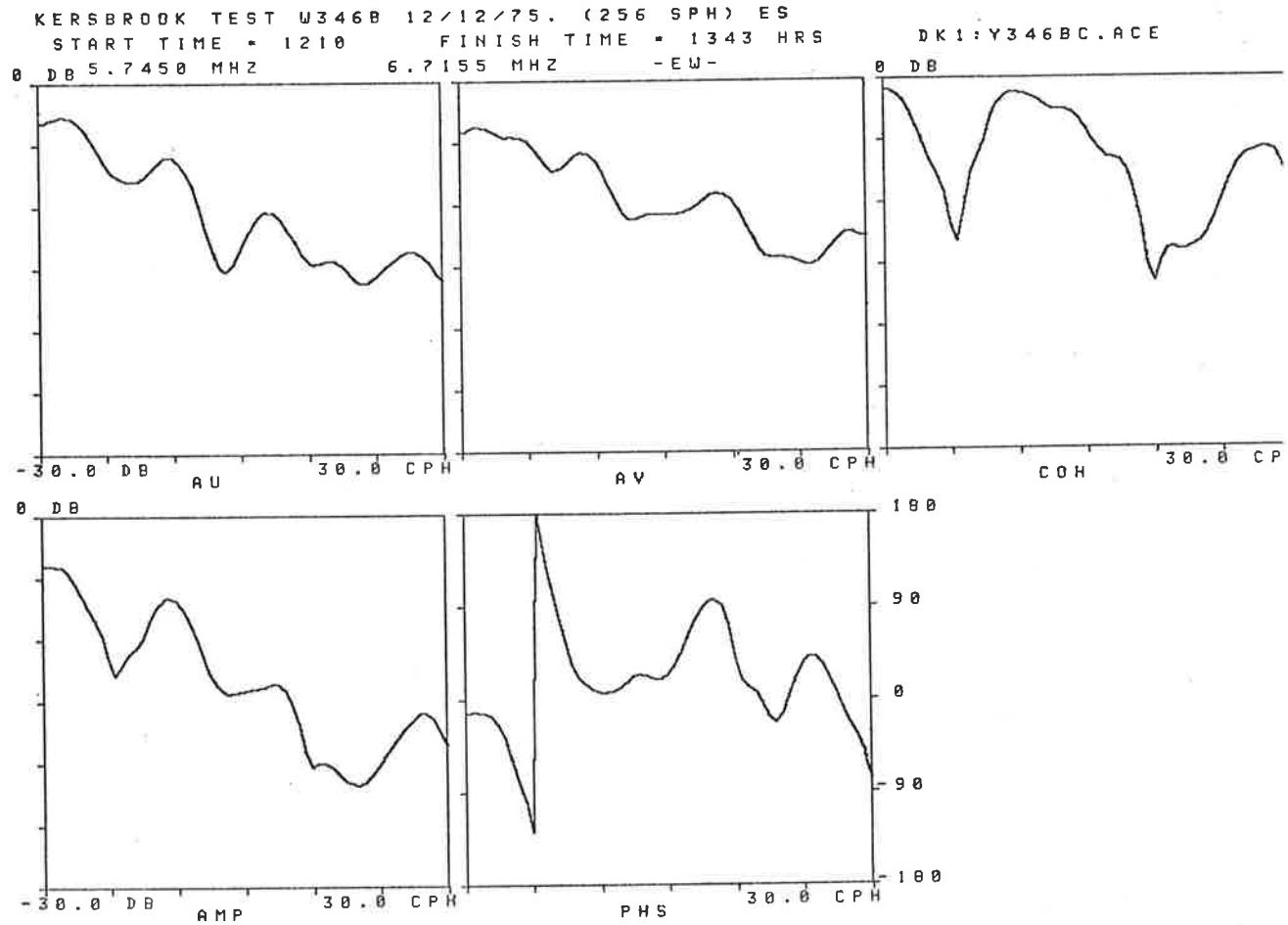

Figure 3.7 Spectra from sporadic E data

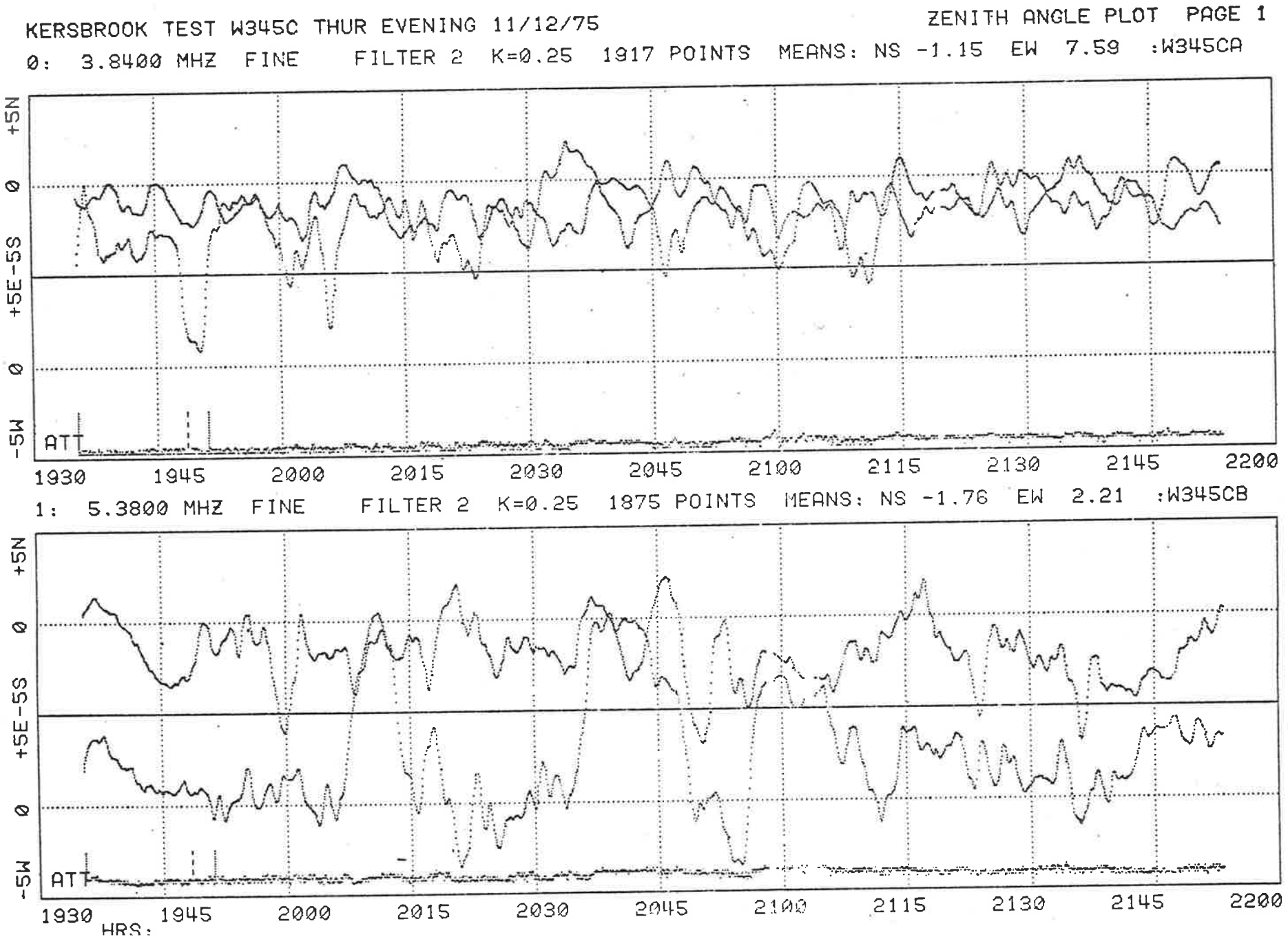

Figure 3.8 Zenith angle data plots from 1930 to 2200 hours on 11/12/75.
(a) 3.84 and 5.38 Mhz frequencies

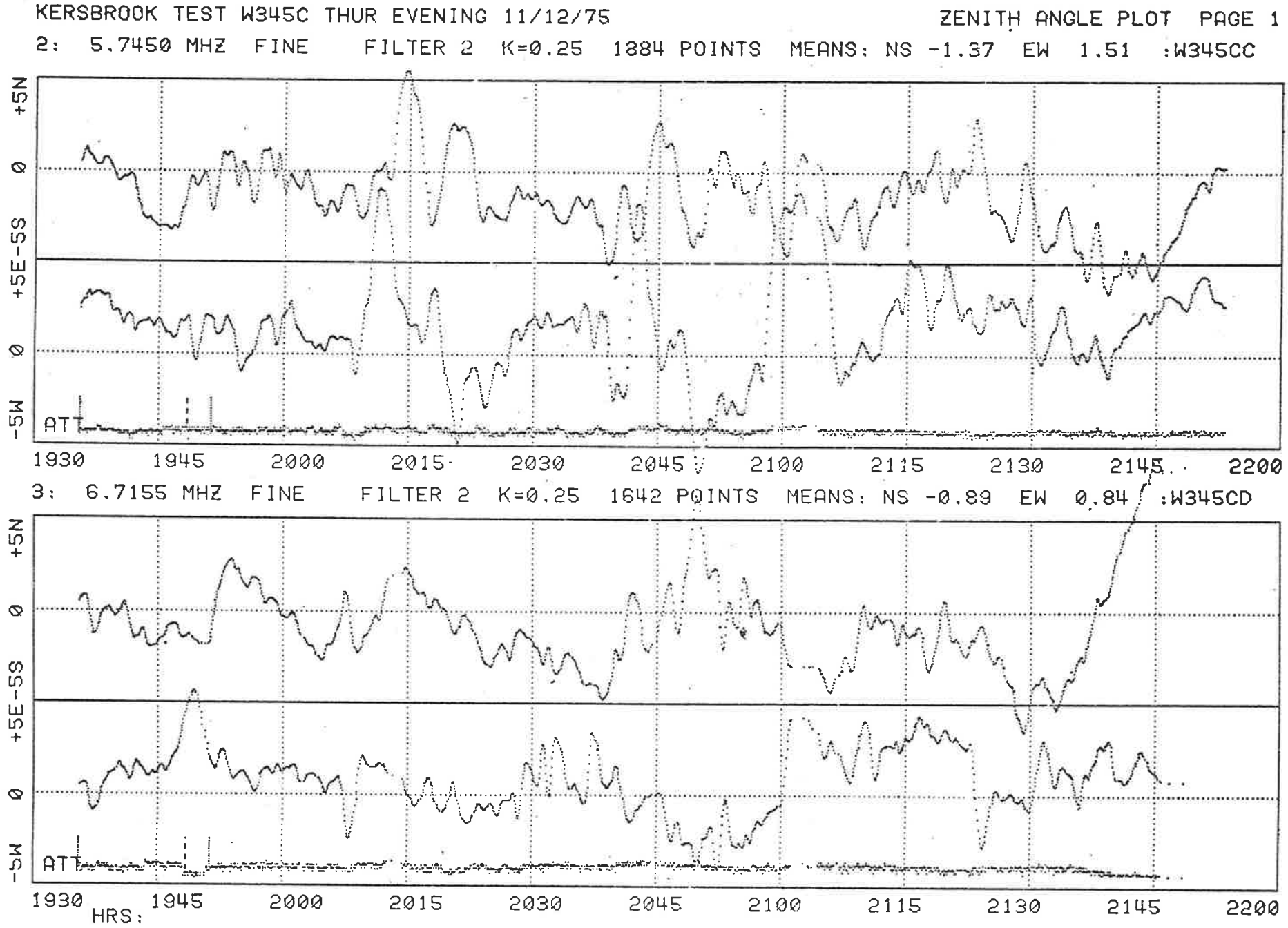

Figure 3.8 Zenith angle data plots from 1930 to 2200 hours on 11/12/75. (b) 5.745 and 6.7155 Mhz frequencies

layer reflection with occasional switching to E layer reflection. The highest frequency of 6.7155 Mhz consists entirely of F region reflection with very little correlation with the 5.745 Mhz signal evident. For this sample of data poor correlation would be found between any pair of signal frequencies.

In figure 9, on the other hand, a definite correlation can be seen between the three higher frequency signals. To a lesser extent there is some correlation between the 3.84 Mhz and 5.38 Mhz signals. Spectra for adjacent pairs of signal frequencies for the data of figure 9 is shown in figure 10. The phase shifts in the gravity wave region of the spectra (i.e. in the region of high coherence at low frequencies) for the 5.38 Mhz and 5.745 Mhz signals are very small, suggesting that these signals are reflected from very nearly the same effective height. This can occur when reflection for these frequencies takes place near the minimum virtual height ($h'F_2$) of the F_2 layer. The selection of ionograms in figure 5(b) shows that this is the case. During the course of the record the F_1 cusp can be seen to flatten out until the ionogram assumes its characteristic evening appearance. The correlation between these signals and the lower and higher frequency signals, is also accounted for, since the effective height of reflection for all four signals is similar.

A sample of early morning zenith angle data is shown in figure 11. A definite change in the character of the data can be seen at sunrise. For the most part the interpretation of night time and early morning data tends to be less certain due to the occasional use of some frequencies for voice communication purposes by other users of these frequencies.

A sample of unfiltered zenith angle data is shown in figure 12. The quantisation in the data points can be seen. Figure 13 displays the same data after filtering with the exponential filter described in appendix A.

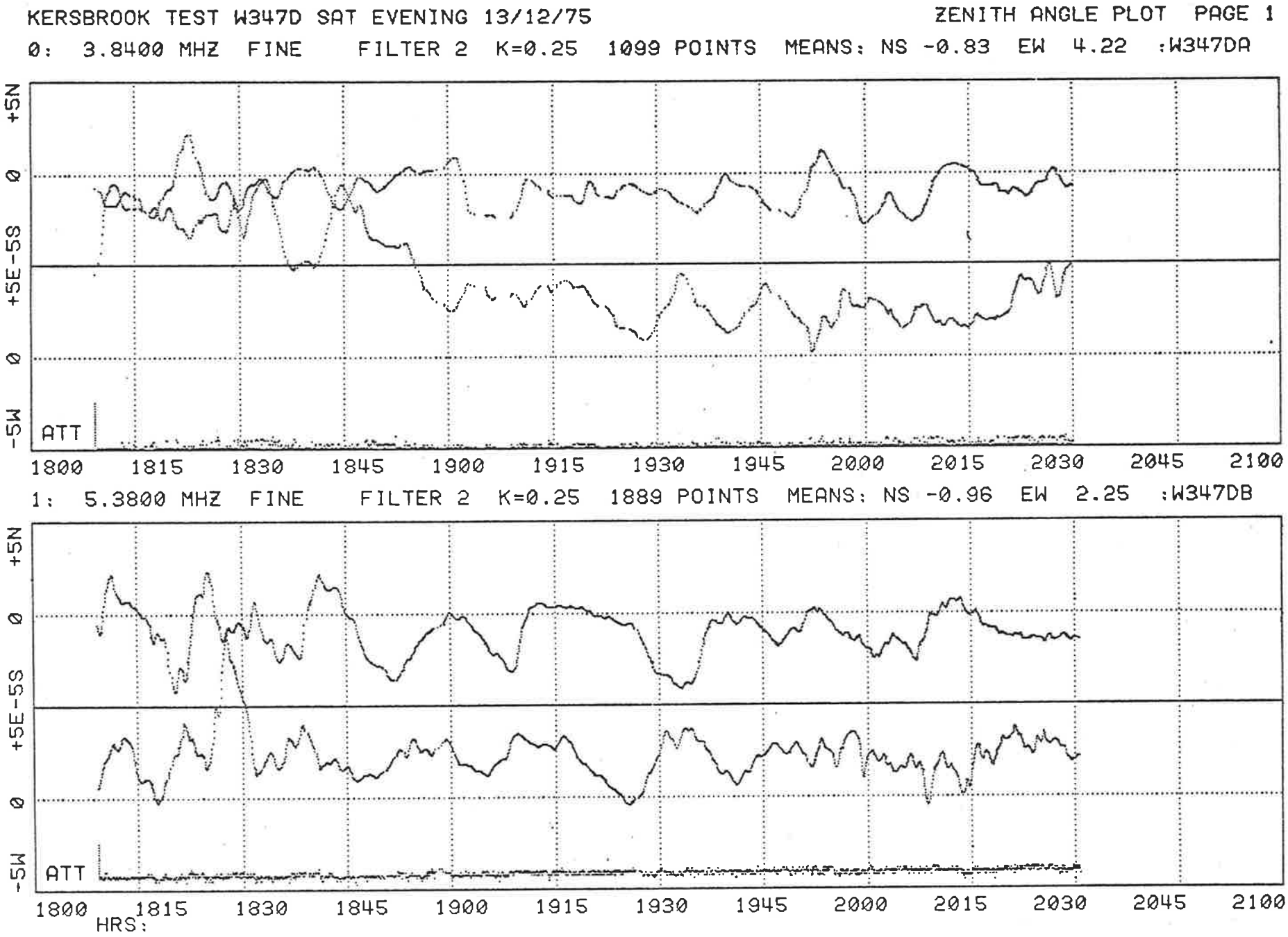

Figure 3.9 Zenith angle data plots from 1800 to 2030 hours on 13/12/75.
(a) 3.84 and 5.38 Mhz frequencies

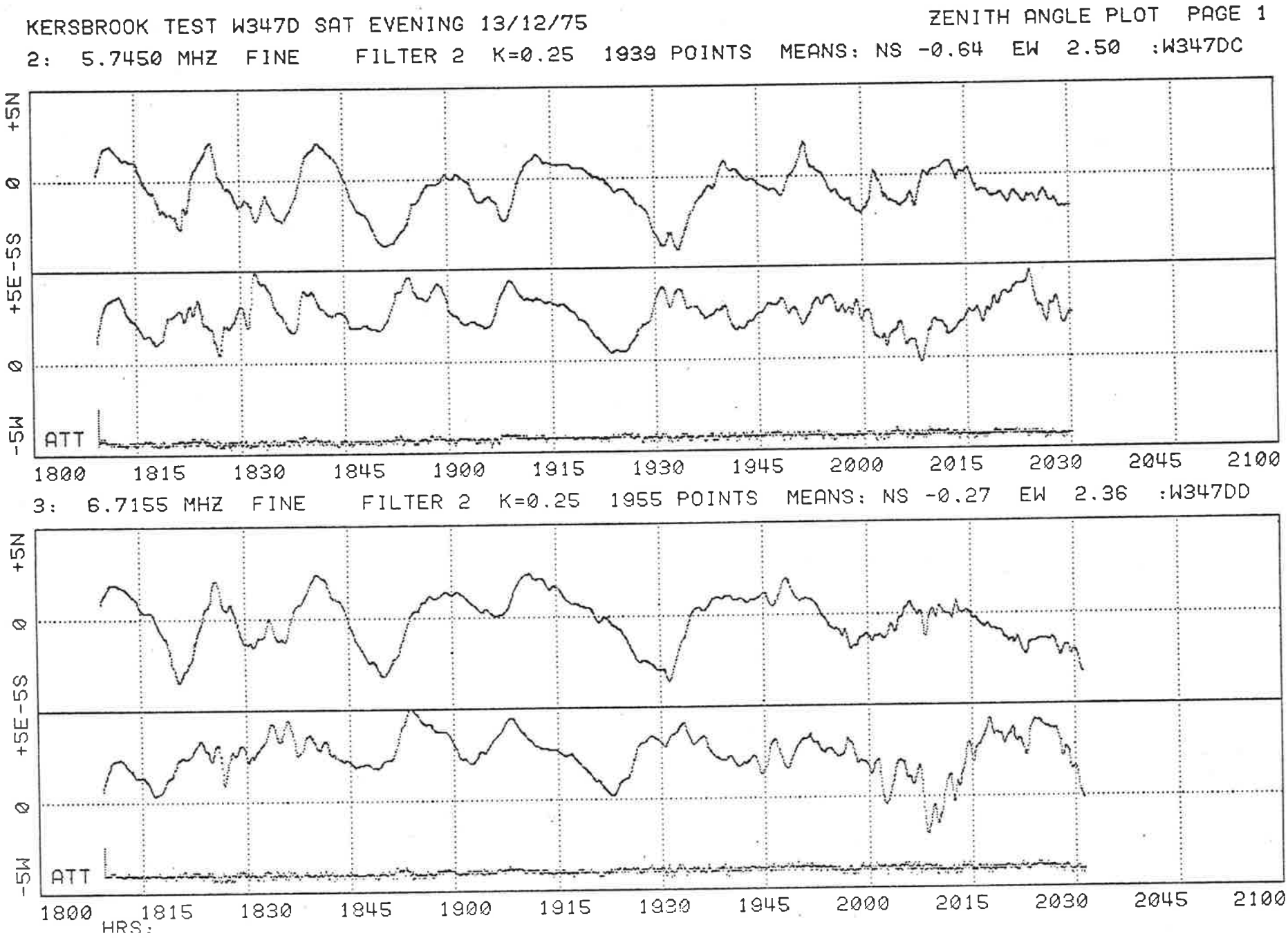

Figure 3.9 Zenith angle data plots from 1800 to 2030 hours on 13/12/75.
(b) 5.745 and 6.7155 Mhz frequencies

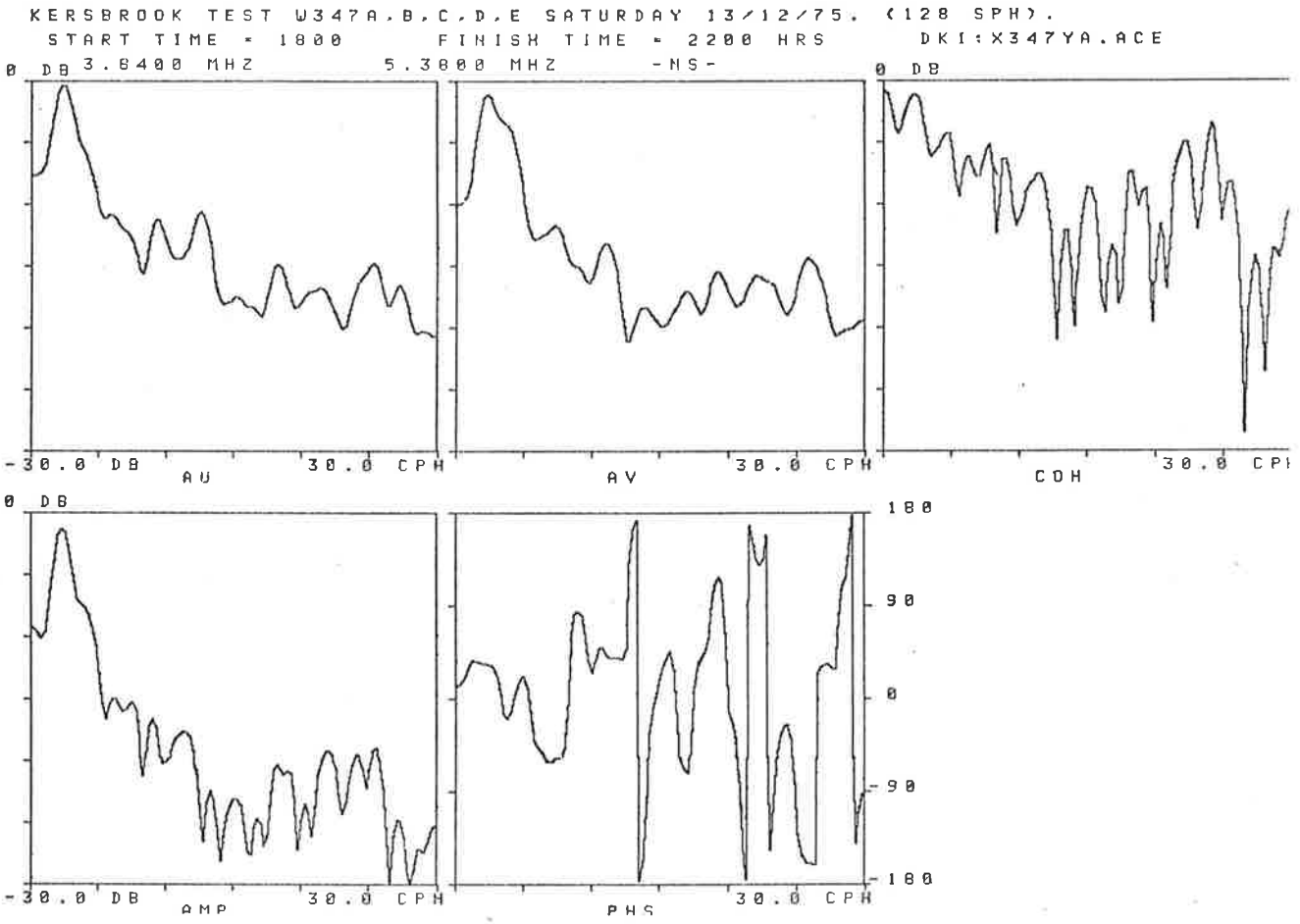

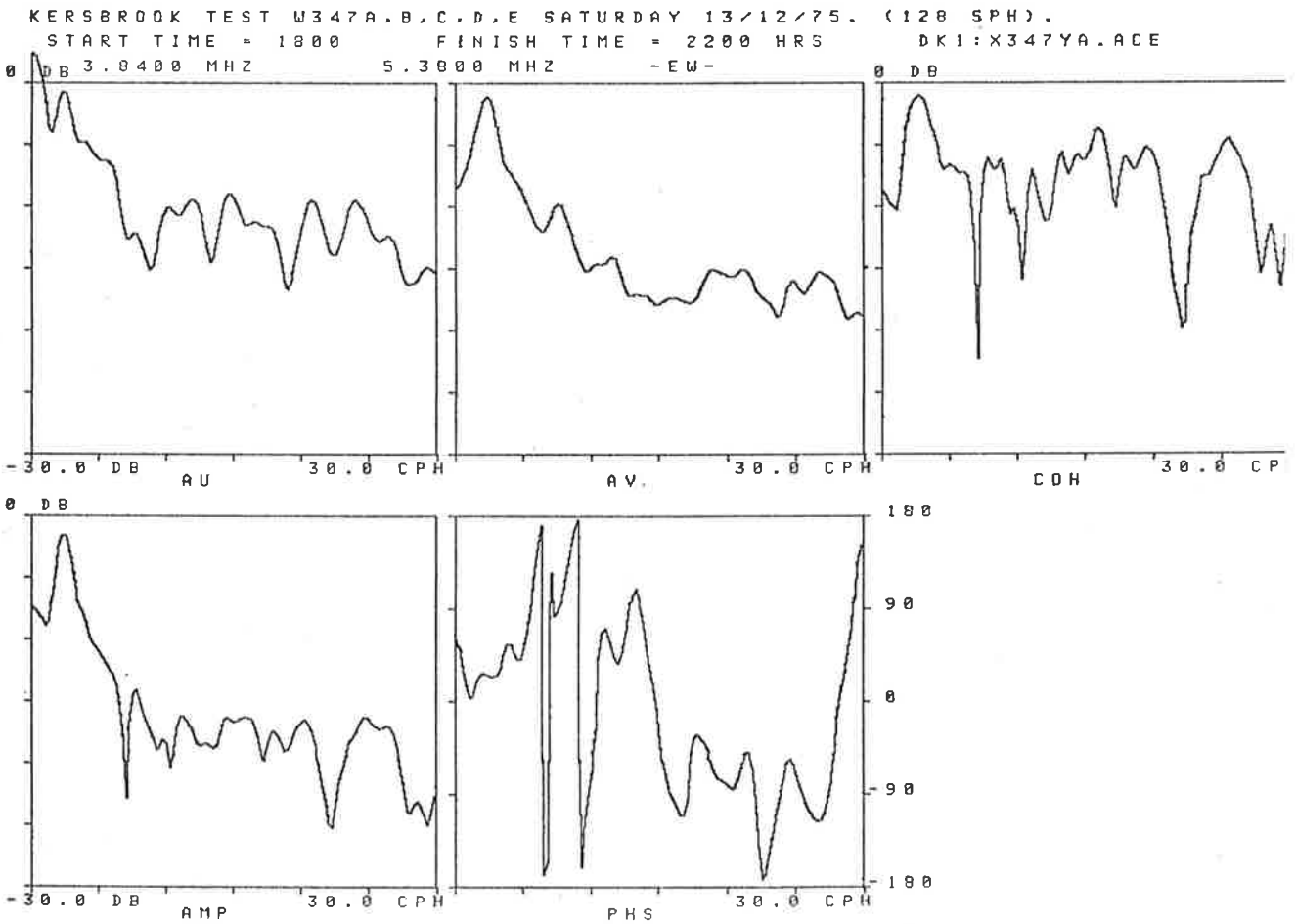

Figure 3.10 Spectra between adjacent signal frequencies for the zenith angle data shown in figure 9. (a) 3.84 and 5.38 Mhz frequencies

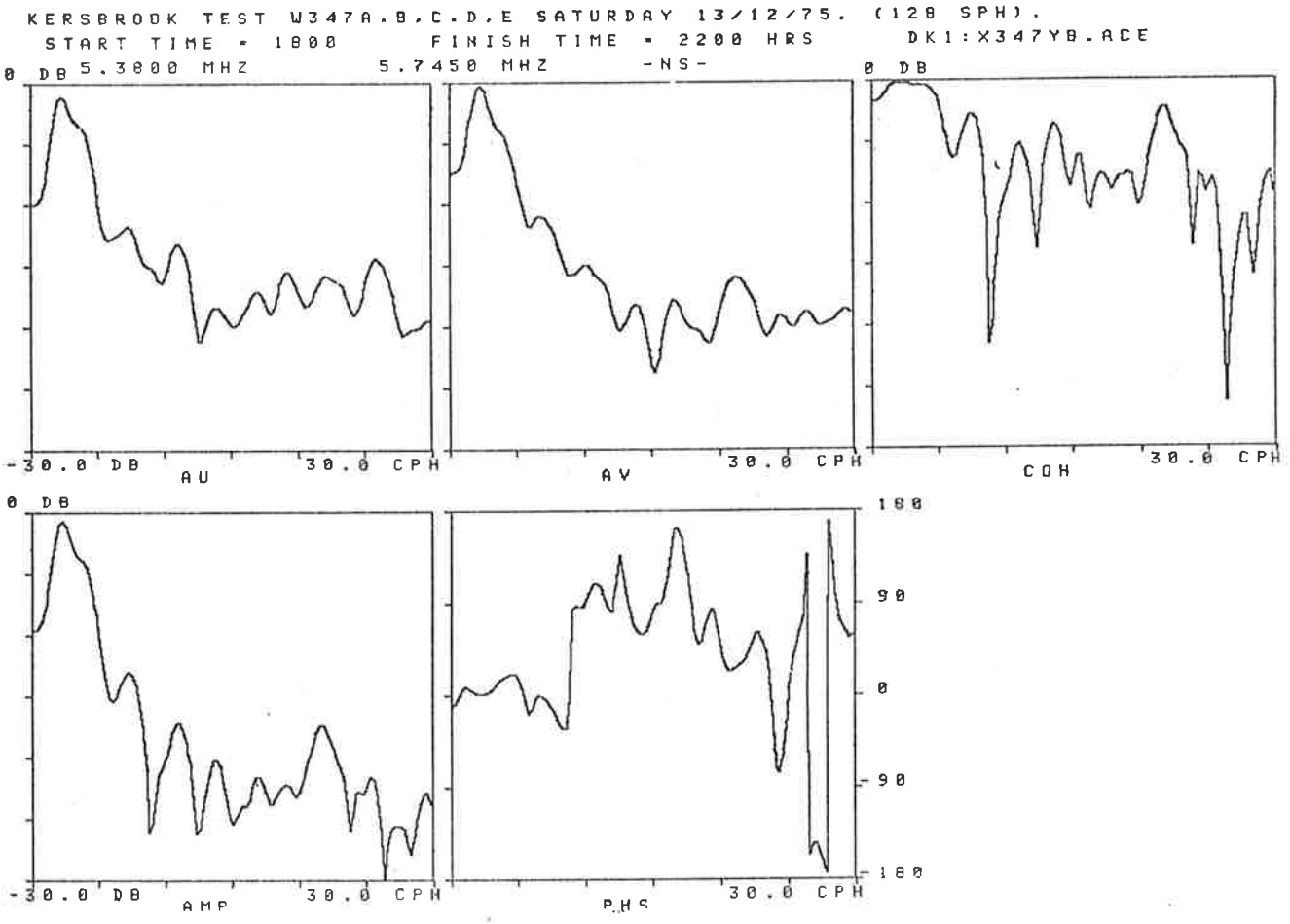

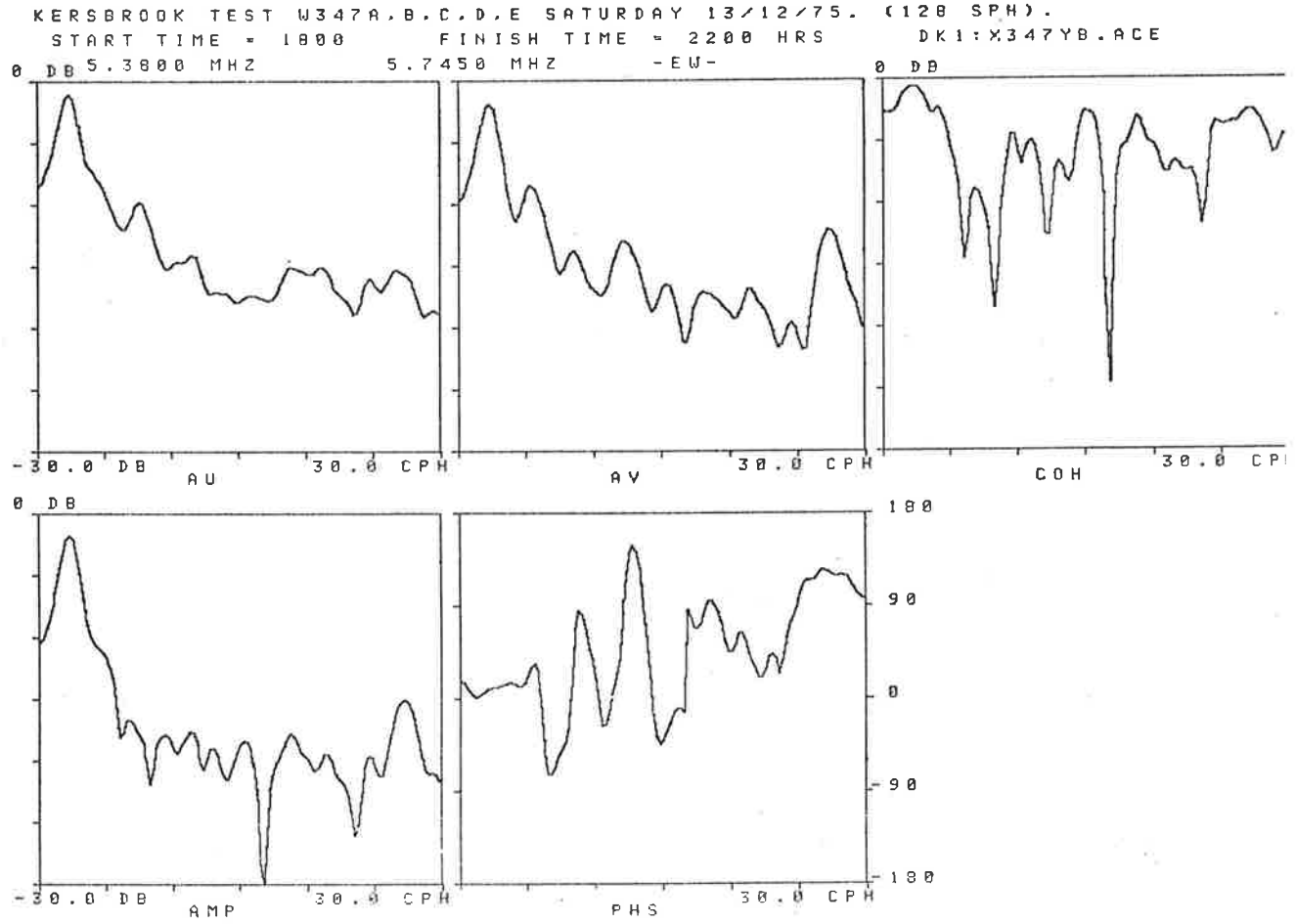

Figure 3.10 Spectra between adjacent signal frequencies for the zenith angle data shown in figure 9. (b) 5.38 and 5.745 Mhz frequencies

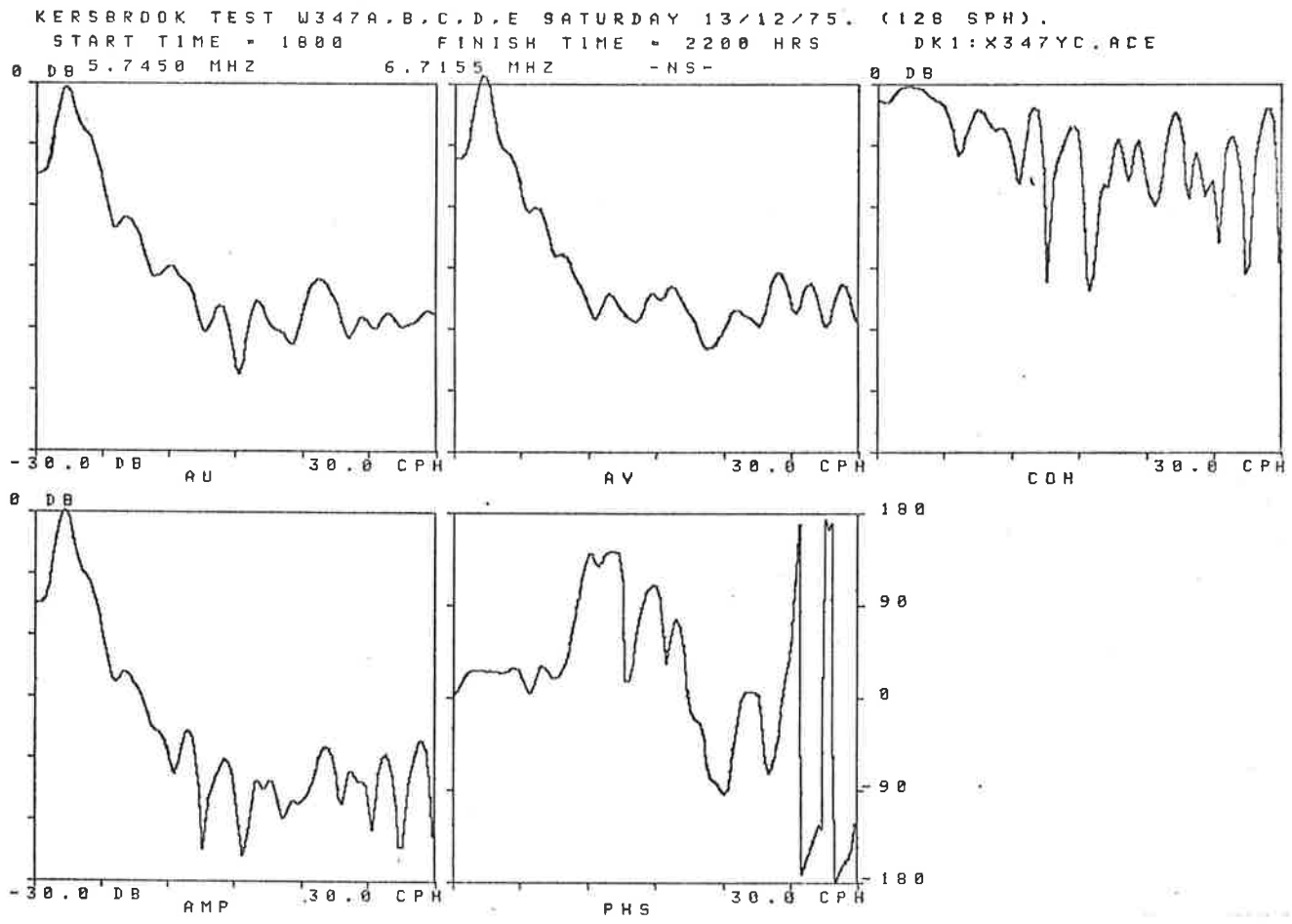

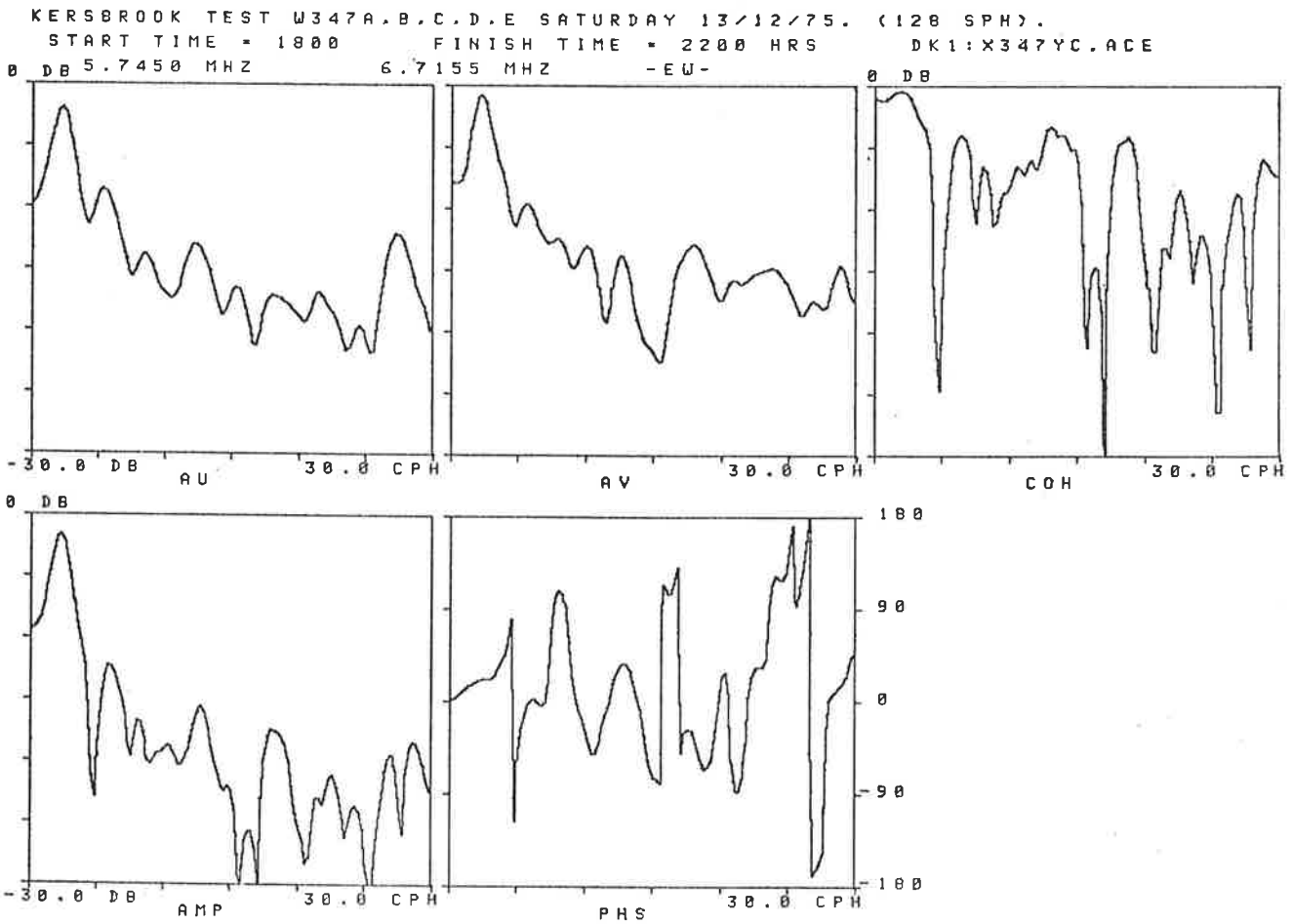

Figure 3.10 Spectra between adjacent signal frequencies for the zenith angle data shown in figure 9. (c) 5.745 and 6.7155 Mhz frequencies

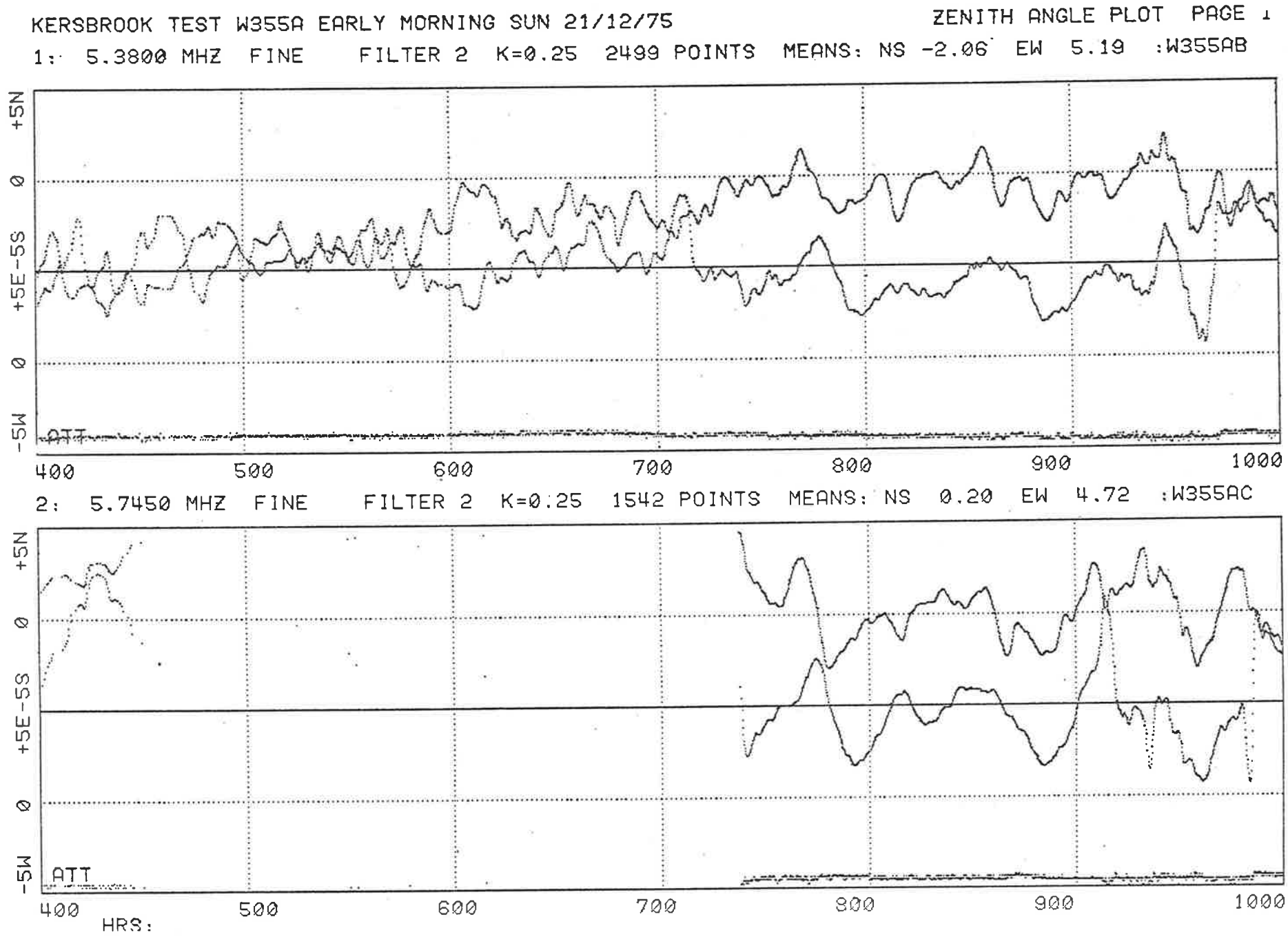

Figure 3.11 Sample of early morning zenith angle data: W355A

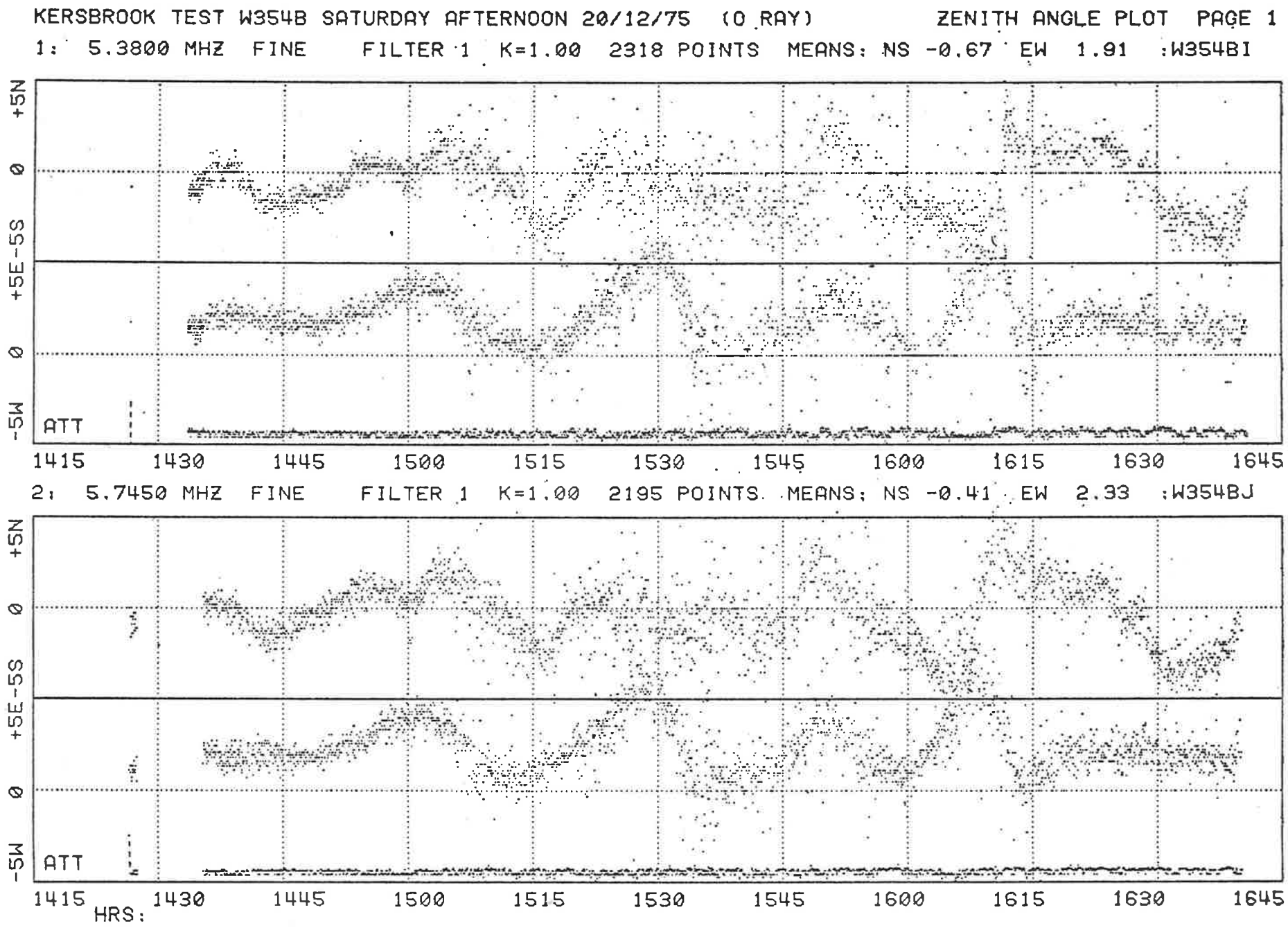

Figure 3.12 Sample of unfiltered data : W354 O-ray

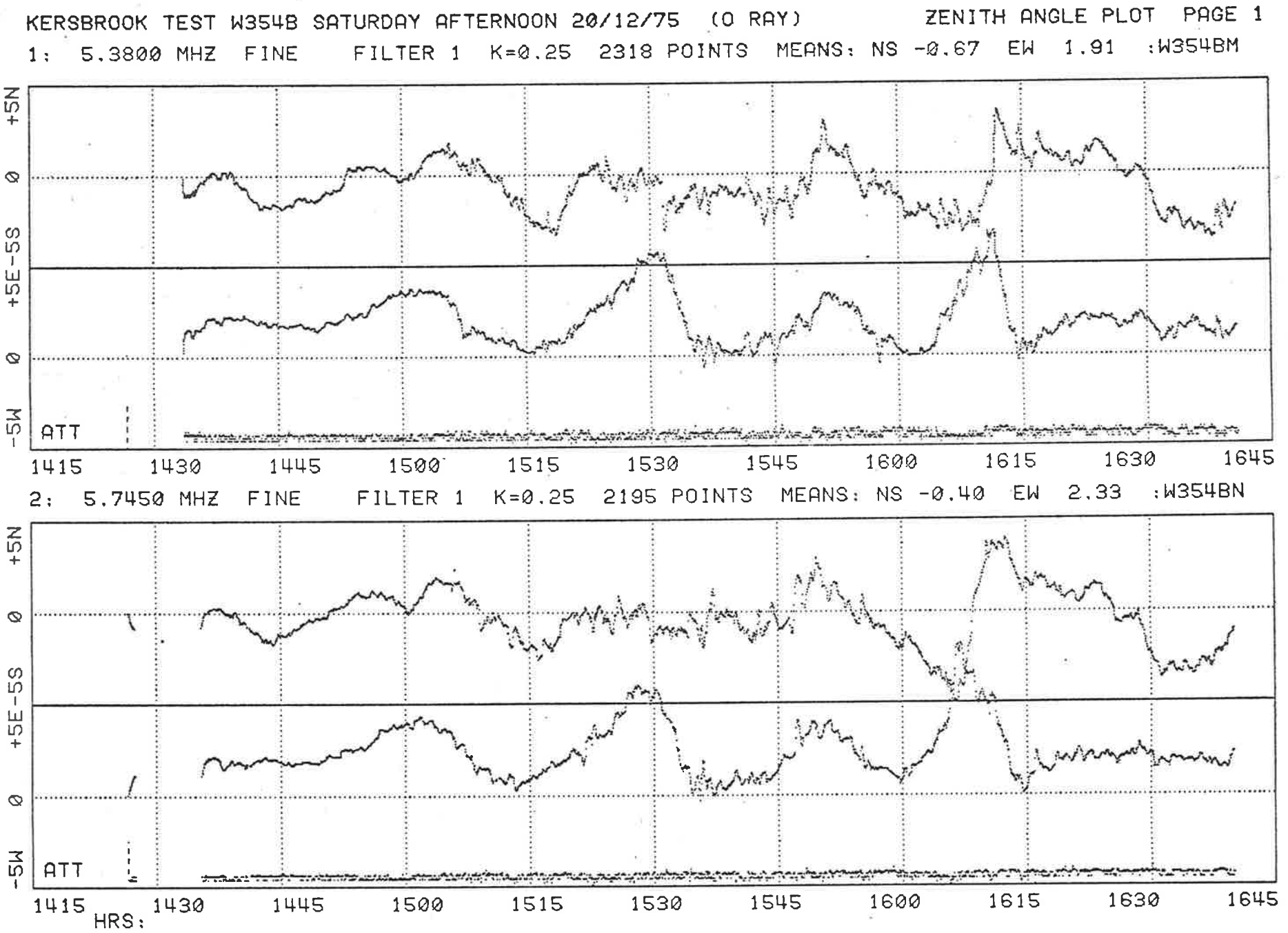

Figure 3.13 The same sample as for figure 12 after smoothing with the exponential filter

The same data sample is used in chapter 5 where plots of this data at equally spaced points and also after FFT filtering can be seen.

A test for the stability of the complete measurement system was carried out by coupling two separate test oscillators to the antenna switching unit inputs. The oscillators were set to 5.38 Mhz and 5.745 Mhz with the help of a frequency counter. A thirty minute sample of unfiltered test data from this configuration is shown in figure 14. The same data, filtered with the exponential filter, with parameters as used for quick look presentation of data is shown in figure 15. A histogram of the unfiltered test data can be seen in figure 16. The conclusion from this test is that noise introduced into the measurements by the measurement system can be substantially reduced by suitable data processing but that a small residual bias is left in the data. Noise can be introduced into the system in a number of ways. The digitally tuned oscillator signals for example are a potential source of phase noise. If cost is not a constraint, commercially available digitally settable synthesizers with adequate phase stability can be used for the generation of local oscillator signals.

An additional sample of zenith angle data is shown in figure 17. An asymmetrical character can be seen in many of the zenith angle excursions resulting from the passage of TID's.

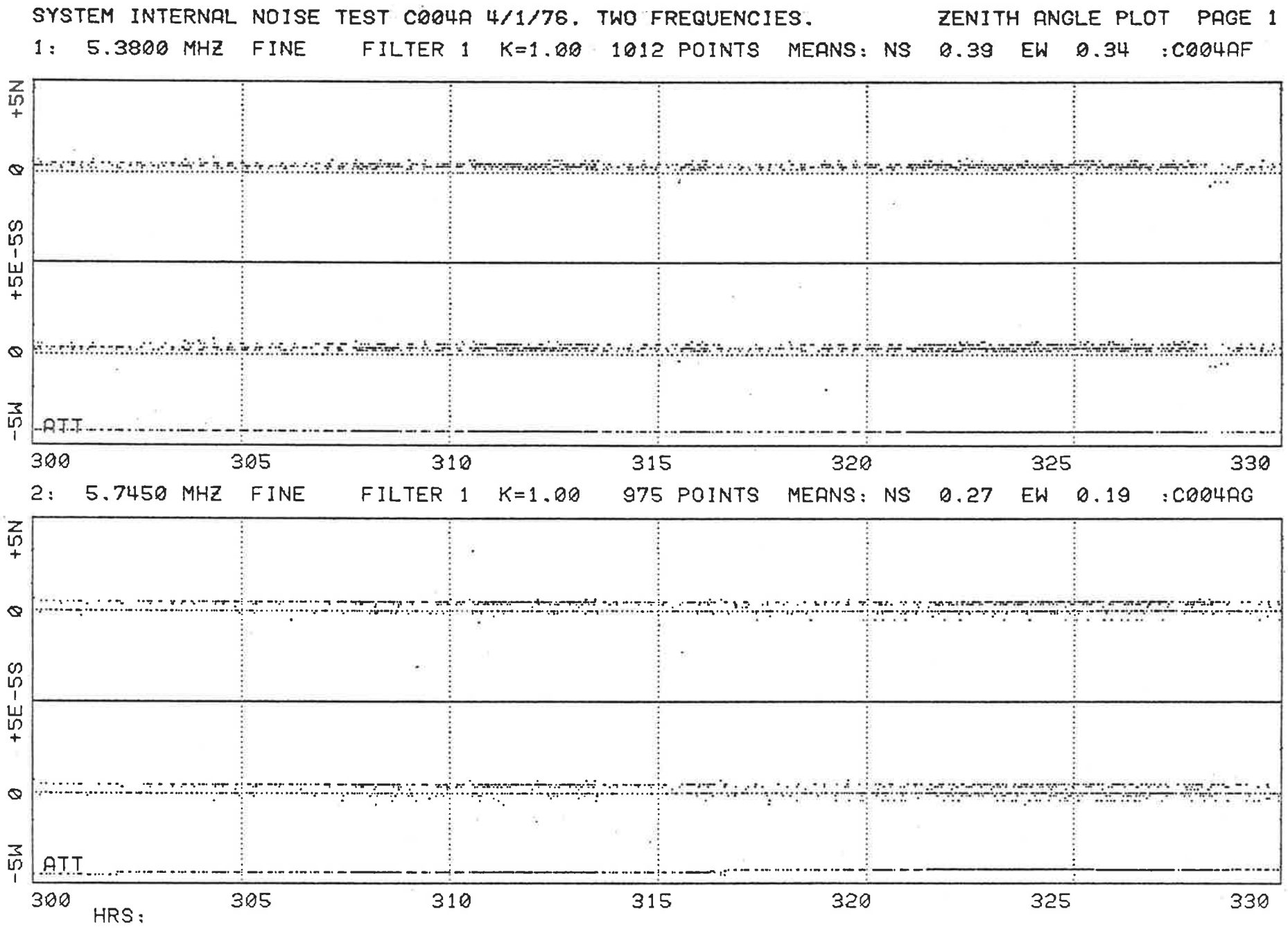

Figure 3.14 Sample of unfiltered data with test oscillators used as input signal sources

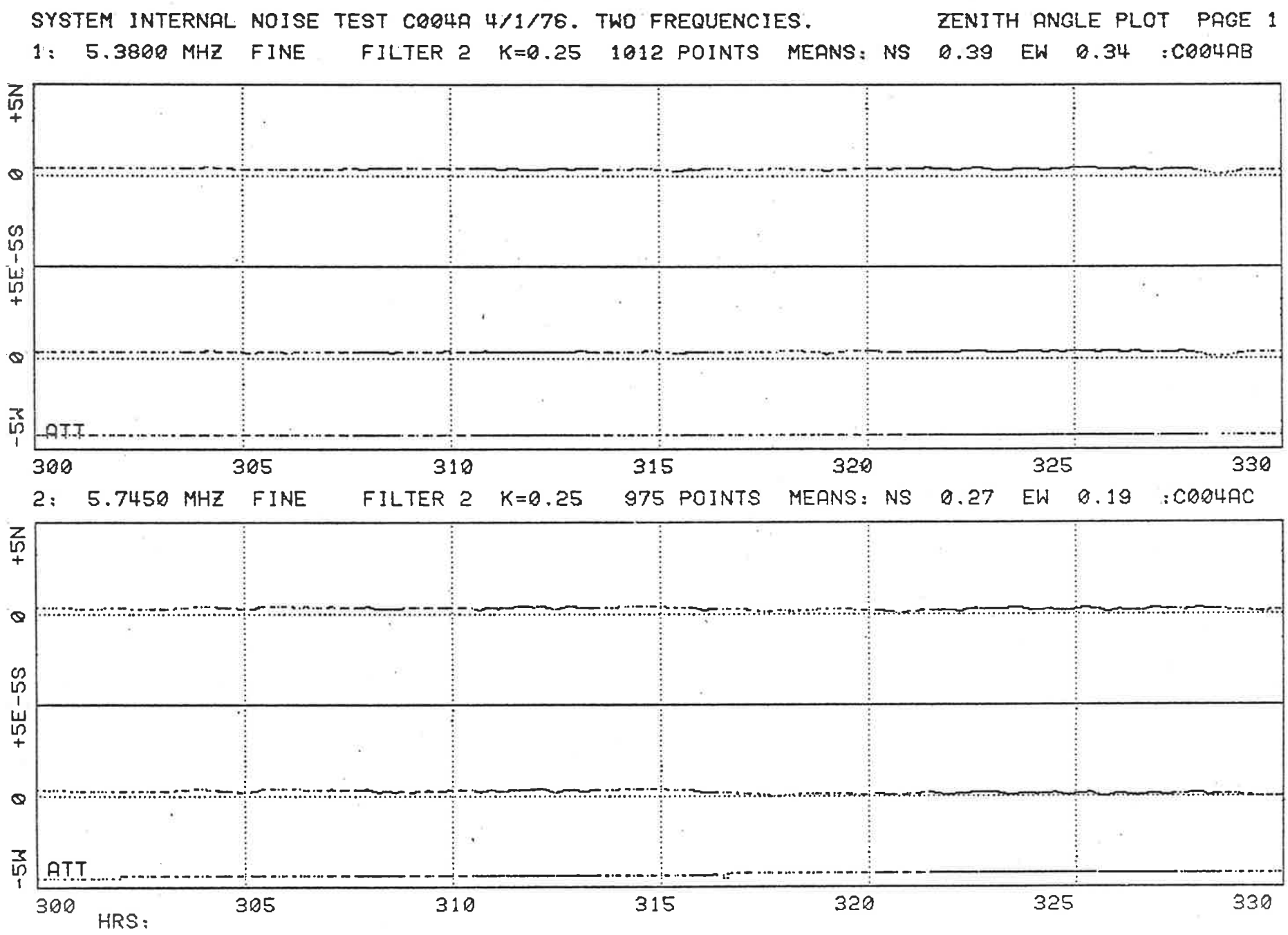

Figure 3.15 The same sample as for figure 14 after smoothing with the exponential filter

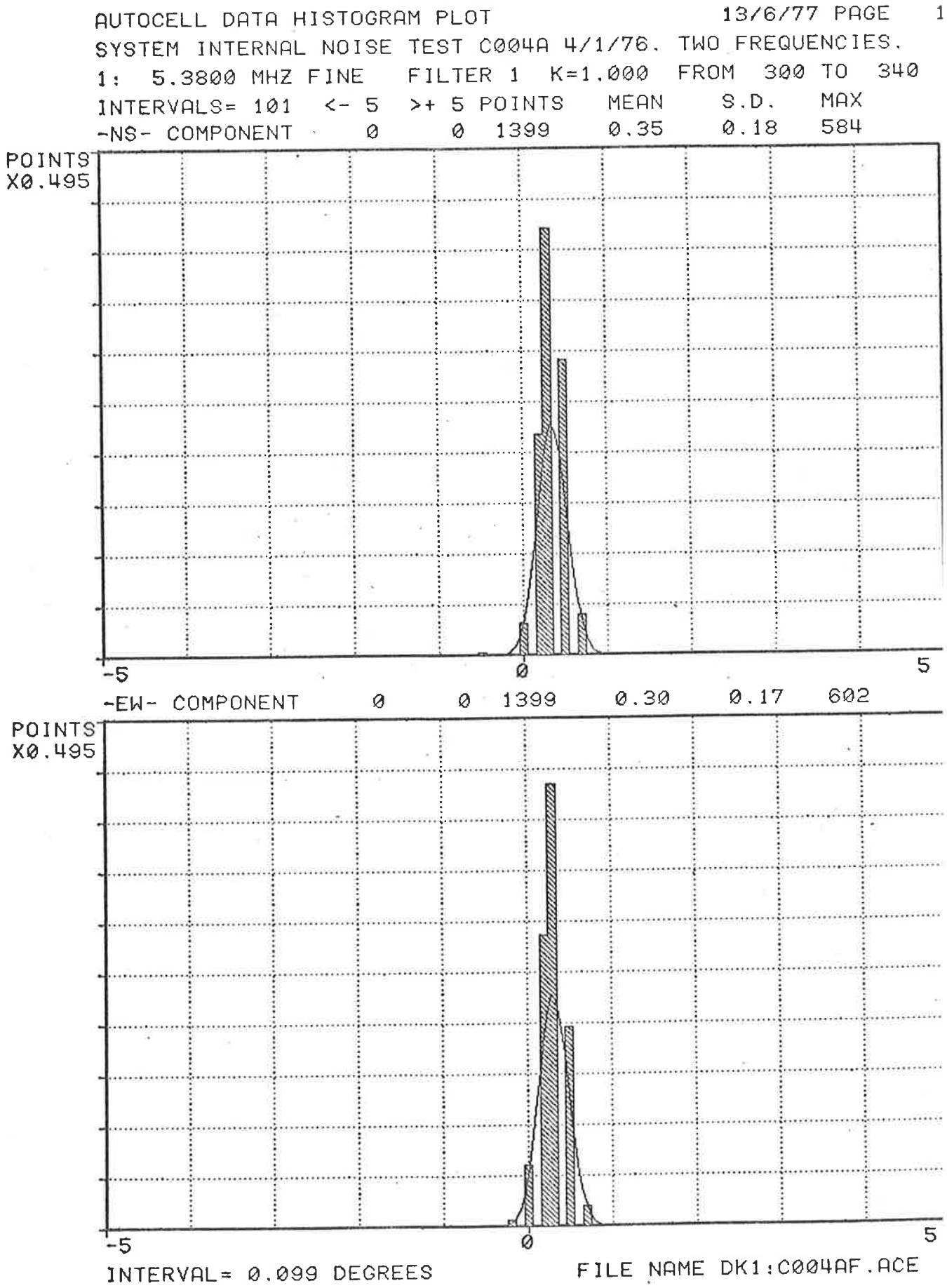

Figure 3.16 Histogram of unfiltered test data from figure 14

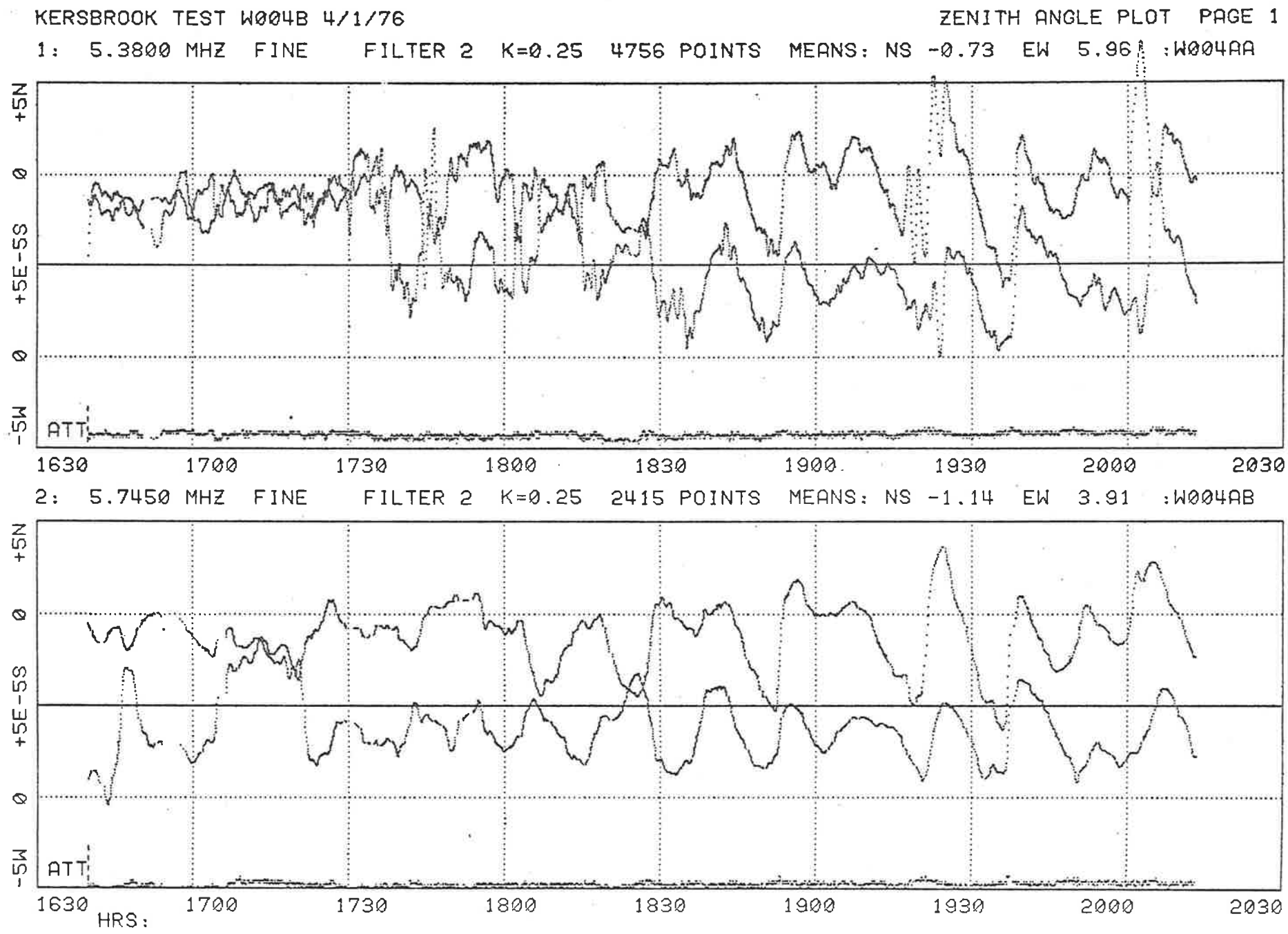

Figure 3.17 Zenith angle data : W004B

CHAPTER 4

SPECULAR REFLECTION OF AN E.M. SIGNAL FROM A DISTORTED IONOSPHERE

4.1 DEVELOPMENT OF A GEOMETRICAL MODEL

A simple geometrical model of specular ionospheric reflection is considered in this chapter. This geometrical reflection model is used mainly for establishing how a travelling sinusoidal reflecting surface can be expected to affect the direction of arrival of a radio signal reflected from it. The conclusions drawn from the model are then of assistance in the interpretation of the data. The model is also useful for direction finding or radio location applications where the transmitted signal, whose point of origin is sought, is reflected from the ionosphere. This application is not considered further.

The ionosphere is considered to be a smooth but distorted reflecting surface. Vector relationships are developed for the description of a reflection point on the surface of the ionosphere at which a signal transmitted from a point D/2 from the origin will be received at a point D/2 from the origin diametrically opposite from the transmitting point. The ground surface is assumed to be flat. Each reflection point is considered to be replaced by a plane reflecting mirror. Expressions for the reflection point are derived using the concepts of geometrical optics.

The technique adopted is essentially that of Bramley (1953) except that numerical techniques are used in place of graphical ones, where solutions of the equations are required. Also the equations are derived initially without approximations other than those implicit in the model. Simplified equations, such as those given by Bramley, can then readily be obtained when required.

Results of the next chapter indicate that at any given time the reflecting surface of the ionosphere can usually best be represented by a spectrum of waves which in general are not travelling horizontally and are not all travelling at the same speed or in the same direction. The assumption that will be made in the present chapter of a single plane wave is therefore somewhat severe for the general case. However, as shown by Bramley, the assumption is justified in practice often enough to be worth pursuing. The very direct experiment carried out by Brownlie et. al. (1973) shows that a vertical incidence signal reflected from the ionosphere is very well represented as a small set of discrete reflections rather than a more diffuse diffraction cone of electromagnetic waves. Thome and Rao (1969) in a direct comparison between a ray tracing model and a geometric reflection model have shown that to a good approximation the major part of the deviation of the path of a signal reflected from the ionosphere occurs in the vicinity of the reflection point.

It has been shown, for example by Davies (1966), that a vertical incidence radio wave in the ionosphere undergoes a spitze in which the e.m. signal at the actual point of reflection may be considerably off vertical, the O-ray being deflected towards the nearer pole and being reflected when its direction of propagation is normal to the Earth's magnetic field, and the X-ray being deflected towards the Earth's equator and reflected when its direction is roughly parallel to the Earth's magnetic field. The practical consequences of the spitze have been investigated by Heisler and Nelson (1967) who show that the main effect is to translate actual reflection points some kilometers to the North or South depending on the polarization and the frequency of the signal. The whole of this part of the trajectory of the e.m. wave will be considered to be inside the ionospheric layer under consideration and is not taken into account in relation to the prob-

lems discussed in this chapter.

The spherical polar coordinate system shown in figure 1 is considered, in which:

$$x = r \sin\theta \cos\gamma$$
$$y = r \sin\theta \sin\gamma \qquad (4.1)$$
$$z = r \cos\theta$$

$\underset{\sim}{A}$ is a vector from the origin which intersects a plane perpendicularly. The plane passes through the point (0,0,h). The plane is hinged along a line which makes an angle γ to the y axis and is tilted downward at the angle θ. $\underset{\sim}{r}$ is any vector from the origin to the plane. From the diagram:

$$r = h \cos\theta \qquad (4.2)$$

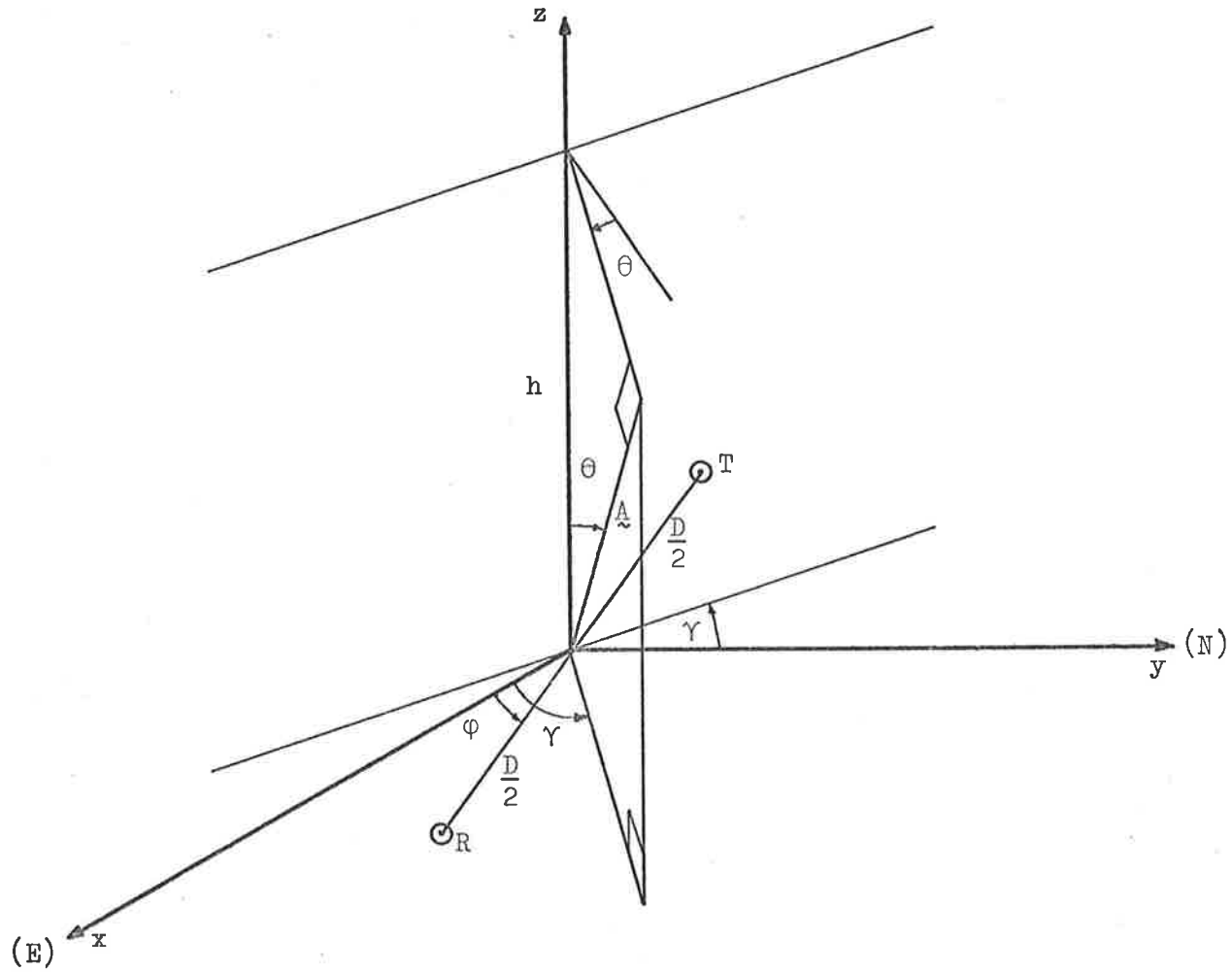

FIGURE 4.1 Geometrical construction used to determine the reflection point coordinates of a tilted ionosphere

The vector $\underset{\sim}{A}$ has components, from (1) and (2):

$$x_A = h \sin\theta \cos\theta \cos\gamma$$
$$y_A = h \sin\theta \cos\theta \sin\gamma \qquad (4.3)$$
$$z_A = h \cos^2\theta$$

Use is made of the property of a scalar product, that the dot product of perpendicular vectors is zero, to derive an equation of the plane:

$$\underset{\sim}{A}\cdot(\underset{\sim}{A}-\underset{\sim}{r}) = 0$$
$$\underset{\sim}{A}\cdot\underset{\sim}{r} = A^2 = h^2 \cos^2\theta \qquad (4.4)$$

The resulting equation of the plane is:

$$\sin\theta \cos\gamma\, x + \sin\theta \sin\gamma\, y + \cos\theta\, z = h \cos\theta \qquad (4.5)$$

The left hand side of (5) gives the unit normal of the plane:

$$\sin\theta \cos\gamma\, \underset{\sim}{i} + \sin\theta \sin\gamma\, \underset{\sim}{j} + \cos\theta\, \underset{\sim}{k} \qquad (4.6)$$

The first step of the procedure adopted is to determine a vector from the location of the transmitter (T) perpendicular to the plane to a point twice the distance from T to the plane.

The transmitter site is located at:

$$x_T = -(D/2)\cos\phi$$
$$y_T = -(D/2)\sin\phi \qquad (4.7)$$
$$z_T = 0$$

and the receiver site is located at:

$$x_R = (D/2)\cos\phi$$
$$y_R = (D/2)\sin\phi \qquad (4.8)$$
$$z_R = 0$$

The equations of a line from the transmitting site intersecting the plane perpendicularly are then:

$$\frac{x+(D/2)\cos\phi}{\sin\theta\cos\gamma} = \frac{y+(D/2)\sin\phi}{\sin\theta\sin\gamma} = \frac{z}{\cos\theta} \qquad (4.9)$$

and twice the distance from the transmitting site to the intersection of the line (9) with the plane is found to be, after completing algebraic reduction:

$$\Omega = D \sin\theta \cos(\phi-\gamma) + 2h \cos\theta \tag{4.10}$$

If the required image point is represented by the vector r_I, then the distance from the transmitter site to r_I is given by:

$$\Omega = \sqrt{(x_I-x_T)^2 + (y_I-y_T)^2 + (z_I-z_T)^2} \tag{4.11}$$

Substitution of (7), (9) and (10) into (11) enables z_I to be found and then x_I and y_I can be found from (9). This gives the image point as:

$$\begin{aligned} x_I &= -(D/2)\cos\phi + \sin\theta \cos\gamma\ \Omega \\ y_I &= -(D/2)\sin\phi + \sin\theta \sin\gamma\ \Omega \\ z_I &= \cos\theta\ \Omega \end{aligned} \tag{4.12}$$

where the positive sign has been taken for z_I since only the image point above ground is of interest.

The next step is to find a vector from the image point to the receiver site. The reflection point r in the plane can then be found by substitution of this vector into the equation for the plane. The required equation for the vector $\underset{\sim}{r} = (x,y,z)$ is:

$$\begin{aligned} \underset{\sim}{r}-\underset{\sim}{R} &= a(\underset{\sim}{r}_I-\underset{\sim}{R}) \\ \underset{\sim}{r} &= \underset{\sim}{R} + a(\underset{\sim}{r}_I-\underset{\sim}{R}) \end{aligned} \tag{4.13}$$

where a is a scalar constant, from which the components are:

$$\begin{aligned} x_r &= (D/2)\cos\phi + a(\sin\theta \cos\gamma\ \Omega - D \cos\phi) \\ y_r &= (D/2)\sin\phi + a(\sin\theta \sin\gamma\ \Omega - D \sin\phi) \\ z_r &= a \cos\theta\ \Omega \end{aligned} \tag{4.14}$$

The coordinates (14) are substituted into the equation of the plane (5), which is then solved for the scalar constant a to give, after reduction:

$$a = \tfrac{1}{2} - (D/4h)\tan\theta\cos(\phi-\gamma) \qquad (4.15)$$

Equations (10),(14) and (15) give the coordinates of the reflection point of a smooth curved or plane tilted ionosphere. These equations can be used in a variety of ways, three of which will be illustrated within the remainder of this chapter.

By use of the following approximations;

$$\begin{aligned} \sin\theta &\simeq \tan\theta \\ \cos\theta &\simeq \cos^2\theta \simeq 1 \\ \sin^2\theta &\simeq 0 \end{aligned} \qquad (4.16)$$

the equations given by (10),(14) and (15) readily reduce to the equations used by Bramley.

$$\begin{aligned} x &= \theta(h + D^2/4h)\cos\gamma \\ y &= h\,\theta\sin\gamma \\ z &= h \end{aligned} \qquad (4.17)$$

It should be noted that h is not the effective height (h′) of the ionosphere but is the height at which the reflecting plane cuts the z axis. For ionospheric waves of small amplitude the approximation $h = h'$ can be used as is done by Bramley.

Although the above approximations will not necessarily be used in this chapter some of the notations used by Bramley are retained.

4.2 THE BEHAVIOUR OF THE TILT ANGLE

The first use of equations (10),(14) and (15) will be to determine the behaviour of the tilt angle θ during the passage of a plane, sinusoidal, horizontally propagating ionospheric wave. To facilitate this, the following simplifications are made to the model:

$$\phi = 0, \quad \gamma = 0, \quad D = 0 \qquad (4.18)$$

The equations then reduce to:

$$a = \tfrac{1}{2}$$

$$\Omega = 2h \cos\theta$$

$$x_r = h \sin\theta \cos\theta \qquad (4.19)$$

$$y_r = 0$$

$$z_r = h \cos^2\theta$$

The plane sinusoidal surface of the ionospheric wave is represented by the real part of:

$$z = H + Z_m \, e^{i(\underset{\sim}{k}.\underset{\sim}{r}-wt)} \qquad (4.20)$$

where Z_m is the amplitude of the wave, and H is the height of the wave above ground. The sign of the argument of the exponential function is opposite to that which will be used in the next chapter, this simply means that distance rather than time advances to the right. In the present case (20) reduces to:

$$z = H + Z_m \cos(k(x-vt)) \qquad (4.21)$$

where v is the velocity of the wave.

The geometry of this simplified model is shown in figure 2. Following the notation of Bramley, the argument of the cosine function in (21) will be represented by β :

$$\beta = k(x-vt) \qquad (4.22)$$

then:

$$z = H + Z_m \cos\beta$$

and:

$$\tan\theta = (\partial z/\partial x)_t = kZ_m \sin\beta \qquad (4.23)$$

where θ is the downward slope of the sinusoidal surface.

Substituting from (19) and (23):

$$x_r = z_r k Z_m \sin\beta \qquad (4.24)$$

It will be assumed that k, v, t, H and Z_m are specified. An expression can then be written containing only the coordinate x within the

term β as unknown, as follows:

$$\begin{aligned}\beta &= k(x_r - vt) \\ &= k(z_r k Z_m \sin\beta - vt) \\ &= k((H + Z_m \cos\beta) k Z_m \sin\beta - vt)\end{aligned} \tag{4.25}$$

Once x_r is found, z_r can be found from (21) and θ can then be found from:

$$\tan\theta = x_r / z_r \tag{4.26}$$

The bisection method of numerical analysis (Hamming, 1973) is used to solve (25). This method appears to be the simplest workable means of obtaining a solution. It was found that no more than about 10 iterations were needed in most cases for the accuracy required. Relaxation methods are non convergent.

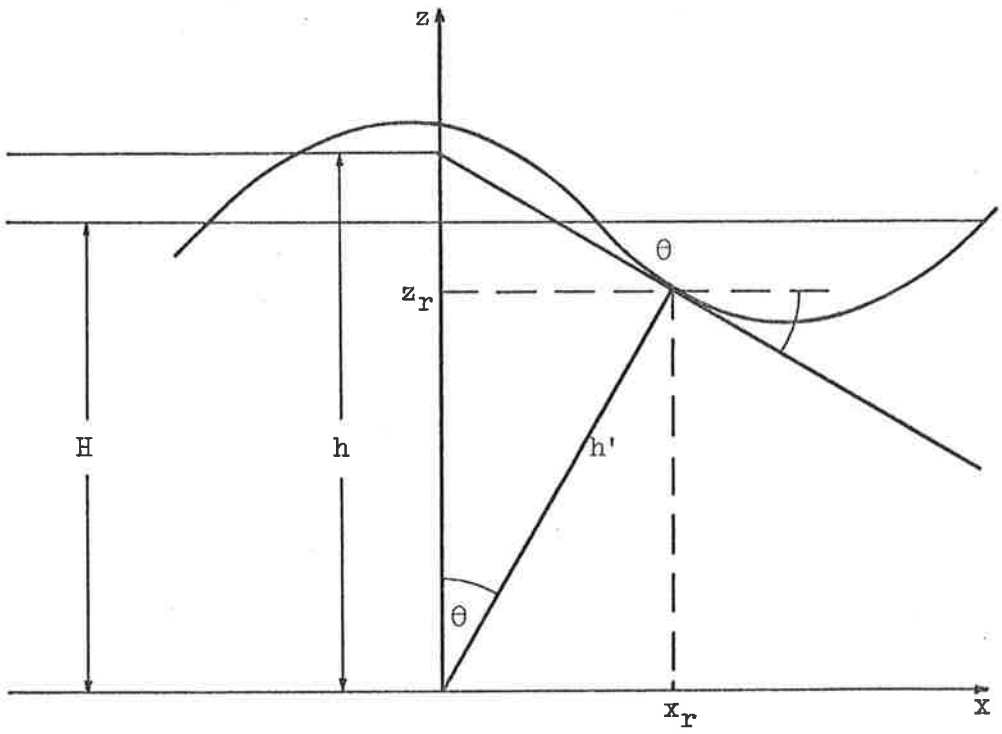

FIGURE 4.2 Model used to determine the behaviour of the tilt angle θ

The function:

$$\beta - k((H + Z_m \cos\beta)kZ_m \sin\beta - vt) \qquad (4.27)$$

is evaluated at successive increments of the unknown x_r over a specified range of values in an initial search phase, until the function changes sign and the bisection method is then applied iteratively until the required accuracy is obtained. The search phase is continued over the whole range specified and all solutions are treated and values stored. A computer plotting programme can then represent the result as a diagrammatic plot, or the procedure can be repeated at successive specified increments of time and θ plotted as a function of time.

The criterion for the onset of multiple reflections can be found as follows. It will be seen that multiple reflections are most prone to occur when the ionospheric surface is concave immediately above the observing point, i.e. at $t = 0$ in the above model. Also multiple reflections will just start to occur when x_r is small. Therefore the following approximations can be made:

$$\sin kx \simeq kx$$

$$\cos kx \simeq 1$$

Substitution of these approximations and putting $t = 0$ into (25) then gives the required condition:

$$k^2 Z_m (H+Z_m) = 1 \qquad (4.28)$$

For practical cases this can be taken as:

$$Z_m \simeq 1/Hk^2 = \lambda^2/(2\pi)^2 H \qquad (4.29)$$

Since λ appears to the second power in (29), ionospheric waves of short wavelength will be prone to give multiple reflections, other conditions being the same.

A series of results from the computer programme are presented in figures 3 and 4. Figure 3 displays a series of snapshots at 2 minute inter-

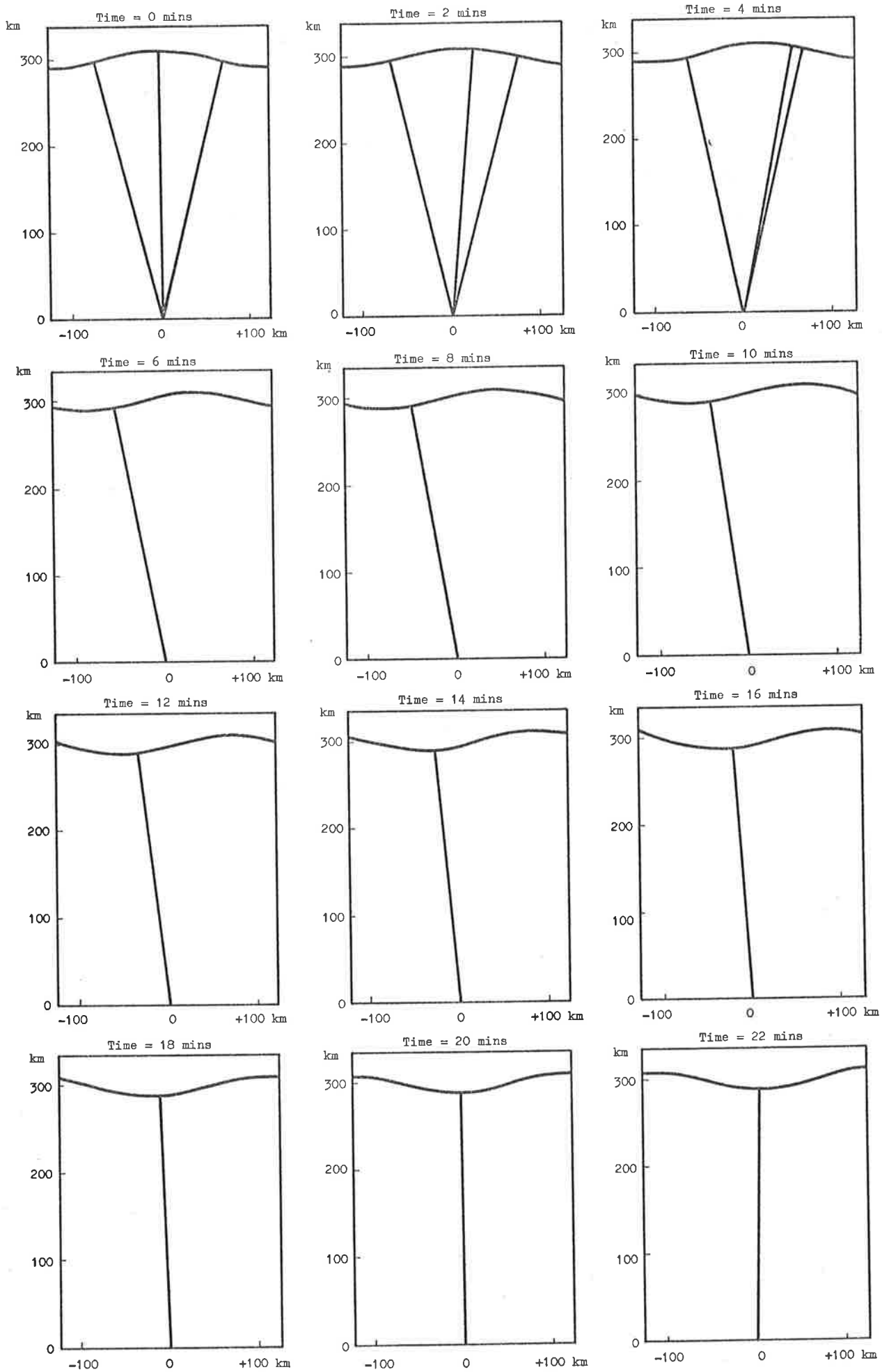

HEIGHT = 300.0 km, AMPLITUDE = 10.0 km, WAVELENGTH = 250.0 km, VELOCITY = 100 m/s

Figure 4.3 Ray paths taken by reflected signals as the travelling wave progresses

vals showing the path or paths taken by the reflected rays. Figure 4 is a series of plots of the tilt angle θ over a period of time for progressively increasing assumed amplitude of the wave. These figures illustrate the following characteristic features of the behaviour of this model. The angle θ as a function of time has an asymmetry which is dependent on the direction of motion of the ionospheric wave. The degree of this asymmetry is dependent on the amplitude Z_m, the wavelength λ and the height H of the wave above the ground but is independent of the speed of the wave.

The asymmetry is imperceptible when $k^2HZ_m \ll 1$ and becomes very marked as $k^2HZ_m \to 1$. When there are three reflection points, these reflection points are symmetrically disposed only at the instant at which the centre of the concave portion of the wave is directly overhead. For the remainder of the time that three reflection points occur two of the reflection points are closer together than the third. This can provide an explanation for the bifurcation sometimes seen in vertical incidence ionograms near the critical frequency, the ionosonde being able to resolve only two reflected signals. When the centre reflection point is directly overhead, the outer reflection paths are equal and less distant than the vertical reflection path. As the ionospheric wave moves overhead the leading reflection path increases and approaches that of the middle reflection path whilst the trailing reflection path diminishes. Three reflection paths of distinctly different length, therefore, exist for only part of the duration of the disturbance. Examples of this type of ionogram are given by Heisler (1963). An example appears in the ionograms shown in the next chapter. A three way split in the ionogram trace near the critical frequency is less frequently seen.

In expression (25), if the term $Z_m \cos \beta$ is neglected by comparison with H then the expression used by Bramley, valid for small amplitude

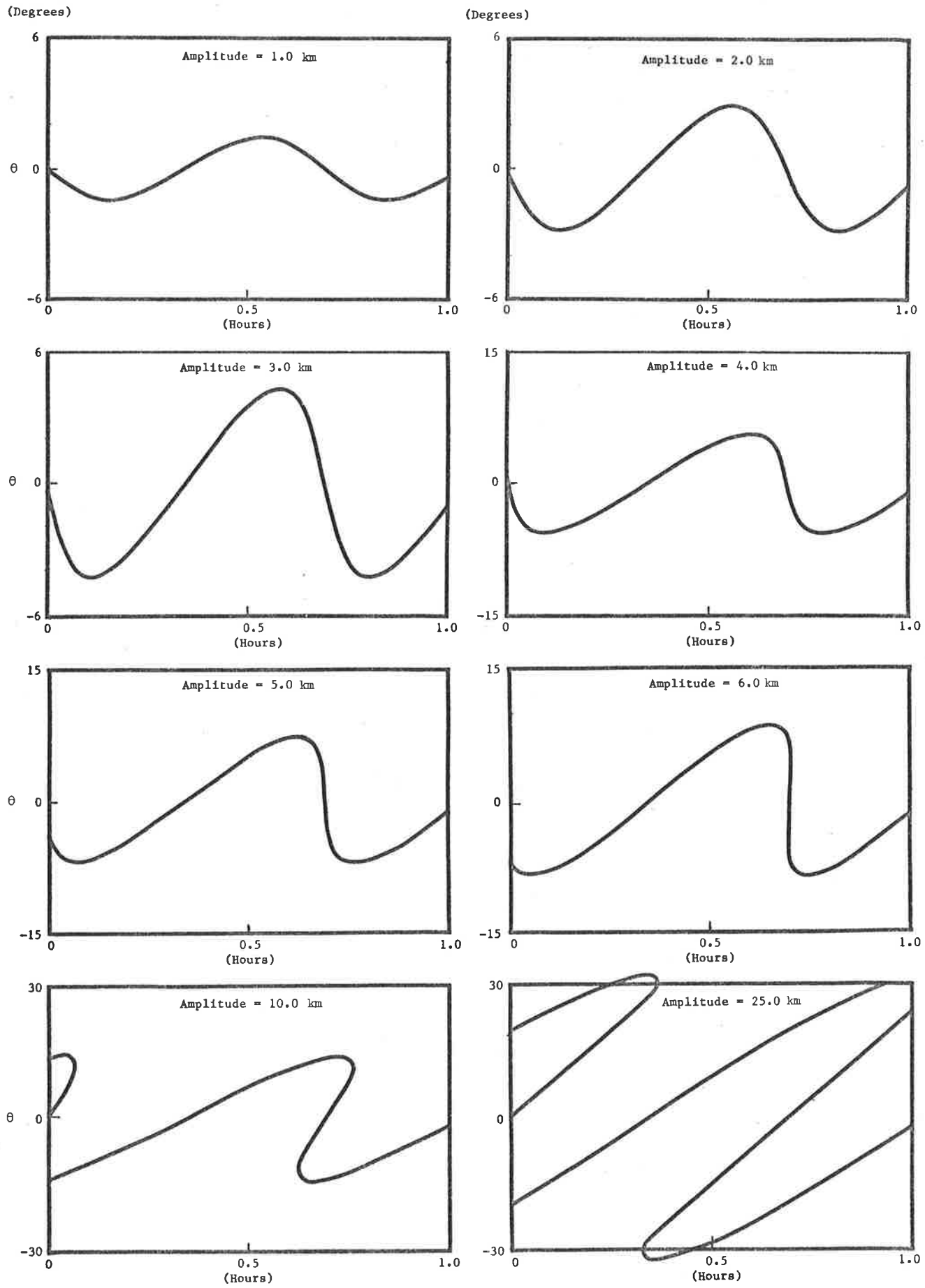

Figure 4.4 Asymmetry displayed by the angle of tilt

waves, is obtained. The procedure used here based on expression (25), is however, also valid for large amplitude waves. As would be expected, the number of reflection points increases to 5, 7 etc., as the factor k^2HZ_m increases above unity. In practice events with five distinct reflection points would be rare. However, waves of short wavelength require only a small amplitude to give rise to multiple reflections and the possibility exists that short wavelength waves could be responsible for spread F effects.

By comparing the sequence in figure 4 for example, with zenith angle values typically obtained, it can be seen that the amplitudes of typical ionospheric waves as far as their ability to reflect e.m. waves is concerned may be of the order of 1 or 2 kilometers. Sufficiently short wavelength waves of these amplitudes could give rise to multiple reflections. Also waves of these amplitudes would not be expected to be readily seen on a sequence of conventional ionograms i.e. no direct relationship would be expected to show up between a zenith angle plot and a time series plot of effective height. Equipment which observes travelling ionospheric disturbances by measuring the direction of arrival of signals reflected from the ionosphere could be expected to be more sensitive to small amplitude waves in the ionosphere than would be a method of observation based on effective height measurement. On the other hand the direction of arrival method of measurement would be less sensitive to slow variations in the height of the ionosphere as a whole than the effective height method of measurement would be.

4.3 FULL SIMULATION OF ZENITH ANGLE DATA

Most of the basic features of the model are displayed by the special case considered above. However, the complete set of equations (10), (14) and (15) can be solved in a similar manner to that of the previous section and the results can then be displayed as zenith angle plots. The assumption that the ionospheric wave is travelling horizontally is retained. The factor β becomes:

$$\beta = k(x\cos\gamma + y\sin\gamma - vt) \tag{4.30}$$

where γ is the angle between the x direction and the direction of the propagation vector $\underset{\sim}{k}$.

The height of the reflecting surface is given by:

$$z_r = H + Z_m \cos\beta \tag{4.31}$$

and as before:

$$\tan\theta = kZ_m \sin\beta \tag{4.32}$$

where θ is the downward slope of the reflecting surface in the direction of the propagation vector.

The x and y components of the reflection point can then be written:

$$\begin{aligned} x_r &= kZ_m \sin\beta\,(\cos\gamma\, z_r + (D^2/4h)\cos\phi\cos(\phi-\gamma)) \\ y_r &= kZ_m \sin\beta\,(\sin\gamma\, z_r + (D^2/4h)\sin\phi\cos(\phi-\gamma)) \end{aligned} \tag{4.33}$$

where z_r is given by (31) and h is evaluated seperately as follows:

From (14):

$$z_r = a\cos\theta\,\Omega$$

$$H+Z_m\cos\beta = \{h-(D^2/4h)\tan^2\theta\cos^2(\phi-\gamma)\}\cos^2\theta \tag{4.34}$$

(34) can be rewritten to give a quadratic expression for h:

$$h^2-(H+Z_m\cos\beta)(1+\tan^2\theta)h-(D^2/4)\tan^2\theta\cos^2(\phi-\gamma) = 0 \tag{4.35}$$

This can be solved for h, however, an adequate approximation for h is taken as:

$$h \simeq (H+Z_m\cos\beta)(1+k^2Z_m^2\sin^2\beta) \tag{4.36}$$

Expressions (33) are solved (as in the previous section) by searching over a suitable range of values of β at suitable incremental steps for a change in sign of the function:

$$\beta - k(x_r \sin\gamma + y_r \cos\gamma - vt) \tag{4.37}$$

and then applying the bisection method for all solutions found. Only a one dimensional search is required since the direction of propagation of the ionospheric wave is assumed to be known, and therefore x_r, y_r and z_r are known at each search point.

When a solution has been found, the zenith angles for the direction of arrival of the signal at the receiving site are calculated from:

$$\alpha_z = \frac{\pi}{2} - \arccos \frac{x_R - x_r}{|\underset{\sim}{R} - \underset{\sim}{r}|}$$

$$\beta_z = \frac{\pi}{2} - \arccos \frac{y_R - y_r}{|\underset{\sim}{R} - \underset{\sim}{r}|} \tag{4.38}$$

Where more than one solution is found, all the solutions are added vectorially before the zenith angles are computed. A zenith angle plot is generated by the computer programme that carries out the above procedures. An output data file is also produced so that additional procedures can be applied to the resulting data.

The value of D and ϕ for the St Kilda - Kersbrook experimental configuration have been used. To avoid confusion, these are shown schematically in figure 5. An illustration of a simulated zenith angle plot is shown in figure 6. It can be seen that offsets in the zenith angle data due to the relative geographical locations of the transmitting and receiving sites are accounted for realistically.

A result from this simulation is the series of plots shown schematically in figure 7. These plots give a series of signatures at directional intervals of 45 degrees from which the directions of motions of specific

wave events in the experimental zenith angle data can be inferred. When polar plots are made from these simulations it is found that the resulting polar plot is a straight line or narrow ellipse pointing in the direction of the wave normal. Consequently an individual wave event would be expected to appear on a polar plot as a straight line or elongated loop, indicating the direction of motion of the wave (with an ambiguity in the sense of the direction).

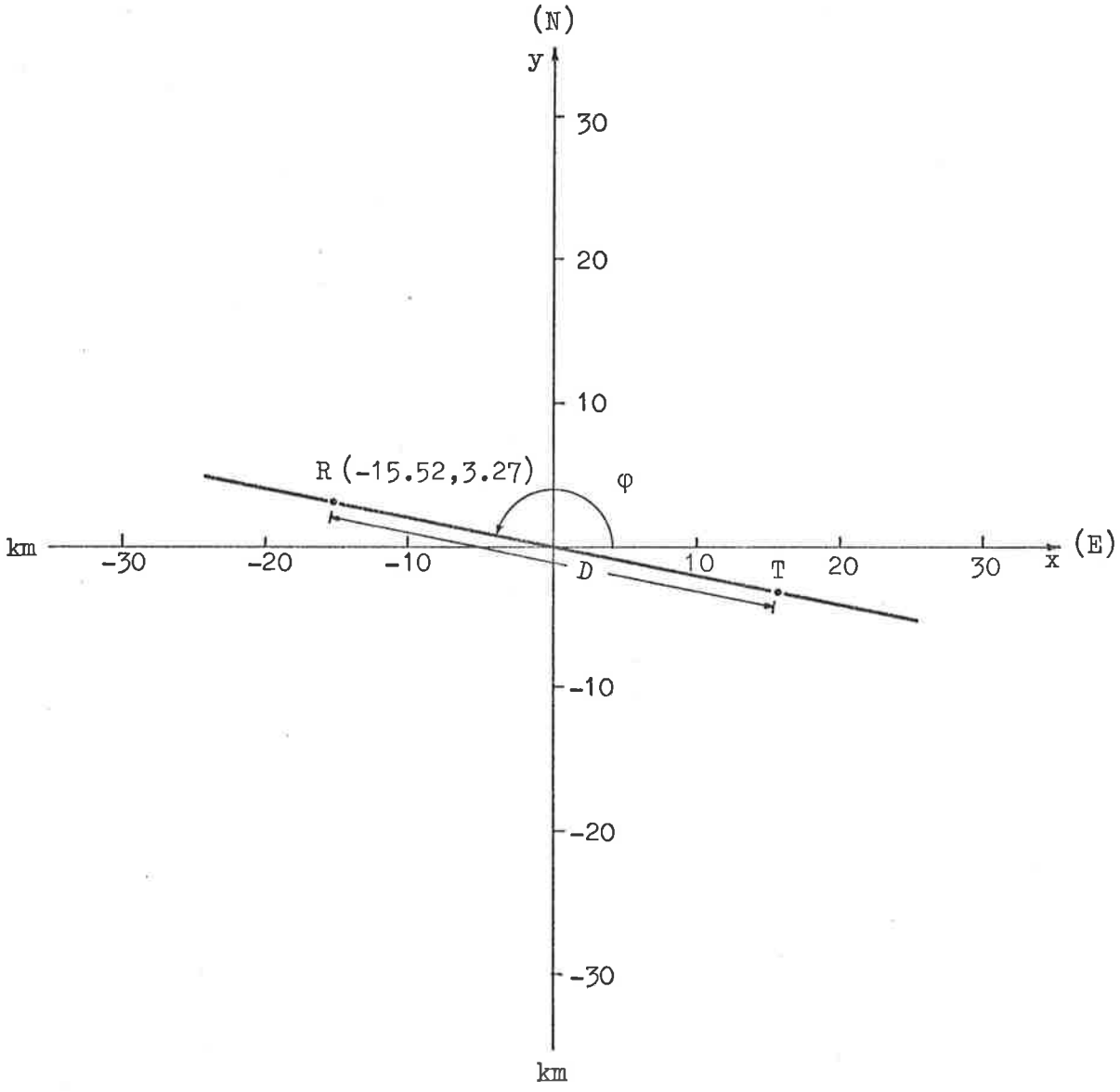

FIGURE 4.5 Experimental configuration of transmitting and receiving sites showing parameter D and ϕ

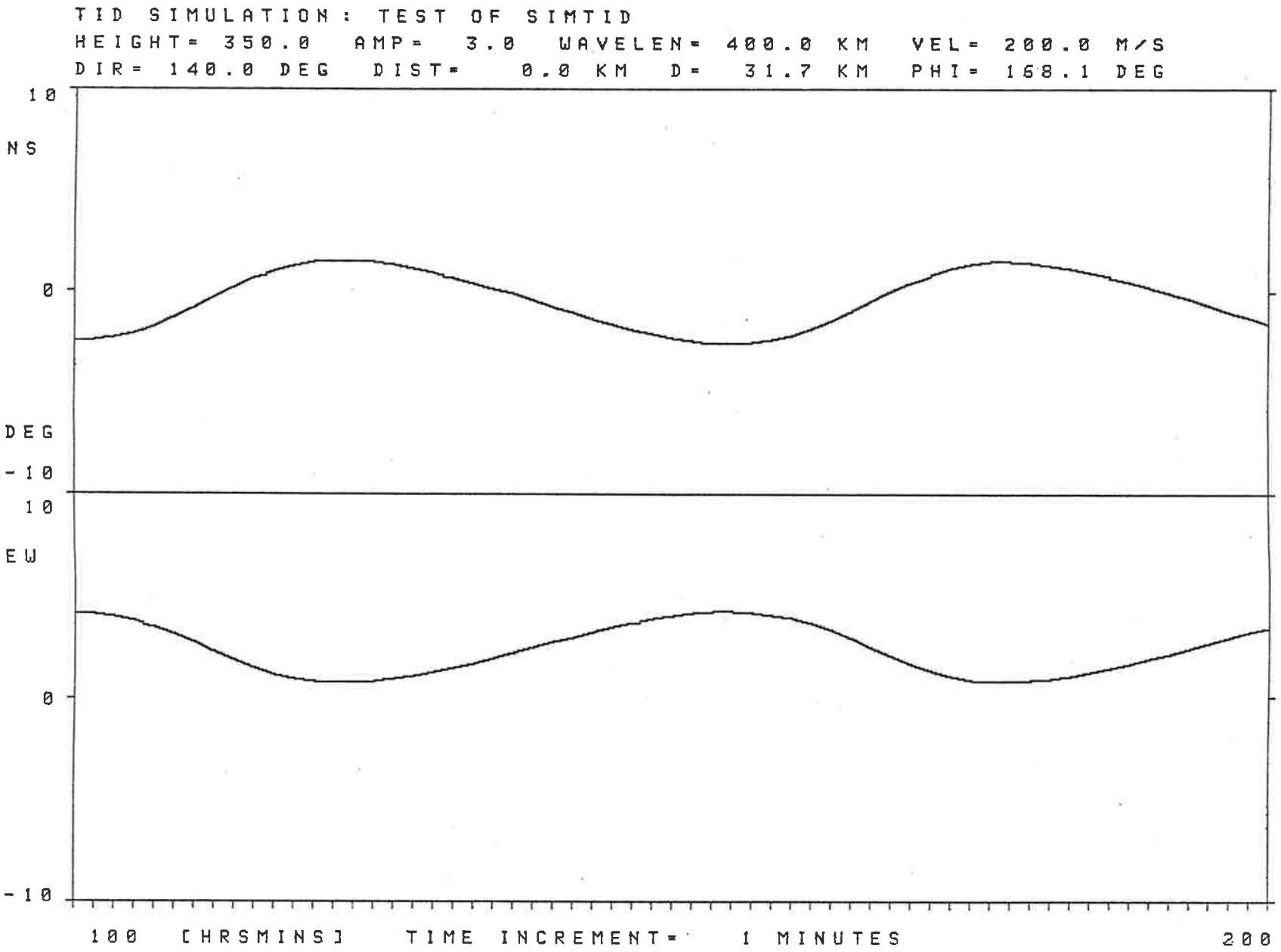

Figure 4.6 Illustration of simulated zenith angle data

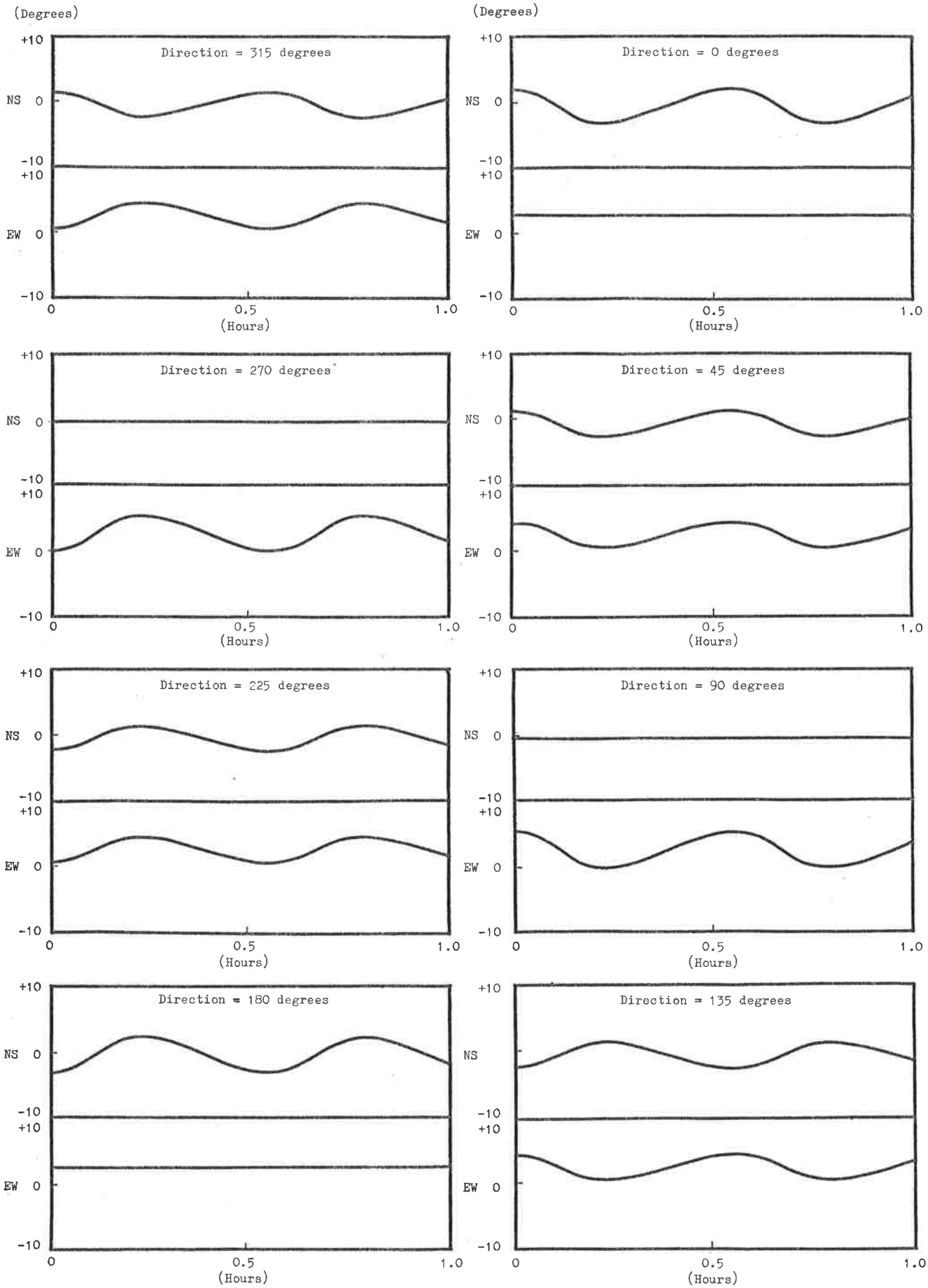

HEIGHT = 350.0 km, AMPLITUDE = 3.0 km, WAVELENGTH = 400.0 km, VELOCITY = 200 m/s

Figure 4.7 Series of zenith angle simulation plots with increments of 45 degrees in the direction of the wave motion

4.4 TILT ANGLE PLOTS

The next procedure to be described makes use of approximations to equations (10), (14) and (15) to convert zenith angle data to tilt and azimuth data. Each azimuth datum corresponds to the instantaneous direction of the normal to the axis of the tilt plane, and the tilt data corresponds to the downward slope of the tilt plane. If a single plane wave were to pass through the ionosphere the azimuth data from this procedure would be a straight line stepping between the direction of motion of the wave and a direction at 180 degrees to the direction of the wave. The tilt data is of interest to observe the order of magnitude of the tilts experienced.

If the angle ϕ for the receiving site had been left in the approximate equations (17), these could have been written as:

$$\begin{aligned} x_r &= h \sin\theta \,(\cos\gamma + (D^2/4h^2)\cos\phi\cos(\phi-\gamma)) \\ y_r &= h \sin\phi \,(\sin\gamma + (D^2/4h^2)\sin\phi\cos(\phi-\gamma)) \\ z_r &= h \end{aligned} \tag{4.39}$$

Since the distance D between transmitting and receiving sites is much less than the height h, the terms containing $D^2/4h^2$ will be omitted entirely. Expressions (39) then reduce to:

$$\begin{aligned} x_r &= h \sin\theta\cos\gamma \\ y_r &= h \sin\theta\sin\gamma \\ z_r &= h \end{aligned} \tag{4.40}$$

the angle γ can then be found from:

$$\gamma = \text{Arctan}\,(y_r/x_r) \tag{4.41}$$

and the tilt angle θ from:

$$\theta = \text{Arcsin}(x_r/h\cos\gamma) \simeq \text{Arctan}(x_r/h\cos\gamma) \tag{4.42}$$

The coordinates of the reflection point (x_r, y_r, z_r) are obtained from:

$$x_r = h' \sin \beta' + (D/2)\cos \phi$$
$$y_r = h' \sin \alpha' + (D/2)\sin \phi \qquad (4.43)$$
$$z_r = h'$$

where α' and β' are the NS and EW zenith angles respectively and h' is taken as the effective height of the ionosphere at the signal frequency being used. The construction for this situation is shown in figure 8. The zenith angles are obtained from the data record to be analysed and the effective height at intervals during the period of the record are obtained from scaled ionograms. A spline in tension (Schweikert, 1966) subroutine is used to obtain smoothly interpolated values of effective height data at the instants corresponding to the zenith angle data points.

The angle γ is converted into an azimuth angle by forming:

$$\gamma' = 90 - \gamma \qquad (4.44)$$

If γ' is negative it is brought into the range 0 to 360 degrees by adding 360 degrees to it. The resulting converted data is plotted by the computer programme. A histogram is constructed for each displayed data at the left hand end of the data, from which the mean and distribution of the data can be seen.

To assist in the interpretation of the plotted results from this procedure, data has been obtained from the TID simulation shown in figure 6 and used as input data to the procedure. The tilt data plot from the present procedure can be seen in figure 9. It can be seen that the angle γ switches through 180 degrees for each half cycle of the zenith angle variation and that the tilt angle θ undergoes a frequency doubling effect. The frequency doubling effect tends to make the tilt data difficult to interpret. A few samples of zenith angle data have been applied to this technique and appear in the next chapter. The characteristic switching through 180 degrees can be seen in a number of places in these plots.

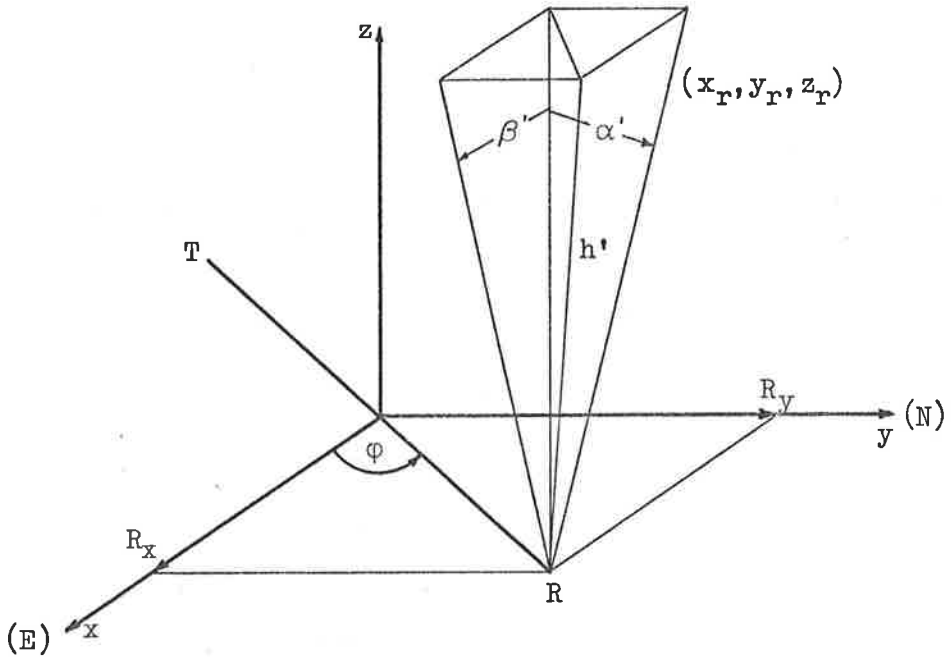

Figure 4.8 Construction for determining the reflection point in terms of zenith angles and effective height

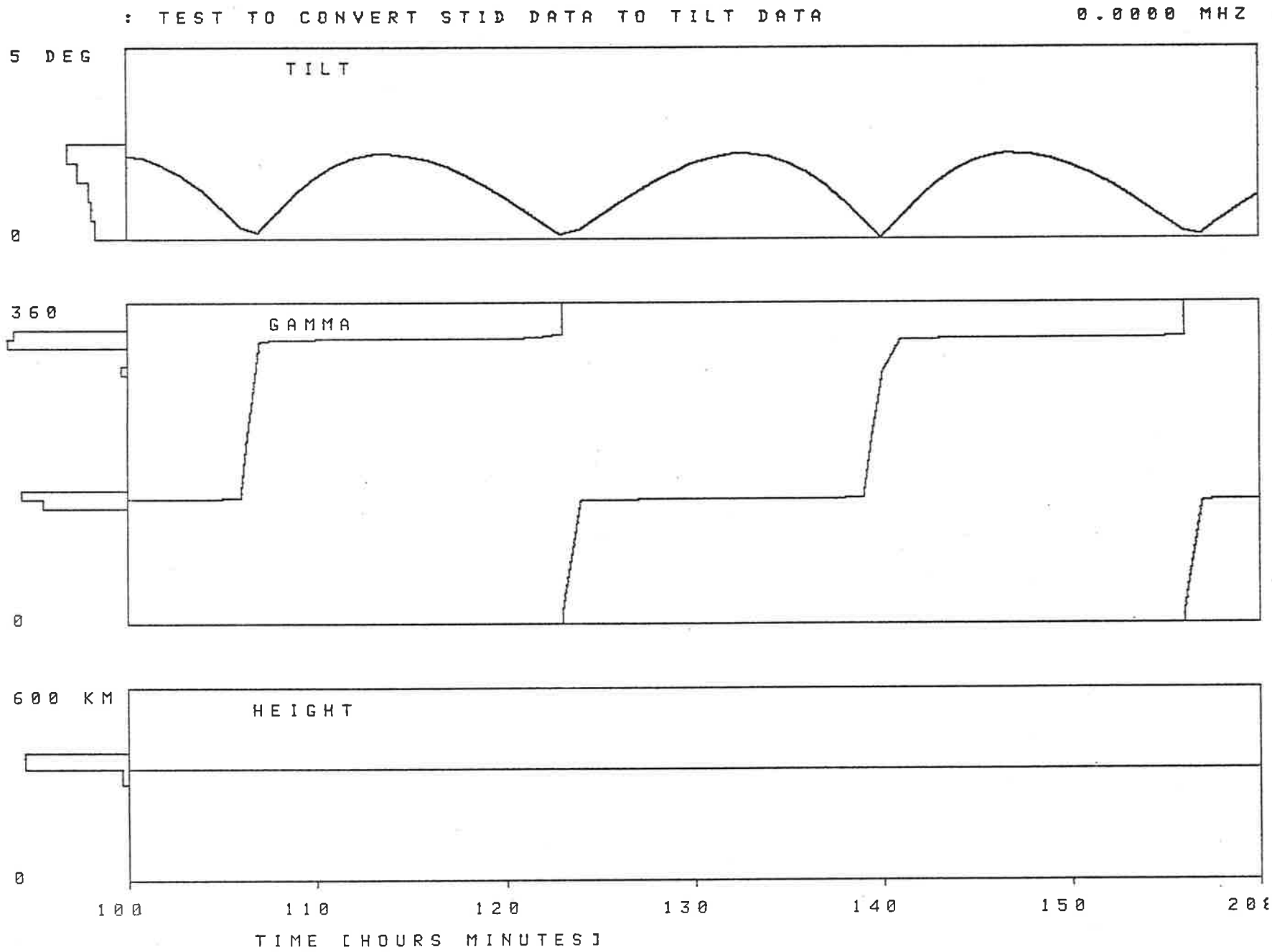

Figure 4.9 Tilt data plot of data from figure 6.

In principle it is possible to make use of the tilt angle results to obtain estimates of the amplitude and wavelength of any well defined events that appear in the tilt plots. If a complete wave period appears in the data, so that the wave period can be estimated, function minimisation techniques can be used to determine the wave parameters. A function of the following form can be used:

$$f = \sum_i \{kZ_m \sin(kW_i - \omega t_i - \phi) - \tan \theta_i\}^2 \qquad (4.45)$$

where: k,Z and ϕ are to be determined such that f is minimised.

ϕ is an arbitrary phase to allow for the time scale in use.

$W_i = x_r \cos \gamma + y_r \sin \gamma$

and θ_i is the angle of tilt.

t_i, W_i and θ_i are obtained and ω is estimated from the tilt data.

Investigations with a simple relaxation approach show that convergence can readily be achieved but that good accuracy may not always be obtained. Values of parameters obtained in this way can be checked against alternative methods of estimation, such as the use of the simulation model.

CHAPTER 5

INTERNAL GRAVITY WAVE ANALYSIS AT IONOSPHERIC ALTITUDES

5.1 THEORETICAL DEVELOPMENT

The theory of wave propagation in an idealized atmosphere suitable for application at ionospheric altitudes has been developed by Hines (1960). The basic relationships derived from this theory are given in the following treatment. These relationships are then used as a means of estimating the horizontal parameters and other characteristics of the wave motions exhibited in the processed zenith angle data.

The idealised model of the atmosphere developed by Hines makes the assumptions that the only forces that need be considered are those due to gravity, pressure gradients and inertia, with viscosity, heat transfer etc. being ignored. The gravitational field is taken to be constant and background winds are assumed to be absent. The atmosphere is assumed to be isothermal and isotropic. The constitutive equation for the fluid is taken to be the perfect gas equation:

$$p = \rho kT/m \tag{5.1}$$

where:

p is the pressure of the gas,

ρ is the mass density,

k is Boltzmann's constant,

T is the absolute temperature,

and m is the molecular mass of the gas.

The simplified equations of fluid motion are:

$$\begin{aligned} D\rho/Dt + \rho\nabla.\underset{\sim}{u} &= 0 \\ \rho\, D\underset{\sim}{u}/Dt + \nabla \underset{\sim}{p} - \rho\underset{\sim}{g} &= 0 \\ Dp/Dt - c^2 D\rho/Dt &= 0 \end{aligned} \tag{5.2}$$

where:

$\underset{\sim}{u}$ is the velocity of fluid motion,

$\underset{\sim}{g} = -g\underset{\sim}{k}$ is the acceleration due to the gravitational field. ($\underset{\sim}{k}$ is used here as a unit vector in the vertical axis direction and is also used elsewhere as the wave number vector).

t is the time,

$c^2 = \gamma p/\rho = \gamma gH$ is the square of the speed of sound,

γ is the ratio of specific heats,

$H = kT/mg$ is the scale height of the atmosphere at the altitude under consideration,

and $D/Dt = \partial/\partial t + \underset{\sim}{u}.\nabla$ is an operator called the convective time derivative and represents the rate of change with time following the motion of the quantity to which it is applied.

The first of equations (2) represents the conservation of mass within the fluid. The second equation represents the conservation of momentum transfer and is the hydrodynamic equation of motion of the gas. The third equation is the adiabatic energy equation.

Small perturbations of the variables are considered to be an adequate approximation and are represented by the primed variables as follows:

$$\begin{aligned} \rho &= \rho_o + \rho' \\ p &= p_o + p' \\ \underset{\sim}{u} &= \underset{\sim o}{u} + \underset{\sim}{u}' \end{aligned} \qquad (5.3)$$

$\underset{\sim o}{u} = 0$ since background winds are ignored.

It is also adequate to represent the horizontal direction of propagation by the single variable x taken to be in the direction of propagation of the wave. The equations are then simplified by the omission of the y direction variable. Plane wave solutions are sought of the form:

$$\frac{p'}{p_o P} = \frac{\rho'}{\rho_o R} = \frac{u_x}{X} = \frac{u_z}{Z} = A\, e^{i(\omega t - K_x x - K_z z)} \tag{5.4}$$

where ω is the frequency of the wave motion, A is an arbitrary constant and K_x, K_z are wave vector components.

The perturbation solution or linearization of equation (2) yields a matrix of coefficients to which two conditions are applied. The first of these is that the determinant of the matrix must vanish for non trivial solutions to exist. This condition gives the dispersion relation:

$$\omega^4 - \omega^2 c^2 (K_x^2 + K_z^2) + (\gamma - 1) g^2 K_x^2 - i\gamma g \omega^2 K_z = 0 \tag{5.5}$$

The second condition is that any three of the quantities P, R, X or Z can be solved as a ratio with the fourth of these quantities, to give the polarization relations relating to air parcel motions.

The form of the solutions taken is:

$$\begin{aligned} P &= \gamma\omega^2 K_z - i\gamma g\omega^2/c^2 \\ R &= \omega^2 K_z + i(\gamma - 1) g K_x^2 - i\gamma g\omega^2/c^2 \\ X &= \omega K_z K_x c^2 - ig\omega K_x \\ Z &= \omega(\omega^2 - K_x^2 c^2) \end{aligned} \tag{5.6}$$

To obtain real solutions of the dispersion relation (5), K_x is taken as purely real and allowed solutions of K_z are found. A choice of solution of K_z is taken such that vertical propagation of phase is provided for. This choice is appropriate for the representation of internal waves. K_x and K_z are taken as:

$$\begin{aligned} K_x &= k_x \\ K_z &= k_z + i\gamma g/2c^2 = k_z + 1/2H \end{aligned} \tag{5.7}$$

Substitution of these values into (5) gives the real valued dispersion relation:

$$k_z^2 = \frac{\omega_g^2 - \omega^2}{\omega^2} k_x^2 - \frac{\omega_a^2 - \omega^2}{c^2} \tag{5.8}$$

where:

$$\omega_g^2 = (\gamma-1)g^2/c^2 \tag{5.9}$$

is the square of the gravity wave cut off frequency, and $\tau_g = 2\pi/\omega_g$ is the period of this cut off frequency. ω_g is sometimes referred to as the Brunt frequency and corresponds to the natural frequency of oscillation of an air parcel in an isothermal atmosphere after being displaced vertically:

$$\omega_a = \gamma g/2c \tag{5.10}$$

is the acoustic cut off frequency.

When suitable values of γ ,g and H for an isothermal atmosphere are substituted into the dispersion relation (8) it is found that $\omega_g < \omega_a$ and that values of ω lying between ω_g and ω_a do not permit non complex solutions of (8). The wave effects considered in this paper have meaningful values of ω below ω_g and consequently emphasis will be placed on these waves, referred to as gravity waves. To a good approximation for this case (8) can be written as the asymptotic approximation:

$$k_z^2 = \frac{\omega_g^2 - \omega^2}{\omega^2} k_x^2 \tag{5.11}$$

The dispersion relation in the form of (8) provides the means of establishing the relationships between the different velocities that can be defined for atmospheric waves. The definitions of these velocities will be considered briefly. The velocities of interest here are the velocities with which the shape or outline of the wave motion propagates rather than the velocities of individual air parcels. Some care needs to be taken when relating measured velocities to the theory. This point has been been noted by Hines (1974).

Perturbation parameters of an individual plane wave are described with the aid of a phase:

$$\phi = \omega t - \underset{\sim}{k}.\underset{\sim}{r} + \phi_o \tag{5.12}$$

the definition of phase velocity from this can be seen by setting ϕ and ϕ_o equal to zero. The resulting expression:

$$t - x/V_{px} - y/V_{py} - z/V_{pz} = 0 \qquad (5.13)$$

where:

$$V_{px} = \omega/k_x \quad , \quad V_{py} = \omega/k_y \quad , \quad V_{pz} = \omega/k_z$$

represents a plane in 3 dimensions, the phase plane, the normal to which is given by:

$$\underset{\sim}{i}/V_{px} + \underset{\sim}{j}/V_{py} + \underset{\sim}{k}/V_{pz}$$

The significant component velocities are the phase trace velocities V_{px}, V_{py}, V_{pz}. Returning to two dimensions, the phase trace velocities are therefore related by an expression of the form:

$$1/V_p^2 = 1/V_{px}^2 + 1/V_{pz}^2 \qquad (5.14)$$

The phase velocity is applicable to an infinite plane wave, which is an unrealisable mathematical abstraction. However, the phase velocity is thought to provide an adequate description of the wave motion in certain respects. A more realistic concept for the description of a travelling wave shape is that of the group velocity in which a superposition of plane waves in a narrow region about a central frequency ω is considered.

The usual definition of group velocity given in the literature is:

$$\underset{\sim}{V}_g = \nabla_k \omega(k) \qquad (5.15)$$

from which the component velocities are vector components given by:

$$V_{gx} = (\partial\omega/\partial k_x)_{k_z} \quad , \quad V_{gz} = (\partial\omega/\partial k_z)_{k_x} \qquad (5.16)$$

Alternatively, a group plane can be defined by applying the condition of "stationary phase", to the phase (12) to give:

$$0 = (d\phi/d\omega) = t - (dk_x/d\omega)x - (dk_z/d\omega)z + (d\phi_o/d\omega) \qquad (5.17)$$

If $d\phi_o/d\omega$ is set equal to zero, equation (17) represents a plane, the group plane with component velocities:

$$V_{gx} = d\omega/dk_x \quad , \quad V_{gz} = d\omega/dk_z \qquad (5.18)$$

The significant component velocities are again trace velocities, or group trace velocities, given by (18), which are related by an expression of the form of (14), with phase subscripts replaced by group subscripts. The discussion of this subject is continued more critically in appendix F where it is shown that if V_{gx}, V_{gz} in (16) are considered to be vector components then at low frequencies the group velocity will exceed the phase velocity by an amount which is limited only by the extent to which the theoretical derivation is valid.

Further abstraction is possible but, for present purposes it will be considered that the observed wave motions are adequately described by the phase and group velocities.

An approximate measurement of the vertical phase velocity is obtained from the zenith angle data by use of cross spectral analysis of the data for two radio wave frequencies to obtain time differences for selected frequency components of the atmospheric waves, and by use of real height analysis to obtain a height difference for the reflection points of the two signals. On the assumption that this velocity represents the vertical phase velocity of the atmospheric wave component, all the remaining velocities, wavelengths and angles of propagation for the wave components can be determined from the dispersion relation (8), if suitable values are chosen for the quantities γ, g, and H. However, since (8) is quadratic in the wave vector components k_x and k_z the signs of the horizontal velocities and angles are undetermined. The required steps to carry out the complete gravity wave analysis will be presented.

Considering the spectral analysis of the zenith angle data it is found that the spectra typically exhibit a low frequency pass band characteristic with a cut off corresponding to the Brunt cut off frequency. The appearance of the spectra does not in general permit a description in terms

of discrete spectral components. The spectra do however give a small number of power spectral density estimates in the pass band portion of the spectra. The phase data $\theta_{xy}(f)$ (see section 2.9) for these estimates from the cross spectral analysis of the zenith angle data permit an estimate to be made of the time difference for the occurence of zero phase for each of these two signals from the relation:

$$\Delta t = \theta_{xy}(f)/\omega \tag{5.19}$$

The vertical phase velocity is then estimated from:

$$V_{pz} = \Delta h/\Delta t \tag{5.20}$$

where Δh is the real height difference in the reflection points of the two e.m. signals. Computations can then be continued in the following order:

$$k_z = \omega/V_{pz} \tag{5.21}$$

$$k_x = \frac{\omega}{c}\sqrt{\frac{c^2k_z^2 + \omega_a^2 - \omega^2}{\omega_g^2 - \omega^2}} \tag{5.22}$$

$$V_{px} = \omega/k_x \tag{5.23}$$

Expression (22) is obtained directly from the dispersion relation (8) by rearrangement. The group velocities can then be obtained from:

$$V_{gx} = \frac{\partial\omega}{\partial k_x} = \frac{V_{px}(\omega_g^2 - \omega^2)}{\omega_g^2 - \omega^2 V_{px}^2/c^2} \tag{5.24}$$

$$V_{gz} = \frac{\partial\omega}{\partial k_z} = \frac{-\omega^2 V_{px}^2}{V_{pz}(\omega_g^2 - \omega^2 V_{px}^2/c^2)} \tag{5.25}$$

The angle of phase propagation is given by:

$$\chi = \text{Arctan}\,(k_z/k_x) \tag{5.26}$$

The maximum possible angle of phase propagation for a given wave frequency (ω) is, from (11):

$$\theta = \text{Arctan}\sqrt{(\omega_g^2/\omega^2 - 1)} \tag{5.27}$$

The angle of group propagation is given by:

$$\phi = \text{Arctan}\,(V_{gz}/V_{gx}) \tag{5.28}$$

when the component velocities V_{gx}, V_{gz} are considered to be vector components. The direction of group propagation is found to be opposite to that of phase propagation in the vertical direction.

The horizontal and vertical wavelengths are found from:

$$\lambda_x = 2\pi/k_x \ , \quad \lambda_z = 2\pi/k_z \tag{2.29}$$

The wave vector k is found from:

$$k = \sqrt{k_x^2 + k_z^2} \tag{5.30}$$

and the corresponding wavelength is:

$$\lambda = 2\pi/k \tag{5.31}$$

The phase velocity for the wave motion is found from:

$$1/V_p^2 = 1/V_{px}^2 + 1/V_{pz}^2 \tag{5.32}$$

Group velocity is calculated both in terms of components as vector or trace components from:

$$V_{gV}^2 = V_{gx}^2 + V_{gz}^2 \quad \text{(vector components)} \tag{5.33}$$

and

$$1/V_{gT}^2 = 1/V_{gx}^2 + 1/V_{gz}^2 \quad \text{(trace components)} \tag{5.34}$$

The direction of energy flow is in the direction of group propagation. The complement of angle (28) will need to be taken if the group velocity is considered to have trace components, as described in appendix F.

The air parcel orbits can be found from the polarization relations (6). The air parcels participating in the wave motions execute elliptical paths. Two quantities related to these orbits can be found from (6). Under the assumption of small ω, these are the angle of tilt of the major axis of the ellipse with the horizontal, given by:

$$\phi_{tilt} = -\tfrac{1}{2}\text{Arctan} \frac{k_z}{k_x}\left(1 - \frac{\omega_g^2}{2\omega^2}\right)^{-1} \tag{5.35}$$

and the x to z axial ratio R of the ellipse:

$$R = \left\{ \frac{\sin^2\phi_{tilt} - 2(k_z/k_x)\cos\phi_{tilt}\,\sin\phi_{tilt} + (\omega_g^2/\omega^2 - 1)\cos^2\phi_{tilt}}{\cos^2\phi_{tilt} + 2(k_z/k_x)\cos\phi_{tilt}\,\sin\phi_{tilt} + (\omega_g^2/\omega^2 - 1)\sin^2\phi_{tilt}} \right\}^{\frac{1}{2}} \quad (5.36)$$

Expressions (35) and (36) have been taken from Georges (1967).

5.2 NUMERICAL RESULTS OF THE ANALYSIS

All of the required calculations are carried out by a computer programme when fed with values of γ, H (km), ω (as a period in units of minutes), $\theta_{xy}(f)$ (degrees), the real height separation Δh (km) and the real height of reflection averaged over the period of the sample of zenith angle data. The value of g is calculated from the real height of reflection z, From (C.I.R.A. 1972):

$$g = 9.793 - 3.086\times10^{-6} z + 7.258\times10^{-13} z^2 \quad (5.37)$$

The calculations are carried out in units of meters, seconds and radians and listed in the more familiar units of kilometers for wavelength, minutes for periods, degrees for angles and meters per second for velocities.

A suitable value for γ is 1.4 for F region heights. Values for H are taken from the real height analysis averaged over the period of the sample of zenith angle data using the method described in section 2.12. Values for H can be compared with values taken for convenience from the Cospar International Reference Atmosphere (1965). Values of H of between 35 km and 45 km are given depending on the time of day and on the solar flux value of $\bar{F}_{2.7}$. A value of averaged flux of 75×10^{-12} W/m^2 c/s has been assumed corresponding to model 2 of the 1965 C.I.R.A. This value is close to the value of solar flux for December 1975 given by Lincoln (1976). The value of H obtained from the real height analysis is slightly higher than the values of H obtained from C.I.R.A. (1965).

Values of the phase $\theta_{xy}(f)$ of the cross spectrum are taken from the spectral analysis using the method of smoothing described in appendix B. Two hour samples of data have been used for the analysis. Longer samples than this would have been desirable from the point of view of increasing the number of estimates in the gravity wave part of the spectrum and of obtaining spectral estimates at lower frequencies. However, longer samples are found to have increased variability of modes effecting the state of the sample and the dynamic range of the spectra are decreased.

Data from Kersbrook test W354 20/12/75 has been used to provide an example of the complete analysis. A two hour sample of data has been taken from 1435 to 1635 hours. Two zenith angle plots of the data are shown in figures 1 and 2. Figure 1 shows equally spaced data, processed as described in section 2.8, that is applied to the spectral analysis programme. The zenith angle plot shown in figure 2 has been further smoothed with the FFT low pass filter described in section 2.10. This sample of data has been taken from the data used for illustrating the appearance of unfiltered data shown in figure 3.12. Ionograms for the period 1430 to 1645 hours are shown in figure 3. It can be seen from the ionograms that reflection from the F region occured throughout the period of the sample. Some activity related to TID's can be seen in figure 3, such as the forked f_oF_2 trace at 1435 hours, however, it is difficult to relate events in the zenith angle plots to events in the sequence of ionograms, as has been mentioned in chapter 4. Spectra for the north-south and east-west components of the data are shown in figure 4. Phase angle data are taken from the low frequency portion of the cross spectrum and below the gravity wave cut off frequency, where the coherence squared function has values greater than 0.5 (-3db). Wave periods of 40, 24 and 17.14 minutes are used in the tabulation of results. Data from the real

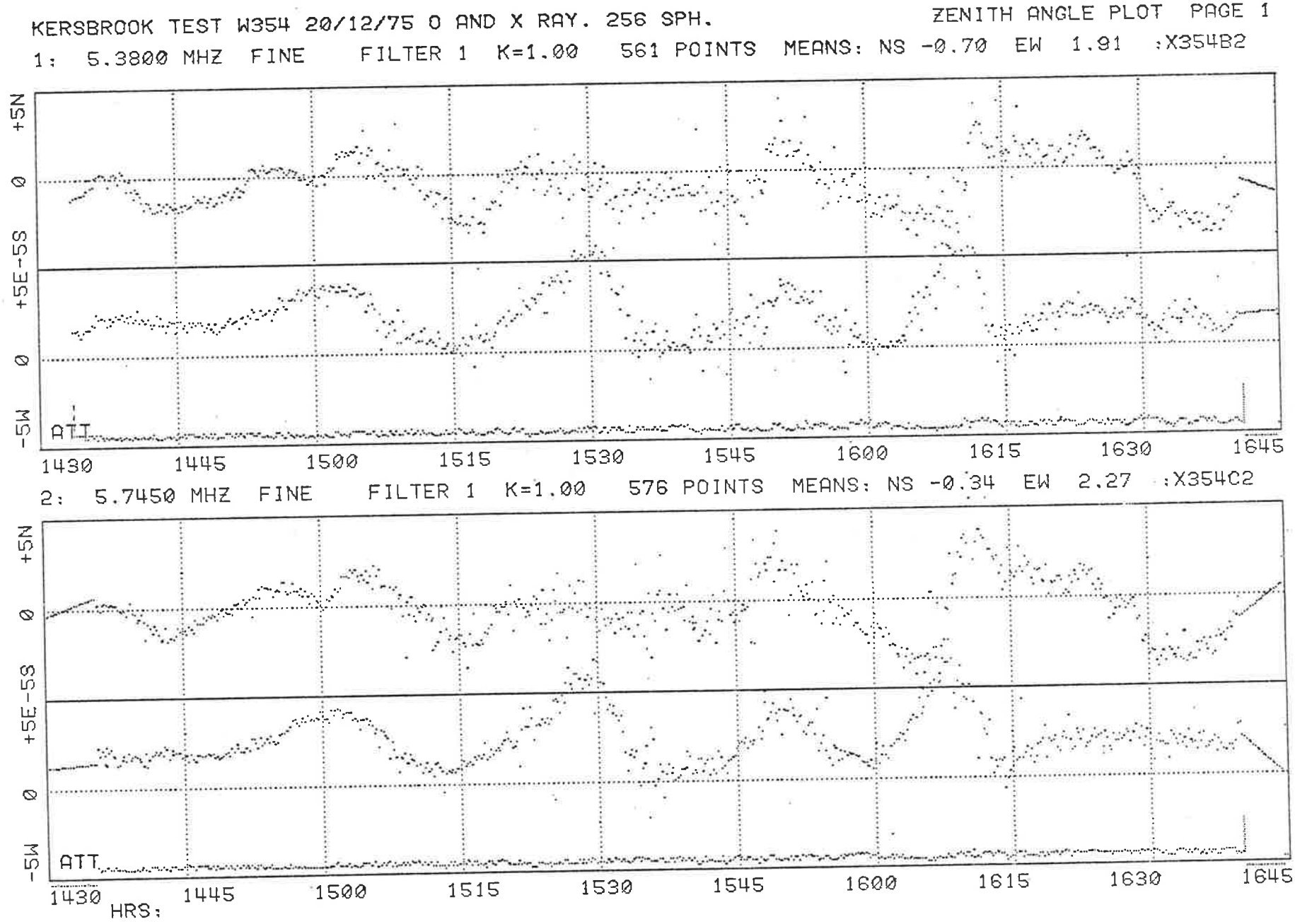

Figure 5.1 Zenith angle plot of evenly spaced data : W354 O-ray

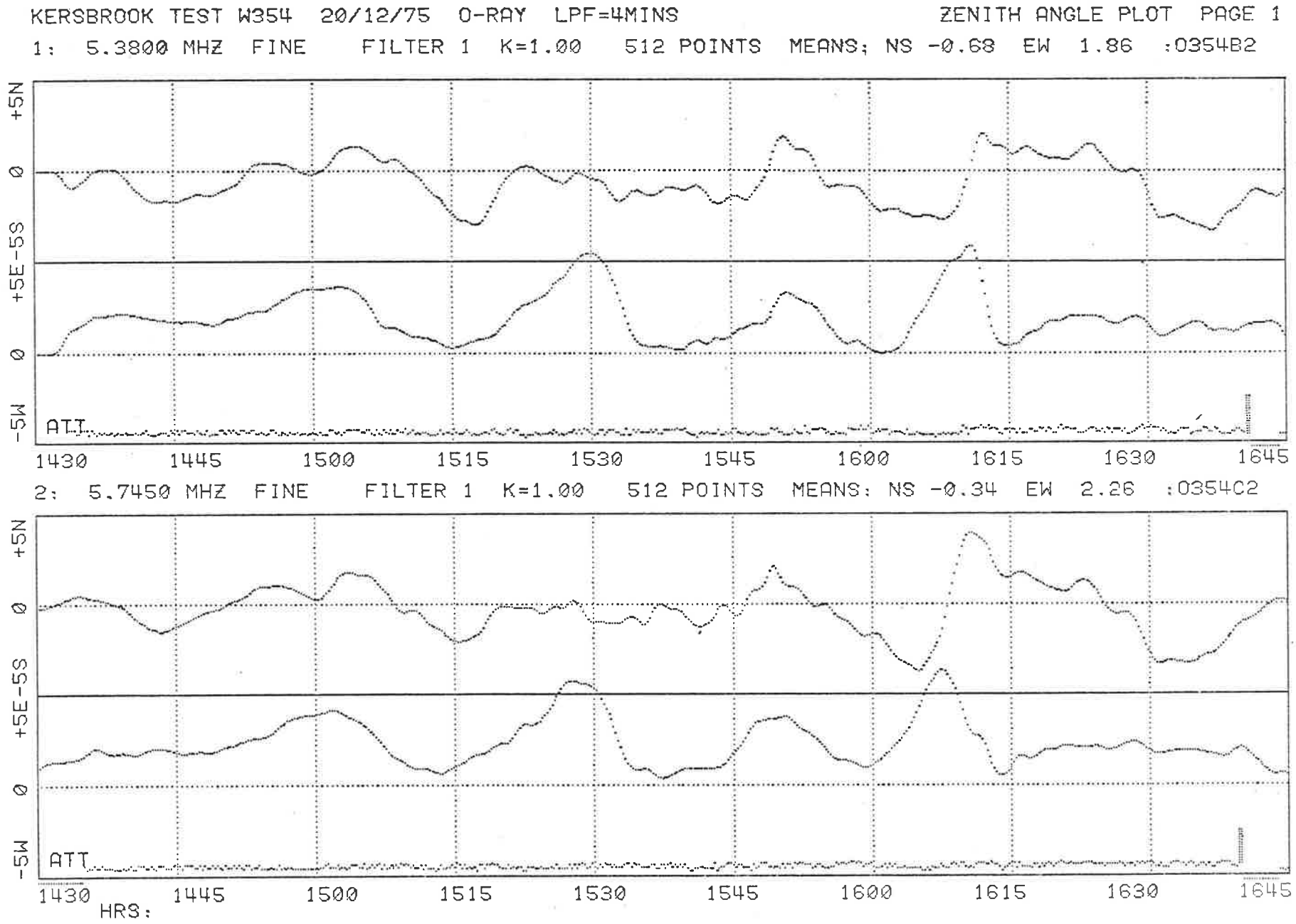

Figure 5.2 Zenith angle plot of low pass filtered data: W354 O-ray

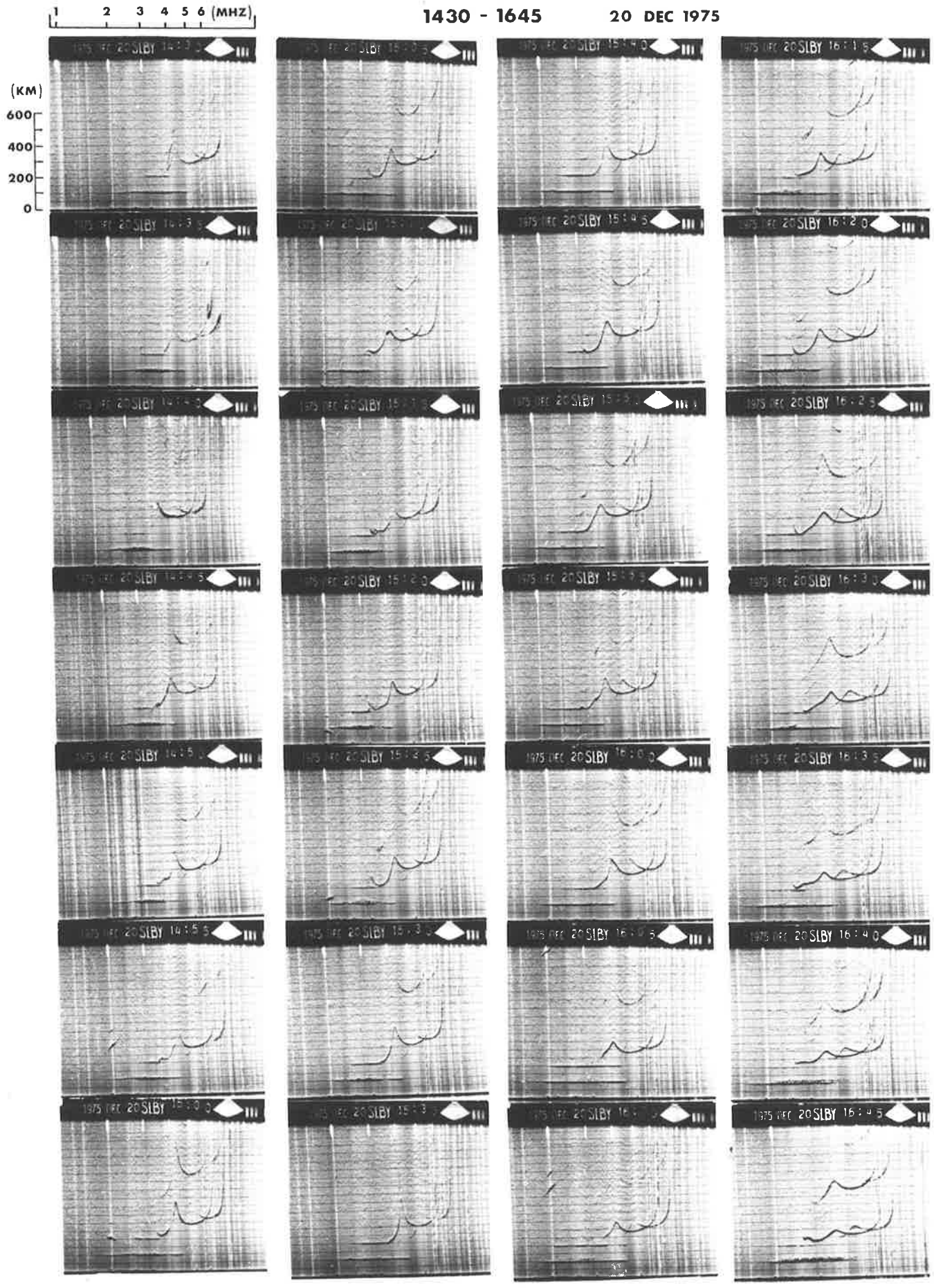

Figure 5.3 Series of ionograms for the period 1430 to 1645 hours: W354

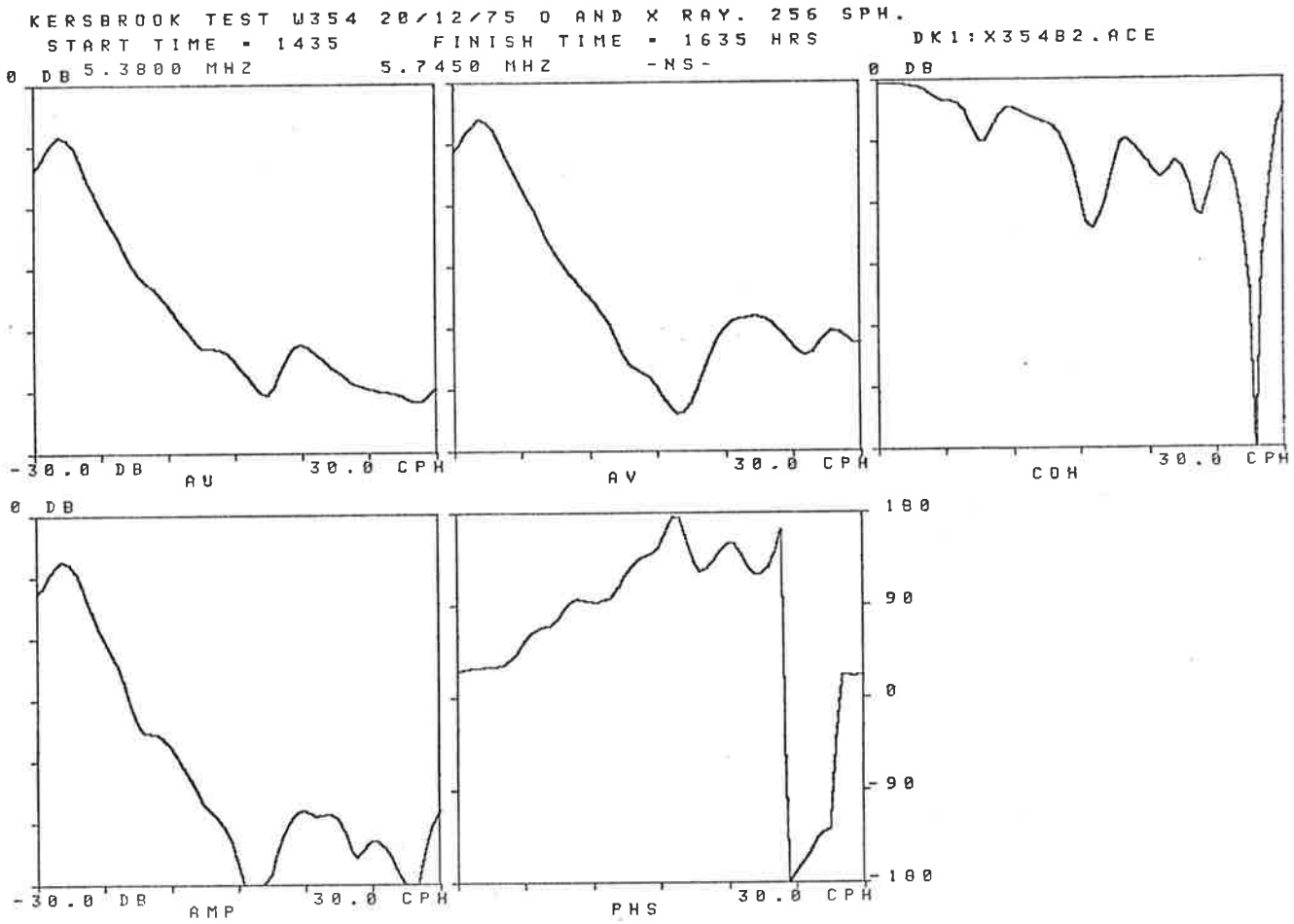

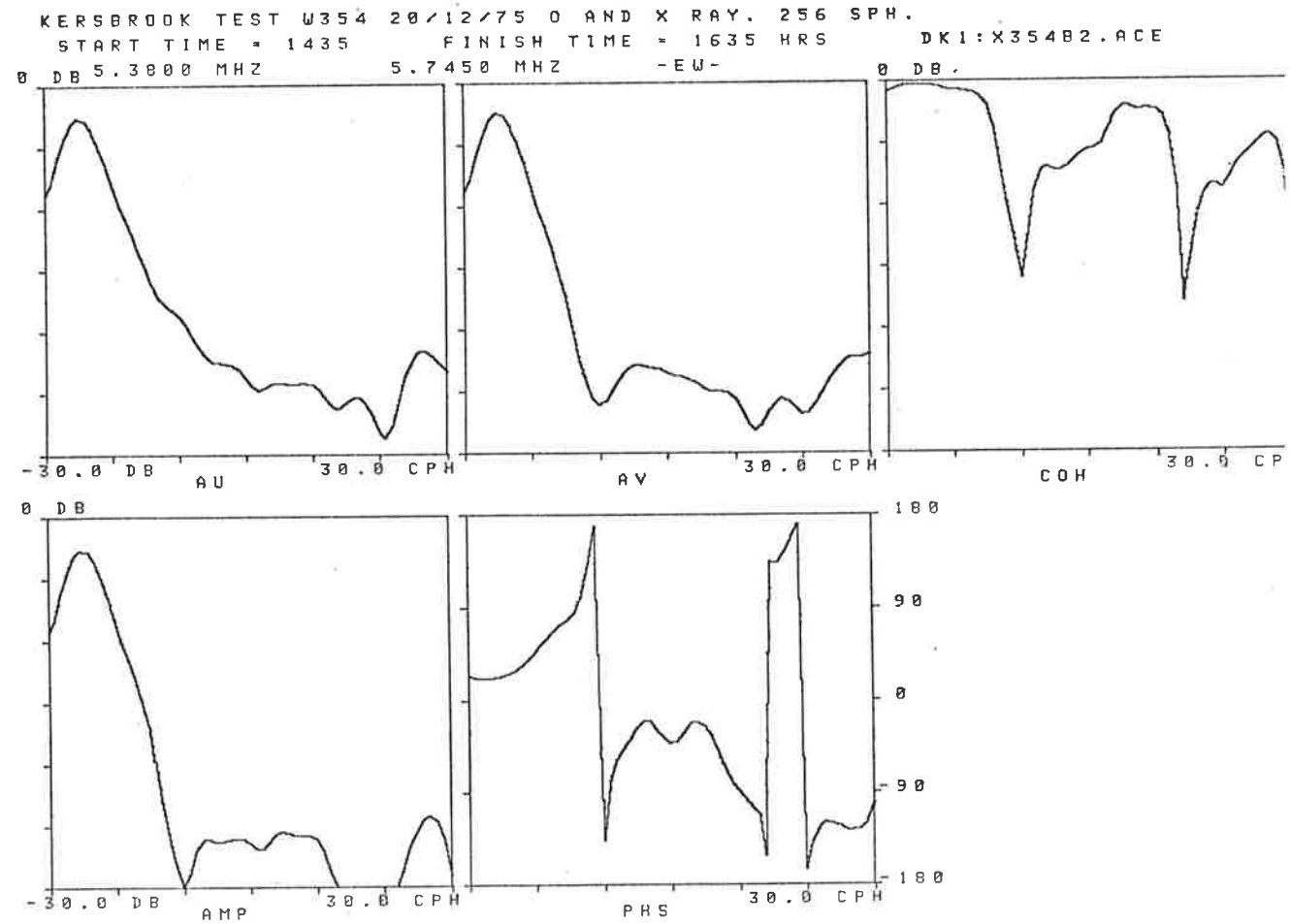

Figure 5.4 Spectral plots of NS and EW components of zenith angle data: W354 O-ray

height analysis has been plotted in figure 5. An average value for the difference in real height of reflection for the 5.38 Mhz and 5.745 Mhz signals of 8.3 km has been taken for the period of the sample.

Relevant numerical data has been collected together in table 5.1.

Horizontal phase velocities shown in table 1 display a negative dispersion, i.e. the velocity decreases with increasing frequency, whereas vertical phase velocities display a positive dispersion. This results in maximum phase velocities occuring at intermediate wave periods. The table also shows that the horizontal velocity of the wave increases with increasing wavelength. In each case, the angle of phase propagation χ is very close to the asymptotic limit θ indicating that the asymptotic approximation is relevant for the data. This can also be seen in the k_x, k_z dispersion diagram shown in figure 6, where the hyperbolic curves of constant ω are seen to be essentially straight lines except near the origin. This is further seen in the values shown for the angle of tilt ϕ_{tilt} of the major axis and ratio R of the axis of the elliptical air parcel orbits, which show that the air parcel motions are very nearly transverse to the direction of phase propagation. The angles χ, θ, ϕ, and ϕ_{tilt} are all given with respect to the horizontal. The direction of phase propagation is downwards as can be seen from the zenith angle plots. Consequently the direction of positive angle is downwards for angles given in the table. The approximation for ϕ_{tilt} and R, based on a small value for ω, produced invalid results for the 17.14 minutes wave component, and are not shown.

The north-south and east-west wave vector components have been added vectorially to give the combined horizontal wavelengths and velocities shown at the bottom of table 1, together with the four possible bearing angles resulting from the ambiguity introduced into the sign of k_x by the

Table 5.1 Gravity wave analysis from experimental data

Kersbrook test W354 20/12/75 O-ray 1435-1635 Hours
Signal frequencies: 5.38, 5.745.Mhz

Scale Height, H=	58.18	km
Acceleration due to gravity, g=	9.16	m/s/s
Ratio of specific heats =	1.40	
Real height separation =	8.30	km
Real height of reflection =	216.00	km
Speed of sound, c=	863.79	m/s
Brunt period =	15.61	minutes
Acoustic cut off period =	14.11	minutes

Wave period (minutes)		N-S Components 40.00	24.00	17.14	E-W Components 40.00	24.00	17.14
$\theta_{xy}(f)$	(deg)	28.83	30.22	32.23	21.84	23.59	28.60
Δt	(min)	3.20	2.01	1.53	2.43	1.57	1.36
λ_z	(km)	103.6	98.9	92.7	136.8	126.7	104.5
λ_x	(km)	242.3	114.7	41.9	317.9	146.4	47.2
λ	(km)	95.3	74.9	38.2	125.7	95.8	43.0
χ	(deg)	66.84	49.25	24.31	66.71	49.14	24.30
θ	(deg)	67.03	49.42	24.37	67.03	49.42	24.37
V_{pz}	(m/s)	43.2	68.7	90.1	57.0	88.0	101.6
V_{px}	(m/s)	101.0	79.7	40.7	132.4	101.7	45.9
V_p	(m/s)	39.7	52.0	37.1	52.4	66.5	41.8
V_{gz}	(m/s)	-36.0	-39.3	-15.3	-47.1	-50.1	-17.2
V_{gx}	(m/s)	85.8	46.1	6.9	112.7	59.0	7.8
V_g	(m/s)	93.0	60.6	16.8	122.1	77.4	18.9
ϕ	(deg)	-67.20	-49.59	-24.42	-67.33	-49.69	-24.44
ϕtilt	(deg)	-22.85	-40.56		-22.76	-40.54	
R		21.1	18.6		16.1	14.5	
k_z	($\times 10^{-6}$)	60.624	63.547	67.773	45.925	49.605	60.140
k_x	($\times 10^{-6}$)	25.927	54.758	150.020	19.767	42.907	133.216
k	($\times 10^{-6}$)	65.935	83.885	164.619	49.999	65.587	146.163
V_{gT}	(m/s)	33.2	29.9	6.3	43.4	38.2	7.1

Combined components

λ_x	(km)	192.72	90.32	31.32
V_x	(m/s)	80.30	62.72	30.45
α	$\pm$(deg)	37.32	38.08	41.60
180- α	$\pm$(deg)	142.68	141.92	138.40

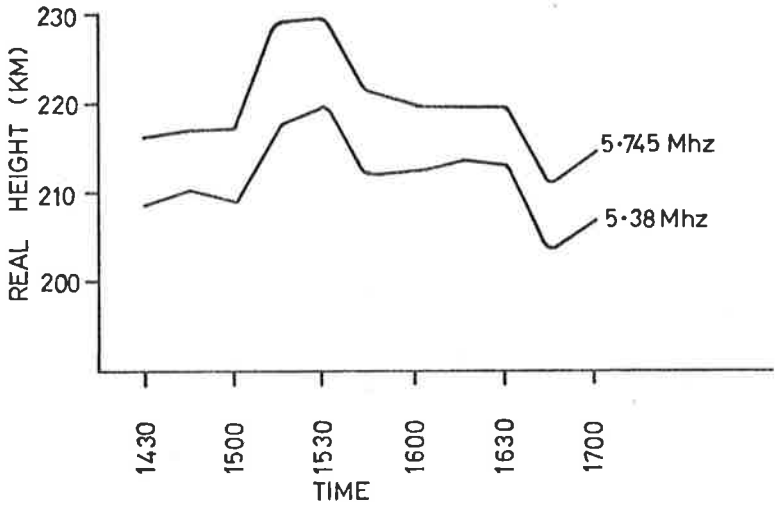

Figure 5.5 True height analysis for 5.38 Mhz and 5.745 Mhz signals : W354 O-ray

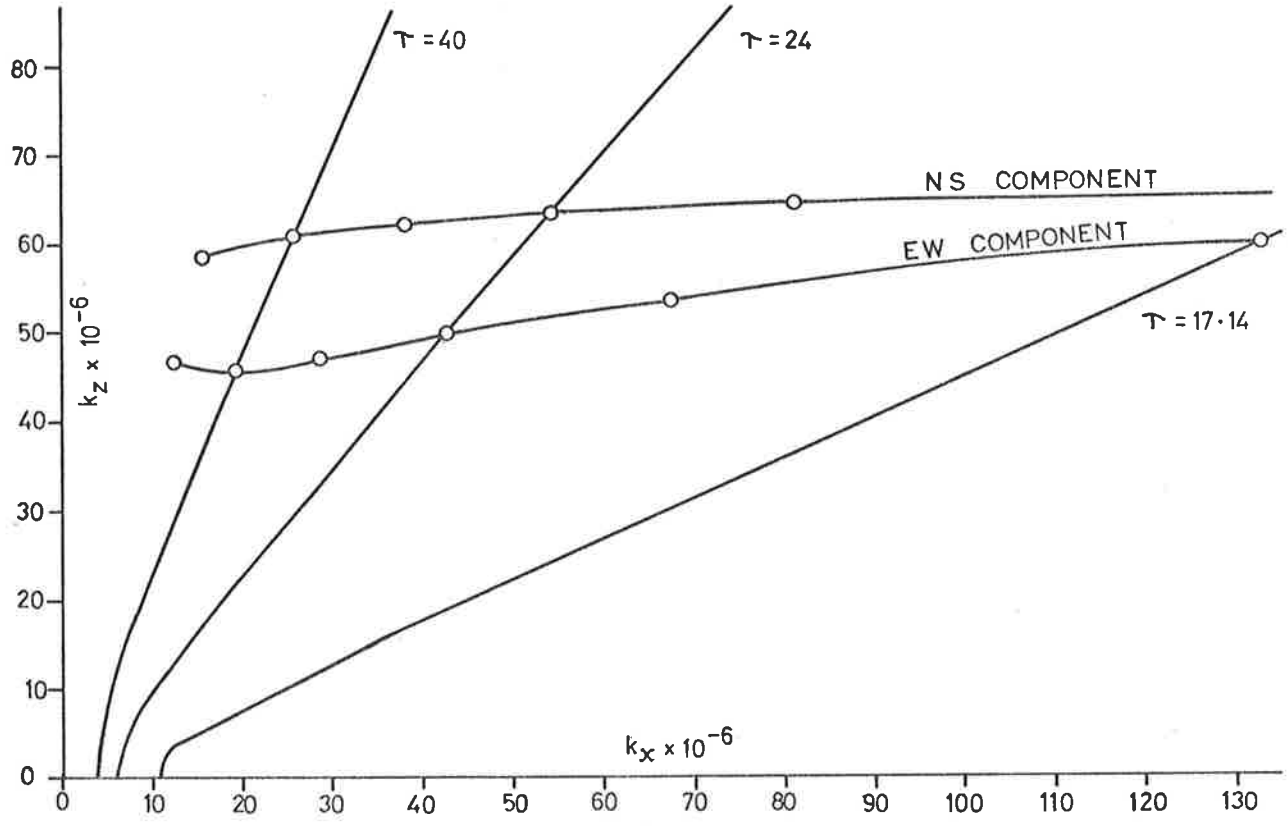

Figure 5.6 k_x, k_z dispersion plot : W354 O-ray

quadratic nature of the dispersion relation.

The velocities obtained by this analysis are comparable, although somewhat lower in this example, to values reported in the literature. For example Herron (1974) gives horizontal phase velocities ranging from 100 m/s at a wave period of 200 minutes to 300 m/s at a wave period of 20 minutes, the sense of dispersion being positive. Munro (1958) gives horizontal speeds of the order of 130 m/s but without dispersion results. Davies and Jones (1971) give their average horizontal velocity for TID's as 200 m/s but do not allow for dispersion. Dispersion curves for horizontal components have been given by Ahmed (1977), which show that both positive and negative dispersion is possible. The different types of dispersion are attributed to different source mechanisms and propagation conditions. A summary of early TID observations giving horizontal speeds and wavelengths is given by Friedman (1966).

Of the four possible bearing angles for the overall average direction of TID movement given by table 1, the angle marked $(180 - \alpha)$ gives values closest to the values of bearings for TID's for December given by Munro (1958). Chapter 4 has described three techniques for determining the directions of individual TID's as seen in the zenith angle data. These are the use of a tilt plot, the use of a polar plot and the use of the simulation plots shown in figure 4.7 in conjunction with a zenith angle plot. The latter method gives the sense of the direction, whereas either of the first two methods gives the bearing angle but not the sense. A tilt plot for the period 1430 to 1645 hours is shown in figure 7 and polar plots are shown in figure 8. The prominant event that occured between 1520 and 1545 hours seen on the tilt plot clearly had a bearing of 85 degrees, which agrees with both the polar plot and the zenith angle plot, with the sense being determined from the zenith angle plot. Considering the remainder of

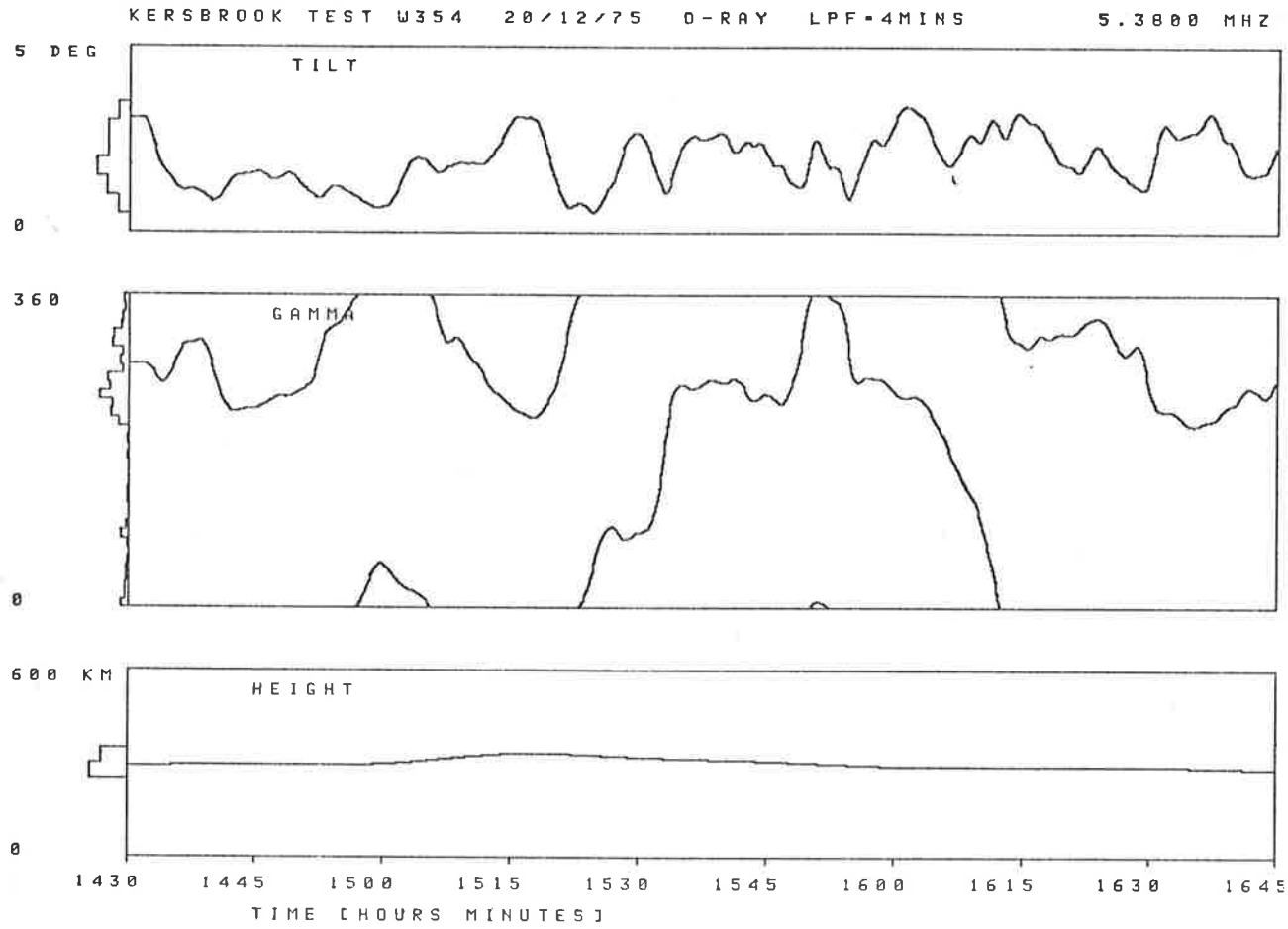

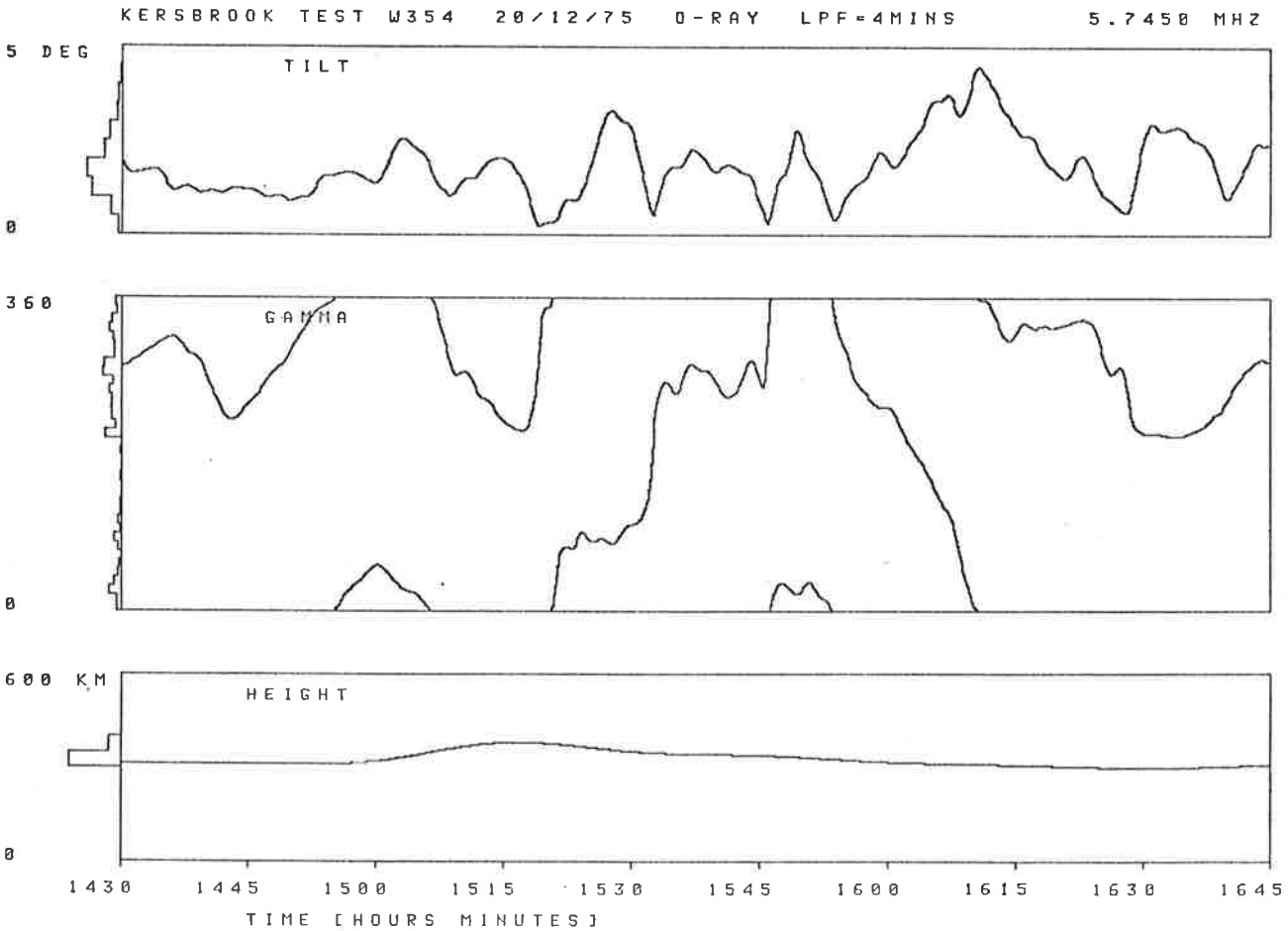

Figure 5.7 Tilt plots for the period 1430 to 1645 hours: W354 O-ray

AUTOCELL DATA POLAR PLOT 2/10/77 PAGE 1
KERSBROOK TEST W354 20/12/75 O-RAY LPF=4MINS
FROM 1435 TO 1535 K=1.000 228 228 0 0 POINTS
1: 5.3800 MHZ FINE FILTER 1 K=1.00 FILE DK1:0354B2.ACE
2: 5.7450 MHZ FINE FILTER 1 K=1.00 FILE DK1:0354C2.ACE

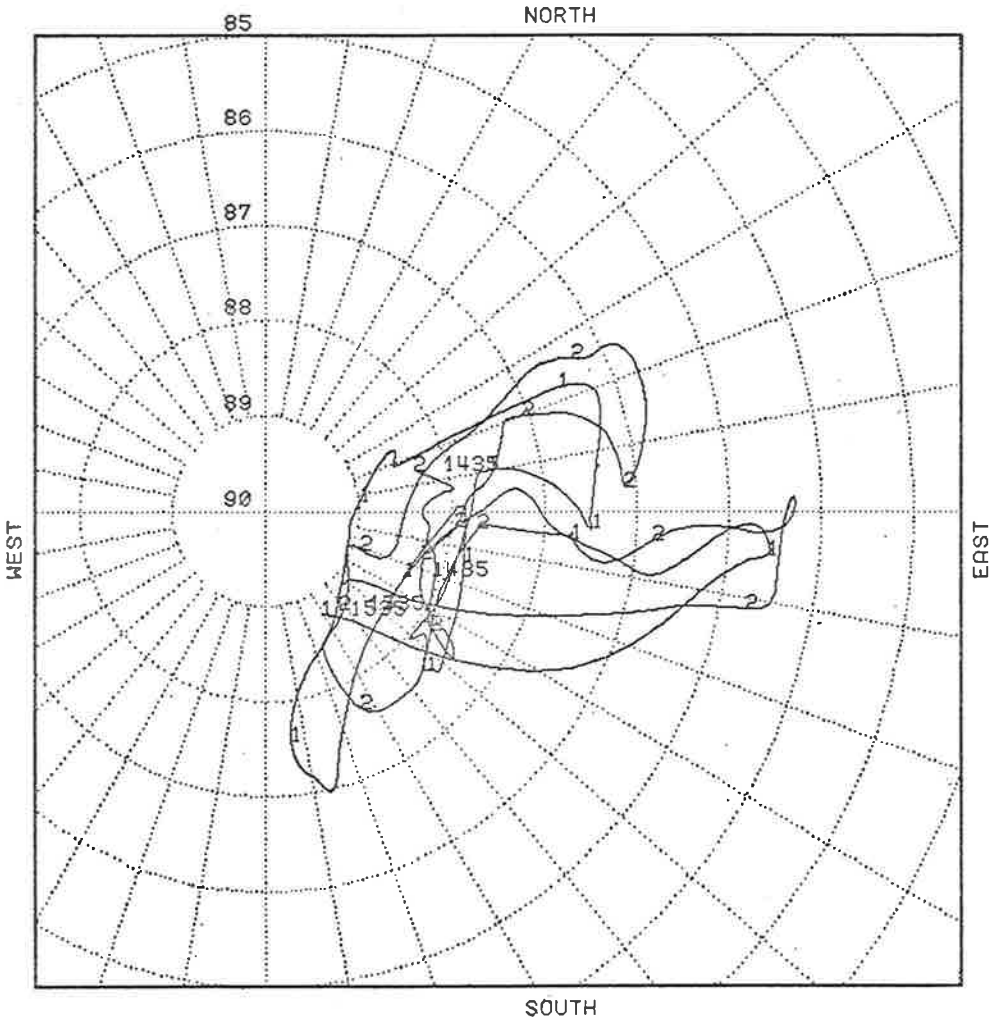

ELEVATION ANGLE V AZIMUTH (10 DEGREES)

AUTOCELL DATA POLAR PLOT 2/10/77 PAGE 2
KERSBROOK TEST W354 20/12/75 O-RAY LPF=4MINS
FROM 1535 TO 1635 K=1.000 227 227 0 0 POINTS
1: 5.3800 MHZ FINE FILTER 1 K=1.00 FILE DK1:0354B2.ACE
2: 5.7450 MHZ FINE FILTER 1 K=1.00 FILE DK1:0354C2.ACE

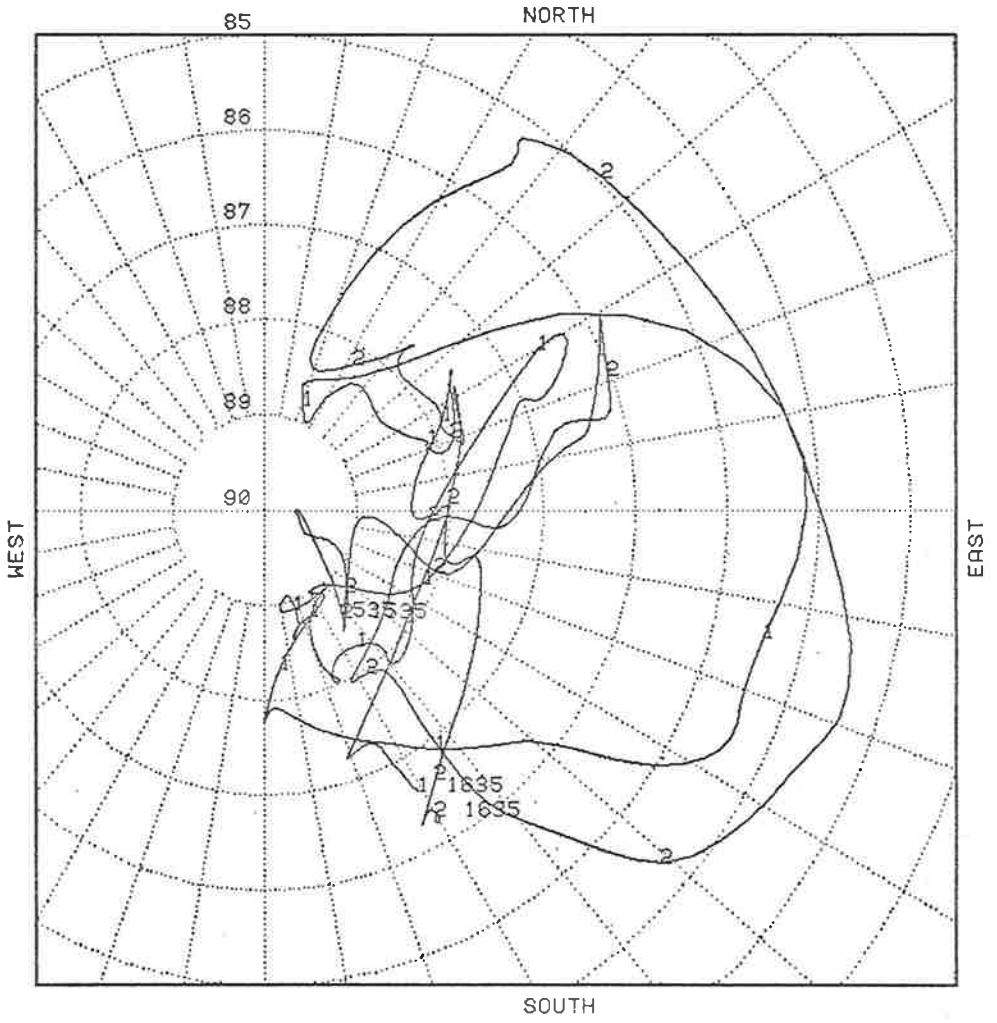

ELEVATION ANGLE V AZIMUTH (10 DEGREES)

Figure 5.8 Polar plots of zenith angle data: W354 O-ray

the plot it is seen that a number of events occur in sequence, some with indicated directions which are appreciably different between one event and the next. Scarcely any of the events, besides the one mentioned above, completes a whole cycle before the next event starts to take place. Consequently it is difficult to assess visually whether any one direction is dominant for comparison with the gravity wave dispersion results. Some method of determining and adding vectorially the velocities of each individual event would be necessary for resolving this comparison.

5.3 DISCUSSION

In considering the results of the dispersion analysis the following practical considerations should be taken into account. Both the cross spectral phase measurement and the real height difference in reflection points represent comparatively small differences in fairly large values. Some care is needed in the scaling of ionograms to obtain the required accuracy. Some degree of correlation is introduced into adjacent values of the phase of the cross spectrum by spectral averaging and also by the application of the cosine bell function. This can result in errors to the phases of adjacent fourier components. The procedures applied in the spectral analysis are a compromise between the effects of noise inherent in the data and the effects introduced by the procedures themselves. A cross correlation analysis can also be used to obtain a time difference in place of the use of (19), however, in this case only one value of time difference is obtained corresponding to the dominent part of the spectrum and this value will have the significance of an average when the spectrum of the data represents a band of frequency components.

The reflection points for the two signals are not truly vertically spaced, due to the occurrence of the spitze discussed in chapter 4. The

horizontal offset of the reflection points would, however, be small for two signal frequencies closs together and with the same polarization. The horizontal offset between the reflection points for the O-ray and the X-ray for a given signal frequency, in an extreme case close to the critical frequency may be of the order of 10 - 15 km in a north-south direction, but is more typically a few kilometers. The offset of the O-ray is appreciably greater than the offset of the X-ray. Any errors introduced by the spitze could be expected to be less when the X-ray is in use than when the O-ray is in use.

The sample of data used for the above analysis represents comparatively stationary F mode reflection conditions. The more general case is for mixed modes to be present. The phase measurement circuitry would tend to accept the dominant mode resulting in switching between modes when multimode conditions are present, reducing the correlation between data for different signal frequencies. The zenith angle data has been shown to consist of a number of partial events rather than one continuous single event. The real height of reflection may vary appreciably during the period of the sample and the signal frequencies used may vary their position with respect to the critical frequency. Therefore both the cross spectral phase values and the real height differences in reflection points represent averages over the conditions prevailing during the sample.

The values of the gravitational constant g and the ratio of specific heats γ are thought to be known to sufficient accuracy for the gravity wave analysis, although a value of 1.5 for γ has been used by some authors. The values calculated for the scale height H may, however, not be correct, depending on the validity of the assumptions underlying the derivation given in appendix D. If the parabolic layer model applicable to the F_1 layer is in fact more nearly correct, the value of H obtained would be

reduced by a factor of $1/\sqrt{2}$. The changes to the calculated values of table 1 that would result are shown in table 2. Horizontal parameters are changed by about 20% at the longer wave periods.

The dispersion relation used may not be the most appropriate one. Dissipative and ducting mechanisms have not been considered in the above analysis, nor have the results of analyses of realistic model atmospheres. In a review of atmospheric gravity waves, Francis (1975) has concluded that medium scale travelling ionospheric disturbances can be described in terms of internal waves whereas the thermal gradient at the base of the thermosphere provides a mechanism for the propagation of evanescent waves of large scale associated with magnetic storms. A description of an experimental observation of the latter type is given by Thome (1968). Of the above two types of waves, the internal wave description is more appropriate for application to the data of this thesis.

Experimental procedures for studying TID's such as "three station" methods generally provide horizontal velocities, whereas the procedure outlined in this chapter provides estimates of vertical velocities. A combination of the two procedures should provide a measure of verification of the theory. Alternatively, some insight might be gained as to which refinements to the theory are physically significant. Herron (1974) has provided data in which both horizontal and vertical phase velocities were measured. A comparison is made between the observed dispersion and the best theoretical fit to gravity wave theory. A degree of agreement is displayed for wave periods between 20 and 50 minutes. Both horizontal and vertical velocities of TID's were measured by Jones (1969) and the results compared with gravity wave theory. A comparison between measured values of the angle of propagation with the horizontal and values calculated from the 1962 U.S. Standard Atmosphere showed a good agreement. This experimental

Table 5.2 Gravity wave analysis from experimental data

Kersbrook test W354 20/12/75 O-ray 1435-1635 hours
Signal frequencies: 5.38, 5.745.Mhz

Scale Height, H=	41.14	km
Acceleration due to gravity, g=	9.16	m/s/s
Ratio of specific heats =	1.40	
Real height separation =	8.30	km
Real height of reflection =	216.00	km
Speed of sound, c=	726.37	m/s
Brunt period =	13.13	minutes
Acoustic cut off period =	11.86	minutes

Wave period (minutes)	N-S Components			E-W Components		
	40.00	24.00	17.14	40.00	24.00	17.14
$\theta_{xy}(f)$ (deg)	28.83	30.22	32.23	21.84	23.59	28.60
Δt (min)	3.20	2.01	1.53	2.43	1.57	1.36
λ_z (km)	103.6	98.9	92.7	136.8	126.7	104.5
λ_x (km)	292.9	149.3	77.2	381.7	189.6	86.8
λ (km)	97.7	82.4	59.3	128.8	105.3	66.7
χ (deg)	70.52	56.48	39.77	70.28	56.25	39.71
θ (deg)	70.84	56.84	40.00	70.84	56.84	40.00
V_{pz} (m/s)	43.2	68.7	90.1	57.0	88.0	101.6
V_{px} (m/s)	122.1	103.6	75.0	159.1	131.6	84.4
V_p (m/s)	40.7	57.2	57.7	53.7	73.1	64.9
V_{gz} (m/s)	-37.3	-47.1	-36.9	-48.1	-59.5	-41.4
V_{gx} (m/s)	109.2	73.1	31.2	142.7	93.2	35.1
V_g (m/s)	115.4	86.9	48.3	150.5	110.6	54.3
ϕ (deg)	-71.16	-57.19	-40.24	-71.38	-57.41	-40.30
ϕ_{tilt} (deg)	-18.91	-33.02		-18.73	-32.93	
R	17.1	13.2		13.1	10.4	
k_z ($\times 10^{-6}$)	60.624	63.547	67.773	45.925	49.605	60.140
k_x ($\times 10^{-6}$)	21.448	42.098	81.430	16.460	33.144	72.419
k ($\times 10^{-6}$)	64.306	76.226	105.944	48.786	59.659	94.135
V_{gT} (m/s)	35.3	39.6	23.8	45.5	50.2	26.8

Combined components

λ_x (km)	232.40	117.27	57.66
V_x (m/s)	96.83	81.44	56.07
α $\pm$(deg)	37.50	38.21	41.65
$180-\alpha$ $\pm$(deg)	142.50	141.79	138.35

data is further considered by Davies and Jones (1971) from which it is concluded that support is given to the view that TID's are caused by propagation of atmospheric gravity waves. Additional verification of the relationship between TID's and gravity wave theory has been made by Thome and Rao (1969) using vertical data from a Thomson scatter facility and horizontal data from a spaced HF radar network. The conclusion was reached that their results supported the gravity wave explanation of TID's but that for the greatest possible accuracy viscous dissipation and ionospheric loss processes should be taken into account.

The degree of success achieved by the experiments of Herron, Jones and of Thome and Rao in supporting the perturbation theory of gravity waves suggests that there is a correspondence between the motions of the neutral atmosphere, on which the gravity wave theory is based, and the motions of the ionised components of the atmosphere, and the free electron component in particular, on which reflection of e.m. waves in the ionosphere depends. This question has been considered by Hooke (1968) who concluded that the motion of the neutral particles parallel to the magnetic field lines is passed on to the ionisation through collisional interaction. The free electron gas moves with the ionised particles to maintain electrical neutrality. The response of the ionised particles to the neutral particles in terms of electron density fluctuations is shown by Hooke (1970a) to be of the order of 5 or 6 percent in the F_2 region and to be appreciably anisotropic, but this consideration is not thought to effect the measurement of phase velocities since the interaction will occur to some extent in equilibrium with neutral gas motions if the time scales of these motions is long by comparison with the collision frequency of the particles. Simplified formulae for the ionisation motions in the F region during the passage of a TID have been given by Georges (1968).

5.4 ADDITIONAL RESULTS

Two additional sets of processed data are given in this section. The first set consists of a sample of extraordinary ray data taken after the ordinary ray sample described in section 2. Evenly spaced zenith angle plots are shown in figure 9 and low pass filtered zenith angle plots are shown in figure 10. Ionograms during the period of the data are shown in figure 11. The ionograms display a continuous transition from day time F region conditions to night time F region conditions. These conditions are reflected in the appearance of the zenith angle plots. The evenly spaced zenith angle data becomes noticably more scattered as night time conditions become established. These conditions are also reflected in the diminished dynamic range of the spectra shown in figure 12.

The gravity wave analysis for the data is shown in table 3. Both the real height separation and the phase angles are less for the X-ray data than for the O-ray data producing very similar results to the data shown in table 1. The tilt and polar plots for this sample are shown in figures 13 and 14 respectively.

The second set of processed data is a sample of ordinary ray data. Evenly spaced and filtered zenith angle data are shown in figures 15 and 16 respectively. The zenith angle data in figure 17 has been included to display the effect of applying a lower frequency cut off to the data. It is somewhat easier to observe directions of wave events with this degree of smoothing. It can be seen from the set of ionograms in figure 18 that a transition to night time conditions occured during the sample in much the same way as for the previous sample. The main difference is the appearance of multimode conditions as the sample progresses and also the additional sets of traces at lower frequencies attributable to oblique echoes. Spectral plots for the data are shown in figure 19 and the gravity wave

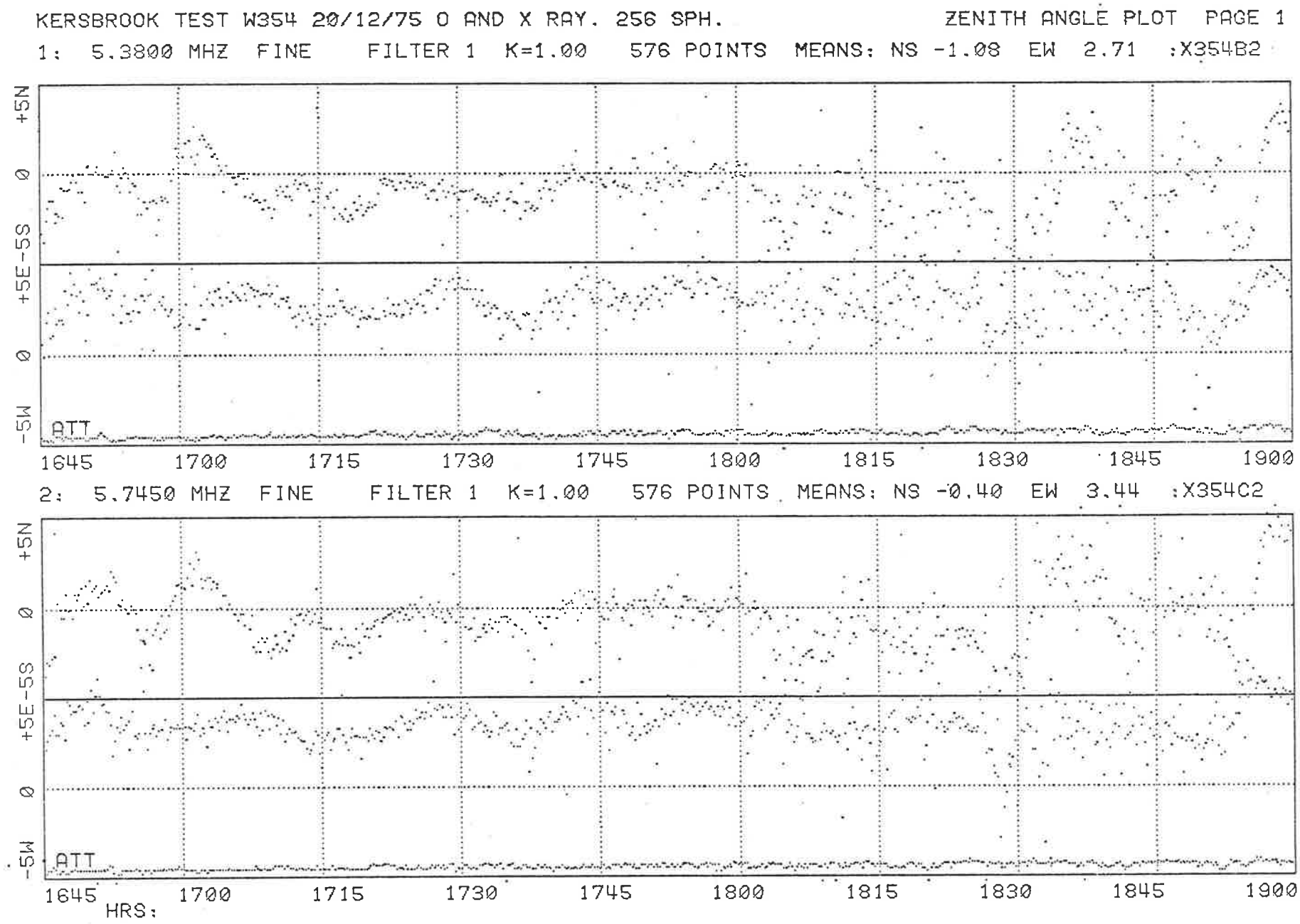

Figure 5.9 Zenith angle plot of evenly spaced data: W354 X-ray

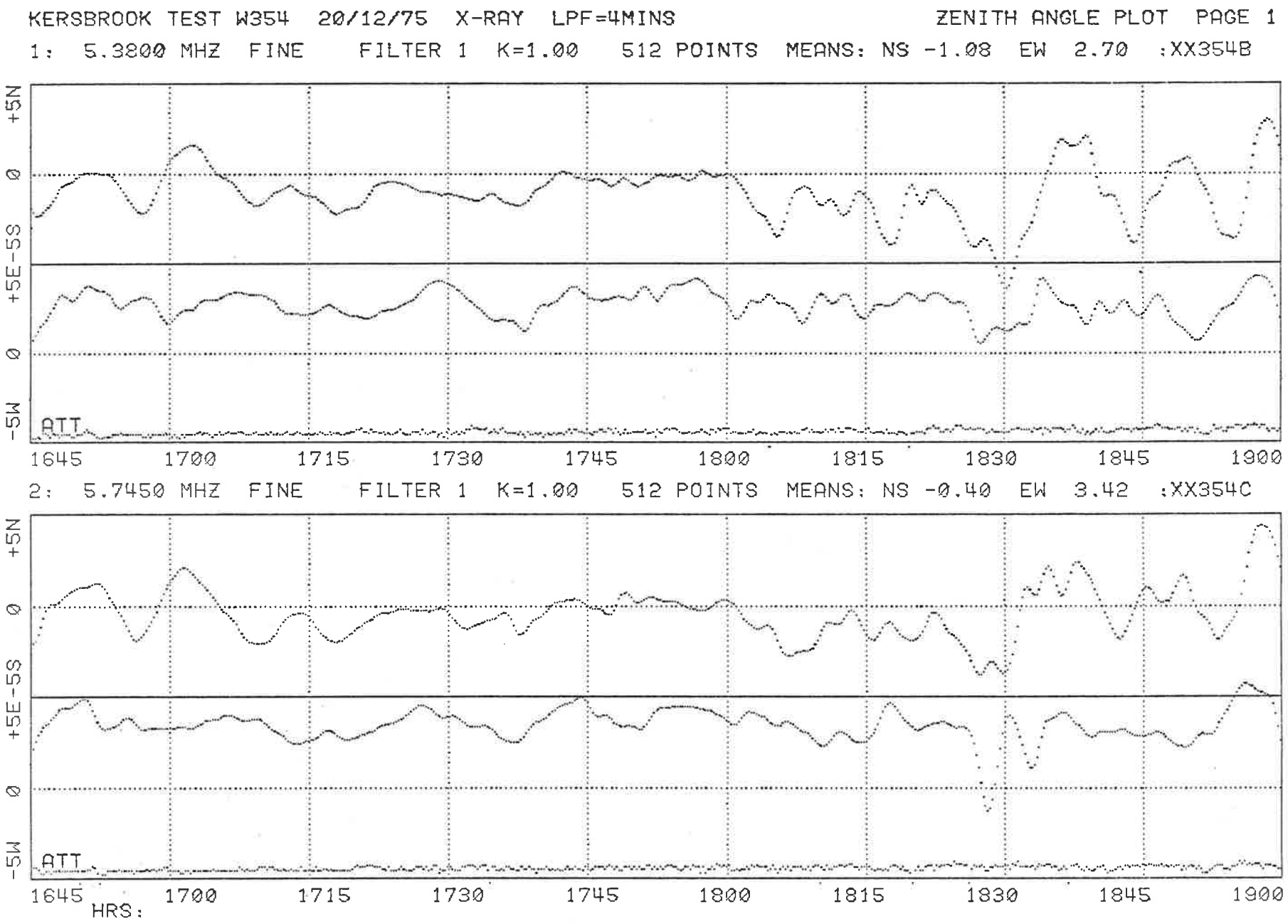

Figure 5.10 Zenith angle plot of low pass filtered data: W354 X-ray

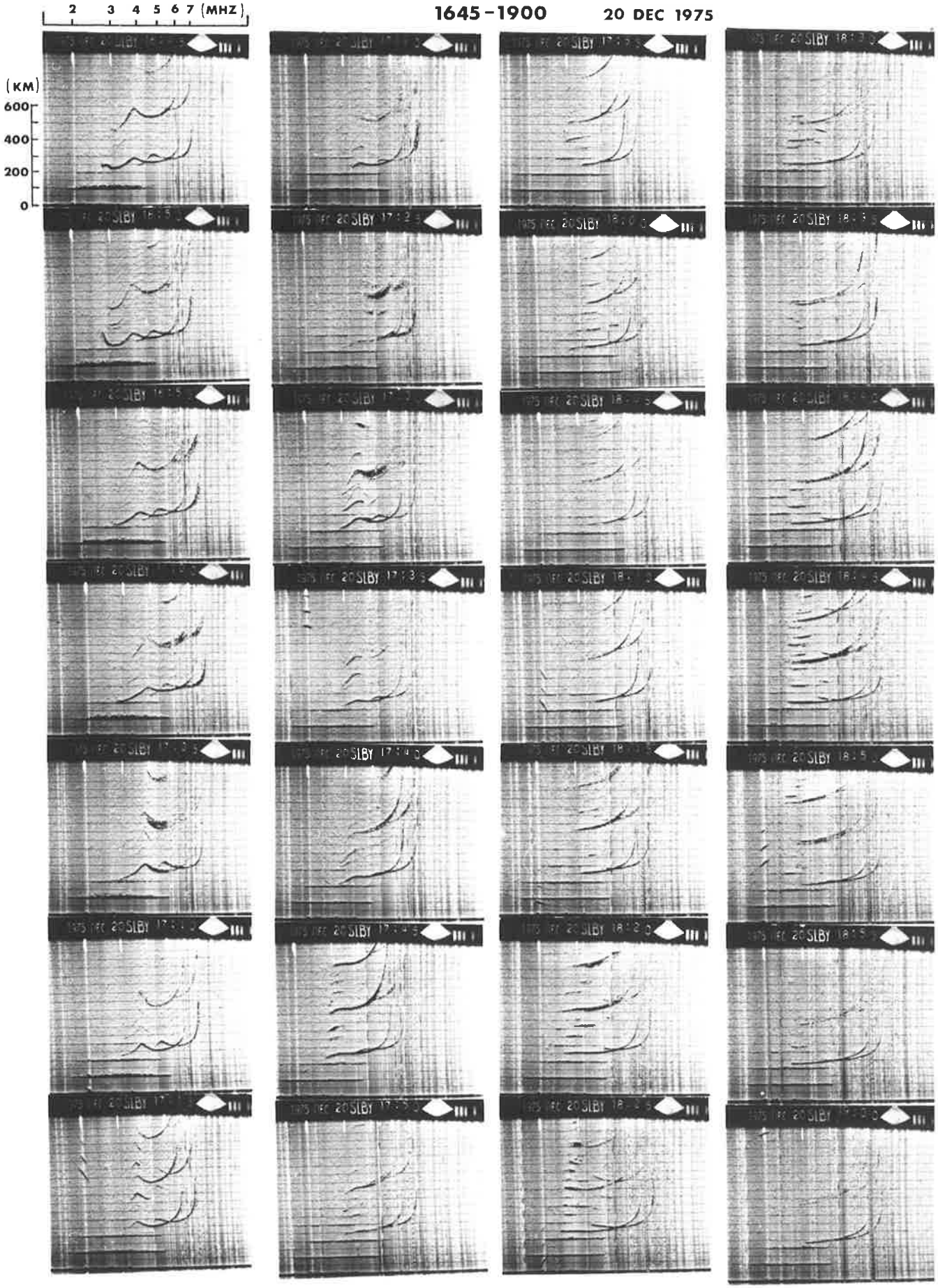

Figure 5.11 Series of ionograms for the period 1545 to 1900 hours: W354

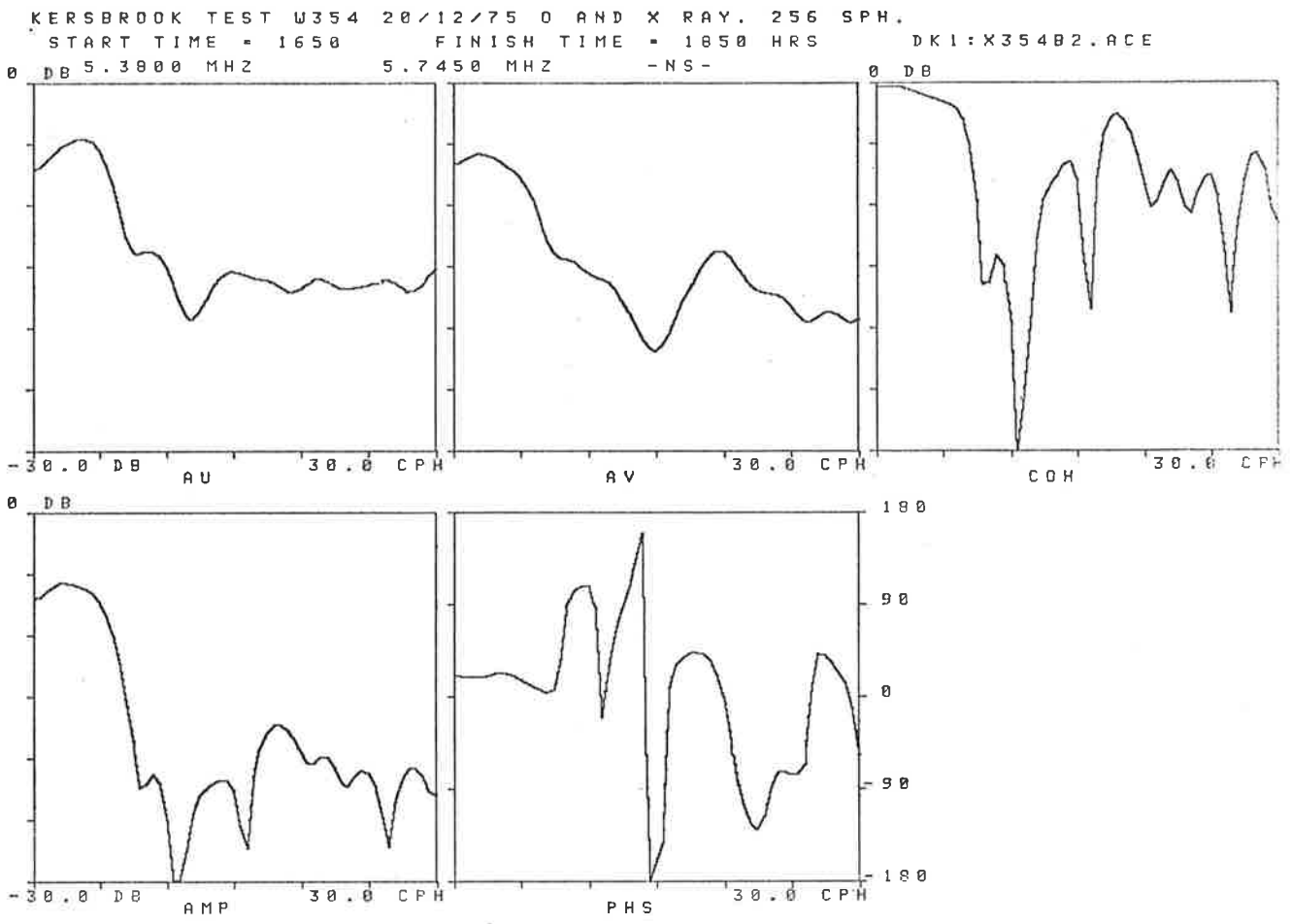

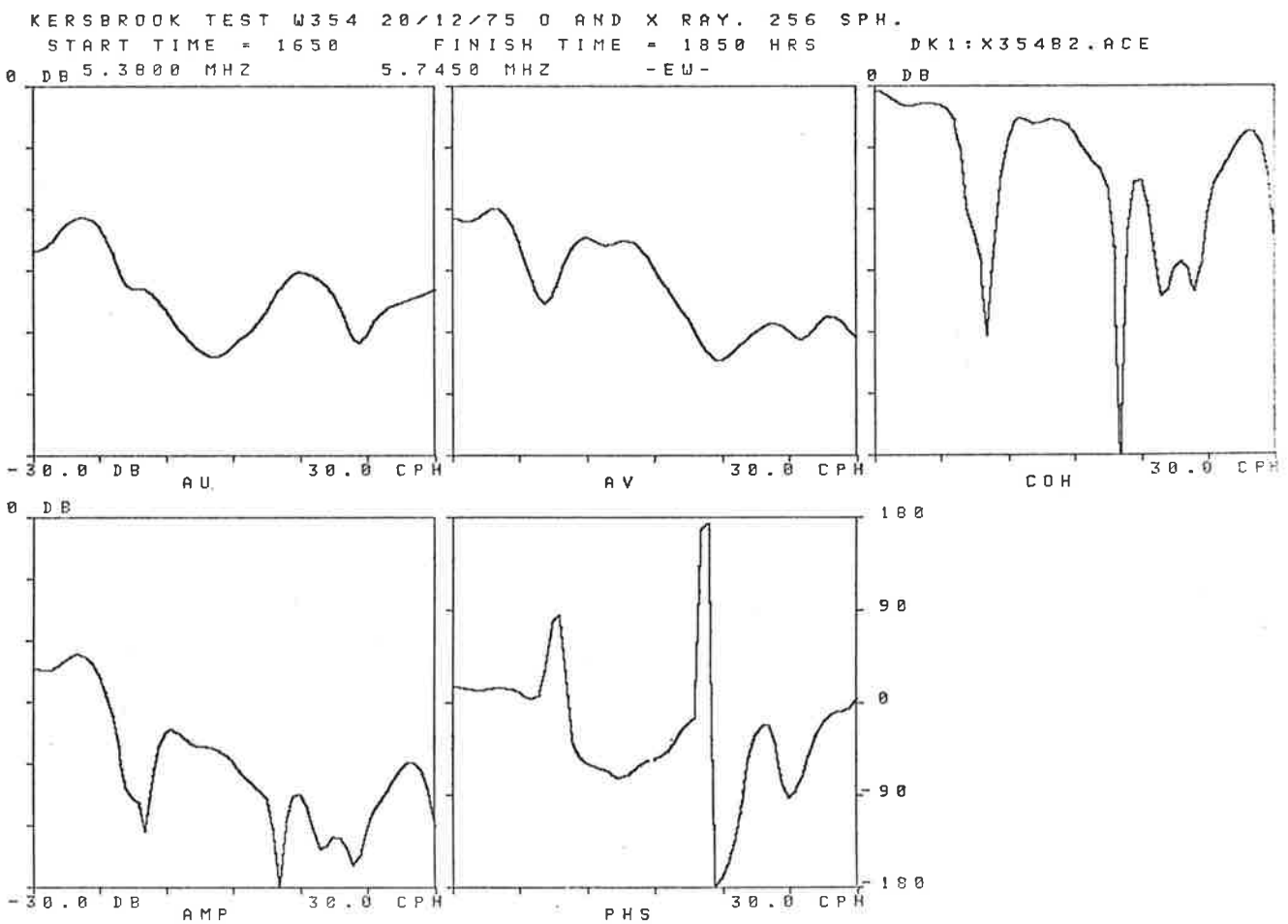

Figure 5.12 Spectral plots of NS and EW components of zenith angle data: W354 X-ray

Table 5.3 Gravity wave analysis from experimental data

Kersbrook test W354 20/12/75 X-ray 1650-1850 hours
Signal frequencies: 5.38, 5.745.Mhz

Scale Height, H=	49.77	km
Acceleration due to gravity, g=	9.19	m/s/s
Ratio of specific heats =	1.40	
Real height separation =	5.91	km
Real height of reflection =	206.00	km
Speed of sound, c=	800.14	m/s
Brunt period =	14.42	minutes
Acoustic cut off period =	13.03	minutes

Wave period (minutes)		N-S Components 40.00	24.00	17.14	E-W Components 40.00	24.00	17.14
$\theta_{xy}(f)$	(deg)	19.35	20.33	23.17	13.32	12.98	15.17
Δt	(min)	2.15	1.36	1.10	1.48	0.87	0.72
λ_z	(km)	110.0	104.7	91.8	159.7	163.9	140.3
λ_x	(km)	280.7	137.9	58.7	401.8	213.0	89.2
λ	(km)	102.4	83.4	49.5	148.4	129.9	75.3
χ	(deg)	68.61	52.80	32.61	68.32	52.42	32.46
θ	(deg)	68.87	53.07	32.73	68.87	53.07	32.73
V_{pz}	(m/s)	45.8	72.7	89.3	66.6	113.8	136.4
V_{px}	(m/s)	116.9	95.8	57.1	167.4	147.9	86.7
V_p	(m/s)	42.7	57.9	48.1	61.8	90.2	73.2
V_{gz}	(m/s)	-38.9	-45.8	-26.0	-55.0	-70.2	-39.4
V_{gx}	(m/s)	102.0	61.5	16.8	146.5	95.7	25.6
V_g	(m/s)	109.2	76.7	30.9	156.5	118.7	46.9
ϕ	(deg)	-69.13	-53.34	-32.85	-69.41	-53.72	-33.00
ϕ_{tilt}	(deg)	-20.93	-36.85		-20.73	-36.74	
R		18.1	14.9		12.6	9.6	
k_z	($\times 10^{-6}$)	57.144	60.038	68.425	39.336	38.332	44.800
k_x	($\times 10^{-6}$)	22.386	45.564	106.948	15.638	29.498	70.442
k	($\times 10^{-6}$)	61.373	75.370	126.964	42.331	48.368	83.481
V_{gT}	(m/s)	36.3	36.7	14.1	51.5	56.6	21.4

Combined components

λ_x	(km)	230.09	115.76	49.06
V_x	(m/s)	95.87	80.39	47.71
α	$\pm$(deg)	34.94	32.92	33.37
$180-\alpha$	$\pm$(deg)	145.06	147.08	146.63

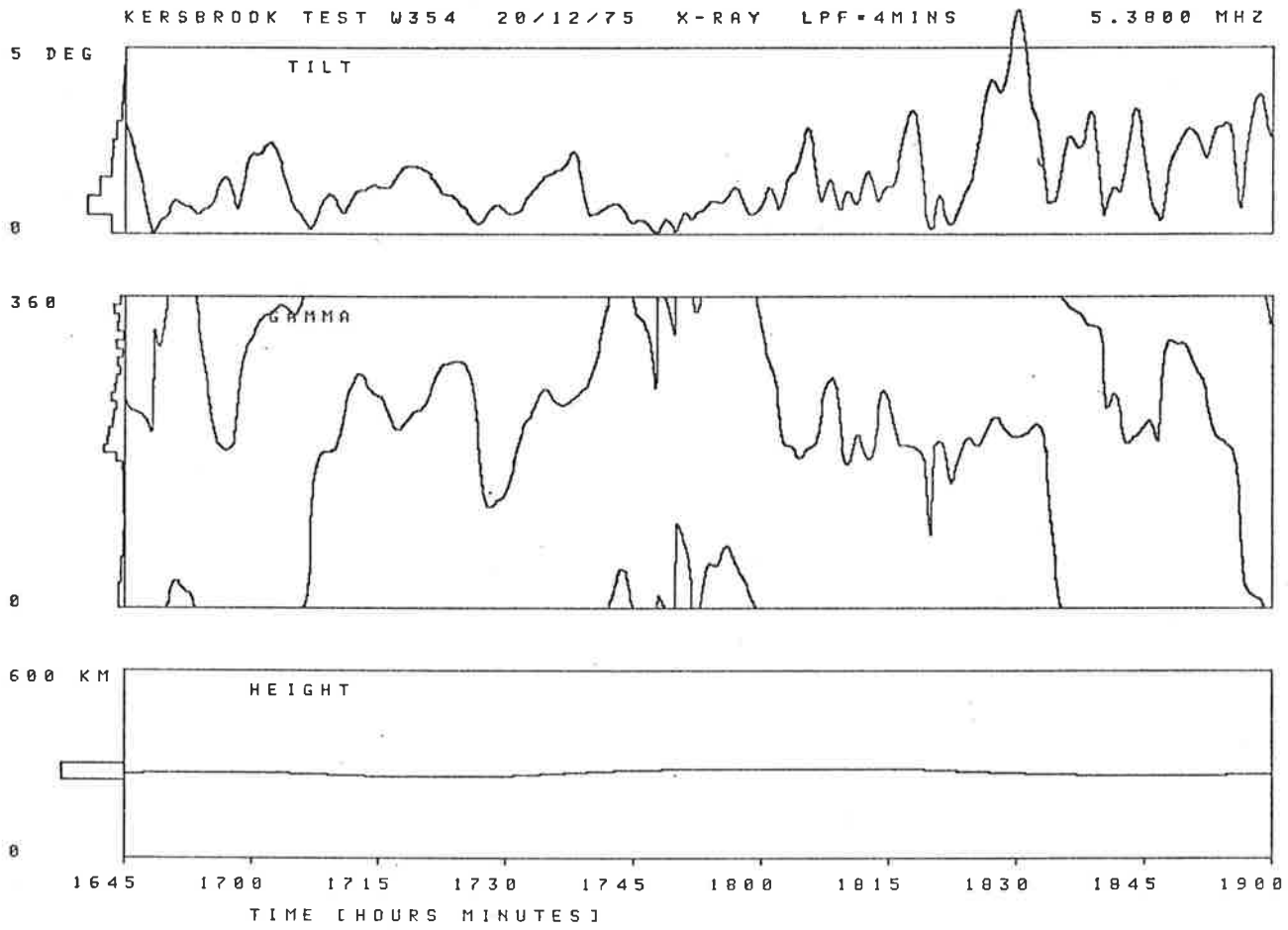

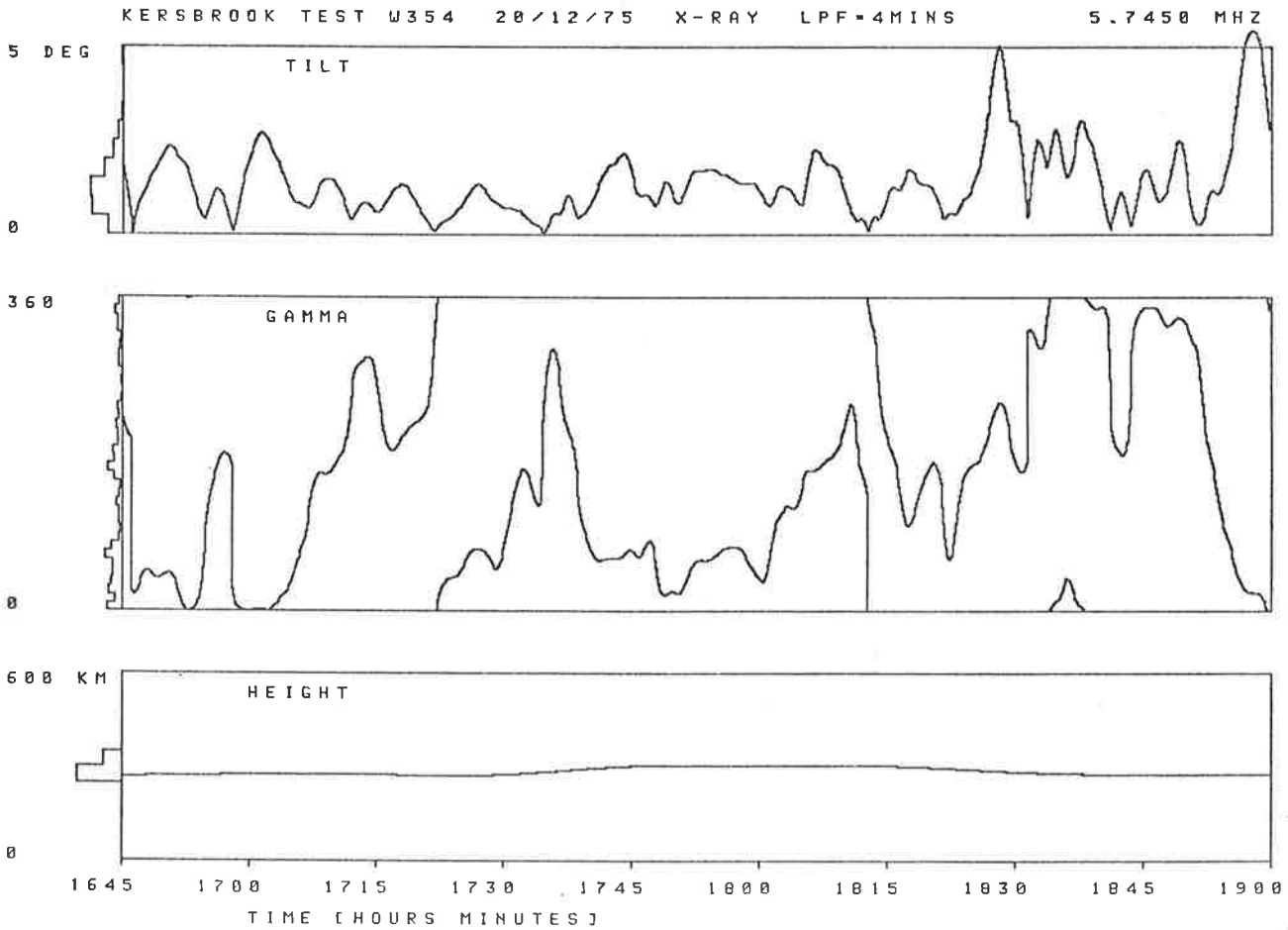

Figure 5.13 Tilt plots for the period 1645 to 1900 hours: W354 X-ray

AUTOCELL DATA POLAR PLOT 2/10/77 PAGE 1
KERSBROOK TEST W354 20/12/75 X-RAY LPF=4MINS
FROM 1650 TO 1750 K=1.000 228 228 0 0 POINTS
1: 5.3800 MHZ FINE FILTER 1 K=1.00 FILE DK1:XX354B.ACE
2: 5.7450 MHZ FINE FILTER 1 K=1.00 FILE DK1:XX354C.ACE

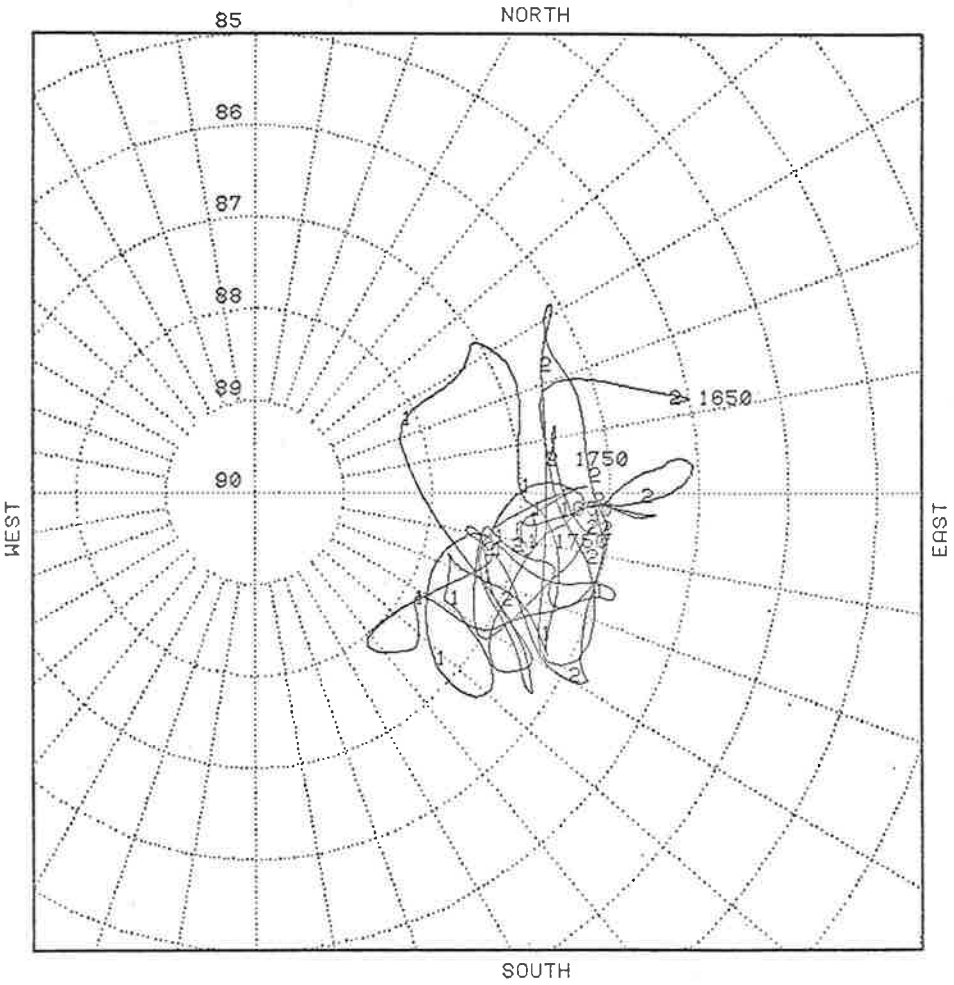

ELEVATION ANGLE V AZIMUTH (10 DEGREES)

AUTOCELL DATA POLAR PLOT 2/10/77 PAGE 2
KERSBROOK TEST W354 20/12/75 X-RAY LPF=4MINS
FROM 1750 TO 1850 K=1.000 227 227 0 0 POINTS
1: 5.3800 MHZ FINE FILTER 1 K=1.00 FILE DK1:XX354B.ACE
2: 5.7450 MHZ FINE FILTER 1 K=1.00 FILE DK1:XX354C.ACE

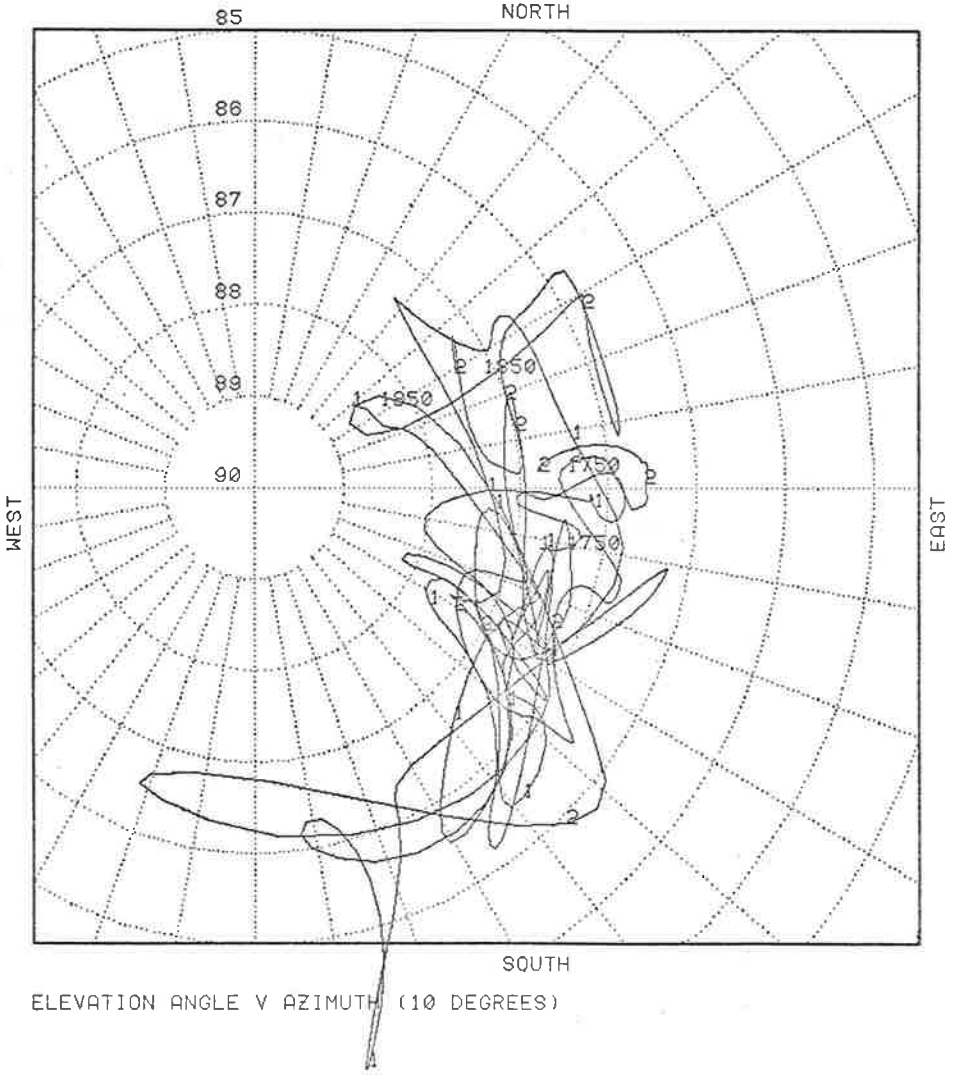

ELEVATION ANGLE V AZIMUTH (10 DEGREES)

Figure 5.14 Polar plots of zenith angle data: W354 X-ray

Table 5.4 Gravity wave analysis from experimental data

Kersbrook test W355 21/12/75 O-ray 1805-2005 hours
Signal frequencies: 5.38, 5.745.Mhz

Scale Height, H=	41.72	km
Acceleration due to gravity, g=	9.11	m/s/s
Ratio of specific heats =	1.40	
Real height separation =	8.35	km
Real height of reflection =	234.00	km
Speed of sound, c=	729.48	m/s
Brunt period =	13.26	minutes
Acoustic cut off period =	11.98	minutes

Wave period (minutes)		N-S Components 40.00	24.00	17.14	E-W Components 40.00	24.00	17.14
$\theta_{xy}(f)$	(deg)	20.60	15.66	13.43	26.54	32.67	37.12
Δt	(min)	2.29	1.04	0.64	2.95	2.18	1.77
λ_z	(km)	145.9	192.0	223.8	113.3	92.0	81.0
λ_x	(km)	401.5	276.1	175.4	315.8	137.3	66.0
λ	(km)	137.1	157.6	138.1	106.6	76.4	51.1
χ	(deg)	70.03	55.19	38.09	70.27	56.17	39.16
θ	(deg)	70.64	56.47	39.33	70.64	56.47	39.33
V_{pz}	(m/s)	60.8	133.3	217.6	47.2	63.9	78.7
V_{px}	(m/s)	167.3	191.7	170.6	131.6	95.3	64.1
V_p	(m/s)	57.1	109.4	134.3	44.4	53.1	49.7
V_{gz}	(m/s)	-50.9	-86.0	-82.7	-40.4	-43.6	-31.4
V_{gx}	(m/s)	149.8	136.1	70.8	117.5	66.6	25.9
V_g	(m/s)	158.2	161.0	108.9	124.3	79.6	40.7
ϕ	(deg)	-71.25	-57.72	-40.59	-71.01	-56.77	-39.50
ϕ_{tilt}	(deg)	-18.88	-33.03		-19.07	-33.41	
R		12.4	7.0		15.8	14.4	
k_z	($\times 10^{-6}$)	43.058	32.733	28.072	55.474	68.287	77.589
k_x	($\times 10^{-6}$)	15.650	22.756	35.818	19.897	45.772	95.259
k	($\times 10^{-6}$)	45.814	39.866	45.508	58.935	82.208	122.859
V_{gT}	(m/s)	48.2	72.7	53.8	38.2	36.5	20.0

Combined components

λ_x	(km)	248.20	122.92	61.74
V_x	(m/s)	103.42	85.36	60.03
α	$\pm$(deg)	51.81	63.56	69.39
180- α	$\pm$(deg)	128.19	116.44	110.61

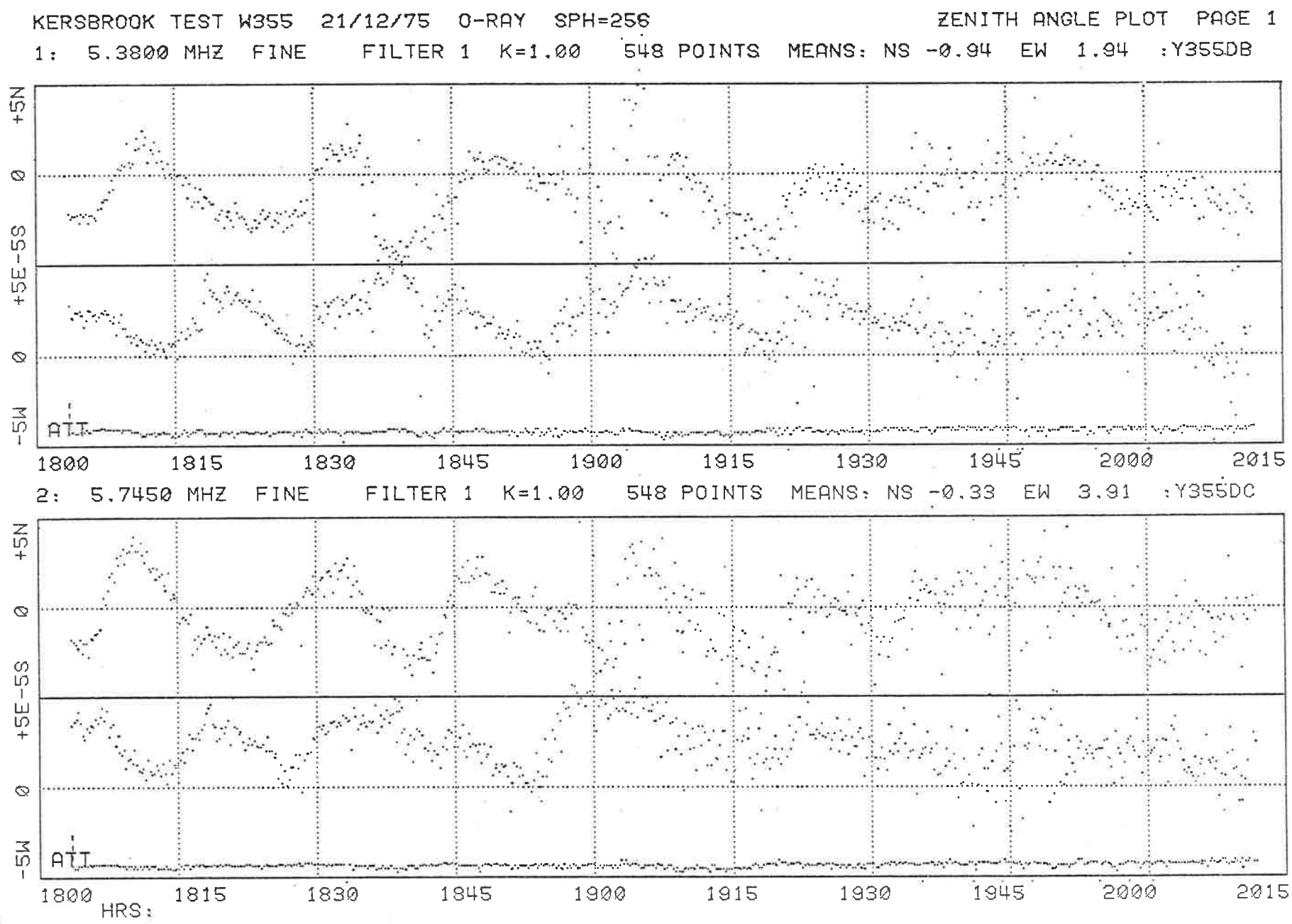

Figure 5.15 Zenith angle plot of evenly spaced data: W355 O-ray

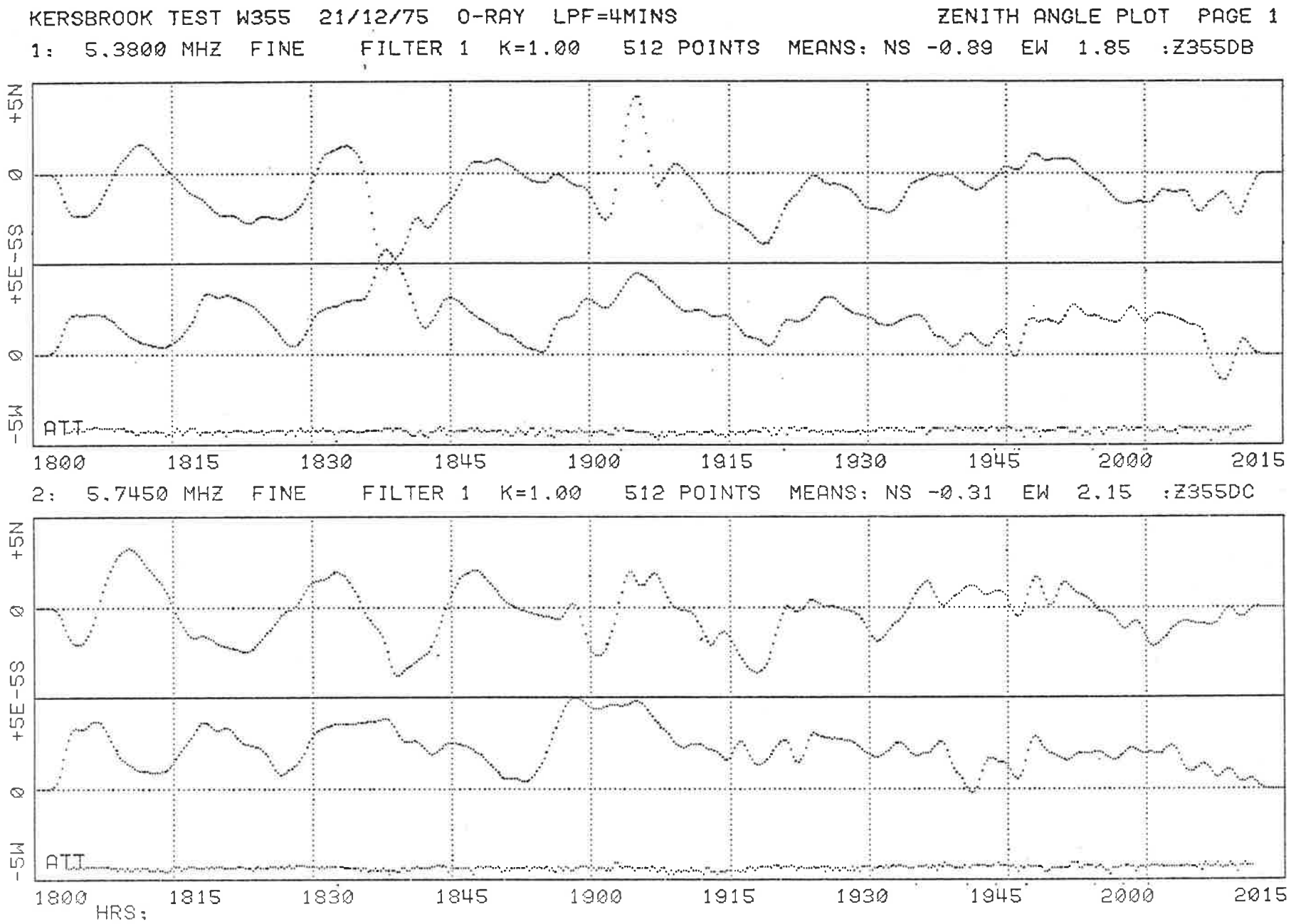

Figure 5.16 Zenith angle plot of low pass filtered data: W355 O-ray

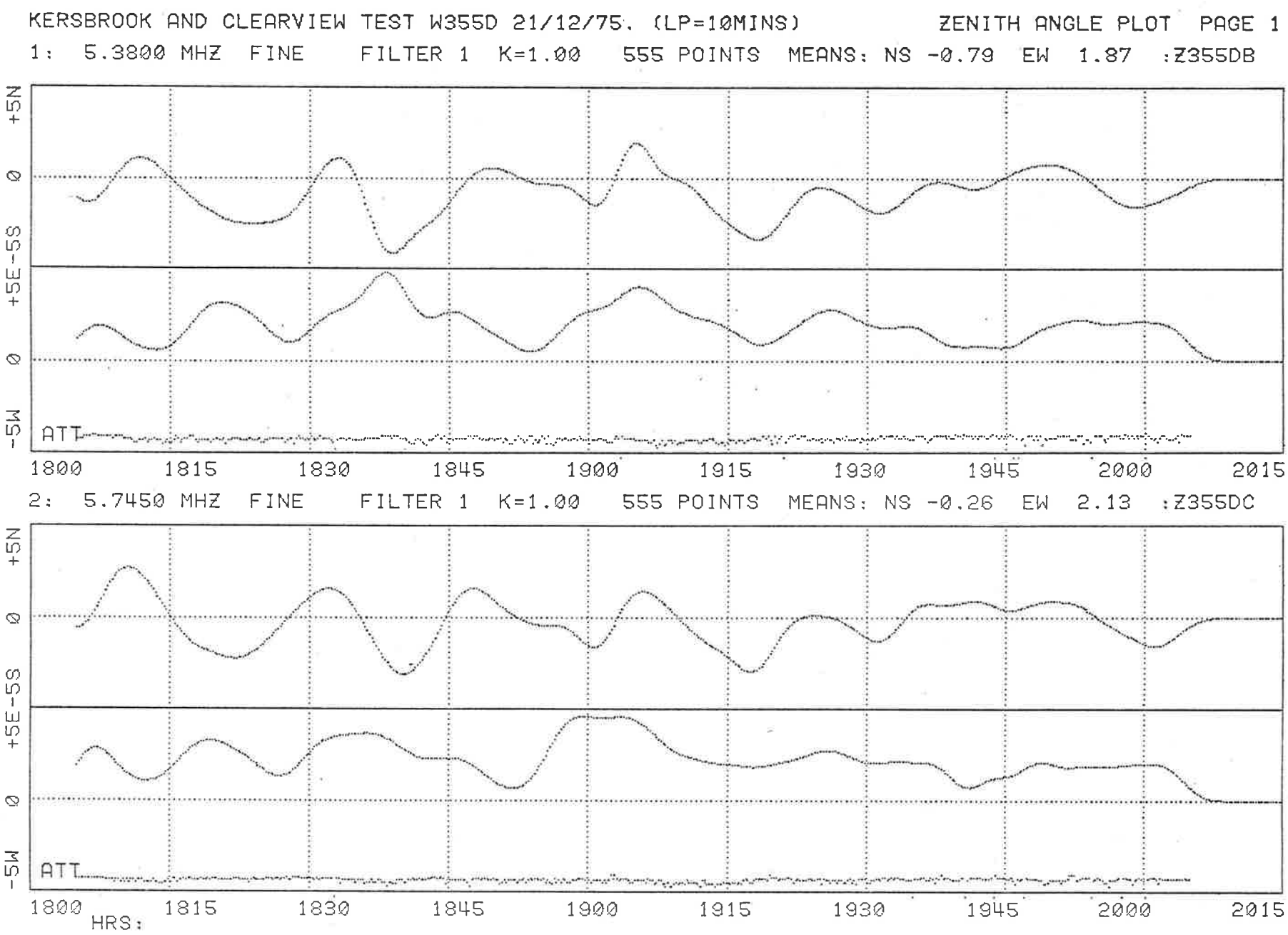

Figure 5.17 Zenith angle plot of low pass filtered data: W355 O-ray (cut off period = 10 minutes)

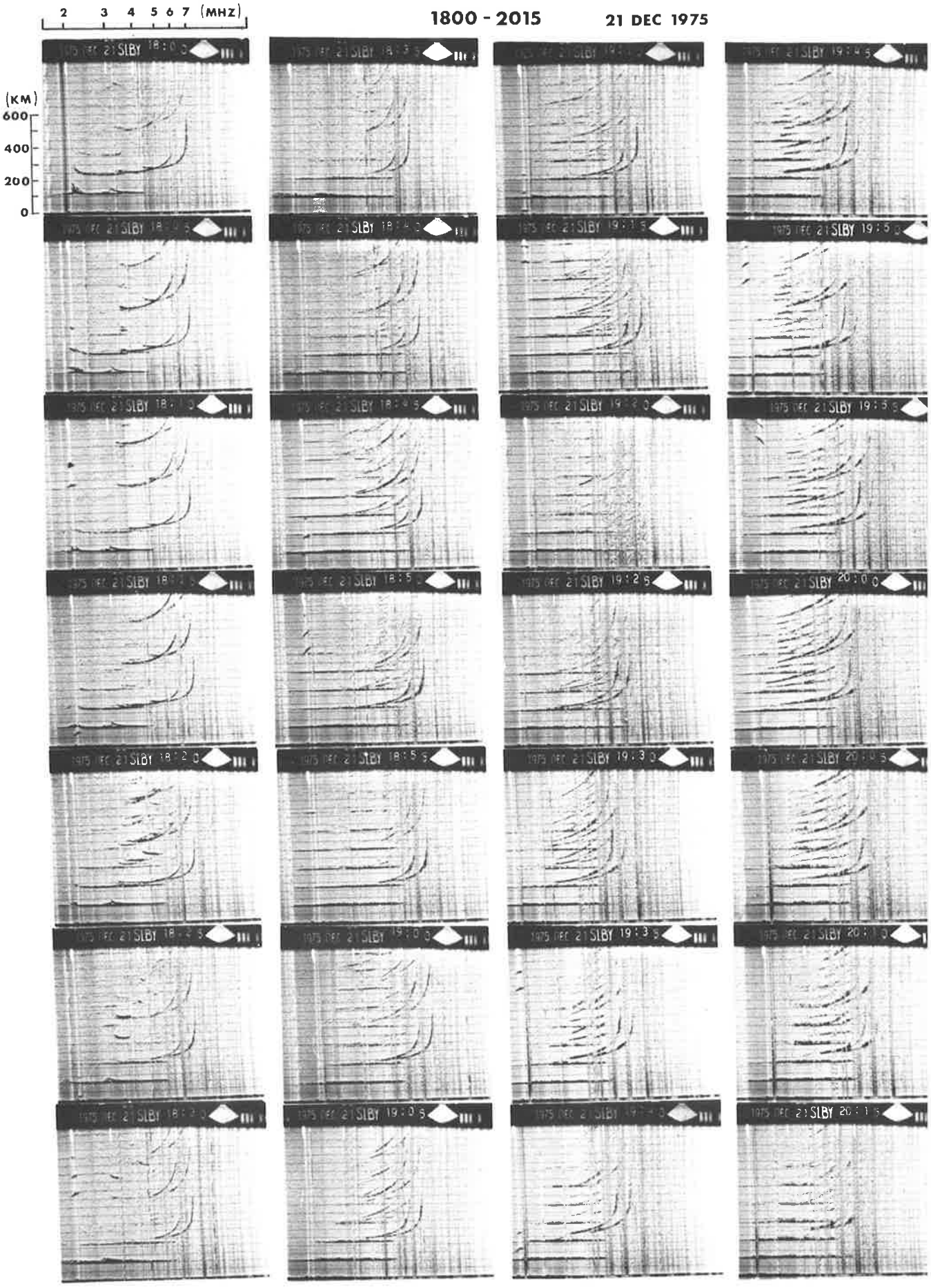

Figure 5.18 Series of ionograms for the period 1800 to 2015 hours: W355

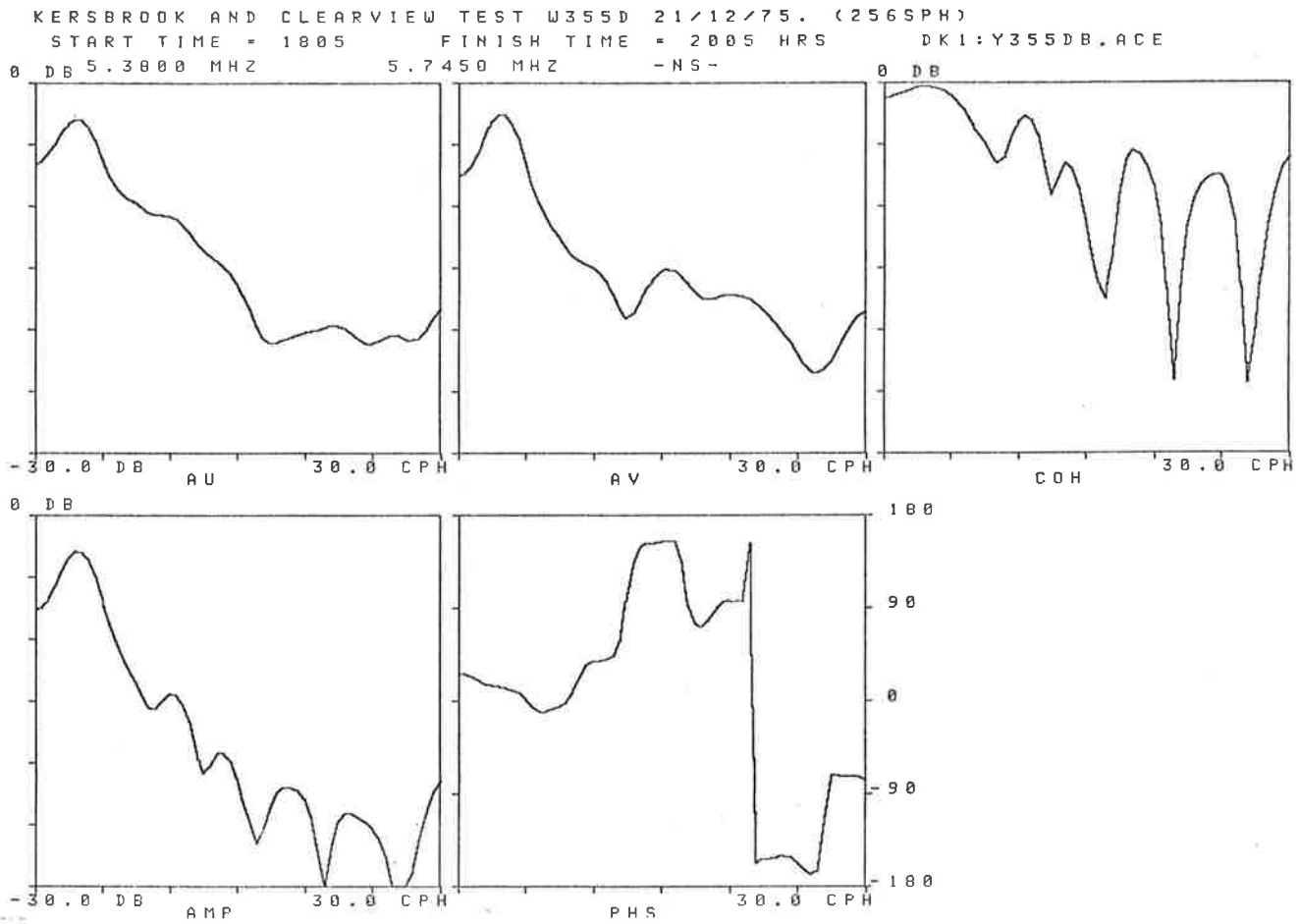

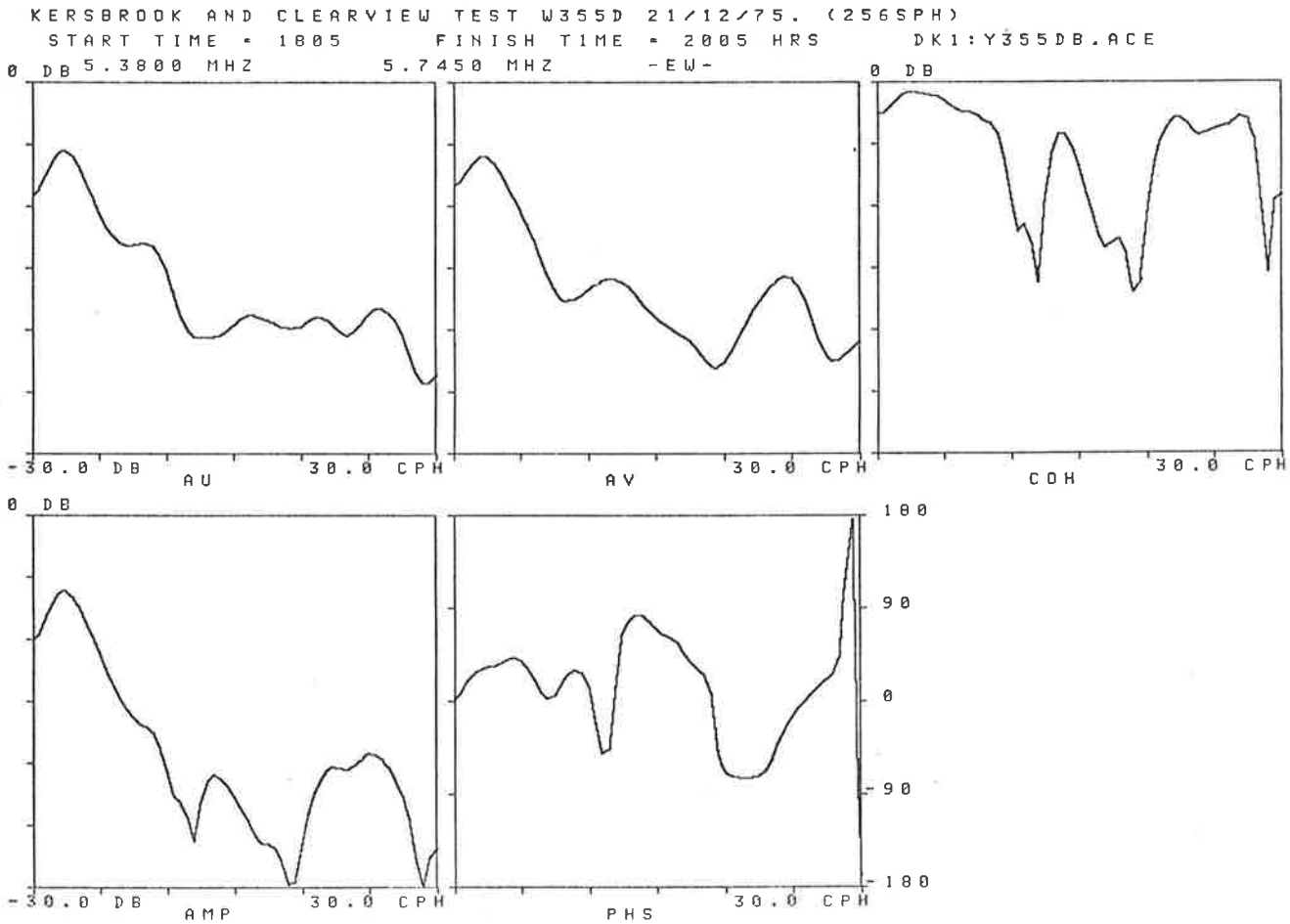

Figure 5.19 Spectral plots of NS and EW components of zenith angle data: W355 O-ray

analysis results are shown in table 4. Once again the results are very similar to the results displayed earlier. Tilt plots are shown in figure 20. The real height data for the 5.745 Mhz signal terminated at 1915 hours due to the critical frequency falling below this frequency. The real height separation has been averaged over a little more than the first half of the sample only. The fact that the 5.745 Mhz signal continued to be received is not completely understood. The slight obliquity may have made this reception possible (Heisler and Whitehead, 1961), or alternatively the critical frequency may have been obscured by attenuation or noise. The isolation of ionospheric components by the aerial polarization circuit is known to be of the order of 28 db under the ideal conditions of near vertical reception and a signal frequency of 5 .745 Mhz and is therefore not a contributory factor. Polar plots are shown in figure 21.

A general conclusion to be drawn from the tilt angle data is that for each of the samples shown average tilts of one or two degrees occured. Occasional peaks in the tilt of over five degrees could occur. Very few well defined TID's appeared in the data with a complete cycle of activity evident. The appearance of the data was characterised more by a succession of numerous partial events.

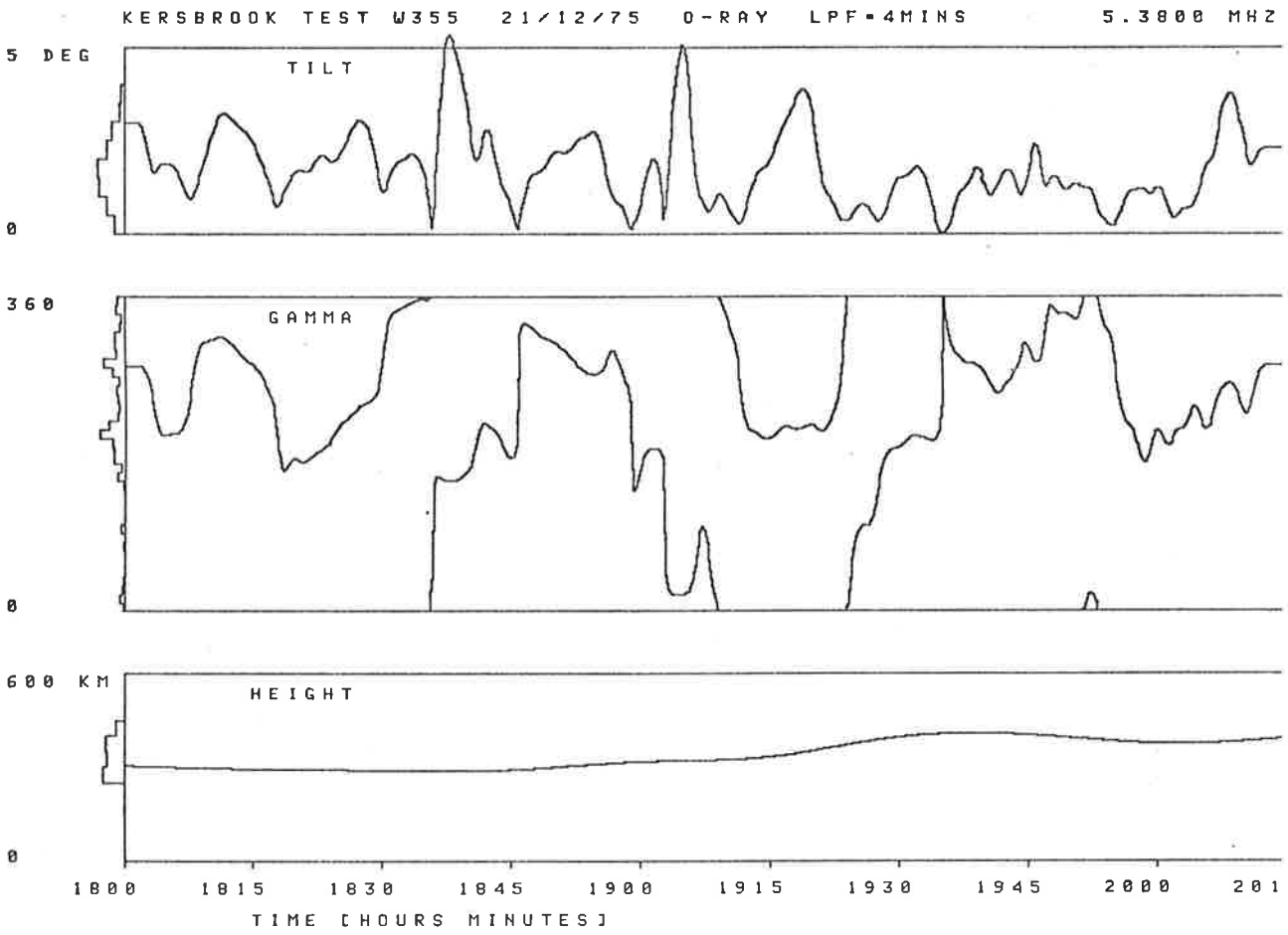

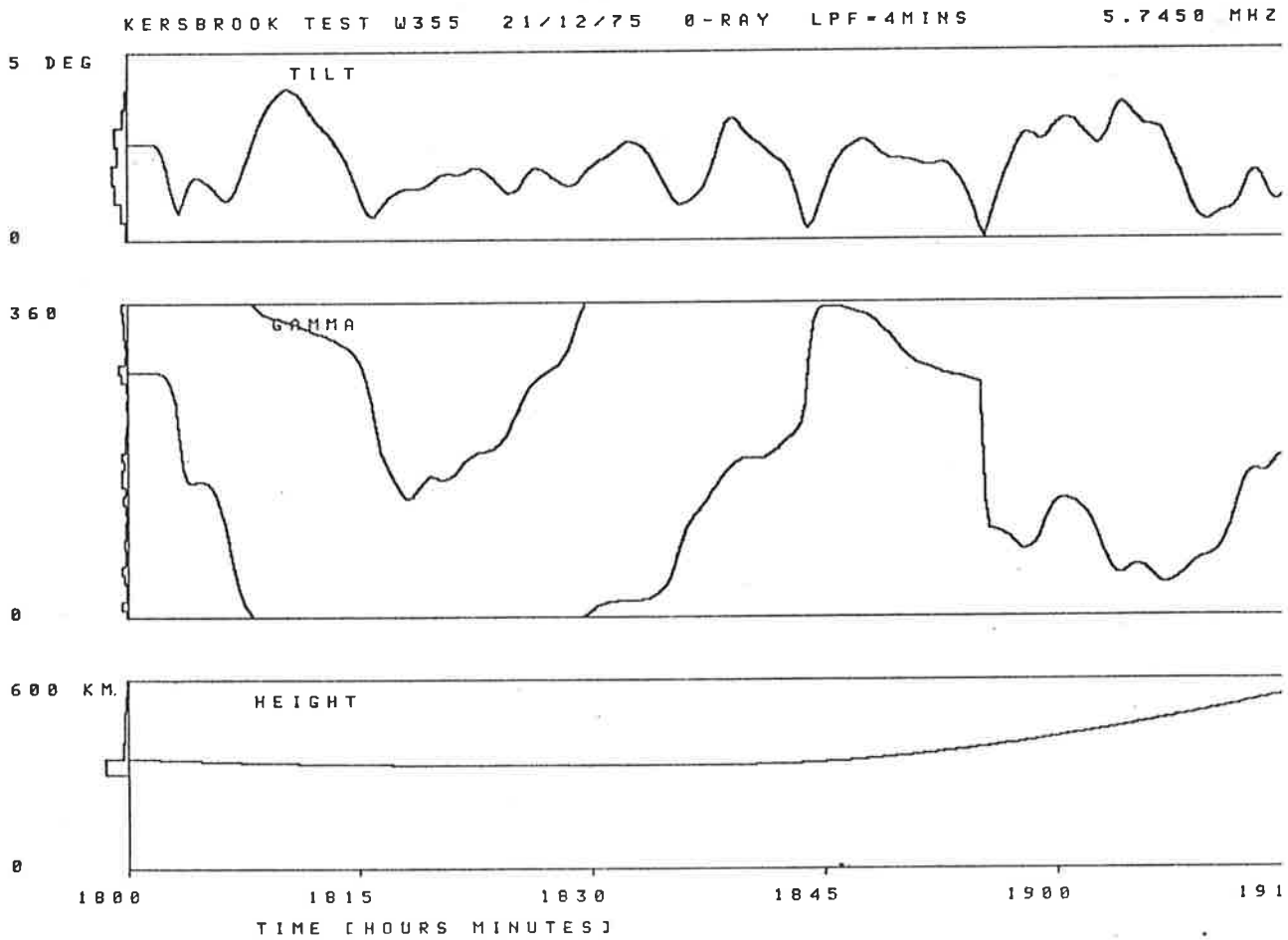

Figure 5.20 Tilt plots for the period 1800 to 2015 hours: W355 O-ray

AUTOCELL DATA POLAR PLOT 2/10/77 PAGE 1
KERSBROOK AND CLEARVIEW TEST W355D 21/12/75. (LP=10MINS)
FROM 1805 TO 1905 K=1.000 256 256 0 0 POINTS
1: 5.3800 MHZ FINE FILTER 1 K=1.00 FILE DK1:Z355DB.ACE
2: 5.7450 MHZ FINE FILTER 1 K=1.00 FILE DK1:Z355DC.ACE

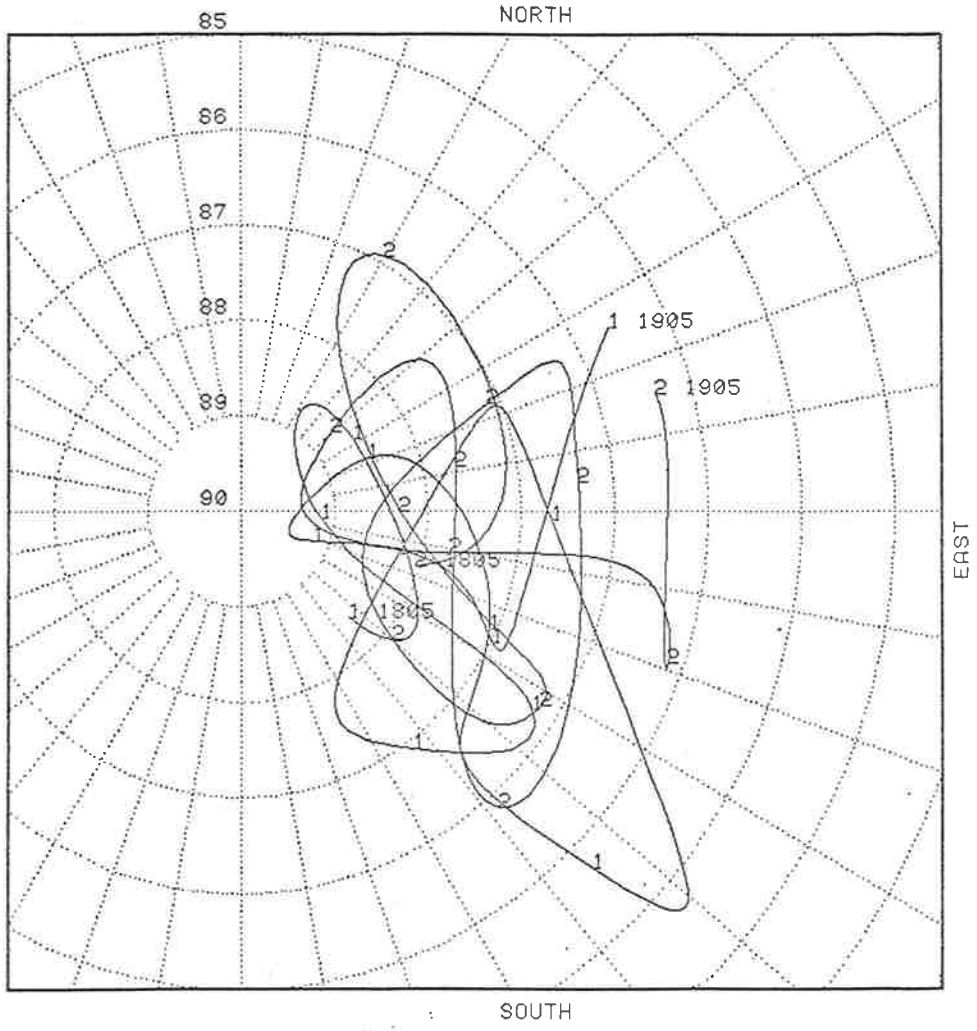

ELEVATION ANGLE V AZIMUTH (10 DEGREES)

AUTOCELL DATA POLAR PLOT 2/10/77 PAGE 2
KERSBROOK AND CLEARVIEW TEST W355D 21/12/75. (LP=10MINS)
FROM 1905 TO 2005 K=1.000 256 256 0 0 POINTS
1: 5.3800 MHZ FINE FILTER 1 K=1.00 FILE DK1:Z355DB.ACE
2: 5.7450 MHZ FINE FILTER 1 K=1.00 FILE DK1:Z355DC.ACE

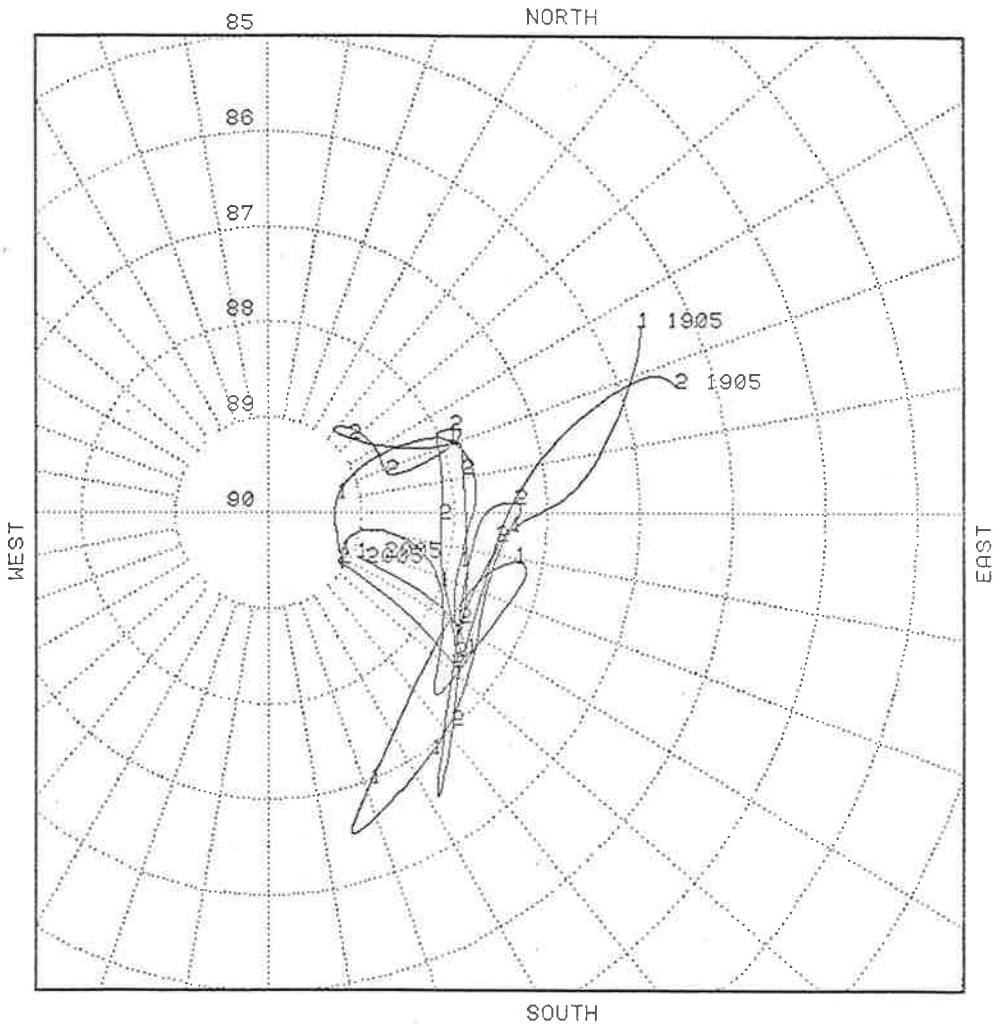

ELEVATION ANGLE V AZIMUTH (10 DEGREES)

Figure 5.21 Polar plots of zenith angle data: W355 O-ray

CHAPTER 6

CONCLUSION

6.1 SUMMARY OF RESULTS OBTAINED

This thesis has described the results of an experimental programme conducted with a fully automated equipment designed to measure the direction of arrival of electromagnetic waves reflected from the ionosphere at a number of selected frequencies. The equipment configuration and the main features of the individual subsystems have been described. A selection of data processing procedures have been developed or adapted for use for the analysis of the experimental data and to assist in the interpretation of the data.

An approach to the three dimensional geometry of reflection from a tilted ionosphere has been developed following the method of Bramley (1953). This model has been used to demonstrate the effects that are seen in the zenith angle plots derived from the experimental phase angle, direction of arrival data and to permit a degree of quantitative evaluation of the parameters of the phenomenon leading to this data. It is demonstrated that a sinusoidal wave assumed to be travelling through the ionosphere will produce an asymmetrical zenith angle plot from which the direction of motion of the wave can be inferred. The degree of asymmetry is dependent on the wavelength and amplitude of the wave and the height of the wave above the surface of the earth but is independent of the velocity of the wave. A computer simulation of zenith angle data from a travelling sine wave has been developed using the parameters of the experimental configuration.

It has further been demonstrated that a direction of arrival method of measurement is sensitive to small amplitude waves and particularly to waves

of short wavelength but is less sensitive to large changes in the height of the ionosphere as a whole. The ionospheric tilts observed in the data had average values of 1 or 2 degrees with peaks exceeding 5 degrees. The data displayed in the zenith angle, tilt and polar plots, during periods of quasi unimodal propagation, has the appearance of a succession of partial events with few events displaying one or more complete cycles of wave motion.

Sequences of ionograms taken at the Salisbury ionosonde station located at approximately the mid point of the path from the transmitting station at Kersbrook to the receiving station at St. Kilda have been used to characterise various features to be seen in the experimental data plots. These ionograms are also used to assess the ionospheric conditions prevailing during the course of the measurement runs from which data has been used for analysis.

Electron density profile analysis together with spectral analysis of zenith angle data for selected periods has been used to obtain estimates of vertical phase velocities of wave motions exhibited in the spectral analysis of the data. Estimates of horizontal velocities and other paramaters of the wave motions have been obtained by application of gravity wave dispersion analysis. These estimates represent an average over the period of the sample. The choice of a suitable period for the sample is determined mainly by the availability of a continuous period of quasi unimodal propagation during which the real heights of reflection of signals with the available frequencies maintains an average separation of the order of 5 to 10 km. The use of data exhibiting propagation via the E layer is ruled out by the latter requirement, as is data which exhibits reflection from the vicinity of the minimum virtual height of the F layer. A wider choice of signal frequencies would be an advantage in the latter case. The

results of this analysis have been compared with the observations of other experimenters (Munro, 1958; Jones, 1969; Herron, 1974; Ahmed, 1977) and have been found to be in reasonable agreement.

The experimental programme was conducted during December 1975 and the first week in January 1976. It has therefore not been possible to investigate seasonal variations in the phenomenon to be seen with the equipment described in this thesis. The main emphasis in this thesis has been placed on developing an understanding of the physical phenomenon underlying the appearance of the data in the various plots produced and in the quantitative interpretation of the results.

APPENDIX A

EXPONENTIAL DIGITAL FILTER

A brief description of the main characteristics of the exponential filter are given in this appendix. A more detailed discussion is given by Warren-Smith (1974). A single section of the filter is designed to behave like a simple low pass analogue resistor-capacitor network. That is, the transient response of the filter is designed to approach an applied input step function in an exponential manner. By discretising the differential equation for the output of the RC network it is possible to obtain the following finite difference equation for the nth sample of the filter:

$$y(nT) = y(nT-T) + K\{x(nT) - y(nT-T)\} \qquad (A.1)$$

which defines the configuration of the filter.

T is the sample interval.

The factor K is related to the time constant of the RC network. The stability of the filter is assured for values of K of $0 < K < 1$. The smaller the value of K the longer is the time constant of the filter. The response characteristics of the filter can be obtained by use of z transform techniques. The transfer function of the filter is given by:

$$H(z) = Kz/\{z-(1-K)\} \qquad (A.2)$$

The frequency response of the filter is found from this to be:

$$|H(e^{j\omega T})| = \frac{K}{1 + (1-K)^2 - 2(1-K)\cos \omega T} \Big/ -\text{Arctan} \frac{(1-K)\sin \omega T}{1-(1-K)\cos \omega T} \qquad (A.3)$$

The weighting function given by:

$$h(n) = K(1-K)^n \qquad (A.4)$$

approximates very closely the exponential weighting function of a continuous RC network for small values of K at the sampling points. The output of the filter therefore approaches the exponentially weighted mean of the input samples.

The ratio of variances between the output and input of the filter, for a random input, can be obtained from the relation:

$$\sigma_y^2 = \sigma_x^2 \sum_{m=0}^{n} h^2(m) \quad , \quad n \to \infty \tag{A.5}$$

where: h(m) is the weighting function for the filter.

A value of K/(2-K) is obtained for the single section filter. The ratio of variances (5) gives a measure of the degree of smoothing achieved by the filter, or allows a means of comparing the smoothing performance of different filter configurations.

It is found that a cascade of filter sections of the type described above results in a significant improvement in smoothing for a given overall transient response time for the cascade. An m'th order filter is therefore preferable to a first order filter. Approximations for the ratios of variances for successive orders of filter follows the sequence K/2, K/4, 3K/16, 5K/32. A value for K of 0.25 has been used with a fourth order filter obtained by applying a second order filter forwards through the data followed by a second application of the second order filter in the reverse direction through the data.

APPENDIX B

A frequently used procedure for smoothing power spectral estimates in spectral analysis is to average a number M of adjacent spectral estimates and assign this averaged estimate to a frequency at the middle of the band of frequencies averaged over. Increasing M increases the confidence that one can theoretically place in the resulting spectral estimate. Due to the low frequency characteristics of gravity waves it is difficult using this technique to get more than two or three smoothed estimates in the gravity wave region of the spectra, for reasonably high confidence intervals. Also in practice it is often found that changes in the value of M will produce changes in the resulting value of the spectral estimate. This behaviour is particularly undesirable in the vicinity of the cut off frequency of the gravity wave spectra since in addition to the above effect, the actual cut off point in the spectrum is obscured. Consequently a different procedure for power spectral smoothing has been adopted. This procedure is to carry out successive elemental running average operations, each of which consists of averaging over three successive raw estimates and asigning the new value to the frequency of the middle estimate. By means of a suitable variation of this procedure for end values, the number of spectral estimates is left unchanged. The averaging is carried out in such a way that values from the previous elemental operation are used in each averaging step before modification by the next averaging step to produce new values. Successive applications of this procedure result in a weighting function for the overall process that is tapered and symmetrical. The resulting spectral estimates have a smooth trend and the relationship of the cut off frequency to the spectra is more easily seen. The number of elemental operations can be specified at the time of processing. Values of $\theta_{xy}(f)$ have been taken for the dispersion analysis of chapter 5 using this process.

The smoothing achieved by this process can be compared with the smoothing obtained by averaging M adjacent spectral estimates by applying A.5. Since this process is a finite impulse response filter, its weighting function can be readily found directly by application of an impulse to the input of the process and determining the output of the process. The ratio of variances for the first six orders of this process are approximately: 0.33, 0.23, 0.19, 0.16, 0.15, 0.14. This can be compared with a ratio of variances of 1/M for the case of averaging M adjacent estimates. The reciprocals of the above series of numbers therefore approximately give the equivalent value of M for the first six orders of the cascaded running mean. The tapered weighting function does, however, introduce some correlation into adjacent values of spectral estimates which may lead to errors in the cross spectral phase values adjacent to peaks in the spectrum.

The sparcity of estimates in the gravity wave region of spectra from TID data has lead to attempts to find alternatives to the use of FFT based spectral analysis methods. The maximum entropy method of spectral analysis has been described by Toman (1976).

APPENDIX C

CORRECTION FACTOR FOR SPECTRAL ESTIMATES

This appendix gives a derivation of the relationship between the area under a power spectral curve and the variance of the time sequence data from which it is obtained.

1. Let x_k , k = 0,1, ... ,N-1

be a time sequence of values to be spectrum analysed. N is the number of values to be used in the analysis. Usually, $N = 2^P$, where P is an integer. Let X_n be the resulting sequence of spectral values.

n = 0,1, ... ,N-1

Parseval's theorem will be required and can be stated as:

$$\frac{1}{N}\sum_{k=0}^{N-1}|x_k|^2 = \frac{1}{N^2}\sum_{n=0}^{N-1}|X_n|^2 \qquad (C.1)$$

A proof can be found in Bogner and Constantinides (1975) or any standard text on Fourier methods.

2. The variance of the input data can be computed from:

$$\sigma^2 = \frac{1}{N-1}\sum_{k=0}^{N-1}(x_k-\bar{x})^2$$

$$= \frac{1}{N-1}\sum_{k=0}^{N-1}x_k^2 - \bar{x}^2 \qquad (C.2)$$

The mean value of the data $\bar{x}$ is made equal to zero as a preliminary step in the spectral analysis and need not be considered further.

3. The power spectral density function for the data is given by:

$$\tilde{G}_n = G_n(f_n) = \frac{2\,\Delta T}{N}|X_n|^2 \qquad (C.3)$$

where ΔT is the time interval between the equally spaced samples and

where $|X_n|^2$ are the raw power spectral estimates produced by the FFT process without modification due to tapering, smoothing etc. The factor of 2 allowes for the fact that the FFT process produces a two sided spectrum only one side of which is used (Bendat, 1971).

The factor 2 $\Delta T/N$ is a correction factor to be applied to the raw power spectral estimates from the FFT. This factor is modified to allow for tapering, smoothing etc. These modifying factors will be considered presently.

Since there are N-1 spaces between the N samples, the sample spacing is:

$$\Delta T = \frac{T}{N-1} \qquad (C.4)$$

where T is the total duration of the sample.

4. The variance of the data is related to the area under the power spectral density function as follows:

$$\sigma^2 = \frac{N}{N-1}\cdot\frac{1}{N}\sum_{k=0}^{N-1}|x_k|^2$$

$$= \frac{N}{N-1}\cdot\frac{1}{N^2}\sum_{n=0}^{N-1}|X_n|^2$$

$$= \frac{1}{T}\sum_{n=0}^{N-1}\frac{T}{N(N-1)}|X_n|^2$$

$$= \frac{1}{T}\sum_{n=0}^{N-1}\frac{\Delta T}{N}|X_n|^2$$

$$= \delta f \sum_{n=0}^{N-1} \tilde{G}_n \qquad (C.5)$$

where δf is the frequency spacing given by $\delta f = 1/T$ (=M/T when M estimates are averaged).

$\tilde{G}_n$ has been substituted from (3) omitting the factor of 2 since the summation here is from 0 to N-1.

The result given by (5) obtains the area under the power spectral density function as a direct summation of the spectral density values. Computation of (2) and (5) effectively becomes a means of checking the computed values of the power spectral density function. The correction factor mentioned earlier has the significance that it provides a scaling factor that enables one to relate the contribution that each spectral estimate has on the variance of the time sequence data.

5. Additional correction factors are required to be applied to (3) to allow for the tapering process used for leakage reduction, the smoothing process applied to the raw spectral estimates for improving the confidence that one can have in these estimates, and to allow for zeroes added to the time sequence data to establish the required number of data points for application of the FFT process.

The application of a 10 percent cosine bell taper modifies the variance of the data applied to the FFT process by a factor of 7/8. The reciprocal of this factor is therefore required to be applied to (3) as an additional correction factor, or taper factor. For a 100 percent cosine bell, or Hanning process the factor is 3/8 in place of 7/8.

For spectral averaging with M consecutive values of raw spectral estimates (or for any alternative averaging process used) a correction is required such that the weighting function for the averaging (i.e. smoothing)

process is normalised.

If zeroes have been added to the time sequence data, the variance of that data including the zeroes, assumes that all N points are data, the effect is corrected for as follows:

Let L be the number of added zeroes. Then there are N-L data values. Let σ_D^2 be the variance computed from the data only.

Then from 2:

$$\sigma^2 = \frac{1}{N-1}\sum_{j=0}^{N-L-1} x_j^2 + \frac{1}{N-1}\sum_{j=N-L}^{N-1} x_j^2$$

$$= \frac{1}{N-1}\sum_{j=0}^{N-L-1} x_j^2$$

since $x_j = 0$ for $N-L \leqslant j \leqslant N-1$

$$\therefore \qquad \sigma^2 = \frac{N-L-1}{N-1} \cdot \frac{1}{N-L-1}\sum_{j=0}^{N-L-1} x_j^2$$

$$= \frac{N-L-1}{N-1}\,\sigma_D^2$$

Hence, the correction factor to apply to the spectral density estimates in (3) is: $(N-1)/(N-L-1)$. The complete expression to take the place of (3) is now (for a 10 percent cosine bell):

$$\tilde{G}_n = \frac{8}{7}\cdot\frac{2\,\Delta T}{N}\cdot\frac{1}{M}\cdot\frac{N-1}{N-L-1}\cdot|X_n|^2$$

$$= \frac{16T}{7NM(N-L-1)}|X_n|^2 \qquad \text{(C.6)}$$

(where averaging of M values of the spectral estimates has been assumed).

APPENDIX D

CALCULATION OF SCALE HEIGHT FROM ELECTRON DENSITY PROFILE ANALYSIS DATA

This appendix considers an approximate method of calculation of the scale height at the F_2 layer peak from electron density profile analysis data. This is done by deriving a parabolic layer approximation from the simple Chapman theory by equating the Chapman production equation for electron density with the appropriate loss equation under assumed equilibrium conditions.

In a review of ionospheric F region theory, Rishbeth (1967) considers the production-loss continuity equation for electron density for the region above the F_1 ledge:

$$\partial N/\partial t = q - \beta N + D\mathfrak{D}N \qquad (D.1)$$

where:

$\partial N/\partial t$ is the rate of change of electron density,

q is electron production,

β is the loss coefficient for the ion-atom interchange process (attachment process).

$D\mathfrak{D}N$ is Ferraro's equation for plasma diffusion,

where:

D is the diffusion coefficient

and $\mathfrak{D}$ is a differential operator.

The Chapman production formula can be written as:

$$q = q_o \exp[1-z-\sec\chi \exp(-z)] \qquad (D.2)$$

where:

$$z = (h-h_o)/H \text{ is the reduced height,} \qquad (D.3)$$

χ is the solar zenith angle,

and the o subscript represents a reference value.

The diffusion term contributes mainly to determining the level at

which the peak occurs.

For a description of the F_2 layer peak, the diffusion term in (1) is set equal to zero and for equilibrium conditions (1) reduces to the equilibrium balance equation:

$$q \simeq \beta N \tag{D.4}$$

This result is substituted into (1) to give a Chapman approximation for the F_2 layer peak:

$$N = N_o \exp[1-z-\sec \chi \exp(-z)] \tag{D.5}$$

For the E and F_1 layers the equilibrium balance equation:

$$q \simeq \alpha N^2 \tag{D.6}$$

for dissociative recombination is more appropriate giving the Chapman approximation:

$$N = N_o \exp\tfrac{1}{2}[1-z-\sec \chi \exp(-z)] \tag{D.7}$$

By expanding (5) and neglecting all terms of higher than second power in z and assuming that the value of χ is small, one obtains the parabolic layer approximation, in a similar manner to that given by Davies (1969).

$$N = N_m \left\{1- \frac{1}{2}\left|\frac{h-h_m}{H}\right|^2\right\} \tag{D.8}$$

where the subscript m refers to values at the peak of the layer.

Alternatively (8) can be written in terms of values at the base of the layer represented by the subscript o:

$$N = N_o \left\{\frac{2(h-h_o)}{\surd 2\, H} - \left|\frac{h-h_o}{\surd 2\, H}\right|^2\right\} \tag{D.9}$$

The corresponding result for the E and F_1 layers is:

$$N = N_m \left\{1- \left|\frac{h-h_m}{2H}\right|^2\right\} \tag{D.10}$$

$$= N \left\{\frac{2(h-h_o)}{2H} - \left|\frac{h-h_o}{2H}\right|^2\right\} \tag{D.11}$$

The quantity $2H$ is often referred to as the semithickness of the layer.

APPENDIX E

LIST OF RAW DATA FILES

DATE	FILE NAME	FREQ Mhz	LOCAL TIME FROM	TO	DATA POINTS	RAY	REMARKS
11/11/75	W315B	5.38	1533	1653	3305		Setting up exercise
29/11/75	W333B	3.84	1717	2218	1245	X	Preliminary test with
		5.38	1713	2219	4933		3 frequencies
		6.7155	1811	2217	599		
7/12/75	W341A	5.38	1415	1805	7321	O,X	Test for comaprison with (h't) data. Figure 3.1
	W341B	3.84	1830	2300	1967		
		5.38	1819	2344	2823		
		6.7155	1851	2320	492		
8/12/75	W342A	3.84	1531	1919	1052	X	
		5.38	1530	1919	3849		
		6.7155	1542	1919	2421		
	W342B	3.84	1924	2425	2761	O	
		5.38	1923	2425	3490		
		6.7155	1923	2239	1067		
9/12/75	W343A	3.84	0031	0823	2698	X	
		5.38	0031	0920	4017		
		6.7155	0039	0852	606		
	W343B	3.84	1126	1342	1407	O	
		5.38	0940	1342	4998		
		6.7155	1202	1342	917		
	W343C	5.38	1403	1512	770	X	
		5.745	1403	1512	1001		
		6.7155	1403	1512	634		
	W343D	5.38	1738	1908	2533	X	
		5.745	1738	1908	2369		
10/12/75	W344A	5.38	1258	1612	3787	O	
		5.745	1258	1612	2787		
		6.7155	1258	1504	748		
	W344B	5.38	1712	2046	2892	O	
		5.745	1712	2046	2902		
		6.7155	1717	2046	1527		
	W344C	5.38	2051	0212	3345	X	
		5.745	2051	0207	2852		
		6.7155	2051	0212	1124		
11/12/75	W345A	5.38	0513	1356	3463	X	
		5.745	0513	1356	3219		
		6.7155	0513	1341	639		
	W345B	3.84	1521	1930	758	X	
		5.38	1517	1930	3003		
		5.745	1517	1930	3178		
		6.7155	1532	1930	379		

	W345C	3.84	1935	2153	1917	X	Figure 3.8
		5.38	1935	2153	1875		
		5.745	1935	2153	1884		
		6.7155	1935	2148	1642		
	W345D	3.84	2158	0004	808	X	
		5.38	2158	0004	659		
		5.745	2158	2343	618		
		6.7155	2201	2328	253		
12/12/75	W346A	3.84	0546	1143	3518	O	Figure 3.3
		5.38	0553	1117	1564		
		5.745	0545	1116	1441		
		6.7155	0546	1143	797		
	W346B	3.84	1146	1404	1603	O	Sample of sporadic E
		5.38	1147	1404	1983		reflection
		5.745	1148	1404	1963		Figures 3.3,4,6,7
		6.7155	1146	1404	1771		Figure 3.5 ionograms
	W346C	3.84	1409	2011	2572	O	Figure 3.3
		5.38	1409	2011	2941		
		5.745	1409	2011	1261		
		6.7155	1409	2011	546		
	W346D	3.84	2025	0001	1130	O	Figure 3.3
		5.38	2025	0000	752		
		5.745	2025	2352	500		
		6.7155	2026	2351	557		
13/12/75	W347A	3.84	0117	0819	2190	X	
		5.38	0117	0907	2256		
		5.745	0132	0907	1472		
		6.7155	0247	0906	1402		
	W347B	5.38	0911	1410	2946	X	
		5.745	0911	1410	3326		
		6.7155	0911	1410	767		
	W347C	5.38	1415	1806	2458	X	
		5.745	1415	1806	2523		
		6.7155	1415	1806	1832		
	W347D	3.84	1809	2030	1099	X	Figures 3.9,10
		5.38	1809	2030	1889		Figure 3.5 ionograms
		5.745	1809	2030	1939		
		6.7155	1809	2030	1955		
	W347E	3.84	2035	2334	1585	X	
		5.38	2035	2334	2052		
		5.745	2035	2334	2022		
		6.7155	2035	2334	1660		
14/12/75	W348A	3.84	2340	0450	2032	X	
		5.38	2340	0448	1907		
		5.745	2340	0450	1657		
		6.7155	2340	0450	1724		
	W348B	3.84	0454	0941	690	X	
		5.38	0454	0956	2151		
		5.745	0454	0956	1663		
		6.7155	0454	0956	1063		

	W348C	5.38	0959	1423	2313	X	
		5.745	0959	1425	2604		
		6.7155	0959	1425	2402		
	W348D	5.38	1428	1650	2040	X	
		5.745	1428	1650	2497		
		6.7155	1428	1650	2783		
	W348E	5.38	1653	1900	2078	X	
		5.745	1653	1900	2046		
		6.7155	1653	1900	2116		
		7.3245	1747	1900	791		
	W348F	3.84	1905	2241	1484	X	
		5.38	1905	2241	1595		
		5.745	1905	2241	1692		
		6.7155	1905	2241	1582		
		7.3245	1905	2241	964		
15/12/75	W349A	3.84	0004	0816	2104	X	
		5.38	0005	0816	1158		
		5.745	0005	0816	1672		
		6.7155	0005	0816	696		
		7.3245	0006	0816	1223		
	W349B	3.84	0820	1057	1189	O	
		5.38	0820	1057	1477		
		5.745	0820	1057	1110		
		6.7155	0820	1057	796		
		7.3245	0820	1057	836		
19/12/75	W353A	5.38	1821	2014	7324	O	Not processed
20/12/75	W354A	3.84	0038	0827	2219	X	
		5.38	0038	1008	2818		
		5.745	0038	1008	1171		
		6.7155	0038	1008	1112		
	W354B	3.84	1427	1640	1407	O	
		5.38	1433	1640	2317		Figures 3.12,13,
		5.745	1427	1640	2187		5.1,2,4,5,6,7,8
		6.7155	1427	1640	1397		Figure 5.3 ionograms
	W354C	3.84	1644	1941	1400	X	
		5.38	1644	1941	2343		Figures 5.9,10,12,13,14
		5.745	1644	1941	2162		Figure 5.11 ionograms
		6.7155	1644	1941	1415		
21/12/75	W355A	3.84	0206	0737	1234	X	Figure 3.11
		5.38	0206	1316	3264		
		5.745	0210	1316	1989		
		6.7155	0207	1316	832		
	W355B	5.38	1340	1735	2114	X	
		5.745	1340	1735	1991		
		6.7155	1340	1735	1886		
		7.3245	1340	1735	799		
	W355C	-					Data lost
	W355D	3.84	1807	2012	1263	O	
		5.38	1803	2012	2009		Figs. 5.15,16,17,19,20,21
		5.745	1803	2012	1963		Figure 5.18 ionograms
		6.7155	1803	2012	1457		

	W355E	3.84	2040	2137	787	O	
		5.38	2040	2137	896		
		5.745	2040	2137	779		
2/1/76	W002A	5.38	1648	1959	4075	O,X	
		5.745	1835	1959	2466		
	W002B	5.38	2004	2248	3248	O	
		5.745	2004	2245	1759		
3/1/76	W003A	3.84	1536	2020	1125	O	Not processed
		5.38	0300	2020	3613		Equipment configuration
		5.745	0801	2020	2582		non standard
4/1/76	W004A	5.38	0432	1610	3711	O	
		5.745	0436	1607	996		
			1512	1611	2615		
	W004B	5.38	1640	2013	4756	O	Figure 3.17
		5.745	1640	2013	2415		

APPENDIX F

DISCUSSION ON THE GROUP VELOCITY OF A GRAVITY WAVE

This appendix discusses an anomalous situation with regard to the representation of the group velocity of a gravity wave that is mentioned in chapter 5. The packet velocities given by Hines (1974) expressed by (5.24) and (5.25) are considered in the literature to be vector components. This, however, leads to a diffuculty. If ω is made small in (5.24) then to a good approximation:

$$V_{gx} \rightarrow V_{px} \tag{F.1}$$

By substitution of (5.8) into (5.25) or more quickly by substitution of (5.11) into (5.25) after neglecting the term $\omega^2 V_{px}^2 / c^2$ it can be seen that for small ω:

$$V_{gz} \rightarrow -V_{pz} \tag{F.2}$$

If V_{gx}, V_{gz} are considered to be vector components whilst V_{px} and V_{pz} are considered to be trace components then the result is obtained that:

$$|V_g| > |V_p| \tag{F.3}$$

since vector components add as:

$$V_{vec}^2 = V_x^2 + V_z^2 \tag{F.4}$$

whereas trace components add as:

$$1/V_{trace}^2 = 1/V_x^2 + 1/V_y^2 \tag{F.5}$$

Specifically, if (1), (2) is applied to packet velocity considered as a vector, then:

$$\begin{aligned} V_g^2 / V_p^2 &\simeq (V_{px}^2 + V_{pz}^2)(1/V_{px}^2 + 1/V_{pz}^2) \\ &= 2 + V_{px}^2 / V_{pz}^2 + V_{pz}^2 / V_{px}^2 \\ &= 2 + (\omega_g^2 - \omega^2)/\omega^2 + \omega^2/(\omega_g^2 - \omega^2) \end{aligned} \tag{F.6}$$

where use has been made of the asymptotic dispersion relation (5.11).

It can be seen from (6) that the ratio of V_g/V_p will increase without limit as ω is made smaller, at least in so far as the approximations inher-

ent in the derivation are valid. This implies that the energy of the wave can advance more rapidly than does the phase wave. If expression (1) is rewritten in more detail as:

$$V_{gx} \simeq V_{px}(1-\omega^2/\omega_g^2) \tag{F.7}$$

it can be seen that:

$$|V_{gx}| < |V_{px}|$$

Similarly (2) is:

$$V_{gz} \simeq -V_{pz}(1-\omega^2/\omega_g^2) \tag{F.8}$$

so that:

$$|V_{gz}| < |V_{pz}| \tag{F.9}$$

If the group velocity components are considered to be vector components then the incongruous result is that whilst the group velocity components are smaller than the phase velocity components the group velocity itself is larger than the phase velocity, (for small values of ω). The difficulty does not exist if the group velocity components are considered to be trace components. However, if this is done a revision to the theory needs to be considered.

The relationship between vector and trace components can be seen in figure 1. Vector components are represented by upper case suffixes and trace components by lower case suffixes. Considering equivalent triangles it can be seen that:

$$V_X/V_Z = V_z/V_x \tag{F.10}$$

and that the slope of the velocity on the assumption that its components are trace components is the compliment of the slope on the assumption of vector components. That is, the group velocity is tangential rather than normal to a curve of constant period in a k_x/k_z diagram.

The direction of energy flow can be found from the real energy flux vector $p\underset{\sim}{U}$ averaged over a cycle. Considering the ratio of components of

the flux vector:

$$\frac{F_x}{F_z} = \frac{\frac{1}{2}\langle p' U'^* \rangle}{\frac{1}{2}\langle p' V_z'^* \rangle} \qquad \text{(F.11)}$$

and substituting for p',U' and V' from (5.6), the ratio (11) reduces to:

$$\frac{F_x}{F_z} = \frac{k_x}{k_z}\left(1 - \frac{\omega_g^2}{\omega^2}\right)$$

This can be seen to be equal to the ratio of (5.24) to (5.25). That is:

$$V_{gx}/V_{gz} = F_x/F_z \qquad \text{(F.12)}$$

which implies that the energy flow is in the direction of the group (or packet) velocity. Since this result is based on the evaluation of a ratio it is independent of any consideration of the group velocity components as trace or vector components.

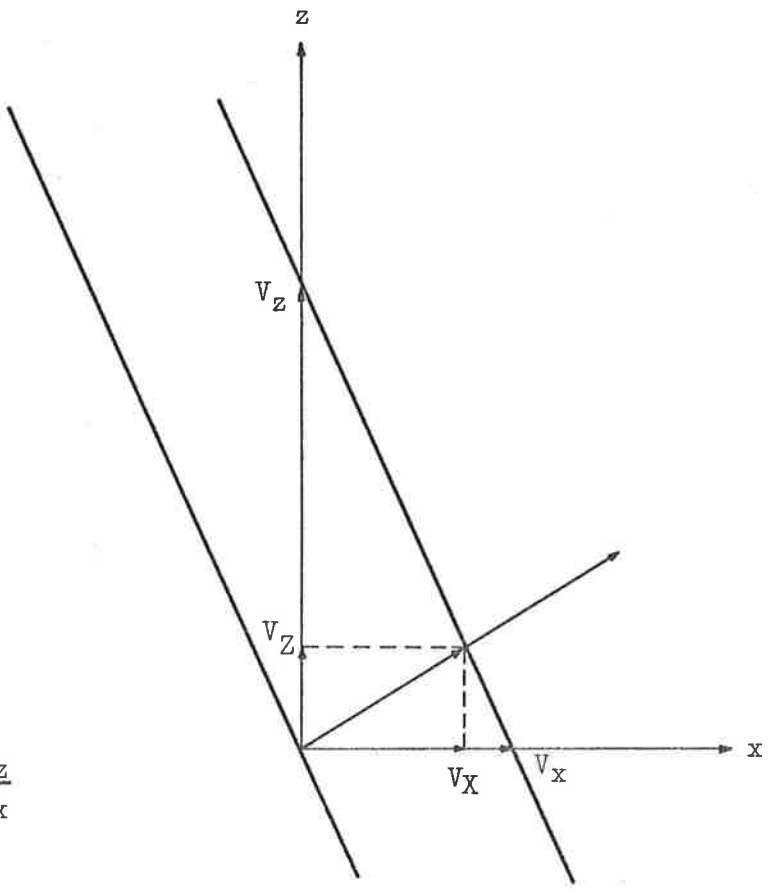

$$\frac{V_X}{V_Z} = \frac{V_Z}{V_x}$$

Figure F.1 Relationship between vector and trace velocity components

BIBLIOGRAPHY

Ahmed M. (1977) "Travelling ionospheric disturbances in the F region". Thesis presented for the degree of Doctor of Philosophy at the University of Adelaide.

Beer T. (1972) "Atmospheric waves in the ionosphere". Contemp. Phys. Vol. 13, No. 3, pp 247-271.

Bendat J. (1971) "Random data - Analysis and measurement procedures". John Wiley publishers.

Bogner R.E. and Constantinides A.G. Editors (1975) "Introduction to Digital Filtering". John Wiley publishers.

Bramley E.N. and Ross W. (1951) "Measurements of the direction of arrival of short radio waves reflected at the ionosphere". Proc. Royal Soc., London, Series A, Vol. 207, pp 251-267.

Bramley E.N. (1953) "Direction finding studies of large scale ionospheric irregularities", Royal Soc. London Proc. Series A, Vol. 220, pp 39-61.

Briggs B.H. and Spencer M. (1954) "Horizontal movements in the ionosphere". Reports on progress in physics. Vol. XVII pp 245-280.

Brownlie G.D., Dryburgh L.G. and Whitehead J.D. (1973) "Measurement of the velocity of waves in the ionosphere. A comparison of the ray theory approach and diffraction theory". J. Atmos. Terr. Phys., Vol. 35, pp 2147-2162.

Burtnyk N., McLeish C.W. and Wolfe J. (1965) "Performance of an interferometer direction finder for the h.f. band". Proc. I.E.E. Vol. 112, No. 11, pp 2055-2059.

COSPAR working group 4 (1965 and 1972) Cospar International Reference Atmosphere (CIRA,1965. North-Holland Publishing Co. CIRA, 1972. Akademie-Verlag, Berlin.)

Croft T.A. and Fenwick R.B. (1963) "Chart for determining the effects of ionospheric tilts using an idealized model". Jnl. of Research of the NBS-D. Radio propagation, Vol. 67D, No. 6, pp 735-745.

Davies K. and Baker D.M. (1966) "On frequency variations of ionospherically propagated H.F. radio signals". Radio Sci. Vol. 1, (New Series), No. 5, pp 545-555.

Davies K. (1966) "Ionospheric Radio Propagation". Dover Publications Inc. First published as National Bureau of Standards, Monograph 80, 1965.

Davies K. (1969) "Ionospheric Radio Waves". Blaisdell Publishing Company.

Davies K. and Jones J.E. (1971) "Three-dimensional observations of travelling ionospheric disturbances". Jnl. Atmos. and Terr. Phys. Vol.33, pp 39-46.

Doupnik J.R. (1963) "A flexible method of determining the electron density distribution in the ionosphere". Scientific report No. 190, Ionospheric Research Laboratories, The Pennsylvania State University.

Francis S.H. (1975) "Global propagation of atmospheric gravity waves: A review". J. Atmos. and Terr. phys. Vol. 37, pp 1011-1054.

Friedman J.P. (1966) "Propagation of internal gravity waves in a thermally stratified atmosphere". Jnl. Geophys. Res. Vol. 71, No. 4, pp 1033-1054.

George P.L. (1972) "H.F. ray tracing of gravity wave perturbed ionospheric profiles". AGARD paper reprinted from conference procedings No. 115.

Georges T.M. (1967) "Ionospheric effects of atmospheric waves". E.S.S.A. tech. report, IER 57-ITSA 54.

Georges T.M. (1968) "Collisional interaction of atmospheric waves with the ionospheric F region". From "Acoustic-gravity waves in the atmosphere" Symposium proceedings, Boulder, Colorado. pp 377-380.

Gething P.J.D. (1966) "High frequency direction finding". Proc. I.E.E. Vol. 113, No. 1, pp 49-61.

Gething P.J.D. (1978) "Radio direction-finding and the resolution of multicomponent fields". Peter Perigrinus Ltd. Publishers.

Hamming R.W. (1973) "Numerical methods for scientists and engineers". McGraw-Hill book Company. Second edition.

Hayden E.C. (1961) "Propagation studies using direction-finding techniques". Jnl. of Research of the NBS-D. Radio Propagation, Vol. 65D, No. 3, pp 197-212.

Heisler L.H. (1958) "Anomalies in ionosonde records due to travelling ionospheric disturbances". Aust. J. Phys. Vol. 11, pp 79-90.

Heisler L.H. and Whitehead J.D. (1961) "The interpretation of F2 critical frequency measurements". J. Atmos. Terr. Phys. Vol. 22, pp 186-191.

Heisler L.H. (1963) "Observation of movement of perturbations in the F-region". J. Atmos. Terr. Phys., Vol. 25, pp 71-86.

Heisler L.H. and Nelson G.D. (1967) "On the divergence of radio rays in the ionospheric medium". J. Atmos. Terr. Phys., Vol. 29, pp 839-855.

Herron T.J. (1974) "Dispersion of ionospheric waves". Nature, Vol. 248, March, pp 213-215.

Hines C.O. (1960) "Internal atmospheric gravity waves at ionospheric heights". Can. J. Phys, Vol. 38, pp 1441-1481, and also 1964, 42, pp 1425-1427. An annotated version appears in "The upper atmosphere in motion". Hines editor, 1974.

Hines C.O. (1963) "The upper atmosphere in motion". Quarterly Journal of the Royal Meteorological Society, Vol. 89, No. 379, pp 1-42. (Napier Shaw prize essay, 1962)

Hines C.O. and Reddy C.A. (1967) "On the propagation of atmospheric gravity waves through regions of wind shear". Jnl. Geophys. Res. Vol. 72, No. 3, pp 1015-1034.

Hines C.O. (1974) "Propagation velocities and speeds in ionospheric waves: A review". J. Atmos. and Terr. Phys. Vol. 36, pp 1179-1204.

Hooke W.H. (1968) "Ionospheric irregularities produced by internal atmospheric gravity waves". Jnl. Atmos. Terr. Phys. Vol. 30, pp 795-823.

Hooke W.H. (1970a) "The ionospheric response to internal gravity waves 1. The F region response". Jnl. Geophys. Res. Space Physics, Vol. 75, No. 28, pp 5535-5544.

Hooke W.H. (1970b) "The ionospheric response to internal gravity waves 2. The lower F region response". Jnl. Geophys. Res. Vol. 75, No. 34, pp 7229-7238.

Hooke W.H. (1970c) "Ionospheric response to an isotropic spectrum of internal gravity waves". Planet. Space Science, Vol. 18, pp 1793-1797.

Jones J.E. (1969) "Observations on travelling ionospheric disturbances by the doppler technique with spaced transmitters". ESSA technical report ERL 142-SDL 11.

Jones T.B. and Reynolds J.S.B. (1975) "Ionospheric perturbations and their effect on the accuracy of h.f. direction finders". The Radio and Electronics Engineer, Vol. 45, No. 1/2, pp 63-73.

Jones T.B., Kantarizis E. and Morgan A.D. (1975) "Simultaneous measurements of the frequency and bearing of h.f. radio waves". Proc. I.E.E. Vol. 122, No. 3, pp 241-244.

Lincoln V.J. (1976) "Geomagnetic and Solar data". J. Geophys. Res. Vol. 81, No. 10, p 1812.

McNamara L.F. (1978) "A comparative study of methods of electron density profile analysis". Report UAG-68 World data centre A for solar-terrestrial physics.

Mitra S.N. (1949) "A radio method of measuring winds in the ionosphere". Proc. I.E.E. Vol. 96, Part 3, pp 441-446.

Morgan A.D. (1974) "A qualitative examination of the effects of systematic tilts, in the ionosphere, on HF bearing measurements". Jnl. Atmos. Terr. Phys. Vol. 36, pp 1675-1681.

Munro G.H. (1950) "Travelling disturbances in the ionosphere". Proc. Roy. Soc. A202, pp 208-223.

Munro G.H. (1953) "Reflections from irregularities in the ionosphere". Proc. Roy. Soc. A219, pp 447-463.

Munro G.H. and Heisler L.H. (1956) "Divergence of radio rays in the ionosphere". Aust. J. Phys. 9, pp 359-372.

Munro G.H. (1958) "Travelling ionospheric disturbances in the F region". Aust. J. Phys. Vol. II, pp 91-112.

Otnes R.K. and Enochson L. (1972) "Digital time series analysis". John Wiley and Sons Publishers.

Phillips G.J. (1951) "A wide band aerial system for circularly polarized waves, suitable for ionospheric research". Proc. Inst. Elec. Eng. 98, Part III, pp 237-239.

Piggott W.R. and Rawer K. editors (1972) "U.R.S.I. Handbook of ionogram interpretation and reduction". 2nd edition, Report UAG-23, World Data Centre A for solar-terrestrial physics.

Pitteway M.L.V. and Hines C.O. (1963) "The viscous damping of atmospheric gravity waves". Canadian Jnl. Phys. Vol. 41, No. 12, pp 1935-1948.

Pitteway M.L.V. and Hines C.O. (1965) "The reflection and ducting of atmospheric acoustic-gravity waves". Canadian Jnl. Phys. Vol. 43, pp 2222-2243.

RACAL Communications Incorporated "Operating manual for twin channel H.F. communications receiver, type RA 153A".

Rice D.W. (1973) "Phase characteristics of ionospherically-propagated radio waves". Nature Phys. Sci. 244, pp 86-88.

Rishbeth H. (1967) "A review of ionospheric F region theory". Proc. I.E.E.E. Vol. 55, No. 1, pp 16-35.

Ross W. (1947) "Fundamental problems in radio direction- finding at high frequencies (3-30Mc/s)". Proc.I.E.E. 94, Part III A pp 154-165.

Ross W., Bramley E.N. and Ashwell G.E. (1951) "A phase-comparison method of measuring the direction of arrival of ionospheric radio waves". Proc. I.E.E. Vol. 98, pp 294-302.

Schweikert D.G. (1966) "An interpolation curve using a spline in tension". J. Math. Phys. 45, pp 312-317.

Thomas J.O. (1959) "The distribution of electrons in the ionosphere". Proc. I.R.E. 47, pp 162-175.

Thome G. (1968) "Long-period waves generated in the Polar ionosphere during the onset of magnetic storms". J. Geophys. Res. Space Physics, Vol. 73, No. 19, pp 6319-6336.

Thome G.D. and Rao P.B. (1969) "Comparison of acoustic-gravity wave theory with HF and UHF observations". Final report. Advanced Research Projects Agency.

Toman K. (1976) "On wavelike perturbations in the F region". Radio Science, Vol. 11, No. 2, pp 107-119.

Treharne R.F., McCue C.G., Jeffrey Z.R. and Hewett B.S. (1965) "Some characteristics of the propagation of skywaves over short ionospheric paths". Proc I.R.E.E. Australia, Vol. 26, No. 8, pp 245-254.

Treharne R.F. (1967) "Vertical triangulation using skywaves". Proc. I.R.E.E. Australia Nov. pp 419-424.

Vincent R.A. (1972) "Ionospheric irregularities in the E-region". Jnl. Atmos. Terr. Phys. Vol. 34, pp 1881-1898.

Walton E.K. (1971) "Studies of travelling ionospheric disturbances with a triple radio interferomenter system". Proceedings of the fourth Allerton-house conference on HF radio direction finding and radiolocation research. RRL publication No. 389.

Warren-Smith D.N. (1974) "A digital filter for data smoothing". Technical memorandum - 1191 (AP) Weapons Research Establishment.

Warren-Smith D.N. and Steer N.J. (1977) "AUTOCELL: An automated high frequency radio interferometer". Technical Report 1644(A) Weapons Research Establishment.